| AD NUMBER |
|---|
| AD910447 |
| LIMITATION CHANGES |

TO:

Approved for public release; distribution is unlimited.

FROM:

Distribution authorized to U.S. Gov't. agencies only; Test and Evaluation; MAR 1973. Other requests shall be referred to Air Force Rome Air Development Center, Attn: OCSE, Griffiss AFB, NY 13441.

AUTHORITY

radc, usaf, ltr, 9 jul 1975

RADC-TR-73-88
Final Technical Report
February 1973

THEORY OF IONOSPHERIC MODIFICATION

University of Colorado

AF30602-72-C-0343

Sponsored by
Defense Advanced Research Projects Agency
ARPA Order No. 1423

Distri...                                                only;
test...                                                 ts
for ...                                                 SE),
GAFB,

The views and conclusions contained in this document are those of the
authors and should not be interpreted as necessarily representing the
official policies, either expressed or implied, of the Defense
Advanced Research Projects Agency or the U. S. Government.

Rome Air Development Center
Air Force Systems Command
Griffiss Air Force Base, New York

# THEORY OF IONOSPHERIC MODIFICATION

M. V. Goldman
D. F. DuBois
J. Weinstock
B. Bezzerides

PUBLICATION REVIEW

This technical report has been reviewed and is approved

RADC Project Engineer

RADC Contract Engineer

ii

# THEORY OF IONOSPHERIC MODIFICATION

M. V. Goldman
D. F. DuBois
J. Weinstock
B. Bezzerides

## Table of Contents

# Table of Contents (Cont'd.)

## Foreword

The principal contractor for the work described in this report is the Department of Astro-Geophysics of the University of Colorado at Boulder. Dr. Donald F. DuBois contributed as a Visiting Professor in the Department of Astro-Geophysics on leave from Hughes Research Laboratories, Malibu, California, where he is Senior Research Scientist. Postdoctoral Research Associates, Drs. R. Berger and E. Williams performed research in collaboration with Drs. Goldman and DuBois. Computer programming was done by D. McKinnis, whose aid we gratefully acknowledge. We wish to thank the National Center for Atmospheric Research for offering the use of their computer facilities for this research. A subcontract was issued to Drs. Weinstock and Bezzerides of the National Oceanic and Atmospheric Administration, Boulder, Colorado.

The format we use here is one of a short self-contained report, together with seven appendices which give further details. Figures originating in the appendides are duplicated in the report when they are cited there, as are references. The appendices are cited in footnotes by their letter. An overall table of contents is provided.

The report proper was prepared by the Principal Investigator, Martin V. Goldman, with the assistance of D.F. DuBois, J. Weinstock, and B. Bezzerides.

The authors of each appendix are indicated on the first page of that appendix.

## Summary

Ionospheric modification experiments over Platteville, Col.[1], and Arecibo, Puerto Rico[2,3] are operated at HF intensities sufficient to drive electrostatic waves unstable in the F-layer plasma, through the process of parametric instability.[4,5] We have studied the nonlinear effects [6,7,8,A] of the waves excited by the HF modifier on:

(a) the modifier propagation, reflection, and deviative absorption[C],

(b) UHF backscattering models[7,B]; and

(c) the nonequilibrium distribution of electrons in the F-layer[B].

It has been found that the electron plasma waves excited by the Arecibo modifier determine the general features and magnitudes of the observed UHF vertical backscattering cross-sections, although there are still some unresolved issues. The most widely accepted current theory is based on ion-acoustic frequency, 35 cm density fluctuations beating with the vertical component of the modifier electric field to produce density fluctuations around the plasma frequency.[4b] The scattering cross-section for other frequencies (VHF to Ghz) and other scattering angles has also been found[6,A]. Much larger cross-sections are predicted at scattering angles which probe plasma waves propagating nearly parallel to the geomagnetic field[6]. Below one GHZ the scattering model is based on the saturation of plasma waves by induced scattering off ions[6,7] (also known as nonlinear ion Landau-damping[9]), provided photoelectrons are ignored. Above about one GHZ the scattering model is based on orbit-perturbation saturation[6,A]. The latter theory is probably also relevant to scattering below 1 GHZ, when photoelectrons are taken into account, although this calculation is still in progress.

We have found that the electron plasma waves excited by the Platteville modifier operating at a peak output of 50 $\mu\omega/m^2$ vacuum intensity at the

2

F-layer cause an additional 10 to 40% nonlinear deviative absorption[C] of the modifier, for a Chapman scale height of 75 km, when the modifier frequency is below $f_oF_2$. At $1500^\circ$K it is stronger (20-40%). Photoelectrons have the effect of reducing the size of the nonlinear altitude range, and hence decreasing the anomalous absorption. We therefore expect stronger anomalous absorption at night, compared to in the daytime. The anomalous absorption which occurs at higher modifier pump powers has also been computed and may be of interest if self-focusing[10] can intensify the present peak power, or if future, more powerful transmitters are developed.

The nonlinear propagation of the modifier into the inhomogeneous ionosphere has been studied[C], neglecting the geomagnetic field. The modifier is essentially a standing wave at altitudes within several kilometers below the reflection point even when there is strong anomalous absorption. There are steep oscillations found in the Poynting flux pattern and hence bands of altitudes at which local anomalous heating should be strongest. The above theory is based on saturation of plasma waves due to induced scattering off ions.

The short wavelength electron plasma waves excited by the Platteville modifier operating at peak output have been found to alter the electron velocity distribution[D]. We have found the rate at which electrons are accelerated by 10-15 cm wavelength plasma waves to energies above 3eV. The flux of such energetic electrons along the geomagnetic field is typically of the order of $10^9$ electrons $cm^{-2}$ $sec^{-1}$, which is sufficient to explain the 6300 Å airglow enhancements observed during modification, and possibly the 5500 Å enhancements as well. The theory is based on perturbed-orbit saturation of electron plasma waves[A,D]. It predicts that the energetic electrons originate at altitudes about 12% of the Chapman scale height below

3

the reflection point.

Interesting new plasma wave effects associated with the geomagnetic field have been found[E,F,G]. Platteville modifier intensities should be sufficient to drive a new parametric instability involving both very low frequency ($\sim 10^{-3}$Hz), long wavelength (600 meter) electrostatic waves propagating transverse to the geomagnetic field and backscattered HF radiation[F]. A crude linear stability analysis predicts a growth rate of several minutes, which is probably too long to account for the wide band attenuation observed in ionosonde experiments. However, given enough time to develop, these waves would constitute field aligned irregularities. A nonlinear saturation theory[G] has been developed for the very low frequency field-aligned waves. The theory predicts a fluctuation level for these waves which is about 1% of the ambient density.

# I. Introduction

This report is concerned with the observable consequences of various plasma wave instabilities which can be excited in the F-layer of the ionosphere by "pump" radio waves[1] in the 5-10Mhz frequency range having vacuum intensities of 25-50 $\mu w/m^2$. Three parametric instabilities which can be excited are examined here in varying degrees: the "decay instability,"[4,7] in which an electron plasma wave and an ion-acoustic wave are excited; the "purely-growing" instability,[11,B] in which an electron plasma wave at the pump frequency and a purely growing mode are excited; and "stimulated diffusion scattering"[F] in which the excited waves consist of a very low frequency diffusion-like mode propagating across the magnetic field, together with a backscattered electromagnetic wave. We have been interested principally in the decay instability, as excited by an ordinary-wave pump in the absence of a magnetic field, for electrons and ions assumed to be the same temperature.[4] The excited waves produce enhanced electron density fluctuations which have been measured in UHF backscattering experiments.[2,3] In order to theoretically compute scattering cross-sections, study the effects of the plasma waves on the electron distribution function, etc., it was necessary to know the nonlinear plasma wave intensity. The determination of this intensity required that we know not only the linear growth rate of the waves, but also the nonlinear decay rate which is ultimately responsible for their saturation. A complete theory further required a knowledge of the nonlinear thermal "noise" sources of the plasma waves.[4b,6,7] Two complementary such nonlinear saturation theories were developed for a homogeneous plasma. The first involves stimulated scattering of the excited plasma waves off ions into less unstable regions of phase space[6,7]; the second involves absorption of the excited plasma waves by electrons whose orbits have been nonlinearly perturbed by the waves.[8] We shall refer to the first of these as "induced-scattering

saturation" (sometimes also referred to as nonlinear ion Landau-damping), and to the second as orbit-perturbation saturation. The induced-scattering saturation mechanism was first presented by DuBois and Goldman at the Ivory Coral Meeting in Albuquerque, New Mexico, August, 1971. A similar theory was also being developed independently at that time by Valeo, Oberman and Perkins.[9] The orbit-perturbation saturation theory was first presented by Bezzerides and Weinstock at the ARPA meeting in Boulder, Col., November, 1971. In Section II below we describe both of these theories and further refinements by the present authors and by others. Also described are the consequences of these theories for the plasma wave spectral intensity distribution, total wave energy, and for the associated anomalous resistivity.

Section III below is devoted to effects of the weak spatial density inhomogeneity in the F-layer on the plasma wave level, and the observable consequences for absorption, scattering and airglow. For the ionosphere, a simple model is found to be adequate: the homogeneous results are taken over, but the density and hence the electron plasma frequency and principally-excited plasma wavelength vary with altitude for a fixed pump frequency. The consequences of this model for the pump propagation towards its reflection point are explored by numerically solving the nonlinear pump wave equation[C] for a vertically plane-layered ionosphere, neglecting geomagnetic field effects. Some nonlinear deviative absorption is found, and we display the pump electric field profile with altitude. The solution gives us the electron density fluctuation spectrum as a function of altitude, and hence determines the UHF scattering cross-section for frequencies in the vicinity of the electron-plasma frequency and the ion-acoustic frequency. The shorter wavelength plasma waves are shown to be capable of accelerating electrons to sufficient energy to excite 6300 Å and possibly 5500 Å

6

collisionally-induced airglow.[D]

    Finally, Section IV treats an interesting instability associated with the geomagnetic field: a process in which the pump undergoes stimulated scattering from a very low frequency ($\sim 10^{-3}$ Hz) diffusion-like mode propagating across the magnetic field with a wavelength given by one-half the local pump wavelength.[E,F,G] This leads to very slow growth of both the diffusion mode and the scattered radiation. Some comparisons are made with stimulated Brillouin scattering. Preliminary work on the nonlinear saturation of the "stimulated-diffusion scattering" instability is described.[G]

## II. Homogeneous nonlinear saturation of the parametric decay instability and anomalous resistivity

### a) Definitions and general properties of nonlinear saturation.

The intensities of the waves excited in the parametric decay instability are measured by the correlation functions of electrostatic field fluctuations, integrated over frequencies near the electron plasma frequency and near the ion acoustic frequency. These frequency-integrated correlation functions[6,7] are called, respectively, $I_1(k,x)$ and $I_2(k,x)$, the former referring to electron plasma waves (which we sometimes call Langmuir waves), and the latter to ion-acoustic waves. $k$ is the propagation wave-number and $x = \hat{e}_0 \cdot \hat{k}$ is the cosine of the angle the propagation vector makes with the pump electric field ($\simeq$ parallel to the geomagnetic field for an ordinary wave near its reflection point). For equal electron and ion temperatures, the Langmuir wave intensity spectrum generally obeys a nonlinear rate equation of form

$$\frac{\partial}{\partial t} I_1 = +2\left[\gamma_g - \gamma_L - \gamma_L^{NL}\right]I_1 + 2S_1, \tag{1}$$

$$\text{where } \gamma_g = \gamma_L P f x^2.$$

$\gamma_g$ is the linear growth rate, $\gamma_L$, the linear damping rate, and $\gamma_L^{NL}$ the nonlinear damping rate. The fourth term represents thermal (noise) emission at Langmuir frequencies. $\gamma_L(k) = \gamma_C + \gamma_\chi(k)$ consists of linear collisional damping and (k-dependent) Landau damping. For k below about $0.2\ k_D$, where $k_D$ is the Debye wavenumber, the Landau damping is negligible. The quantity P is a measure of the pump field strength and is given by

$$P \equiv \frac{E_o^2}{4\pi n \Theta}\ \frac{1}{16\gamma_L/\omega_P}, \tag{2}$$

where n is the electron density and $\Theta$, the common electron and ion temperature in energy units. P=1 defines the minimum threshold field, $E_o|_{\text{min.thresh.}}$, for excitation of parametric instability. The P-value tells us how much the pump power is above or below the minimum threshold. The factor, $f = f(k,x)$ is called the frequency mismatch factor and is equal to one for k equal to the frequency-matched wave number, $k_m$, defined by

$$\omega_o = \omega_L(k_m) + \omega_{ia}(k_m), \tag{3}$$

where $\omega_o$ is the pump frequency, $\omega_L(k)$ is the Langmuir frequency $(\omega_p^2 + 3k^2V_e^2)^{\frac{1}{2}}$, and $\omega_{ia}(k)$ is the ion acoustic frequency, $\sim (m_e/m_i)^{\frac{1}{2}} kV_e$. For $k<k_m$, the mismatch factor f is < 1. Note $k_m$ is fixed by the density, temperature, and pump frequency. The nonlinear damping rate $\gamma_L^{NL}(k,x)$ depends on $I_1$, and has been the subject of various theories and approximations to be described. The emission term, $S_1$ consists of linear Cerenkóv and/or bremunstrahlung emission at the Langmuir frequency $\omega_L(k)$ plus a term, first derived by two of the authors[13,4], representing the beating of Cerenkóv emission at ion-acoustic frequencies with the pump field to produce emission around the Langmuir frequency. It dominates the usual linear emissions even for P < 1.

Since we have assumed azimuthal symmetry about the pump electric field, the solution to equation 1 for some appropriate model of the nonlinear damping rate $\gamma_L^{NL}$ gives $I_1(t,k,x)$ for a homogeneous plasma. Asymptotic time-independent solutions $I_1(k,x)$ obtained by setting the right side of equation 1 equal to zero and solving the resulting nonlinear equation are called saturated steady-state intensity spectra. $I_1$ and $I_2$ are necessary in order to compute scattering cross-sections or anomalous resistivities. In all of the saturation theories developed for the equal temperature decay instability the ion acoustic spectrum $I_2$ is simply proportional to

9

$I_1$ and given by $I_2 = \left[\gamma_g k^2 / k_D^2\right] I_1$. In the ionosphere the intensity of parametrically excited ion-acoustic waves turns out to be much lower than that of the Langmuir waves. Physically, the ion acoustic waves are heavily damped quasi-modes which are "dragged" along by the strongly enhanced Langmuir modes.

Another quantity of interest is the total energy, $\bar{E}$, in Langmuir waves for a given electron density, temperature and pump frequency (hence, for a given $k_m$)

$$\bar{E} \equiv \int \frac{d^3\underline{k}}{(2\pi)^3} \frac{I_1(\underline{k})}{4\pi} \tag{4}$$

The two theories for $\gamma_L^{NL}$ to be described below have both been solved in various approximations for $I_1(\underline{k})$, $\bar{E}$ and for the high frequency electromagnetic anomalous dissipative conductivity, $\sigma_T^{NL}$. An expression for the (transverse) anomalous dissipative conductivity, $\sigma_T^{NL}$, applicable to either theory is given by,

$$\frac{\sigma_T^{NL} |E_0|^2}{2} = 2 \int \frac{d^3\underline{k}}{(2\pi)^3} \gamma_g(k) \frac{I_1(\underline{k})}{4\pi} \tag{5}$$

This is a simple expression of energy conservation. The energy loss rate of the pump (left side) is balanced by the total energy gain (summed over $\underline{k}$ on the right side) of Langmuir waves, due to their linear growth at the rate $\gamma_g = x^2 f P \gamma_L$, indicated in the rate equation 1.

b) Saturation of Langmuir waves by induced scattering off ions

In this theory, the parametrically unstable Langmuir waves are scattered off ions out of the unstable region of phase space where $\gamma_g(\underline{k})$ is largest and into more stable regions. The scattering rate, $\gamma_L^{NL}$, is proportional to the intensity of Langmuir waves and the process is therefore said to be

10

"induced" or "stimulated." (The scattered waves are entirely electrostatic in this process, which is not to be confused with electromagnetic scattering.) The earliest theory[14,7] made the crude approximation that $I_1$ was independent of x and therefore that the Langmuir waves were isotropically distributed in angle about the direction of the pump electric field. We will refer to this as the isotropized theory. In the published form of this work[7] $I_1(k)$ spread continuously from $k_m$ to lower k as P was increased, and the total energy, E, was found to increase as $P^2$. An estimate of the radar backscatter cross-section was also made at this time and appeared to give too large a result in comparison with the Arecibo experiments. Later, more refined computations[15,6,9], still based, however, on resonant approximations for dielectric functions (and for f), and on the so-called derivative approximations for $\gamma_L^{NL}$ led to an angular distribution of Langmuir waves, $I_1(x)$ which was highly peaked along the pump electric field (i.e., at x = 1). For the iono- sphere, this means peaking along the geomagnetic field direction. The width in k of the angle-averaged anisotropic spectrum, $\bar{I}_1(k) = \int_{-1}^{+1} \frac{dx}{2} I_1(k,x)$ was found to be 0.67 $(m_e/m_i)^{\frac{1}{2}}P$. The anomalous dissipative conductivity $\sigma_T^{NL}$ was found from the energy balance equation (5) by further noting that the induced scattering process represented in this saturation theory by $\gamma_L^{NL}$ merely redistributes the energy among Langmuir waves of different $\underline{k}$ without acting as an energy sink for the entire collection of waves integrated over $\underline{k}$. By integrating the rate equation (1) over $\underline{k}$ it was therefore possible to show that the right side of equation (5) was still correct if the growth rate $\gamma_g$ were replaced by the damping rate $\gamma_L$, provided the emission term $S_1$ was negligible (valid for P > 1). Physically, this says that the only real energy sink in this theory is the linear damping rate of plasma waves. The energy flows from the pump to the plasma waves, is then

11

redistributed in $\underline{k}$-space by the nonlinear saturation mechanism, and is finally delivered to the plasma particles by the collisional and Landau damping present in $\gamma_L$. For $k_m$ in the collision-damped region, therefore, the anomalous dissipative conductivity $\sigma_T^{NL}$ is given by

$$\sigma_T^{NL} = 4\gamma_c \bar{E}/E_o^2, \tag{6}$$

The results of Reference 6 and of other and more refined theories of this saturation all give slightly different numerical factors for $\bar{E}$, but all yield a $\sigma_T^{NL}$ in terms of $\bar{E}$, through equation (6). The results of these theories can be summarized by using a multiplicative parameter $\eta$, such that

$$\bar{E} = 4\eta \frac{\gamma_c}{\omega_P} P^2 n\theta \tag{7}$$

The values of $\eta$ corresponding to each theory are given in Table 1. Some of these theories make more accurate predictions for the structure of $I_1(k,x)$. The time-dependent solutions[16,17] of equation 1 provide estimates of the time scale necessary for the establishment of the steady state spectrum in the ionosphere. In the case of rapid pump turn-on a time of 15 m sec is required to establish the steady state spectrum if $P = 5$, while 5 m sec is required if $P = 20$. The spectrum may develop adiabatically with the pump, if the latter is turned on slowly enough. The rise time must be slower than 0.75 seconds for $P = 5$, or 3 seconds for $P = 20$. The most accurate of the 1-D time-dependent[17] solutions yields a discrete structure in k, consisting of peaks at values of k corresponding to Langmuir waves shifted in frequency by multiples of the ion acoustic frequency. This structure was also found independently by Kuo and Fejer.[18] The most complete refinement of our theory to date appears to be the numerical integration by Kuo and Fejer[19] of the rate equation (1), in time, wave number, and angle, using the exact dielectric function and no derivative

12

approximation for $\gamma_L^{NL}$. The most interesting feature of their solution is angular spreading which increases with P and is out to about $20^O$ at $P = 2$. The earlier k-structure is again found, leading to umbrella-shaped discs of Langmuir-wave intensity in $\underline{k}$-space. No values for the total energy $E$ are given in this work, but our earlier isotropized model leads us to expect an $\eta$-value of between 1 and 2.

Induced scattering of Langmuir waves off ions appears to be the dominant saturation mechanism for matched wavenumbers, $k_m < .23k_D$, in the collision-damped region, and the orbit-perturbation process to be discussed in the next section appears to be the dominant saturation for matched wave numbers in the Landau-damped region, $k_m > .23k_D$. In Appendix C, in addition to treating effects of spatial inhomogeneity on the nonlinear pump propagation, we have extended the induced-scattering saturation theory of $\sigma_T^{NL}$ somewhat, to include Landau-damping (qualitatively), four-mode effects (which raise the threshold when $\omega_{ia} < \gamma_L$), and broad spectrum effects (at high pump powers). Refer to Appendix C for details.

c) Saturation of Langmuir waves by orbit-perturbation

This saturation mechanism involves absorption of the parametrically excited Langmuir waves by electrons whose orbits have been nonlinearly perturbed by the waves. Sometimes it is called resonance-broadened Landau-damping. The theory of the nonlinear damping rate, $\gamma_L^{NL}$ and the spectrum $I_1(\underline{k})$ is described in detail in Appendix A and in Reference 8. Energy comparisons have shown that for frequency matched wave-numbers $k_m$ in the Landau-damped region $k_m > .23k_D$, orbit-perturbation is the dominant saturation mechanism. For smaller $k_m$, Landau-damping is exponentially weak since there are so few electrons whose velocities match the wave phase velocity. The resonance broadening effect for $k_m < .23k_D$ (at least for the pump intensities

13

of interest in the ionosphere) can't reach back far enough into the velocity distribution to find an appreciable number of electrons. For these wave numbers, the induced-scattering saturation described in the previous section dominates. Physically, the distinction between the two theories is made by asking whether or not a wave is scattered <u>out</u> of the unstable region (large $\gamma_g$) of phase space by the induced-scattering mechanism before it is <u>locally</u> absorbed by resonance broadened Landau-damping. Thus, a comparison of the rates for the two processes should be made. A careful treatment of the region $k_m \approx 0.2k_D$, where the two rates are apparently comparable has not been made to date. As we shall see in the next section, plasma waves with $k_m$ values in both nonlinear saturation regimes are always excited, although at different altitudes.

The validity of orbit perturbation theory requires that the correlation time of the fluctuating electric field be short compared to an electron trapping bounce time. This is guaranteed if the total wave energy density is less than the particle energy density, a condition which is satisfied for ionosphere parameters.

The spectrum obtained is broad in angle, provided $Px^2 \geq 1$, and narrow in k. In the Landau-damped region of the ionosphere the spectrum is confined to a half width, $\Delta k \approx 3 \times 10^{-4} k_m$, about the frequency-matched wave number, $k_m$. The angular part of the spectral intensity is given by

$$I_1(x) \equiv \int \frac{dk}{(4\pi)^2} k^2 I_1(\underline{k}_1 x) = 4\pi v\theta \times 3.4 \left\{ \frac{\ln (1 + r)Px^2 - r}{(k_D/k_m)^2 + 4.5} \right\}^2 , \qquad (8)$$

where r is the ratio of the collision damping rate $\gamma_c$ to the Landau-damping rate evaluated at $k_m$. This expression is valid provided $Px^2 \geq 1$. We see from eq$^n$ (8) that the spectrum becomes increasingly broad in angle.

14

as the pump is increased, finally reading isotropy. Figure 1 is a sketch of $I_1(x)$ as a function of $\theta = $ arc cosine $x$. The maximum spreading angle is given by $x^2_{min} = P^{-1}$, $\theta_{max} = $ arc cosine $x_{min}$. The total saturated wave energy density is given by

$$\frac{\bar{E}}{4\pi n \theta} = \frac{6.75}{\left[(k_D/k_m)^2 + 4.5\right]^2} \left\{ \left[\ln(1 + r)P\right]^2 - 4\left[\ln(1 + r)P - 2\right] - \frac{8}{\sqrt{1 + r\,P}} \right\}$$

(9)

For $k_m$ in the Landau-damped region, so that $r \ll 1$, the total wave energy density $\bar{E}$ is seen to increase rather slowly with the pump ratio $P$ for $P$ large. In Figure 2 we illustrate $\bar{E}$ as a function of $P$ for $k_m = 0.2k_D$, or $r = 1$. From the curve one observes that $\bar{E}$ increases approximately as $P$. Equation (5) may again be employed to give the nonlinear high-frequency dissipative conductivity, $\sigma_T^{NL}$. A direct application of (5) yields

$$\sigma_T^{NL}\Big|_{orbit \ perturbation} = \frac{\alpha}{3\pi} \gamma_L P \frac{\bar{E}}{E_o^2}$$

(10)

$\alpha$ is a numerical factor resulting from the angular dependence of $I(x)$. It varies slowly between 1 and 2 as a function of $P$. $\bar{E}$ is given by equation (9), and by Figure 2.

Whereas for the induced-scattering saturation mechanism the energy flowed from the pump to the waves where it was redistributed in k-space and eventually delivered to the particles via linear damping, the perturbed-orbit saturation mechanism predicts the energy to flow from the pump to the waves, and finally to the particles via the nonlinear process of resonance-broadened Landau-damping. Finally, it is interesting to note that (10) has met with considerable success in comparisons with numerical simulations.

15

Kruer and Dawson[20] have determined from numerical simulations an effective electron-ion collision rate, $\nu \equiv 4\pi\sigma_T^{NL}$ of precisely the same form as equation (10). Further details of perturbed-orbit saturation theory may be found in Appendix A.

III. Effect of density inhomogeneity in the ionosphere: applications of nonlinear saturation theory to absorption, scattering and airglow.

a) Anomalous absorption and the modifier field pattern. We have taken into account some important effects of density inhomogeneity on parametric instabilities in the ionosphere through the following simple model[C]: The homogeneous theory of the previous section is assumed to hold at each altitude, provided the local values of the plasma frequency and the pump (modifier) electric field amplitude at that altitude are used. The pump electric field is not assumed given, but is found locally in an assumed vertically plane-layered ionosphere, in terms of the incident vacuum intensity. The self-consistent pump field solution includes the effect of nonlinear pump depletion caused by the flow of power from the pump to the parametrically excited plasma waves at each altitude. This effect is contained in the dissipative nonlinear conductivity, $\sigma_T^{NL}$, in the wave equation for the pump. Effects of inhomogeneity on the linear parametric instability theory should not be important for the ionosphere because the scale height exceeds the electron mean free path[21]. We are also ignoring effects of inhomogeneity in the saturation theory and on the plasma wave propagation. (Some preliminary estimates of inhomogeneous plasma wave propagation effects have been carried out by Arnush[22], neglecting saturation, and by Perkins[22], with saturation included.) Basically, our model is one of nonlinear ordinary wave pump propagation vertically upwards through a linear density-altitude profile with a horizontal magnetic field

16

(or no magnetic field). Only after the pump field is found self-consistently in this manner do we know the plasma wave intensity spectrum as a function of altitude. As in the linear solution, the local pump wavelength is much larger than the wavelength of the excited plasma waves — one justification for using locally homogeneous theory for the latter. The frequency matched wave-number defined in equation (3) is now a function of altitude, since $\omega_p^2 = 4\pi n e^2/m$ is a function of altitude. Ignoring $\omega_{ia}$ relative to $\omega_p$, the matched wave number is

$$\frac{k_m^2}{k_D^2} = \frac{1}{3} \frac{\Delta z}{H} , \tag{11}$$

where H is the scale height and $\Delta z$ is distance below the reflection altitude. Thus, Langmuir waves of different wavenumbers are excited at different altitudes: long wavelengths are excited above short wavelengths. Since the shorter plasma waves are Landau-damped and the longer ones collisionally damped, the induced-scattering saturation mechanism should be valid at the higher altitudes and the orbit-perturbation mechanism at the lower altitudes. The situation is illustrated in Figure 3.

We have solved the following nonlinear inhomogeneous wave equation[C] for the modifier, including linear damping and the nonlinear damping represented by $\sigma_T^{NL}$, defined in equations 6 and 7:

$$\frac{\partial^2 E}{\partial z^2} + \left[ 1 - \frac{\omega_p^2(z)}{\omega_o^2} \left( 1 - \frac{\nu_{ei}(z)i}{\omega_o} \right) + \frac{4\pi i \sigma_T^{NL}}{\omega_o} (E_o, z) \right] E = 0 \tag{12}$$

The geometry is shown in Figure 4. z is measured in units of $c/\omega_o$. $z = 0$ is the reflection point and $z = z_o$ is the point of incidence.

The first set of computer runs have been performed using the following set of parameters:

$$n_o = 5 \times 10^5 \text{ cm}^{-3}$$

$$\theta_{e_i} = 0.2\text{eV} = 2319^o\text{K (daytime)}$$

$$\alpha \equiv (m_e/m_i)^{1/3} = .00583 \text{ (oxygen)}$$

$$\omega_o/2\pi = \text{modifier (pump) frequency} = 6.35 \text{ Mhz} \tag{13}$$

Derived quantities based on the above parameters are:

$$\omega_{pe_o} = 4 \times 10^7 \text{ radians/sec}$$

$$\nu_{ei_o} = 2\gamma_{co} = 350 \text{ Hz}$$

$$\Lambda^2_{th} \quad \frac{E^2_{o_{th}}}{4\pi n_o \theta_e} = 16 \frac{\gamma_{co}}{\omega_p} = 7 \times 10^{-5}$$

$$I_{th} = \frac{c}{8\pi} E^2_{o_{th}} = 168 \text{ } \mu\text{W/m}^2 \text{ (locally)} \tag{14}$$

The peak plasma frequency $\omega_{pe_o}$ is equal to the pump frequency, $\omega_o$. $\nu_{ei_o}$ is the electron-ion collision frequency at the reflection altitude. The threshold for the parametric instability is indicated as $I_{th}$, and should be understood as the value which $\frac{cE^2_o}{8\pi}$ (including swelling due to inhomogeneity) must exceed locally to excite the parametric decay instability. We consider two scale heights: $H = 37.5$ km ($z_o \equiv \frac{\omega_o}{c} H = 5000$) and $H = 75$ km ($z_o \equiv \frac{\omega_o H}{c} = 10^4$).

The integrated total absorption is numerically measured by the quantity $1 - R$, where $R = |E_{ref}/E_{inc}|^2$ is the power reflection coefficient at the "source point" $z = z_o$. We also compute for each case the integrated purely linear reflectivity $R_{lin}$, obtained by integrating the wave equation using only the linear dissipative conductivity. These results compare favorably (within 50%) with the value of $R_{lin}$ calculated from geometric optics.

18

$$R_{lin} = e^{-\frac{8}{3}\frac{\nu_{ei}}{\omega_o} z_o}$$

The quantity $R_{lin} - R = (1 - R) - (1 - R_{lin})$ is a measure of the anomalous absorption (excess beyond linear).

In Figure 5 both $1 - R$ (left axis) and $R_{lin}-R$ (right axis) are shown for an incident vacuum intensity of 50 $\mu W/m^2$, which is about the maximum presently available at the Platteville transmitter[1] in Colorado. (Approximately one half this value is attainable at Arecibo, Puerto Rico. The absorption is plotted as a function of the multiplicative scaling parameter, $\eta$, defined in equation (7) and Table 1. As explained in Table 1, the results of the best available theories indicate $\eta$-values between ½ and 3/4.

For a scale height of 37.5 km, the linear absorption $1 - R = 9\%$ for the above parameters of (13) and (14). The excess nonlinear (anomalous) absorption $R_{lin}-R$ is between 9% and 23% depending on $\eta$. The behavior of $R_{lin}-R$ with $\eta$ is roughly linear.

For a scale height of 75 km, the linear absorption is $1 - R_{lin} = 17\%$ for the same parameters. The excess nonlinear absorption $R_{lin} - R$ is between 14% and 33%, depending on $\eta$. Longer density scale lengths are therefore seen to lead to stronger absorption. The physical reason is that the absorption region is "stretched," although from the above results it appears that this is a stronger effect for the linear absorption than the nonlinear contribution (presumably because the nonlinear absorption region is thinner spatially).

The above results are for relatively high daytime electron temperatures. Strictly speaking, the effects of photoelectrons on the plasma wave damping should be included for daytime parameters. We have crudely estimated the effects of photoelectrons in a separate data run by adjusting the Landau

19

damping to be three times larger than the collisional damping of the Langmuir

waves at a matched wave number of $k_m \approx 0.1k_D$. (Ordinarily the Landau

damping is much smaller than the collision damping.) The factor 3 was

chosen as an average. At this density and temperature downward propagating

plasma waves have a photoelectron damping rate equal to the collisional

damping rate and upward propagating plasma waves have photoelectron damping

five times collisional damping. (The photoelectrons originate mainly at

lower altitudes.) Also, there should not be many photoelectrons at energies

beyond $\frac{m}{2}(\frac{\omega_p}{k})^2 \approx 20eV$. This has the effect of raising the threshold for

parametric instability by a factor of ~4 at altitudes in the vicinity of

$z/z_o = .03$ and by more below. It does not alter the nonlinear conductivity

at higher altitudes because the phase velocities at the correspondingly

smaller matched wave numbers are too high to allow wave resonance with

photoelectrons. The net effect is to condense the spatial region of nonlinear

absorption. For all parameters the same as in Figure 5, but photoelectrons

included in the above manner, and a scale height of 75 km, we find for $\eta =$

$2/3$, $R_{lin} - R = 11\%$ anomalous absorption compared to $14\%$ anomalous absorption

without photoelectrons; and for $\eta = 2$, $R_{lin} - R = 27\%$ anomalous absorption,

compared to $33\%$ anomalous absorption, without photoelectrons. Photoelectrons

thus appear to reduce the percent of anomalous absorption by a factor of

about $20\%$. When photoelectron damping of Langmuir waves is a strong effect,

or, indeed even if the normal Landau damping region is to be treated

properly, the absorptive conductivity arising from orbit perturbation

saturation[8,A] must be used rather than the conductivity associated with

weak turbulence saturation, which we have been using here. We are presently

putting into effect a program for doing this.

We have also made some runs at lower electron temperature (.13eV =

$1500^{\circ}K$). Since the linear absorptive conductivity goes as $\nu_{ei}$ and hence as $\theta_e^{-3/2}$, the linear absorption should and did increase. The nonlinear absorption also increased, although not as strongly as the linear absorption. Making some numerical comparisons for the H = 75 km shown in Figure 5, but with all other parameters except temperature the same, we find the linear absorption $1 - R_{lin}$ increased from 17% to 26% as $\theta_e$ is decreased from $2320^{\circ}K$ to $1500^{\circ}K$, whereas the anomalous absorption $R_{lin} - R$ increased from 14% (.2eV) to 19% (.13eV) for $\eta = 2/3$ and from 33% (.2eV) to 39% (.13eV) for $\eta = 2$. Nighttime anomalous absorption would thus appear to be stronger than daytime anomalous absorption, although orbit perturbation effects must be included to really determine whether this is true. Daytime neutral collisional absorption of the modifier (pump) at lower altitudes (D-region) would make daytime anomalous absorption still weaker.

In Figure 6 we have plotted the absorption $1 - R$ as a function of incident intensity for the scale height H = 75 km using the same $\eta$-values and other, fixed parameters as in Figure 5. The absorption goes up somewhat more slowly than linear.

In Figure 7 we plot the pump radiation electric field amplitude squared versus altitude. The pump amplitude is normalized to the incident amplitude and the altitude is in units of $c/\omega_0$. For the parameters of (13) and (14) this distance is 7.5 meters. The spatial wave patterns are plotted for an incident vacuum intensity of 50 $\mu W/m^2$, a scale height of 75 km ($z_0 = 10^4$), and a nonlinear scaling parameter $\eta = 2$. The density is $5 \times 10^5$ $cm^{-3}$ and the temperature is 0.2eV. Results are shown both for a purely linear absorptive conductivity and for the linear plus nonlinear absorptive conductivity. The peak of the Airy function swelling pattern is indicated by X for comparison. The effect of pump depletion is evident. The peak swelling factor at the first maximum is reduced from 82 with no absorption to 71

21

with linear absorption, to 56 with linear plus nonlinear absorption. The
amplitudes at all the maxima are reduced by somewhat smaller percentages.
For the case shown we are not very far above threshold even at the first
maxima of the field pattern. Based on the actual swelling at the first
maximum of the curve which includes linear plus nonlinear absorption we
find $P = 17$. If we had used the Airy function swelling factor this number
would have come out to be $P \sim 24$.

In Figure 8 we have plotted the negative of the total Poynting flux
in units of the incident flux for the same parameters as in Figure 7. In
the absence of any absorption this net flux must vanish. The lower curve
in Figure 8 includes only linear absorption. The upper curve includes both
linear and nonlinear absorption. The steeper regions of the oscillating
flux are the regions where the absorption is strongest, and correspond to the
maxima of $E_o(z)$. The curve including both linear and nonlinear absorption
shows stronger oscillations than the curve including only linear absorption
because $\partial J / \partial z \propto \sigma^{NL} E_o^2 \propto E_o^4$. Also, the curve including both linear and non-
linear absorption rises to a higher value at $z = z_o$ than the curve with
linear absorption alone because the smaller the reflected wave at that point,
the higher the net Poynting flux.

b) <u>UHF scattering near the plasma frequency.</u> The peak intensity of the
HF modifier probe at Arecibo is $25~\mu W/m^2$. The plasma waves probed by the
430 Mhz incident wave in backscattering experiments are propagating close
to the vertical and have wavenumber $k = 4\pi \times 430~\text{Mhz}/c = 0.18~\text{cm}^{-1}$. The
pump electric field is assumed to lie along the geomagnetic field direction,
so that the vertical is some $42^o$ from the pump direction and $x^2 \equiv \cos^2 42^o =$
0.55. $k_D$ depends on the reflection density (i.e., on $f_o$) and temperature.
It ranges from $k_D = 3.4~\text{cm}^{-1}$ for $f_o = 6~\text{Mhz}$, $\theta_e = 2400^o K$ to

22

$k_D = 2$ cm$^{-1}$ for $f_0 = 8.2$ Mhz, $\theta_e = 1500^\circ$K. The second value is for the set of parameters cited by Kantor [3]. Thus, $k/k_D$ ranges from .05 to .09 depending on time of day or night. The frequency-matched plasma waves are therefore in the collision-damping rather than the Landau-damping regime, so the saturation theory appropriate to cross-section calculations above threshold is the one based on induced-scattering of Langmuir waves off ions rather than perturbed-orbit theory. At these wavenumbers, photoelectrons cannot play a very important role in the Landau damping of even the upward propagating Langmuir waves, because the associated phase velocity would correspond to photoelectron energies of at least 25eV, where the photo-electron flux rapidly decreases. From equation (11) we see that the altitude from which the scattering return is expected is given by $\Delta z/H = 7.5 \times 10^{-3}$ to $2.4 \times 10^{-2}$, or from about 0.5 to 2 kilometers below the reflection height. The true swelling factor to these altitudes , for a modifier with $\lesssim 5$ $\mu$W/m$^2$ incident intensity, based on the solutions described in the previous section, is $\sim$ 40-60 provided the altitude happens to correspond to a maximum in the midifier field. In general, this is unlikely. Kantor[3] has verified the standing wave pattern by allowing the density profile to sink without track-ing the modifier frequency to it. For plasma waves propagating in the pump direction at this altitude, the pump peaks would be between 2 and 8 times threshold (P = 2 to 8). This value is sensitive to $f_0$, since the threshold power goes as $n_0^{3/2}$. P = 2 corresponds to an 8 Mhz pump; P = 8 corresponds to a 6 Mhz pump. These values are based on an (optimistic) 75 km scale height. Even the most detailed theory[18] predicts a less than 20$^\circ$ angular spread of plasma waves about the pump direction for P = 2, and effects of inhomogeneity suggested by Perkins[22] would probably also be insufficient to spread the saturated spectrum to 42$^\circ$ with any appreciable intensity.

23

Since $x^2 = 0.55$, the Langmuir waves probed by the scatter experiment are probably below the threshold for parametric instability for this case. On the other hand for lower HF frequencies if one happens to catch a pump field maximum it is possible that the saturated spectrum has spread[18] as far as $42°$, in which case a far larger cross-section would be observed. This may account for some of the variability of the scattering results.

The detailed comparisons by Perkins[23], Harker[23], and Meltz and Tomljanovich[23] of Arecibo scattering measurements[2,3] with the anisotropic and isotropic nonlinear saturation theories of the scattering cross-section led to the conclusion that the measured waves were usually stable. The magnitude of the Arecibo scattering measurements at $42°$ to the pump can then be understood by using the anisotropic angular spectrum of DuBois and Goldman[6] and Valeo, et al.[9], at low P values. At this angle the only nonlinearity entering the cross-section is the pump-enhanced ion-acoustic Cerenkov emission term first predicted in 1967 by DuBois and Goldman[4b]. This arises from the beating of the modifier with the ion-acoustic frequency Cerenkov emission to produce emission at the Langmuir wave frequency. This emission is larger by a factor $P\omega_L/\omega_{ia}$ than the direct Langmuir bremsstrahlung emission. The scattering model for low P at $\theta = 42°$ is called critical fluctuation theory. It predicts that the cross-section increases linearly with P at the Langmuir frequency. For large P, or for $\theta$ close to 0 for smaller P, the cross-section should increase as $P^2$ times a large coefficient. A dramatic increase (by as much as three orders of magnitude for an increase of P by 5) in the cross-section should be characteristic of this regime.

The considerable detail of the Arecibo backscatter spectrum presents many spectral features besides the plasma peak to be explained by theory. The critical fluctuation theory predicts a ratio of peak intensity of the

24

enhanced Stokes Langmuir line (downshifted from the pump frequency by the ion-acoustic frequency) to the ion-acoustic line, which is in agreement with experiment.[7,3] Likewise, the ratio of the anti-Stokes line (Langmuir line upshifted from the pump frequency by the ion-acoustic line) to the Stokes line is in agreement with experiment.[3] A spectral peak shifted by exactly the pump frequency has been identified as the high frequency component of the purely-growing instability, which is a different branch of the dispersion relation. In Appendix B, the critical fluctuation intensity is computed for the purely growing instability. Assuming values of P which appear to explain the features of the parametric decay instability, we compute the ratio of the purely-growing line to the decay line (Stokes line). This ratio of cross-sections turns out to be larger by a factor of 2 or 3 than the ratios observed at Arecibo. This factor could arise from the assumption of equal electron and ion temperatures. In addition to indicating that the decay line peak and the growing line peak should be of comparable order of magnitude, as observed, the theory predicts a variability in the ratio with heater frequency and scale height, since the observed purely growing mode is excited at a lower altitude than that of the decay instability. One feature which has still not been explained consistently with the critical-fluctuation theory is the structure of the so-called broad bump in the incoherent scatter data near the stokes frequency. The shape is qualitatively similar to that predicted in detailed spectral shape calculations[17,18]; however, these theories require that the pump te well above threshold. The scattering models constructed by the Boulder group predict, in addition to the below and above threshold behavior indicated above, a third dramatically different regime, which has not yet been probed experimentally. As explained above,

25

the values of $k_m/k_D$ probed by the 430 Mhz scatter are .05 to .09. A factor
of 3 or 4 increase in the incident scattering wave frequency would bring
the frequency-matched wave number into the Landau-damping regime. Thus, the
use of an L-band (1.3 GHz) probe should give cross-sections characteristic of orbit
perturbation saturation. The detailed predictions here are given in Appendix
A, although we note from Figure 1 that the spectrum will be broad in angle
even for P of order 2, so large scattering cross-sections may be expected.

c) Acceleration of electrons and airglow.

The large enhancements of 6300 $\overset{o}{A}$ airglow over Boulder and Arecibo suggest
that the electron velocity distribution function is significantly altered
during ionospheric modification. The alteration of the velocity distribution
can have important consequences: for example, the formation of energetic
tails may cause plasma wave instability or change the saturation results of
orbit perturbation theory. In Appendix D, a theory for quantitatively
predicting the change in the electron velocity distribution has been developed.
Such changes are primarily due to acceleration of electrons by short wave-
length ($\sim$ 15 cm) Langmuir waves propagating at Landau-damped altitudes. The
electrons mainly affected are those whose velocities are close to the wave
phase velocity. The altitudes from which the accelerated electrons originate
are illustrated in Figure 3. The airglow measurements provide a direct
measurement of the enhanced photon flux from atomic excitations. The photon
flux is, in turn, a measure of the enhanced flux of electrons responsible
for the excitation. In Appendix D it is found that $5 \times 10^4$ electrons per
c.c. are produced per second in the proper velocity range to excite 6300 $\overset{o}{A}$
airglow, when $P \approx 3$, and $k_m/k_D \approx 0.2$. The total wave energy for these parameters
is $10^{-3} n\theta$, according to perturbed-orbit theory. From this a flux of $10^9$
electrons per $cm^2$ per sec. results. This flux appears sufficient to explain

26

the observed 50 Rayleigh enhancements of the 6300 Å airglow over Boulder. The acceleration mechanism is made possible by the resonance broadening predicted by orbit-perturbation theory, which accelerates electrons which are as much as a thermal velocity away from the wave phase matched velocity (at 5 thermal velocities).

## IV. Effects of the geomagnetic field: stimulated diffusion scattering

### a) The diffusion mode

In addition to supporting wave-like responses to density perturbations, a homogeneous plasma can respond with a diffusion-relaxation of the perturbation. As an example, electron-ion collisions can cause a random walk of particles across the magnetic field. This leads to a diffusion mode with wave vector very close to orthogonal to the magnetic field. The situation is illustrated in Figure 10. Diffusion along the magnetic field lines occurs much more rapidly than diffusion across the field, provided the electron cyclotron frequency is much larger than the electron-ion collision frequency, a condition which is satisfied in the ionosphere. The cross-field diffusion coefficient in the simplest approximation is

$$D_\perp = \nu_{ei} R_e^2 (1 + \theta_i/\theta_e),  \tag{14}$$

where $\nu_{ei}$ is the electron-ion collision frequency and $R_e$ is the electron gyro-radius. The linear fluctuation-dissipation theorem predicts an equilibrium electron density fluctuation spectrum associated with this diffusion mode, having $\underline{k} \perp \underline{B}$, and a bell-shaped frequency structure around zero with half-width given by

$$\Delta\omega \approx D_\perp k^2.  \tag{15}$$

The integrated spectrum in equilibrium is independent of $\nu_{ei}$ or B and is of the same order of magnitude as the integrated low frequency spectrum in the absence of B. The high frequency scattering cross-section is directly proportional to the electron density fluctuation spectrum. Baron and Petriceks[24] may have observed this structure in L-band scattering experiments orthogonal to the geomagnetic field.

28

For the F-layer, with $\nu_{ei}$ assumed to be 400 Hz and $R_e = 2$ cm, $D_\perp$ is of the order 3000 $cm^2$/sec. VHF, UHF, and L-band back-scattering experiments probe wave numbers given by $k = 4\pi f_i/c$, where $f_i$ is the incident frequency. The theory, therefore, predicts central line returns with very narrow frequency widths for back-scattering orthogonal to magnetic field lines. The width is given by

$$\Delta\omega \approx 5 \times 10^{-4} f_i^2 ,$$

(16)

$f_i$ in MHz

Thus, for example, $\Delta\omega \approx 13$ Hz for a probe at 157 MHz and $\Delta\omega \approx 1$ kHz at L-band. The above results do not take into account the modifier or its possible effects on the intensity of the diffusion mode. In Appendix E we derive further details of the diffusion mode, using more refined approximations. The mode is found to propagate only within $10^{-6}$ radians of strict orthogonality to the geomagnetic field.

b) Stimulated diffusion scattering

A new electromagnetic parametric instability has been found in which an O-wave modifier acts as a pump to drive unstable the diffusion mode described in the previous note, together with a scattered O-wave. Figure 11 shows the simple geometry for which the calculation has been performed. The incident and scattered wave vectors are orthogonal to $\underline{B}$ and the wave vector of the diffusion mode is also orthogonal. The lowest threshold is found to occur for back-scattering, in which case, $k_{diffusion} \approx 2k_{pump}$. The threshold we have obtained is less than a factor of two higher than the threshold for the parametric decay instability. A pump with local vacuum intensity of $50\mu W/m^2$ incident upon the F-layer with a 75 km scale length

29

should be an order of magnitude above the threshold for this instability. The parametric coupling converts the diffusion mode into a very low frequency propagating mode of real frequency $\omega = k^2_{diff} D_1 /\sqrt{2}$. The backscattered O-wave differs from the pump by this frequency. The pump wave number, $k_{pump}$, near the reflection point is much smaller than the free-space wave number, and is given by

$$k_{pump} = .066 \, \omega_o/c,$$

for a 100 km scale length. For a 6 MHz modifier, the diffusion mode frequency is on the order of $10^{-3}$ Hz and the parametric growth rate is on the order of minutes, which appears long in comparison with common spread-f onset times. We have also calculated the growth rate of stimulated Brillouin scattering, and find it to be on the order of 200 Hz, which gives a growth time of several milliseconds, and appears short compared to spread-f times. The details of stimulated diffusion scattering can be found in Appendix F. A preliminary saturation theory for this instability is given in Appendix G, where density fluctuations on the order of $10^{-2}$ times the ambient density are found.

## Table 1

Values of the scaling parameter $\eta$ appearing in the total plasma wave energy $E$ or, equivalently, the absorptive nonlinear conductivity $\sigma_T^{NL}$.

| $\eta$ | Theory |
|---|---|
| $\frac{1}{6}$ | Resonant approx. for $f(k)$, cutoff at $k_c$. Analytic saturated theory of Ref. 6. |
| $\frac{3}{8}$ | Resonant approx. for $f(k)$ no cutoff at $k_c$. Analytic saturated theory of Ref. 9. |
| $\frac{1}{2}$ | Resonant approx. for $f(k)$, cutoff at $k_c$. Time-dependent numerical integration (B. Godfrey, D.F. DuBois, M.V. Goldman[16]) |
| $\frac{3}{4}$ | Exact $f(k)$. No cutoff at $k_c$. Time-dependent 1-D numerical integration. W. Kruer, E. Valeo[17]. |
| ? | Exact $f(k)$. No cutoff at $k_c$. Time-dependent 2-D numerical integration. J. Fejer, Y.Y. Kuo[19]. |
| 2 | Value used by F. Perkins and by G. Meltz and N. Tomljamovich in recent geometric optics approximations[19] to the nonlinear absorption problem. |

## Figure Captions

Figure 1: The angular spectrum (equation (8)) from orbit-perturbation theory as a function of the angle between the pump field and $\underline{k}$.

Figure 2: Total wave energy $\bar{E}/n\theta_e$ from orbit-perturbation theory versus the pump ratio P for $k_m/k_D \approx 0.2$, or $r = 1$. (see equation 9)

Figure 3: Linear Langmuir wave damping mechanisms as a function of altitude below the reflection height. The electrons producing airglow are accelerated from the Landau-damping region where orbit-perturbation saturation applies.

Figure 4: Geometry for normal incidence of electromagnetic wave on a plane-layered inhomogeneous plasma. The spatial coordinate z is in the dimensionless units of $c/\omega_0$, the free-space wavelength over $2\pi$.

Figure 5: Integrated absorption $1 - R$, $R = |E_{refl}/E_{inc}|^2$, for incident intensity $I_{inc} = cE_{inc}^2/8\pi = 50\mu W/m^2$ ($\pm 2\%$) and various values of the nonlinear scaling parameter $\eta$ defined in equation (6) and Table 1. Both linear and nonlinear absorption are included and the following parameters are used: $n = 5 \times 10^5$ cm$^{-3}$, $\theta_e = 0.2$eV ($2319^\circ$K), $f_{modifier} = 6.35$ Mhz, $\nu_{ei} = 350$ Hz. The ions are assumed to be oxygen. Scale heights of 37.5 km ($z_0 = 5000$) and 75 km ($z_0 = 10^4$) are used. The right side scale on each plot is $R - R_{linear}$, which is a measure of the relative percent of nonlinear absorption.

Figure 6: Integrated linear and nonlinear absorption, $1 - R$, $R = |E_{refl}|^2/|E_{inc}|^2$ as a function of incident intensity, $I_{inc} = cE_{inc}^2/8\pi$. The nonlinear scaling parameter $\eta$ is defined in equation (6) and Table 1. The scale height is $H = 75$ km and the integrated linear absorption is shown as well.

32

Figure 7: Pump radiation electric field amplitude squared (in units of incident amplitude squared) versus altitude (in units of $c/\omega = 7.5$ meters). Lower altitudes are towards the right and the lowest altitude shown is ~1 km below the reflection height. Linear and linear plus nonlinear cases are plotted for an incident vacuum intensity of $50\mu W/m^2$, a scale height of H = 75 km ($z_0 = 10^4$), and a nonlinear scaling parameter $\eta = 2$ (see equation (6) and Table 1). The density is $5 \times 10^5 cm^{-3}$ and the temperature is 0.2eV. The peak of the Airy function swelling factor is shown by X for comparison. The integrated linear absorption is $1 - R = 17\%$, whereas the integrated linear and nonlinear absorption is an additional 33%.

Figure 8: Negative of Poynting flux in units of incident flux for parameters of Figure 6.

Figure 9: The component of the diffusion tensor along the geomagnetic field versus velocity along the geomagnetic field. $\omega_e$ is the plasma frequency at the reflection point and $v_e$ is the electron thermal velocity. $D(v)$ is a maximum at v near 5 thermal velocities where the value of $D(\underline{v})$ is about $10^{20}$ $cm^2$ $sec^{-3}$.

Figure 10: Relaxation of a density perturbation in a homogeneous plasma by diffusion across the magnetic field.

Figure 11: Simple geometry used for stimulated diffusion back-scattering. The diffusion mode has twice the wave number of the incident pump.

33

FIGURE 1

34

$$\frac{\langle |\delta E|^2 \rangle}{4\pi NKT_e} \quad (10^{-2})$$

FIGURE 2

35
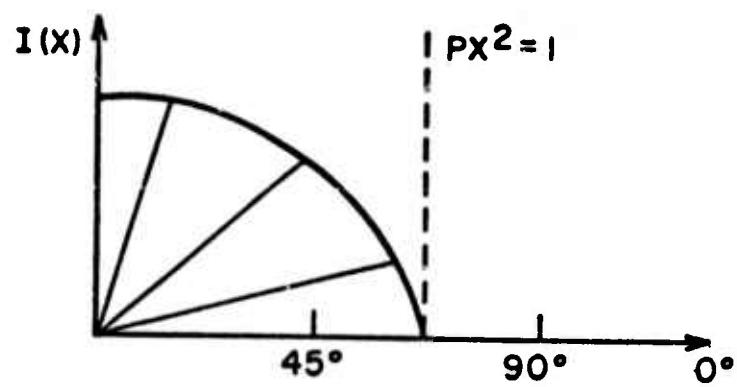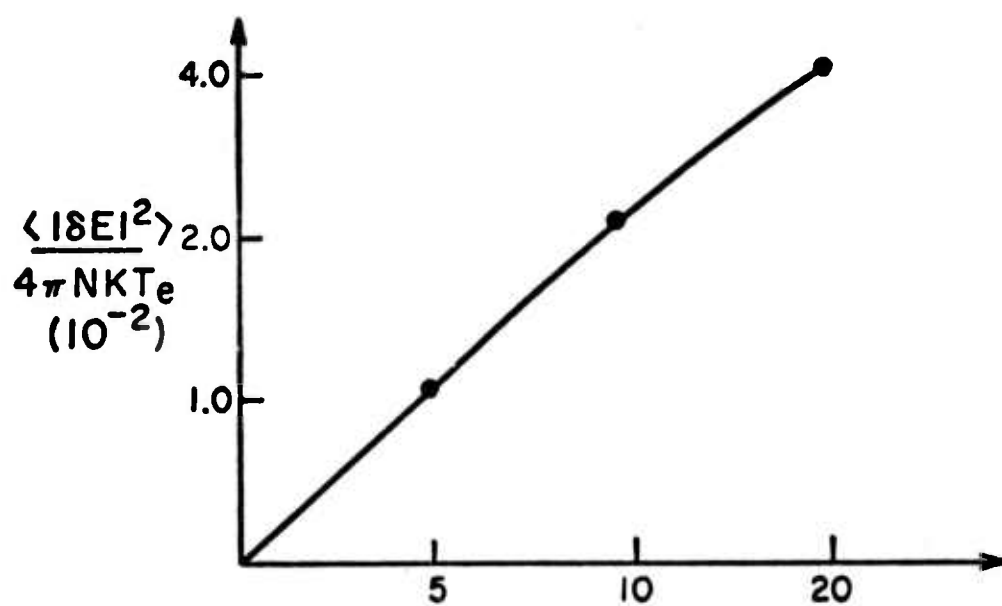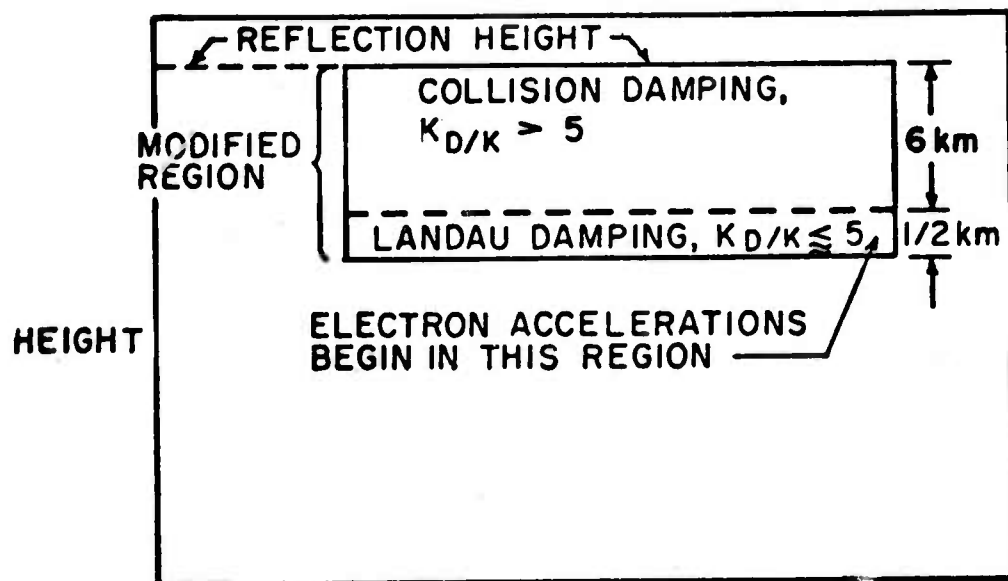
FIGURE 3

**FIGURE 4**

FIGURE 5
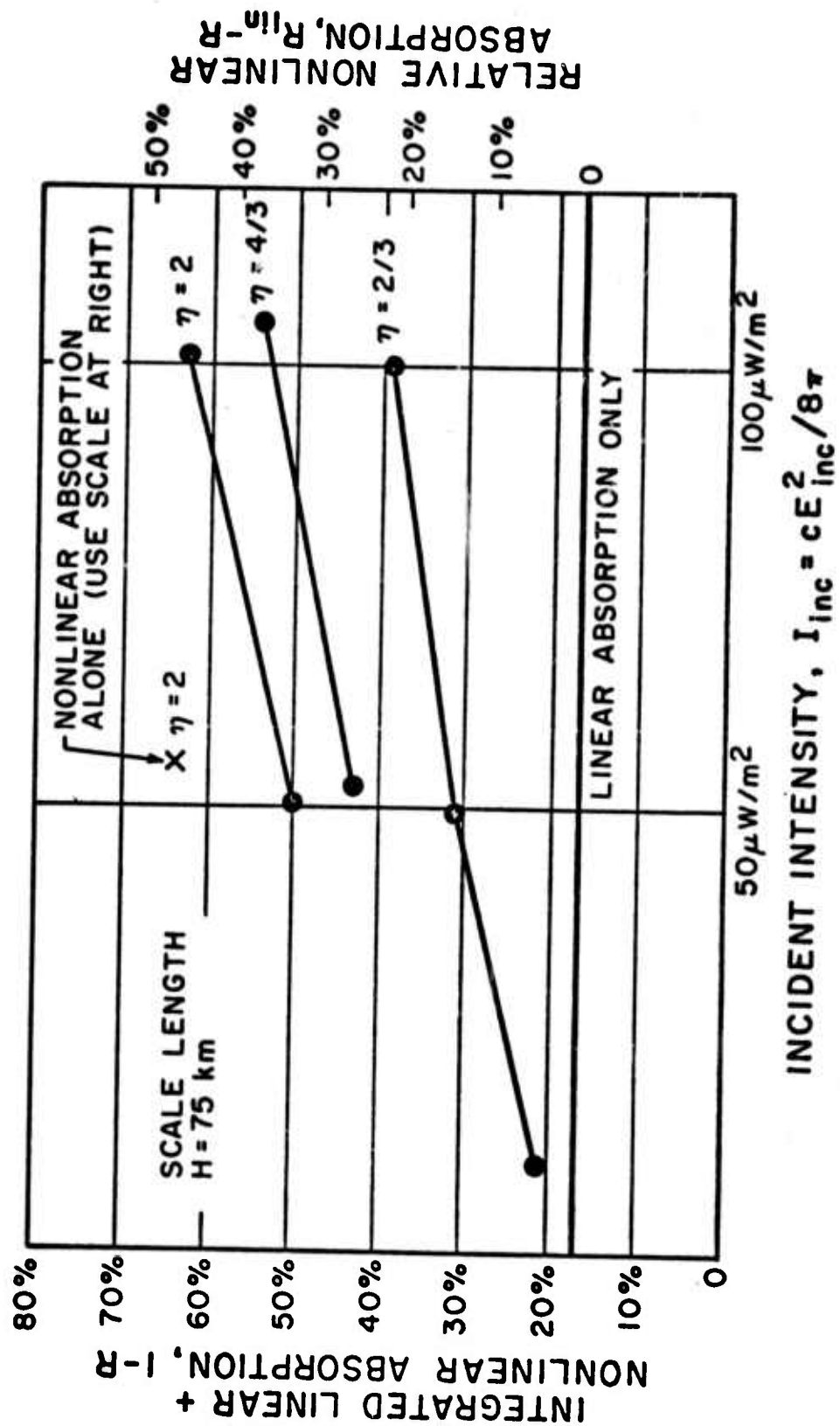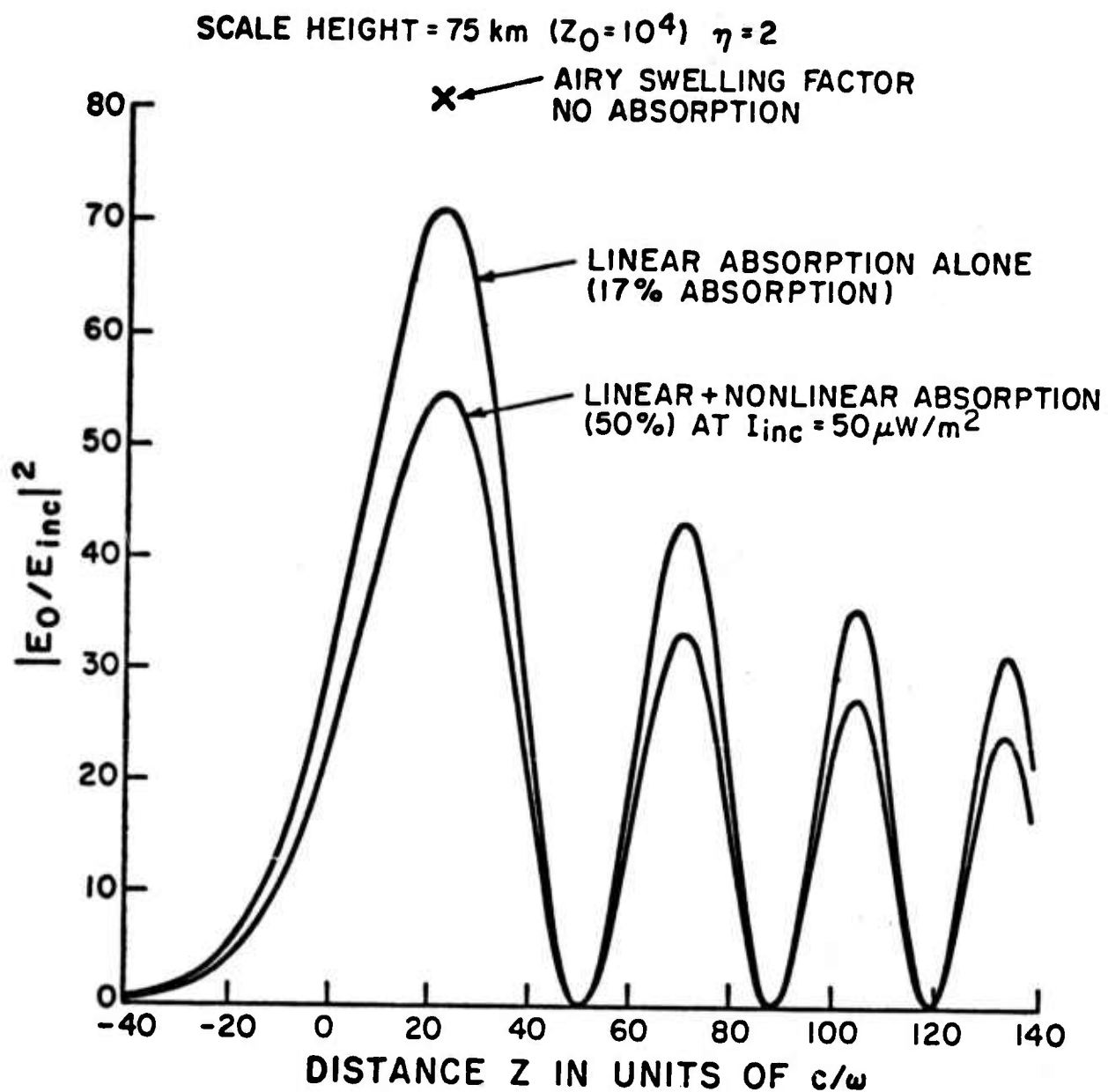
38

FIGURE 6

SCALE HEIGHT = 75 km $(Z_0 = 10^4)$ $\eta = 2$

× ← AIRY SWELLING FACTOR
NO ABSORPTION

LINEAR ABSORPTION ALONE
(17% ABSORPTION)

LINEAR + NONLINEAR ABSORPTION
(50%) AT $I_{inc} = 50 \mu W/m^2$

FIGURE 7

40

SCALE HEIGHT = 75 km ($Z_0 = 10^4$) $\eta = 2$

LINEAR + NONLINEAR
ABSORPTION (50%)
AT $I_{inc} = 50\,\mu W/m^2$

LINEAR ABSORPTION
ALONE (17%)

NEGATIVE POYNTING FLUX, $-J/J_{inc}$

DISTANCE Z IN UNITS OF $c/\omega$

FIGURE 8

41

FIGURE 9

42

$$\frac{\partial n_{1e}}{\partial t} - D \frac{\partial^2 n_{1e}}{\partial y^2} = 0, \quad n_e \approx n_i$$

$$D = \nu_{ei} R_e^2 \left(1 + \frac{\Theta_e}{\Theta_i}\right)$$



$n_{1e}(t_0)$

$n_{1e}(t_1)$

$n_{1e}(t_2)$

FIGURE 10

43

FIGURE 11

44
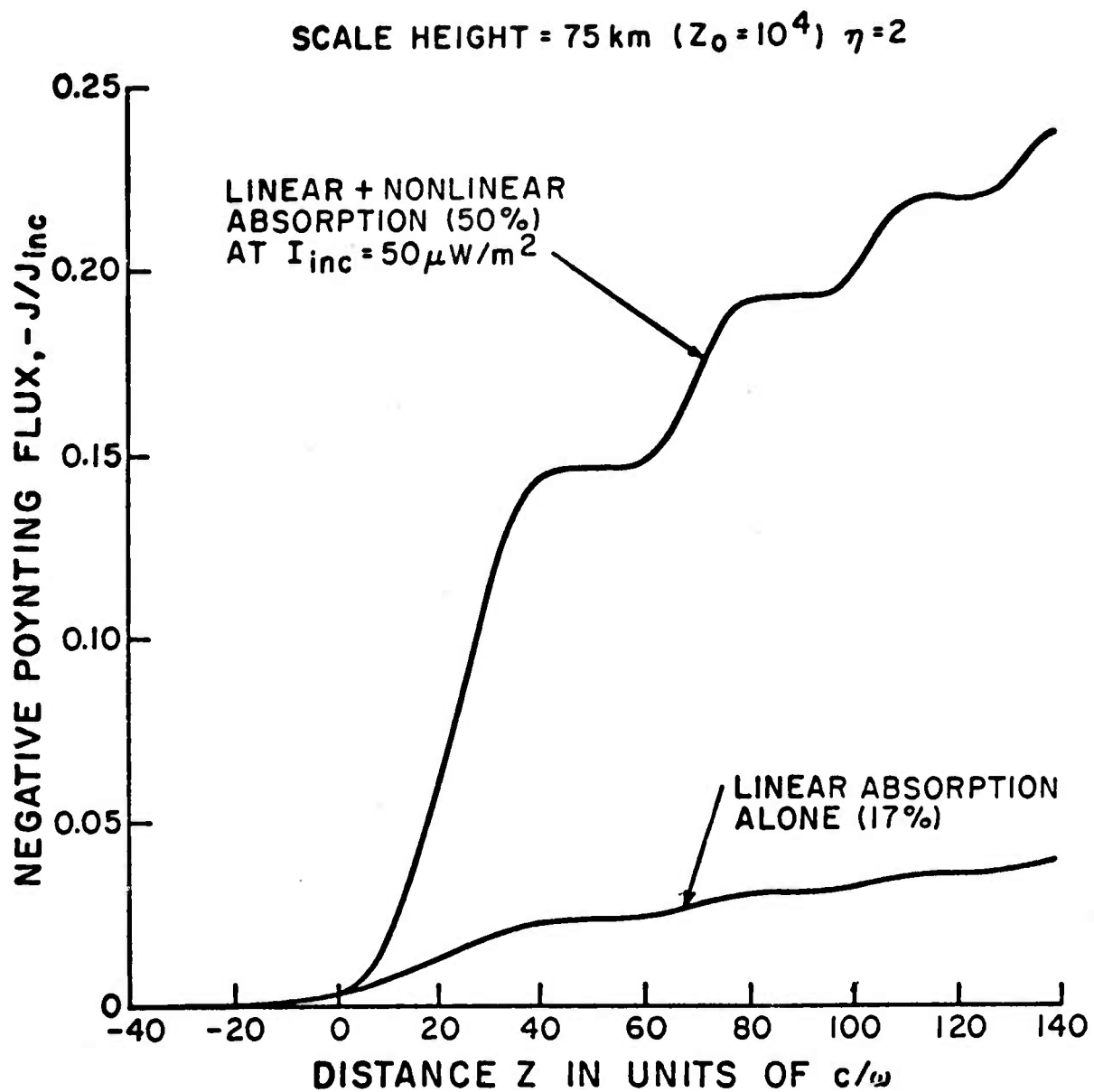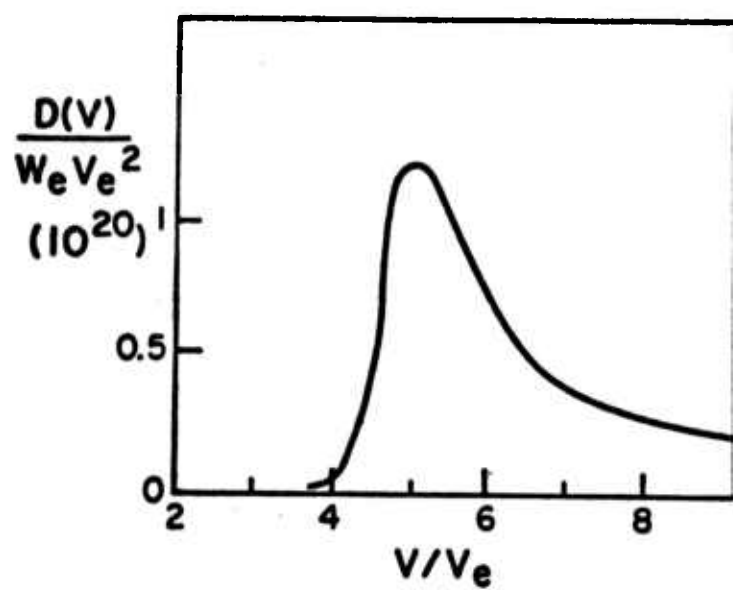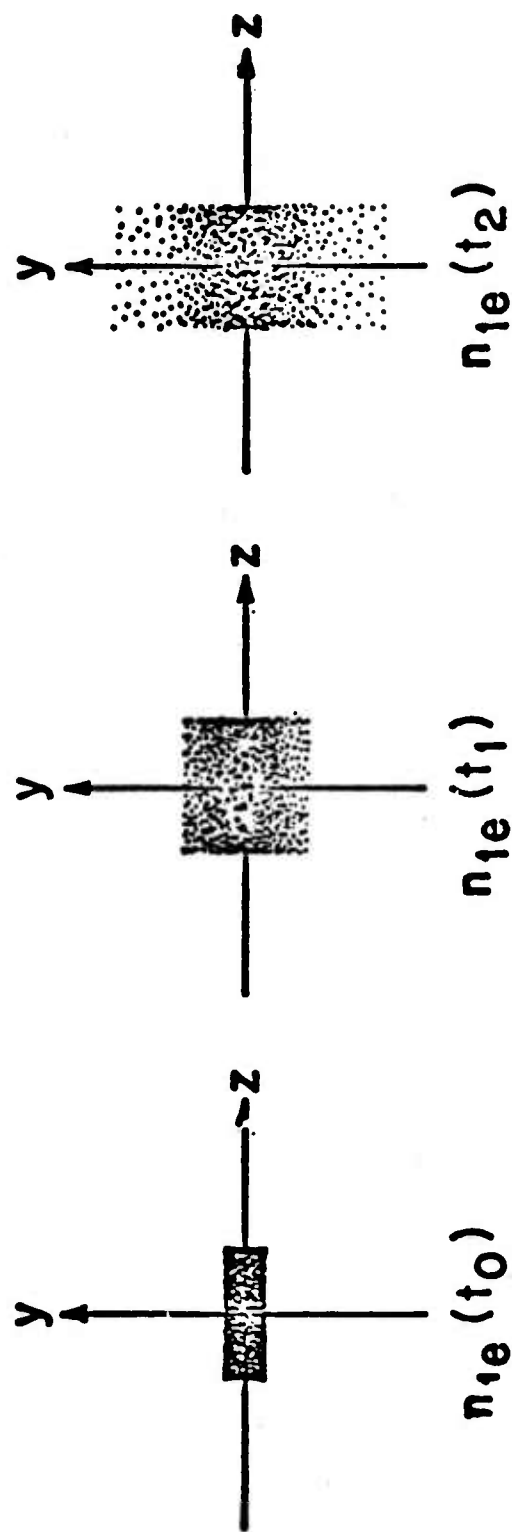
## References

A. Appendix A: Nonlinear Saturation of Parametric Instabilities: Spectrum of Turbulence and Enhanced Collision Frequency

B. Appendix B: Critical Fluctuation Level for the Purely Growing Parametric Instability

C. Appendix C: Nonlinear Wave Optics of Parametric Pump Radiation in an Inhomogeneous Plasma

D. Appendix D: Electron Acceleration

E. Appendix E: Linear Theory of Diffusion Modes

F. Appendix F: Stimulated Diffusion Scattering

G. Appendix G: Nonlinear Saturation of Parametrically Excited Field Aligned Irregularities


1. R. Cohen and J. D. Whitehead, Journal of Geophysical Research 75, 6439 (1970).

2. H. E. Carlson, W. E. Gordon, R. L. Shower, "High Frequency Induced Enhancements of the Incoherent Scatter Spectrum at Arecibo." J. Geophys. Research 77, 1242-1250 (1972).

3. I. J. Kantor, "Plasma Waves Induced by HF Radio Waves," Ph.D. Thesis submitted 7/72 to Rice University.

4. D. F. DuBois and M. V. Goldman, Phys. Rev. Lett. 14, 544 (1965); and Phys. Rev. 164, 207 (1967).

5. F. W. Perkins and P. K. Kaw, J. Geophys. Research 76, 282 (1971).

6. D. F. DuBois and M. V. Goldman, Phys. Rev. Lett. 28, 218 (1972).

7. D. F. DuBois and M. V. Goldman, Physics of Fluids 15, 919 (1972).

8. B. Bezzerides and J. Weinstock, Phys. Rev. Lett. 28, 481 (1972); also see Appendix A.

9. E. Valeo, F. Perkins and C. Oberman, Phys. Rev. Lett. 28, 340 (1972).

10. N. M. Tomljanovich, "Self-Focusing of Electromagnetic Waves in Plasmas," Summary of ARPA Theoretical Meeting of 17 November 1972, p. 94.

11. K. Nishikawa, Journ. Phys. Soc. Japan 24, 916, 1152 (1968).

12. M. A. Biondi, D. P. Sipler, R. D. Hake, Jr. J. Geophys. Research 75, 6421-24 (1970).

13. M. V. Goldman, _Ann. Phys._ (New York) $\underline{38}$, 95 (1966).

14. Ivory Coral Meeting, Albuquerque, New Mexico, August, 1971.

15. Boulder Ivory Coral Theoretical Meeting, November, 1971.

16. M. V. Goldman and D. F. DuBois, "Nonlinear Laser Heating of a Plasma," Technical Report #AFWL-TR-72-101, Kirtland Air Force Base, Albuquerque, New Mexico, September, 1972. Also reported on at the Anomalous Absorptive Conference, Boulder, Colorado, March, 1972.

17. W. L. Kruer and E. J. Valeo, "Nonlinear Evolution of the Decay Instability in a Plasma with Comparable Electron and Ion Temperatures," PPL MATT-919, August 1972 (to be published in _Phys. Fluids_).

18. Y. Kuo and J. A. Fejer, _Phys. Rev. Lett._ $\underline{29}$, 1667 (1972).

19. J. A. Fejer and Y. Y. Kuo, "Structure in the Nonlinear Saturation Spectrum of Parametric Instabilities," Preprint December, 1972.

20. W. L. Kruer and J. M. Dawson, _Phys. Fluids_ $\underline{15}$, 446 (1972).

21. F. W. Perkins and J. Flick, Princeton University, Plasma Physics Laboratory Report No. MATT-833 (1971).

22. Anomalous Absorption Conference, Boulder, Colorado, March, 1972.

23. Ivory Coral Theoretical Meeting, SRI, November, 1972.

24. M. Baron and J. Petriceks, _J. Geophys. Research_ $\underline{21}$, 5325 (1967).

APPENDIX A

# NONLINEAR SATURATION OF PARAMETRIC INSTABILITIES:
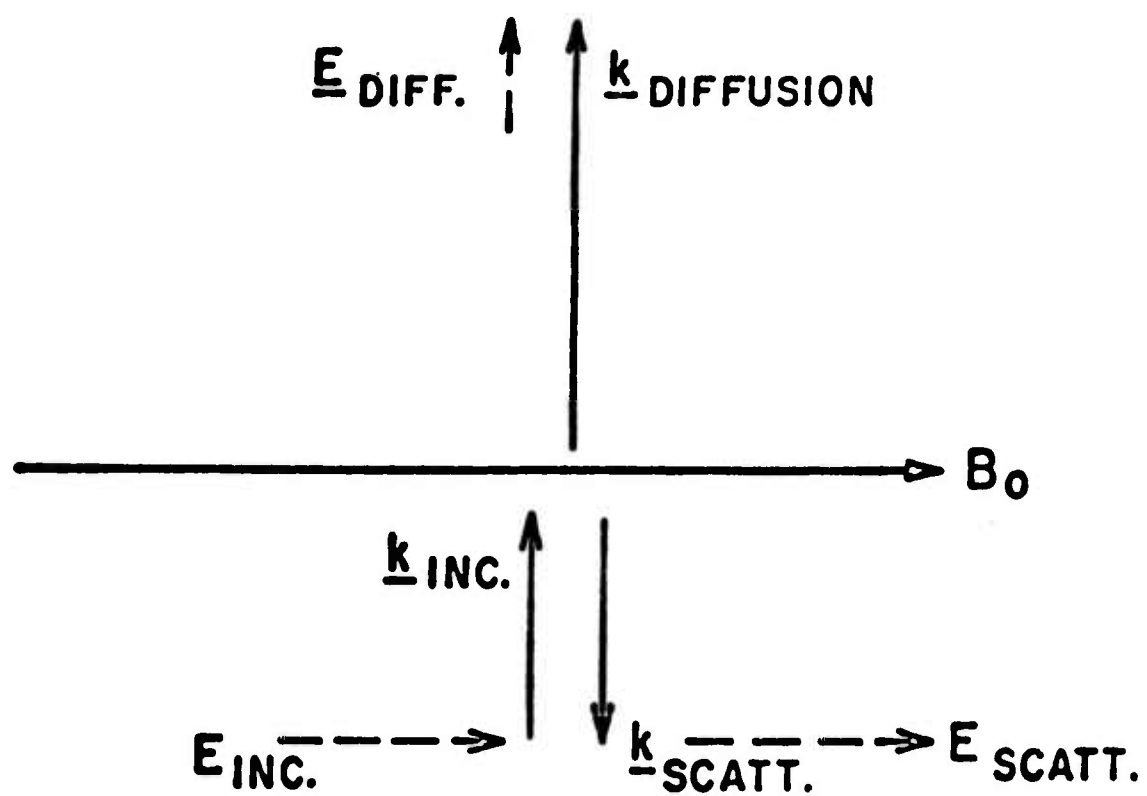# SPECTRUM OF TURBULENCE AND ENHANCED COLLISION FREQUENCY

Jerome Weinstock and Bandel Bezzerides

# ABSTRACT

We consider the nonlinear saturated state of parametric instabilities driven by an externally applied electromagnetic pump field oscillating near the plasma frequency. For short wave lengths or strong pump fields, modifications of electron and ion orbits are the dominant saturation mechanism. A calculation is made of the saturated spectrum of Langmuir waves excited by the decay instability for $T_e \approx T_i$. The spectrum is found to be broad in angle, in the absence of a magnetic field, and this has been confirmed by computer simulations. A calculation has also been made of the enhanced collision frequency and heating rate $\nu^*$. It is found that; (a) $\nu^*$ increases rapidly with pump intensity when the intensity is small, (b) $\nu^*$ increases very slowly, logorithmically, with intensity when the intensity is large, and (c) $\nu^*$ significantly depends on whether the ratio of matching wave number to Debye wave number is greater or less than 0.2. These predictions have all been confirmed by computer simulations and by a laboratory experiment. A previous calculation of the authors for the saturation of the decay and oscillating two-stream instabilities with $T_e \geq T_i$ was limited to just the total fluctuation energy at saturation.

# I. INTRODUCTION

The theory of parametric excitation of waves in a plasma is of consider-
able interest because of its role in laser heating and ionospheric modifications.
A problem of particular current interest is the nonlinear stabilization of
the excited waves once the instability threshold is exceeded. Data is now
available from a wide range of experimental situations which provide valuable
information about the final saturated state of the plasma. Computer simula-
tion studies,[1] ionospheric incoherent scatter,[2] airglow measurements,[3] and
conventional laboratory plasma experiments[4] all suggest the existence of a
saturated state of highly excited waves. Clearly, any attempt at a theoretical
understanding of this state must provide the nonlinear mechanism which finally
limits the level to which the turbulent fluctuations can grow. In particular,
the saturated state of the parametric decay instability, induced by an
incident electromagnetic wave $E_o \sin \omega_o t$, has been the object of intense
current research. Several nonlinear mechanisms have been presented to limit
wave growth. Pustovalov and Silin have considered the nonlinear damping
of acoustic waves by induced scattering from ions for the case $T_e \gg T_i$.[5]
Kruer and Dawson[1] have considered the effects of particle trapping for
strong instabilities. DuBois and Goldman,[6] and Valeo, Oberman, and Perkins[7]
have calculated the effects of scattering of the parametrically unstable
Langmuir waves by ion density fluctuations. The authors[8] have calculated
the role of the deflection and heating of electrons and ions by <u>unstable
waves</u>, both Langmuir and acoustic. Saturation is achieved, with this mechanism,
when the rate at which the parametric instability feeds energy into the unstable
waves is equal to the rate at which scattered electrons and ions remove energy
from the unstable waves.[8] It is interesting to note that in the former

A2

mechanisms[5,6,7] it is assumed that the particle orbits are unperturbed by the presence of unstable waves. In the latter mechanism,[8] on the other hand, the distortion of particle orbits by unstable waves is the crucial nonlinear effect leading to saturation. A comparison of the results of different mechanisms will be presented in Sec. V. The nonlinear saturation due to the scattering of particles by unstable waves was calculated[8] by the method of <u>perturbed orbit theory</u>. The results were compared with recent computer simulation studies of Kruer and Dawson.[1] Quantitative agreement for the total saturated wave energy was obtained over a wide range of pump powers which encompassed both the parametric decay and the oscillating two-stream instability for the case $T_e \gg T_i$.

In this paper we complete the task begun in our earlier work, i.e., we present the solution to the more comprehensive problem of determining the <u>spectral distribution</u> of excited waves saturated by the effect of perturbed orbits. Here we treat specifically the parametric decay instability spectrum for approximately equal ion and electron temperatures. As will be clear subsequently, the approach is not limited to this case, and we will report the detailed spectrum results for other regimes in a future publication. In fact, the general procedure is applicable to a wide assortment of problems whenever strong wave-particle interactions contribute to the saturation.

We find as the principal result of our work an angular spectral intensity $I(x)$ of Langmuir waves which is given by

$$\frac{I(x)}{4\pi n \theta_e} \sim \frac{27}{8} \left[ \frac{\log[(1+r)Px^2 - r]}{(k_D/k_m)^2 + 9/2} \right]^2 \tag{1}$$

where x is the cosine of the angle between the pump and the wave vector <u>k</u>. P is the ratio of the pump intensity to threshold intensity for instability

at the matching wavenumber $k_m$, $n\theta_e$ is the kinetic energy density of electrons, and $r = r(k_m)$ is the ratio of the collisional to Landau damping decrements for the matched wave number $k_m$. The value of $k_m$ is obtained from the matching condition $\omega_0 = \omega_L (k_m) + \omega_a (k_m)$, where $\omega_0$ is the pump frequency, $\omega_L$ is the Langmuir frequency, and $\omega_a$ is the acoustic frequency. The main feature of this spectrum is that it is broad in angle with a rather slow dependence on pump intensity and angle, through the simple factor $Px^2$, with a cutoff at $Px^2 \leq 1$. Thus the spectrum broadens in angle, ultimately reaching isotropy, with increased driver intensity P. The k-spectrum is characterized by a half width $\Delta k$ on the order of the linear width $\Delta k_0$ of excited waves. The half width can be greater or less than $\Delta k_0$, depending on the ratio of matching wave number to Debye wave number. These results are in sharp contrast to those obtained by the scattering of Langmuir waves by ion fluctuations. There one finds the spectrum narrowly confined to the direction along the pump polarization with spreading to lower k values as the pump intensity is increased.[6,7]

A basic objective in any calculation of the saturated wave state is the increased wave damping decrement due to the nonlinearity. In Sec. II we derive the nonlinear susceptibilities and dielectric function in the presence of the external pump $E_0 \sin \omega_0 t$. Nonlinear susceptibilities are determined by accounting for the perturbed orbits of the particles. The effects of perturbed orbits are characterized by a deflection frequency, $\omega_d$, by describing the rate at which an electron is _deflected_ by a wavelength due to unstable waves. This frequency is explicitly calculated in terms of the spectra intensity. The nonlinear damping decrement due to waves is then determined, from the nonlinear

A4

susceptibilities, in terms of $\omega_d$ and, hence, the spectral intensity. In steady state the parametric growth rate is balanced by this nonlinear damping decrement, and results in a nonlinear equation for the spectral intensity. In Sec. III this equation is analytically solved for the saturated spectrum. In Sec. IV we calculate the anomalous collision frequency and heating rate, and in Sec. V the results are illustrated for specific cases, including the ionosphere. A comparison is made between the results of nonlinear perturbed orbit theory and nonlinear Landau damping. For small values of P we find that the nonlinear saturation of the parametric decay instability for the particular case in which $T_e \sim T_i$ is governed by perturbed orbits for $k \gtrsim k_D/5$ and is governed by nonlinear Landau damping for $k \lesssim k_D/5$, where $k_D$ is the Debye wave number and $k$ is the wave number of excited Langmuir wave. This demarcation in $k$ is influenced by the pump ratio P. For large enough P saturation by perturbed orbits is important for all $k$. A brief summary of the results is given in Sec. VI.

## II. NONLINEAR DIELECTRIC FUNCTIONS AND WAVE DAMPING RATE

We consider an isotropic, homogeneous plasma in the presence of a homogeneous, external, sinusoidal field $\underline{E}_o \sin \omega_o t$. It is well known that such a field will excite parametric instabilities in the plasma when the intensity of the field exceeds the threshold for instability. In particular, Langmuir waves are driven unstable when $E_o^2/4\pi n\theta_e > E_{th}^2/4\pi n\theta_e = 16 \; \gamma_L/\omega_L$, for $T_e \gtrsim T_i$, where $\gamma_L$ is the linear damping decrement, $\theta_e$ is the electron kinetic energy and n is the electron density. These waves continue to grow until nonlinear effects develop which saturate this growth. Here we shall calculate the nonlinear state of this instability at saturation.

The ultimate goal of our nonlinear calculation is the spectral density of the longitudinal electric field fluctuations $I(\underline{k},\omega) = \lim\limits_{T,V \to \infty} (TV)^{-1} \langle |E(\underline{k},\omega)|^2 \rangle$, where $E(\underline{k},\omega)$ is the space-time Fourier component of the saturated field fluctuations, and T and V are representative of a time interval of observation and the volume of the system, respectively. For the parametric decay instability $I(\underline{k},\omega)$ is dominated by resonances in the neighborhood of $\omega_L$ and $\omega_o - \omega_L \approx \omega_a$.

$$I_L(\underline{k}) = \int_{\substack{high \\ frequency}} \frac{d\omega}{2\pi} \; I(\underline{k},\omega) \; .$$

$$I_a(\underline{k}) = \int_{\substack{low \\ frequency}} \frac{d\omega}{2\pi} \; I(\underline{k},\omega) \qquad (2)$$

Since the low frequency wave density is precisely known in terms of the high frequency wave density,[11] it is sufficient to focus on the high frequency density $I_L(\underline{k})$. The spectral density $I_L(\underline{k})$ satisifes the kinetic wave equation

$$\frac{\partial}{\partial t} I_L(\underline{k}) = - 2\gamma_p^{NL} (\underline{k}) \; I_L(\underline{k}) + 2 \; S_p (\underline{k}) \; , \qquad (3)$$

A6

where $\gamma_p^{NL}(\underline{k})$ is the total damping rate of the Langmuir waves (the high frequency waves whose spectral density is $I_L(\underline{k})$ will be referred to as Langmuir waves). $S_p(\underline{k})$ is the rate of generation of wave fluctuations due to particle dis-creteness effects in the plasma (thermal noise). The detailed form of $S_p$ is not important except close to instability threshold. To obtain $\gamma_p^{NL}$ we derive the nonlinear dielectric function in the presence of the pump and the nonlinear waves. In the Appendix we show that for $T_e \geqslant T_i$,

$$\gamma_p^{NL} = \gamma_L^W + \gamma_L - P \gamma_L f \chi^2 . \tag{4}$$

Here the last term on the right hand side is the parametric growth rate in which $\gamma_L$ is the total linear damping decrement with $\gamma_L = \gamma_{\mathcal{L}} + \nu_c$, where $\gamma_{\mathcal{L}} \equiv \omega_L \sqrt{\pi/8} \; (k_D/k)^3 \exp[- 1/2(k_D^2/k^2 + 3)]$ is the Landau damping decrement with Debye wave number $k_D$, and $\nu_c$ is the collisional damping decrement. The pump ratio $P = P(k)$ is the ratio of actual pump intensity to the threshold intensity at the wave number $k$:

$$P \equiv \frac{1}{16} \left(\frac{\omega_{pe}}{\omega_o}\right)^2 \; \frac{\omega_a \, \omega_L}{\gamma_a \, \gamma_L(k)} \; \left(\frac{E_o^2}{4\pi n \theta_e}\right) . \tag{4a}$$

It is important to bear in mind, later, that $P$ varies with $k$ through $\gamma_L(k)^{-1}$. The resonance function $f$ measures the degree of frequency mismatch for excited waves of wave number $\underline{k}$:[9]

$$f = f(k) = [1 + (\Delta\omega/2 \, \gamma_a)^2 \; (\omega_a + \delta)^2/\omega_a \delta]^{-1}, \quad k < k_c \tag{5}$$
$$= 0 \qquad\qquad\qquad\qquad , \quad k > k_c ,$$

where $\Delta\omega = \omega_o - \omega_L(k) - \omega_a(k)$, and $\delta(k) = \omega_o - \omega_L(k)$, from which $k_c$ is defined as $\delta(k_c) = 0$.

In Eq. (4) $\gamma_L^W$ denotes that part of the damping decrement which is due to nonlinear wave interactions. It has been established[8,11,12] that such nonlinear effects are determined by the method of perturbed orbits as

$$\gamma_L^W + \gamma_{\chi} = (\frac{\partial}{\partial \omega} \text{Re } \epsilon^{NL})^{-1} \text{Im } \epsilon^{NL} \tag{6}$$

$$\epsilon^{NL} = 1 + \sum_s \chi_s^{NL} (\underline{k}, \omega) \tag{7}$$

$$\chi_s^{NL} (\underline{k},\omega) = -i \frac{\omega_{ps}^2}{k^2} \int_o^\infty dt \int d^3v \, \exp[i(\omega - \underline{k} \cdot \underline{v})t]$$

$$x \quad \langle \exp[-i\underline{k} \cdot \delta \underline{r}_s(t)] \rangle \, \underline{k} \cdot \frac{\partial \langle F_s(\underline{v}) \rangle}{\partial \underline{v}} \tag{8}$$

where $\epsilon^{NL} \equiv \epsilon^{NL}(\underline{k},\omega)$ denotes the nonlinear dielectric function at frequency $\omega$ and wavevector $\underline{k}$ and $\chi_s^{NL}(\underline{k},\omega)$ denotes the nonlinear susceptibility of species s, $\omega_{ps}$ is the plasma frequency, $\langle F_s(\underline{v}) \rangle$ is the background velocity distribution function, and $\delta \underline{r}_s(-t)$ is the nonlinear deflection or perturbation of the particle orbit at time t due to the action of the fluctuating $\delta\underline{E}$. $\delta\underline{r}_s(t)$ is given by

$$\delta\underline{r}_s(t) = \frac{e}{m_s} \int_o^t dt' \, t' \quad \delta\underline{E}[\underline{r}_s(t - t'), t'] \tag{9}$$

where e is the charge and $m_s$ is the mass. It should be noted that $\delta\underline{E}$, in Eq. (9), is evaluated along the actual particle orbit $\underline{r}_s(t)$ given by

$$\underline{r}_s(t) = \underline{r} - t\underline{v} + \delta\underline{r}_s(t)$$

where $\underline{r}$ is the particle position at t = o.

Equations (6) - (9) will be used to determine $\gamma_L^W$ in terms of $\langle \delta\underline{E}\ \delta\underline{E} \rangle$, and then $\gamma_L^W$ will be substituted into Eqs. (4) and (3) to obtain a closed equation for $\langle \delta\underline{E}\ \delta\underline{E} \rangle$. It is clear that a major task in carrying out this program is to evaluate the right side of Eq. (8) for $\chi_s^{NL}$ in terms of $\langle \delta\underline{E}\ \delta\underline{E} \rangle$. However, it has been demonstrated previously that this task is readily accomplished by means of a cumulant expansion as follows:[10]

$$\langle \exp\,[-i\underline{k}\cdot\delta\underline{r}_s(-\tau)]\rangle = \exp[-\tfrac{1}{2}\,\langle(\underline{k}\cdot\delta\underline{r}_s(-\tau))^2\rangle + \sum_{n=3} C_n/n!], \qquad (10)$$

where $C_n$ is the cumulant of the nth order moment of $i\underline{k}\cdot\delta\underline{r}_s$ and is assumed negligible for $n \geq 3$. From Eq. (9) the mean square displacement term in the exponent of Eq. (10) is given after transformations of the time integrals by:[12]

$$\tfrac{1}{2}\langle(\underline{k}\cdot\delta\underline{r}_s(\tau)^2\rangle = \frac{e^2}{m_s^2}\ \int_0^\tau\!dt\ t\ \int_0^t\!dt'(t-t')\langle\underline{k}\cdot\delta\underline{E}(\underline{r},T)\ \underline{k}\cdot\delta\underline{E}(\underline{r}_s(T-t'),t')\rangle\ . \qquad (11)$$

Expanding $\delta\underline{E}$ in terms of its Fourier components $\underline{E}(\underline{k},\omega) = \hat{\underline{k}}\ E(\underline{k},\omega)$ and using the spectral definition in Eq. (2) we find that Eq. (11) may be written:[12]

$$\tfrac{1}{2}\langle(\underline{k}\cdot\delta\underline{r}_s(-\tau))^2\rangle = \frac{e^2}{m_s^2}\,\mathrm{Re}\int_0^\tau\!dt\,t\int_0^t\!dt'\ (t-t')\sum_\nu\int\frac{d^3k'}{(2\pi)^3}\ (\underline{k}\cdot\hat{\underline{k}}')^2\ I_\nu(\underline{k}')$$

$$x\quad \exp[-i(\omega_\nu(k')-\underline{k}'\cdot\underline{v})t' - \tfrac{1}{2}\langle(\underline{k}'\cdot\delta\underline{r}_s(-t'))^2\rangle \qquad (12)$$

where $\underline{k}'$ denotes the wave vector and $\nu$ stands for either the Langmuir or acoustic mode. This equation has previously been investigated in the diffusion limit to obtain resonant broadened wave-particle contributions. Here we shall calculate an important nonresonant contribution as well. Thus, in the asymptotic limit of large $\tau$, compared to the correlation time of the electric field along

A9

the particle orbit, Eq. (12) becomes:

$$\frac{1}{2}\langle[\underline{k}\cdot\delta\underline{r}_s(-\tau)]^2\rangle \sim \frac{1}{3}\tau^3\,\underline{k}\cdot\underline{D}(\underline{v})\cdot\underline{k} + \frac{1}{2}\tau^2\,[\omega_d^{nr}(\underline{v})]^2 \tag{13}$$

where the diffusion term $\underline{D}(\underline{v})$ and the frequency $\omega_d^{nr}(\underline{v})$ are defined by

$$\underline{D}(\underline{v}) \equiv \frac{e^2}{m^2}\,\text{Re}\,\sum_{\nu}\int\frac{d\underline{k}'}{(2\pi)^3}\,\hat{\underline{k}}'\hat{\underline{k}}'\,I_\nu(\underline{k}')\int_0^\infty dt'\,\exp\{-i[\omega_\nu(\underline{k}')-\underline{k}'\cdot\underline{v}]t'-\frac{1}{2}\langle[\underline{k}'\cdot\delta\underline{r}_s(-t)]^2\rangle\} \tag{14a}$$

$$[\omega_d^{nr}(\underline{v})]^2 \equiv -\frac{e^2k^2}{m^2}\,\text{Re}\,\sum_{\nu}\int\frac{d\underline{k}'}{(2\pi)^3}(\hat{\underline{k}}\cdot\hat{\underline{k}}')^2\,I_\nu(\underline{k}')\int_0^\infty dt'\,t'\,\exp\{-i[\omega_\nu(\underline{k}')-\underline{k}'\cdot\underline{v}]t'$$

$$-\frac{1}{2}\langle[\underline{k}'\cdot\delta\underline{r}_s(-t')]^2\rangle\} \tag{14b}$$

The resonant broadened diffusion tensor $\underline{D}(\underline{v})$ has been previously introduced by Dupree[11] and one of us.[12] The quantity $\omega_d^{nr}(\underline{v})$, on the other hand, is introduced in Eq. (13) for the first time. A short discussion of $\omega_d^{nr}$ and its relative importance compared to $\underline{k}\cdot\underline{D}(\underline{v})\cdot\underline{k}$ is thus in order here. To understand the quantities $\underline{k}\cdot\underline{D}\cdot\underline{k}$ and $\omega_d^{nr}$ it is useful to introduce the characteristic deflection time, $\tau_d$, or deflection frequency, $\omega_d = \tau_d^{-1}$ defined by

$$\langle[\underline{k}\cdot\delta\underline{r}_s(-\tau_d)]^2\rangle \equiv 1 \tag{15}$$

so that $\tau_d(\underline{v})$ <u>is the time it takes a particle to be "deflected" the distance of a wavelength from its unperturbed orbit</u>, and $\omega_d = \omega_d(\underline{v})$, <u>is the frequency with which such deflections occur.</u>[13] $\omega_d(\underline{v})$ is a function of $\underline{v}$ since the orbit $\underline{r}(t)$ is a function of $\underline{v}$. Now, in terms of $\omega_d(\underline{v})$ it is seen from the t' integral in Eq. (14a) that $\underline{D}(\underline{v})$ is essentially zero unless $\underline{v}$ satisfies

$$|\omega(\underline{k}') - \underline{k}'\cdot\underline{v}| < \omega_d(\underline{v})\,, \tag{16a}$$

Hence, $\underline{D}(\underline{v})$ is referred to as a resonant broadened diffusion tensor. On the other hand, it is seen from the t' integral in Eq. (14b) that the frequency $\omega_d^{nr}(\underline{v})$ is large and positive when $\underline{v}$ is such that

$$|\omega(\underline{k}') - \underline{k}'\cdot\underline{v}| > \omega_d(\underline{v}) \ll \omega(\underline{k}') , \quad \text{all } \underline{k}' \tag{16b}$$

in which case (14b) reduces to

$$\left[\omega_d^{nr}(\underline{v})\right]^2 = \frac{e^2 k^2}{m^2} \sum_{\nu} \int_{V_1} \frac{d\underline{k}'}{(2\pi)^3} \left\{ \frac{(\hat{\underline{k}}\cdot\hat{\underline{k}}')^2 \, I_\nu(\underline{k}')}{[\omega_\nu(\underline{k}') - \underline{k}'\cdot\underline{v}]^2} \left[1 + 0\left(\frac{\omega_d}{\omega_\nu - \underline{k}'\cdot\underline{v}}\right)^2\right]\right\} \tag{17}$$

where the subscript $V_1$ denotes that $\underline{k}'$ is restricted to $|\omega - \underline{k}'\cdot\underline{v}| > \omega_d$. Hence, $\tau^2[\omega_d^{nr}(\underline{v})]^2$ is a nonresonant contribution to $\langle[\underline{k}\cdot\delta\,r(-\tau)]^2\rangle$. We shall thus refer to $\omega_d^{nr}(\underline{v})$ as the <u>nonresonant deflection frequency</u>. It describes diffusion due to <u>the action of waves nonresonant with the particle</u> when $|\omega - \underline{k}'\cdot\underline{v}| \gg \omega_d$. Similarly one could describe the resonant broadened frequency $\omega_d^r(\underline{v})$ by

$$\omega_d^r(\underline{v}) \equiv [\tfrac{2}{3}\,\underline{k}\cdot\underline{D}(\underline{v})\cdot\underline{k}]^{1/3} \tag{18}$$

in which case Eq. (13) can be written as

$$\langle[\underline{k}\cdot\delta\underline{r}_s(-\tau)]^2\rangle \sim \tau^3[\omega_d^r(\underline{v})]^3 + \tau^2[\omega_d^{nr}(\underline{v})]^2 , \tag{19}$$

so that for values of $\underline{v}$ such that $\omega_d^r(\underline{v})$ is small, i.e., for small $\underline{D}(\underline{v})$, we have $\omega_d \sim \omega_d^{nr}$. In general, both resonant and nonresonant terms, $\omega_d^r$ and $\omega_d^{nr}$, must be included to calculate the susceptibility in Eq. (8). However, it is found that one term will usually dominate the other depending on the spectral distribution $I_\nu(\underline{k}')$ and the mode frequency $\omega(\underline{k})$. A more detailed analysis of $\omega_d^r$ and $\omega_d^{nr}$, and their relative importance is given in a forthcoming publication. (The relative value of $\omega_d^r$ and $\omega_d^{nr}$ is discussed in Appendix C for Langmuir waves. It is demonstrated there that $\omega_d^{nr} > \omega_d^r$ when $\langle|\delta E|^2\rangle\,(4\pi n\theta_e)^{-1} \geqslant (k/k_D)^4$ for the case of parametrically excited Langmuir waves.)

A11

With Eq. (13) and (10) substituted into (8) we have for the nonlinear electron susceptibility $\chi_e^{NL}$

$$\chi_e^{NL}(\underline{k},\omega) = -i \frac{\omega_{ps}^2}{k^2} \int_0^\infty d\tau \int d^3v \, \exp\{i(\omega-\underline{k}\cdot\underline{v})\tau - 1/3 \, \underline{k}\cdot\underline{\underline{D}}\cdot\underline{k}\tau^3$$

$$- 1/2(\omega_d^{nr})^2 \, \tau^2\} \, \underline{k}\cdot\frac{\partial\langle F(\underline{v})\rangle}{\partial\underline{v}} \quad . \tag{20}$$

We can now evaluate $\chi^{NL}$ for both its real and imaginary parts. The real part of $\chi^{NL}$ determines the nonlinear frequency shift of Langmuir waves. The evaluation of Re $\chi^{NL}$ is given in Appendix B where it is found that for Langmuir waves

$$\text{Re}\chi_e^{NL} \approx -\frac{\omega_{pe}^2}{\omega^2}\left(1 + \frac{3 k^2 v_e^2}{\omega_{pe}^2}\left[1 + \frac{\langle\delta E^2\rangle}{4\pi n\theta_e}\right]\right) \quad , \tag{21a}$$

where $\langle\delta E^2\rangle$ is the mean square amplitude of the Langmuir waves. The nonlinear Langmuir frequency $\omega_L^{NL}$ is given, in the presence of turbulence, by

$$\omega_L^{NL} \approx \omega_{pe}^2\left(1 + \frac{3 k^2 v_e^2}{\omega_{pe}^2}\left[1 + \frac{\langle\delta E^2\rangle}{4\pi n\theta_e}\right]\right) \tag{21b}$$

Equation (21b) explicitly shows how the Langmuir frequency shift, due to non-linearity, scales with the wave energy density $\langle\delta E^2\rangle \, (4\pi)^{-1}$. This shift is small when the total wave energy density is much less than the thermal energy density. It should be noted the frequency shift appears as an *effective temperature* increase $v_e^2 \rightarrow v_e^2(1 + \langle\delta E^2\rangle \, (4\pi n\theta)^{-1})$.

We now turn to Im $\chi^{NL}$, from Eq. (20), which determines the nonlinear damping. First we must perform the t integration in Eq. (20). We find that there are two cases for which this integration is elementary: Case (1) is for $(\omega_d^{nr})^2 \gg (\underline{k}\cdot\underline{\underline{D}}\cdot\underline{k})^{2/3}$. In this case one can neglect $(\underline{k}\cdot\underline{\underline{D}}\cdot\underline{k})\tau^3$ in Eq. (20), so that the $\tau$

A12

integral is a simple Gaussian and $\text{Im } \chi_e^{NL}$ is given by

$$\text{Im } \chi_e^{NL} = - \frac{\omega_{pe}^2}{k^2} \int d\underline{v} \; \underline{k} \cdot \frac{\partial \langle F_e \rangle}{\partial \underline{v}} \; \frac{\sqrt{\pi/2}}{\omega_d^{nr}(\underline{v})} \; \exp\left[ - \frac{(\omega - \underline{k} \cdot \underline{v})^2}{2(\omega_d^{nr})^2} \right] \qquad (22a)$$

Case (2) is for $(\underline{k} \cdot \underline{D} \cdot \underline{k})^{1/3} \gg \omega_d^{nr}$. In this case we cannot ignore the term $(\underline{k} \cdot \underline{D} \cdot \underline{k})\tau^3$ in Eq. (20) since this term dominates $(\omega^{nr})^2 \, \tau^2$. However, if we consider the $\tau$ integral as a function of $\underline{v}$ then we find that the main contribution comes from the range of $\underline{v}$ satisfying $|\omega - \underline{k} \cdot \underline{v}| \lesssim \sqrt{2}(1/3 \; \underline{k} \cdot \underline{D} \cdot \underline{k})^{1/3}$. Outside this range of $\underline{v}$ the $\tau$ integral is negligibly small and even slightly negative. Hence, we need only consider $\underline{v}$ in the range $|\omega - \underline{k} \cdot \underline{v}'| \lesssim \sqrt{2}(1/3 \; \underline{k} \cdot \underline{D} \cdot \underline{k})^{1/3}$. For $\underline{v}$ inside this range the imaginary part of the $\tau$ integral is accurately approximated by

$$\text{Im} \int_0^\infty d\tau \; \exp\{ i(\omega - \underline{k} \cdot \underline{v})\tau - \frac{1}{3} \underline{k} \cdot \underline{D} \cdot \underline{k} \; \tau^3 - \frac{1}{2}(\omega_d^{nr})^2 \; \tau^2 \}$$

$$\frac{1/3 \, \Gamma(1/3)}{[(1/3 \; \underline{k} \cdot \underline{D} \cdot \underline{k})^{2/3} + 1/2 \; (\omega_d^{nr})^2]^{1/2}} \; \exp\left\{ - \frac{(\omega - \underline{k} \cdot v)^2}{4[1/3 \; k \cdot D \cdot k)^{2/3} + 1/2(\omega_d^{nr})^2]} \right\}, \quad (22b)$$

$$((1/3 \; \underline{k} \cdot \underline{D} \cdot \underline{k})^{1/3} \gg \omega_d^{nr})$$

where $\Gamma(1/3)$ is the Gamma function evaluated at $1/3$. The two cases (22a) and (22b) can be combined into one expression for $\text{Im } \chi_e^{NL}$ as follows:

$$\text{Im } \chi_e^{NL} = - \frac{\omega_{pe}^2}{k^2} \int d\underline{v} \; \underline{k} \cdot \frac{\partial \langle F_e \rangle}{\partial \underline{v}} \; \frac{\sqrt{\pi/2}}{\omega_d(\underline{v})} \; \exp\left[ - \frac{(\omega - \underline{k} \cdot \underline{v})^2}{2\omega_d^2(\underline{v})} \right], \qquad (23a)$$

with

$$\omega_d^2(\underline{v}) = \frac{(\frac{2}{3}^{3/2} \; \underline{k} \cdot \underline{D} \cdot \underline{k})}{\omega_d(\underline{v})} + [\omega_d^{nr}(\underline{v})]^2 , \qquad (23b)$$

A13

Equation (23) reduces to case (1) for $\omega_d^{nr} \gg (1/3 \underline{k} \cdot \underline{D} \cdot \underline{k})^{1/3}$, and reduces to case (2) for $(1/3 \underline{k} \cdot \underline{D} \cdot \underline{k})^{1/3} \geqslant \omega_d^{nr}$. It is shown in Appendix C that case (1) obtains when the total wave energy $\langle \delta E^2 \rangle$ roughly satisfies $\langle \delta E^2 \rangle (4\pi n \theta_e)^{-1} > (k/k_D)^4$ and that case (2) obtains when, roughly, $\langle \delta E^2 \rangle (4\pi n \theta_e)^{-1} < (k/k_D)^4$

We now consider the velocity integral in Eq. (23). This integral is complicated by the dependence of $\omega_d(\underline{v})$ on $\underline{v}$ through the Doppler shifted frequency $\omega_L - \underline{k}' \cdot \underline{v}$ indicated in Eqs. (14) and (17). A significant simplification is possible, however, since in Eq. (23) $\omega_d(\underline{v})$ can be approximated by its value at $v_\perp = 0$, where $v_\perp$ denotes the vector component of $\underline{v}$ perpendicular to $\underline{k}$, with $v_\parallel$ the component $\underline{v}$ parallel to $\underline{k}$; that is, $\omega_d(\underline{v}) \simeq \omega_d(v_\parallel)$. The simplification arises since the main contribution to the integrand in Eq. (23) comes from $v_\perp \leqslant v_e = (\theta_e/m_e)^{1/2}$, and $v_\parallel \simeq \omega/k \equiv v_p$, where $v_p$ denotes the wave phase velocity. Consequently, for $v_p \gg v_e$ we have in Eq. (23) $v_\parallel \gg v_\perp$, and therefore

$$\underline{k}' \cdot \underline{v} \simeq (\underline{k}' \cdot \hat{\underline{k}}) \, v_\parallel \tag{24}$$

in $\omega_d$ so that $\omega_d(\underline{v}) \sim \omega_d(v_\parallel)$. Integrating $\langle F_s \rangle$ over $\underline{v}_\perp$, we find that Eq. (23) reduces to

$$\operatorname{Im} \chi_e^{NL}(\underline{k},\omega) = \frac{\omega}{2} \frac{k_D}{kv_e^2} \int_{-\infty}^{\infty} v_\parallel \, v_\parallel \, \frac{e^{-G_e(v_\parallel)}}{\omega_d(v_\parallel)} \, , \tag{25}$$

where

$$G_e(z) = \frac{1}{2} \left(\frac{v_\parallel}{v_e}\right)^2 + \frac{\omega^2}{2\omega_d^2(v_\parallel)} \left(1 - \frac{v_\parallel}{v_p}\right)^2 \tag{26}$$

A14

The integrand in Eq. (25) is highly peaked in the neighborhood of $v_\parallel = v_p$ for $\omega_L^2/2\omega_d^2 \gg 1$. Indeed, for $\omega_d \to o$ the integrand peaks precisely at $v_\parallel = v_p$, reproducing the well-known linear result of Landau damping. In the present nonlinear case the finiteness of $\omega_d$ extends or broadens the integrand to include velocities with $v_\parallel < v_p$ thereby resulting in increased damping. (This broadening of the integrand to wider ranges of velocity is referred to as a broadening of resonant wave-particle interactions).

To evaluate Eq. (25) we apply Laplace's method of asymptotic integration to obtain:

$$\mathrm{Im}\ \chi_e^{NL}(\underline{k},\omega) = \omega\ \frac{\sqrt{\omega}}{2}\left(\frac{k_{De}}{k}\right)^3\left(\frac{\omega}{\omega_{pe}}\right)\left\{\frac{v_c}{v_p^2\ \omega_d(v_c)}\ \frac{\exp\text{-}G_e(v_c)}{\sqrt{G_e^{\parallel}(v_c)}}\left[1 + 0\left(\frac{\omega_d^2}{\omega^2}\right)\right]\right. \tag{27}$$

where primes denote derivatives with respect to arguments, and $v_c$ is determined by $G_e^{'}(v_c) = o$, or with Eq. (26),

$$\frac{v_c}{v_p} = \left(\frac{v_e}{v_p}\right)^2\left(\frac{\omega_L}{\omega_d}\right)^2\left(1 - \frac{v_c}{v_p}\right)\left\{1 + \frac{1}{2}\left(1 - \frac{v_c}{v_p}\right)v_p\ \frac{d}{dv_\parallel}\ \log\ \omega_d^2\Big|_{v_\parallel = v_c}\right\} \tag{28}$$

The nonlinear damping decrement can now be obtained by substituting (27) into (7) and the resulting expression into (6). We thus find with $\partial\ \mathrm{Re}\ \epsilon^{NL}/\partial\omega = 2\omega_{pe}^2(\omega_L^{NL})^{-3}$,

$$\gamma_L^W = \omega_L^{NL}\ \sqrt{\pi/8}\left(\frac{k_{De}}{k}\right)^3\ \frac{v_c}{v_p^2}\ \frac{(\omega_L/\omega_d)}{\sqrt{G^{\parallel}(v_c)}}\ \exp\{- G_e(v_c)\} - \gamma_{\mathcal{L}}$$

or, equivalently, using the value of $\gamma_{\mathcal{L}}(k)$,

$$\gamma_L^W = \gamma_{\mathcal{L}}(k)\ \{\exp[A(\underline{k},v_c) - a] - 1\} \tag{29}$$

where

$$A(\underline{k},v_c) = \frac{1}{2}\left\{\left(\frac{k_{De}}{k}\right)^2 + 3\right\}\left(1 - \left(\frac{v_c}{v_p}\right)^2\right) - \frac{1}{2}\left(\frac{\omega_L}{\omega_d}\right)^2\left(1 - \frac{v_c}{v_p}\right)^2\ ,$$

$$a = -\log\left\{\frac{v_c}{v_p^2}\ \frac{\omega_L^{NL}}{\omega_L}\ \frac{\omega_L^{NL}/\omega_d}{\sqrt{G_e^{\parallel}(v_c)}}\right\}\ . \tag{30}$$

A15

Equation (29) gives the nonlinear wave damping $\gamma_L^W$ in terms of $v_c$ and $\omega_d$ $(v_c)$. To obtain $\gamma_L^W$ in terms of the spectrum we use Eq. (14) to express $\omega_d$ in terms of the spectrum $I(\underline{k})$ and then use Eq. (28) to also express $v_c$ in terms of the spectrum. Let us, then, turn to Eqs. (23b) and (14) so as to evaluate $\omega_d$ in terms of $I(\underline{k})$. To obtain $\omega_d(\underline{v})$ we must substitute Eq. (14) for $\omega_d^{nr}$ and $\underline{k} \cdot \underline{D} \cdot \underline{k}$ into Eq. (23b). This is done in Appendix D where it is demonstrated that $\omega_d(\underline{v})$ is approximately given by

$$\omega_d^2(\underline{v}) = \frac{e^2}{m_e^2} \int \frac{d\underline{k}'}{(2\pi)^3} \frac{(\underline{k} \cdot \hat{\underline{k}}')^2 \, I_L(\underline{k}')}{(\omega - \underline{k}' \cdot \underline{v})^2 + 3\omega_d^2(v_c)} \tag{31}$$

(Equation (31) is a synthesis of the contributions of $\underline{k} \cdot \underline{D} \cdot \underline{k}$ and $\omega_d^{nr}$ to $\omega_d$. From Appendix D one sees that the contribution to Eq. (31) from the region of $\underline{k}'$ for which $|\omega - \underline{k}' \cdot \underline{v}| > \sqrt{2}\,\omega_d$ comes from $\omega_d^{nr}$, whereas the contribution from the region $\underline{k}'$ for which $|\omega - \underline{k}' \cdot \underline{v}| < \sqrt{2}\,\omega_d$ comes mostly from $\underline{k} \cdot \underline{D} \cdot \underline{k}$ .) To perform the $\underline{k}'$ integration, with $\underline{v} = v_\parallel \hat{\underline{k}}$, in Eq. (31) we introduce polar coordinates:

$$\omega_d^2(v_\parallel) = \frac{e^2}{m^2} k^2 \int \frac{k'^2 dk'}{2\pi} \left( \int_0^1 \frac{dx'}{2\pi} \int_0^{2\pi} \frac{d\phi'}{2\pi} + \int_{-1}^0 \frac{dx'}{2\pi} \int_0^{2\pi} \frac{d\phi'}{2\pi} \right)$$

$$\times \quad \frac{(\hat{\underline{k}} \cdot \hat{\underline{k}}')^2 \, I_L(\underline{k}')}{[\omega_L - k'v_\parallel(\hat{\underline{k}} \cdot \hat{\underline{k}}')]^2 + 3\omega_d^2} \tag{32}$$

where $\phi'$ is the azimuthal angle that $\underline{k}'$ makes with the pump direction $\hat{\underline{e}}_0$ and $x' = \hat{\underline{k}}' \cdot \hat{\underline{e}}_0$ is the direction cosine of $\underline{k}'$ with respect to the pump. We next change variables $\underline{k}' \to -\underline{k}'$ in the second term on the right of Eq. (32), use $I(\underline{k}') = I(-\underline{k}')$, denote $(k'/k) \equiv y$ and $(kv_\parallel/\omega_L) \equiv z$ to obtain

$$\omega_d^2(v_\parallel) = \frac{e^2}{m^2} k^2 \int_0^\infty k'^2 \frac{dk'}{2\pi} \int_0^1 \frac{dx'}{2\pi} \int_0^{2\pi} \frac{d\phi'}{2\pi} \, (\hat{\underline{k}} \cdot \hat{\underline{k}}')^2 \frac{I(k')}{\omega_L^2}$$

$$\times \left( \frac{1}{(1 - yz \, \hat{\underline{k}} \cdot \hat{\underline{k}}')^2 + 3\omega_d^2/\omega_L^2} + \frac{1}{(1 + yz \, \hat{\underline{k}} \cdot \hat{\underline{k}}')^2 + 3\omega_d^2/\omega_L^2} \right)$$

$$= \frac{e^2}{m^2} k^2 \int_0^\infty k'^2 \frac{dk'}{2\pi} \int_0^1 \frac{dx'}{2\pi} \int_0^{2\pi} \frac{d\phi'}{2\pi} \, \frac{I(k'x')}{\omega_L(k')^2} \, (xx' + \sqrt{1-x^2}\sqrt{1-x'^2} \cos\phi')^2$$

$$\times \left\{ \frac{1}{[1 - yz(xx' + \sqrt{1-x^2}\sqrt{1-x'^2} \cos\phi')]^2 + 3\omega_d^2/\omega_L^2} + (z \to -z) \right\} \quad (33)$$

To obtain the last equation in (33) we have explicitly introduced the azimuthal symmetry of the spectrum, about the pump, by $I(\underline{k}) = I(k',x')$, and we have defined the direction cosine of $\underline{k}$ by $x \equiv \hat{\underline{k}} \cdot \hat{\underline{e}}_0$ so that $\hat{\underline{k}} \cdot \hat{\underline{k}}' = xx' + \sqrt{1-x^2}\sqrt{1-x'^2} \cos\phi$. The $\phi'$ integration in Eq. (33) is tabulated and yields, with $(3\omega_d^2/\omega_L^2) << 1$ and $yz \leq 1$,

$$\frac{\omega_d^2(v_\parallel)}{\omega_L^2} = \left(\frac{v_e}{v_p}\right)^2 \left(\frac{\omega_{pe}}{\omega_L}\right)^2 \int_0^\infty k'^2 \, \frac{dk'}{2\pi} \int_0^1 \frac{dx'}{2\pi} \, \frac{I(k',x')}{4\pi n\theta_e} \, \frac{1}{(yz)^2}$$

$$\times \left\{ \left( 1 - \frac{1}{B} + \frac{yz[xx'(1-yz\,xx') + yz(1-x^2)(1-x'^2)]}{B^3} \right) + (z \to -z) \right\} \quad (34a)$$

$$B^2 \equiv (yz)^2 (x-x')^2 + (1-yz)[1 + yz(1-2xx')] + 3\frac{\omega_d^2}{\omega_L^2} \quad (34b)$$

A17

and we have, for convenience, normalized $\omega_d$ to $\omega_L$ and $I(k',x')$ to $(4\pi n \theta_e)$. We have also replaced $\omega_L(k')$ in Eq. (33) by $\omega_L(k)$ which is justified in Sec. III-C by the narrowness of the spectrum $I(k',x')$ in $k'$.

To perform the $x'$ integration in Eq. (34a) we use the fact that $1/B^2$ is sharply peaked about $x = x'$, for $yz \sim 1$. In fact, $B^2$ can be asymptotically expressed by

$$B^2 \sim (x - x')^2 + \epsilon$$

$$\epsilon = (1 - yz)\,[1 + yz(1 - 2xx'] + 3\omega_d^2/\omega_L^2$$

$$\epsilon \ll 1, \quad y \sim 1, \quad z \sim z_c \sim 1, \quad (1 - yz_c) > o$$

$$z_c \equiv kv_c/\omega_L \equiv v_c/v_p \tag{35}$$

That $y \sim 1$ follows from the fact that $I(k',x')$ is narrowly peaked about $k' = k_m$ (see Sec III-C) so that $y \sim 1$ for $k \sim k_m$. Also, we have $(1 - z_c) \ll 1$ for $I(x)\,(4\pi n \theta_e)^{-1} \ll 1$, as is verified by Eq. (38). Hence $(1 - yz) \ll 1$ for $z \sim z_c$, $k \sim k_m$. Since $\omega_d^2/\omega_L^2 \lll 1$ it follows that $\epsilon \ll 1$ for $z \sim z_c$, $k \sim k_m$. With Eq. (35) it is clear that $1/B^3 \gg 1$ at $x = x'$ and that the main contribution to integration in Eq. (34a) comes from $x' \sim x$, unless $I(k',x')$ is very narrow in $x'$. In fact, $I(k',x')$ is found in Sec. III-A to be rather broad in $x'$ so that Eq. (34a) becomes

$$\frac{\omega_d^2(v_\parallel)}{\omega_L^2} = \left(\frac{v_e}{v_p}\right)^2 \left(\frac{\omega_{pe}}{\omega_L}\right)^2 \int_0^\infty k'^2 \; \frac{dk'}{(2\pi)^2} \frac{I(k',x)}{4\pi n \theta_e} \; \frac{1}{yz}$$

$$\times \int_0^1 dx' \; \frac{[xx'(1-yz\;xx') + yz\,(1-x^2)(1-x'^2)]}{B^3} \quad , \tag{36}$$

A18

The $x'$ integral is straightforward with the result, for $y \sim 1$,

$$\frac{\omega_d^2(v_\parallel)}{\omega_L^2} = \left(\frac{v_e}{v_p}\right)^2 \left(\frac{\omega_{pe}}{\omega_L}\right)^2 \frac{I(x)}{4\pi n\theta_e} \left(\frac{1}{z^2}\right) \left(\frac{z(1-x^2) + x^2(1-z)}{(1-z)(1 + z - 2z\,x^2)}\right)$$

$$\times \left(\frac{1-x}{\sqrt{(1-x)^2 + \eta^2}} + \frac{x}{\sqrt{x^2 + \eta^2}}\right) \quad , \quad (z \sim z_c) \tag{37}$$

where $I(x)$ denotes the angular spectrum defined by

$$I(x) \equiv \int k'^2 \frac{dk'}{2\pi} \frac{I(k'x)}{2\pi} \quad , \text{ and}$$

$$\eta^2 \equiv \frac{1}{z_c^2}(1-z_c)(1 + z_c - 2z_c x^2) \ll 1, \text{ for } \frac{I(x)}{4\pi n\theta_e} \ll 1$$

Equation (37) expresses $\omega_d^2(v_\parallel)$ in terms of both the angular spectrum $I(x)$ and $z_c$. However, $\omega_d(v_\parallel)$ and $z_c$ are related to each other by Eq. (28), and substituting Eq. (37) and, its derivative, into Eq. (28) we find the following explicit relation for $I(x)$ in terms of $z_c$,

$$\frac{I(x)}{4\pi n\theta_e} = \frac{1 + 1/2 \, p}{q} \, z_c(1 - z_c)^2, \tag{38a}$$

or

$$\frac{I(x)}{4\pi n\theta_e} = 3/2(1-z_c)^2 \ , \text{ for } z_c \sim 1 \tag{38b}$$

where $p$ and $q$ are near unity and vary slowly with $x$ and $z_c$. They are defined by

$$\frac{1}{2}\,p \equiv \frac{z_c(1-x^2) + x^2(1-z_c)}{1 + z_c - 2z_c x^2}$$

$$2\,q = \frac{1-x}{\sqrt{(1-x)^2 + \eta^2}} + \frac{x}{\sqrt{x^2 + \eta^2}} \tag{39}$$

A19

We can use (38) and (39) to eliminate $I(x)$ or $z_c$ from (37) to obtain, with $\omega_{pe}^2/\omega_L^2 \approx 1$.

$$\frac{\omega_d^2(z_c)}{\omega_L^2} = \left(\frac{v_e}{v_p}\right)^2 \frac{(1-z_c)}{z_c} (1 + 1/2\ p) , \qquad (40a)$$

and

$$\frac{\omega_d^2(z_c)}{\omega_L^2} \approx \sqrt{\frac{3}{2}} \left(\frac{v_e}{v_p}\right)^2 \sqrt{\frac{I(x)}{4\pi n\theta_e}} , \qquad (40b)$$

which explicitly gives $\omega_d$ in terms of $I(x)$. Finally, to obtain $\gamma_L^W$ in terms of $I(x)$ we use Eqs. (38a) and (40a) to eliminate $(1-z_c)$ and $\omega_d(z_c)$ from Eqs. (29) and (30). The result for $\gamma^W$, neglecting the small quantity a compared to A, is

$$\gamma_L^W = \gamma_\ell(k) \left[ \exp\{(\tfrac{2}{3})^{\frac{1}{2}} \left(\tfrac{2}{3}\frac{k_D^2}{k^2} + 3\right) \sqrt{\frac{I(x)}{4\pi n\theta_e}} \sqrt{1+F}\} - 1 \right] \qquad (41a)$$

$$\approx \gamma_\ell(k) \left[ \exp\{(\tfrac{2}{3})^{\frac{1}{2}} \left(\tfrac{2}{3}\frac{k_D^2}{k^2} + 3\right) \sqrt{\frac{I(x)}{4\pi n\theta_e}}\} - 1 \right] , \qquad (41b)$$

where F is an algebraic function of $I(x)$ and x, whose magnitude is less than 1/2, implicitly defined by Eqs. (38a), (40a) and (41a), and which rapidly approaches zero as $I(x) (4\pi n\theta_e)^{-1} \to o$. F is thus a minor correction and can be ignored for almost all purposes.

Equation (41), to our knowledge, gives for the first time an expression for the angular dependence of the nonlinear wave damping rate due to strong turbulence (perturbed orbits). We note that $\gamma_L^W$ is a highly nonlinear function of the angular spectrum $I(x)$. This result is in marked distinction to nonlinear Landau damping, for example, in which $\gamma_L^W$ is linear in $I(x)$. It is clear that a result such as Eq. (41) could not be obtained within the confines of weak turbulence theory. Having obtained $\gamma_L^W$ in terms of $I(x)$ we can proceed to calculate $I(x)$ from the wave equation.

A20

## III. STEADY-STATE SPECTRUM OF WAVES

### A. Angular Spectrum

The object of this section is to calculate the saturated angular spectrum from the wave equation. To do this we substitute $\gamma_L^W$, given by (41), into the wave equation (3) at steady state.

$$\frac{1}{2} \frac{\partial}{\partial t} I(k) = -(\gamma_L^W + \gamma_L) I(\underline{k}) + \gamma_L \, Pf(k)x^2 + S(\underline{k}) = 0 \qquad (42)$$

It is seen in Eq. (42) that the increased damping due to nonlinear waves, $\gamma^W$, plus the linear damping rate, $\gamma_L$, must be sufficiently large to balance the growth rate $\gamma_L Pfx^2$ for each mode $(\underline{k})$. More precisely, $\gamma_L^W$ must be slightly larger in order to overcome the noise source S. S is only important near threshold where we can take[14]

$$S(\underline{k}) = 4\pi\theta_e \, \gamma_L \left\{ 1 + Pfx^2 \, \frac{\omega_{pe}}{\omega_o - \omega_L(\underline{k})} \right\} \equiv S(k,x) \qquad (43)$$

(The first term in brackets is the usual rate of generation of Langmuir waves due to Cerenkov and Bremstrahlung emission. The second term is the Cerenkov emission at the low frequency coupled through the pump to act as an additional enhanced source for Langmuir waves and significatly dominates the first term.) At steady-state Eq. (42) can be formally solved for the spectum as

$$I(k,x) = \frac{S(k,x)}{\gamma_L^W + \gamma_L - \gamma_L \, Pfx^2} \qquad (44)$$

To solve Eq. (44) approximately for the angular spectrum I(x) we first add and subtract $\gamma_\ell$ to the denominator of the right side of Eq. (44) and divide both the numerator and denominator by $\gamma_\ell + \gamma_L (Pfx^2 - 1)$. The result may be written:

$$\frac{\gamma_L^W + \gamma_\ell}{\gamma_\ell + \gamma_L(Pfx^2-1)} - 1 = \frac{I_o}{I(k,x)} \quad , \tag{45}$$

where $I_o$ is defined by

$$I_o = \frac{S}{\gamma_\ell + \gamma_L(Pfx^2-1)} \quad , \tag{46}$$

and is of the order of magnitude of the thermal noise level of spectral
intensity. For unstable modes we must have $I(k,x) \gg I_o$, particularly near
the peak value of $I(k,x)$ at $k \approx k_m$. Hence, for $k \approx k_m$ Eq. (44) leads to

$$\gamma_L^W(k,x) - \gamma_L(k)(Pfx^2 - 1) \approx 0, \quad \frac{I_o}{I} \ll 1 \quad , \tag{47}$$

This merely states that at saturation the total growth rate of the strongly
excited modes is near zero. Let us define $r \equiv r(k) \equiv \nu_c/\gamma_\ell(k)$ to be the ratio
of the collision damping to Landau damping decrements, and

$$\gamma_L(k) = (1 + r)\,\gamma_\ell(k) \quad . \tag{48}$$

Substituting Eq. (48) in Eq. (47) at $k = k_m$ and using the expression for
$\gamma_L^W(k_m,x)$ given by Eq. (41), with $f(k_m) = 1$, we obtain from Eq. (47)

$$\exp\left\{\left(\tfrac{2}{3}\right)^{\frac{1}{2}}\left[\frac{2}{3}\left(\frac{k_D}{k_m}\right)^2 + 3\right]\sqrt{\frac{I(x)}{4\pi n\theta_e}}\,\sqrt{(1+F)}\right\} - (1+r)\,Px^2 + r = 0 \quad . \tag{49}$$

Solving Eq. (49) for $I(x)$ we finally have the desired expression for the saturated
angular spectrum $I(x)$:

$$\frac{I(x)}{4\pi n\theta_e} = \frac{\frac{27}{8}\,[\log\{(1+r)\,P\,x^2-r\}]^2}{\left[\left(\frac{k_D}{k_m}\right)^2 + \frac{9}{2}\right]^2}(1+F)^{-1} \quad , \qquad Px^2 \geq 1 \tag{50a}$$

A22

$$\approx \frac{\frac{27}{8} [\log \{(1+r)P\, x^2 - r\}]^2}{\left[\left(\frac{k_D}{k_m}\right)^2 + \frac{9}{2}\right]^2} \quad , \text{ since } 0 \leq F \leq 1/2 \qquad (50b)$$

providing $P\, x^2 > 1$. Equation (50) describes the saturated angular spectrum $I(x)$ of parametrically excited Langmuir waves in terms of the ratios $P$, $(k_D/k_m)$ and $r$. Note that the saturated spectrum is spread over all angles for which $P\, x^2 > 1$ and is thus quite broad in angle for $P \geq 2$. Furthermore, this angular spread coincides with the angles that are linearly excited by the instability ($P\, x^2 > 1$). This result justifies our previous assumption of a broad spectrum which was used in Sec. II. Note, too, that as $P$ increases the spectrum tends to become isotropic.

### 2. Total Wave Energy Density

The total saturated wave energy density

$$\frac{\langle |\delta E|^2 \rangle}{4\pi} = \int \frac{\frac{dk}{(2\pi)^3}}{4\pi} I(k) = 2 \int_0^1 dx \int k^2 \frac{dk}{2\pi} \frac{\frac{I(k,x)}{2\pi}}{4\pi} = \frac{1}{2\pi} \int_0^1 dx\, I(x) \ , \qquad (51)$$

is obtained by substituting Eq. (49) in Eq. (51) with the result

$$\frac{\langle \delta E^2 \rangle}{4\pi n \theta_e} = \frac{27}{4} \int_{1/\sqrt{P}}^1 dx\ \frac{[\log \{(1+r)P\, x^2 - r\}]^2}{\left[\left(\frac{k_D}{k_m}\right)^2 + \frac{9}{2}\right]^2}$$

which becomes

$$\frac{\langle \delta E^2 \rangle}{4\pi n \theta_e} \approx \frac{(27/4)}{\left[\left(\frac{k_D}{k_m}\right)^2 + \frac{9}{2}\right]^2} \left\{ [\log(1+r)P]^2 - 4[\log(1+r)P - 2] - \frac{8}{\sqrt{(1+r)P}} \right\} \quad (52)$$

for $(1+r)P \gg r$. The total wave energy is thus seen to increase rather slowly with the pump power ratio $P$ when $P$ is large, and to be quite small in the Landau damped regime, $r < 1$, and large in the collision damped regime, $r > 1$.

A23

## C. k-Dependence of Spectrum

Thus far we have determined the variation of the saturated spectrum with angle, given by Eq. (50) and the total spectral energy, given by Eq. (52). To complete the determination of the spectrum we now consider the dependence of the excited wave intensity on wave number k. However, to simplify matters we shall be content, in this paper, to limit ourselves to the gross features of the k dependence. In particular, we shall only calculate the half-widths of the spectrum at half maximum. The values of k at the half-width shall be denoted by $k_{\frac{1}{2}}$ which, in general will vary with the angle cosine x. Hence, if we denote the value of k at the peak of the spectrum by $k_p$, then by definition we have

$$\frac{I(k_{\frac{1}{2}},x)}{I(k_p,x)} = \frac{1}{2} . \tag{53}$$

This equation can be solved for $k_{\frac{1}{2}}$ by making use of Eq. (44) for $I(k_{\frac{1}{2}})$ and $I(k_p)$. To simplify the analysis let us add unity to each side of Eq. (45) and then take the logarithm of both sides to obtain

$$\log\frac{(\gamma_L^W + \gamma_{\mathcal{L}})}{\gamma_{\mathcal{L}}} - \log\left[1 + \frac{\gamma_L}{\gamma_{\mathcal{L}}}(Pfx^2-1)\right] = \log(1 + \frac{I_0}{I}) \sim \frac{I_0}{I(k,x)} . \tag{54}$$

The first term on the eft of Eq. (54) is determined by Eq. (41) as

$$\log\left(\frac{\gamma_L^W + \gamma}{\gamma_{\mathcal{L}}}\right) \sim (\frac{2}{3})^{\frac{1}{2}}\left[\frac{2}{3}\left(\frac{k_D}{k}\right)^2 + 3\right]\sqrt{\frac{I(x)}{4\pi n\theta_e}}$$

$$\equiv A(k) \tag{55}$$

Equations (54) and (55) determine $I(k,x)$ in terms of $I(x)$ or $A(k)$. Solving (54) and (56) for $I(k_{\frac{1}{2}},x)$ and $I(k_p,x)$ in terms of $A(k)$ and substituting these solutions into Eq. (53) we have, neglecting the variation of $I_0$ with k,

A24

$$A(k_{\frac{1}{2}}) - \log \{(1+r(k_{\frac{1}{2}})) \, P(k_{\frac{1}{2}}) \, f(k_{\frac{1}{2}}) \, x^2 - r(k_{\frac{1}{2}})\}$$

$$= 2[A(k_p) - \log \{(1+r(k_p)) \, P(k_p) \, f(k_p) \, x^2 - r(k_p)\}] , \qquad (56)$$

where we have used Eq. (48). Equation (56) may be rewritten to give

$$(A(k_{\frac{1}{2}}) - \log \{(1+r(k_{\frac{1}{2}})) \, P(k_{\frac{1}{2}}) \, f(k_{\frac{1}{2}}) \, x^2 - r(k_{\frac{1}{2}})\}) - (k_{\frac{1}{2}} \to k_p)$$

$$= A(k_p) - \log \{(1+r(k_p)) \, P(k_p) \, f(k_p) \, x^2 - r(k_p)\}$$

$$= \frac{I_o}{I(k_p, x)} \qquad (57)$$

For the sake of simplicity we consider the solution of Eq. (57) for $(1+r) \, P \gg r$. Then Eq. (57) becomes

$$A(k_{\frac{1}{2}}) - A(k_p) + \log \left\{ \frac{(1+r(k_p)) \, P(k_p) \, f(k_p)}{(1+r(k_{\frac{1}{2}})) \, P(k_{\frac{1}{2}}) \, f(k_{\frac{1}{2}})} \right\} = \frac{I_o}{I(k_p, x)} \qquad (58)$$

with (A9), $\quad P(k_p)/P(k_{\frac{1}{2}}) = \dfrac{\gamma_L(k_D)}{\gamma_L(k_{\frac{1}{2}})} = \dfrac{\gamma_{\angle}(k_{\frac{1}{2}}) \, (1+r(k_{\frac{1}{2}}))}{\gamma_{\angle}(k_p) \, (1+r(k_p))} , \qquad (59)$

so that Eq. (58) becomes

$$A(k_{\frac{1}{2}}) - A(k_p) + \log \left\{ \left( \frac{\gamma_{\angle}(k_{\frac{1}{2}})}{\gamma_{\angle}(k_p)} \right) \left( \frac{f(k_p)}{f(k_{\frac{1}{2}})} \right) \right\} = \frac{I_o}{I(k_p, x)} \qquad (60)$$

or with (55)

$$\left[ \left( \frac{2}{3} \right)^{3/2} \sqrt{\frac{I(x)}{4\pi n \theta_e}} - \frac{1}{2} \right] \left[ \left( \frac{k_D}{k_{\frac{1}{2}}} \right)^2 - \left( \frac{k_D}{k_p} \right)^2 \right] + \log \frac{f(k_p)}{f(k_{\frac{1}{2}})} = \frac{I_o}{I} \qquad (61)$$

Since, as will be seen, the spectrum is relatively narrow in k we can approximate $k_p \approx k_m$ in (61) and expand the left-hand-side about $k = k_p \approx k_m$. For $I(x)/4\pi n \theta_e \ll 2(3/4)^3$, we can then write for (61),

A25

$$\left(\frac{k_D}{k_m}\right)^2 \left[ + \frac{\Delta k}{k_m} - \frac{3}{2}\left(\frac{\Delta k}{k_m}\right)^2 \right] + \left(\frac{\Delta k}{\Delta k_o}\right)^2 = \frac{I_o}{I} \ , \qquad (62)$$

where we have used from Eq. (5) that

$$f(k)^{-1} = 1 + \frac{(k - k_m)^2}{(\Delta k_o)^2} + \dots \ , \quad \frac{k - k_m}{\Delta k_o} < 1 \ , \qquad (63)$$

and $\Delta k_o$ is the "linear width" given by

$$\Delta k_o \approx \frac{k_D}{3}\left(\frac{m_e}{m_i}\right)^{\frac{1}{2}} \ . \qquad (64)$$

For $\Delta k/k_m \ll 2/3$ and $I_o/I \ (k_m,x) \ll 1$, Eq. (62) is solved to yield two solutions for $\Delta k$ corresponding to the half-width of I on either side of the peak value of I. Those solutions are,

$$\Delta k_{(1)} \approx 0 \ , \qquad (65a)$$

$$\Delta k_{(2)} \approx - \Delta k_o \left(\frac{\Delta k_o}{k_D}\right)\left(\frac{k_D}{k_m}\right)^3 \qquad (65b)$$

Equations (65a) and (65b) show that the k-spectrum $I(k,x)$ is skew-symmetric about $k_m$ towards lower values of k. For a hydrogen plasma with $k_m/k_D \sim 0.2$, we note that $\Delta k_{(2)}$ from Eq. (65b) implies a k width equal to the linear width $\Delta k_o$. Equations (65a) and (65b) apply to the case where $I_o/I \ll 1$, i.e., above threshold for instability. At threshold we expect, on physical grounds, that the width of the spectrum $\Delta k$ to be equal to the linear width $\Delta k_o$.

A26

## D. Fine Structure of Angular Spectrum

Thus far we have ignored the explicit effects of F on the spectrum in Eq. (41). We have been able to do so because $|F| < 1/2$ and, generally speaking, F will not alter the total spectral energy by more than about 30%. However, for large enough P we find that F can have an unexpected and surprising effect on the shape of the angular spectrum. Namely, F can cause the spectrum to peak at a substantial angle to the direction of the pump. That F can influence the shape of $I(x)$ at large P is easy to understand, since for large enough P it can be seen that $I(x)$ as given by Eq. (41b) varies very slowly with x, and indeed, tends to become isotropic for $P \gg 1$. Hence, for large P, the x variation of $I(x)$ may well be influenced by the subdominant quantity F in Eq. (41a). That F causes $I(x)$ to maximize at $x \neq 1$, i.e., that $I(x)$ peaks off the pump direction, is illustrated for the particular case of $P = 10$ and $k_m/k_D = 0.21$. For this case we evaluate F by numerically solving the set of Eqs. (29), (30), (38a), (39), (40a), and (41a) to obtain an approximate value for F. This numerically evaluated F is then used in Eq. (50b) to evaluate $I(x)$. These numerical results are summarized in Fig. 4 where we plot F, $\log(Px^2)$ and $I(x) \sim (1 + F)^{-1} (\log Px^2)^2$ as functions of $\theta = \cos^{-1}x$. It is seen in Fig. 4 that $I(x)$ peaks at $x \approx 0.9$ which corresponds to an angle of about 26° off the pump direction. For weaker pumping, smaller P, the peak in $I(x)$ tends to lie along the pump direction. It is interesting to note that in a recent computer simulation, by Biskamp and Chodura,[15] of the current driven ion acoustic instability the angular distribution exhibits the same structure as Fig. 4 with a peak at about an angle of 40° with the current direction. Although the ion acoustic instability is quite different from the parametric instability, it should be noted that the saturation mechanisms and the angular dependence of the linear growth rates are both similar for the two instabilities.[16]

A27

## IV. ANOMALOUS COLLISION FREQUENCY AND DISSIPATION RATE

With the saturated spectrum given by Eq. (50) we are in a position to calculate the anomalous collision frequency and dissipation due to the Langmuir waves. The dissipation is governed by the temporal evolution of the averaged electron distribution function $\langle F_e(\underline{v},t) \rangle$[12]

$$\frac{\partial \langle F_e(\underline{v},t) \rangle}{\partial t} = \frac{e}{m} \ \underline{E}_o \ \sin \omega_o t \ \cdot \frac{\partial \langle F_e(\underline{v},t) \rangle}{\partial \underline{v}}$$

$$+ \ \frac{\partial}{\partial \underline{v}} \cdot \underline{\underline{D}}(\underline{v}) \cdot \frac{\partial}{\partial \underline{v}} \ \langle F_e(\underline{v},t) \rangle \tag{66}$$

where $\underline{\underline{D}}(\underline{v})$ is the resonance broadened diffusion tensor defined by Eq. (14a). Equation (66) has been rigorously derived in Ref. 12 for any external field. The kinetic energy density, K.E., of electrons in the rest frame, oscillating with pump, is defined by

$$K.E. \equiv n \int d\underline{v} \ \frac{1}{2} \ m_e (\underline{v} - \underline{v}_o)^2 \ \langle F_e(\underline{v},t) \rangle \tag{67}$$

where $\underline{v}_o = - eE_o \cos(\omega_o t)/(m\omega_o)$. Substituting Eq. (66) into the time derivative of (67), we use an integration by parts to show that the first term on the right side of Eq. (66) vanishes and we are then left with

$$\frac{\partial K.E.}{\partial t} = \frac{1}{2} \ nm_e \int d\underline{v} (\underline{v} - \underline{v}_o)^2 \ \frac{\partial}{\partial \underline{v}} \left( \underline{\underline{D}}(\underline{v}) \cdot \frac{\partial \langle F_e \rangle}{\partial \underline{v}} \right)$$

$$= - \ nm_e \int d\underline{v} (\underline{v} - \underline{v}_o) \cdot \underline{\underline{D}}(\underline{v}) \cdot \frac{\partial \langle F_e \rangle}{\partial \underline{v}}$$

$$\approx - \ nm_e \int d\underline{v} \ \underline{v} \cdot \underline{\underline{D}}(\underline{v}) \cdot \frac{\partial \langle F_e \rangle}{\partial \underline{v}} \tag{68}$$

A28

since the main contribution to Eq. (68) comes from $v \sim v_p$ and $v_o < v_e \ll v_p$.
Substituting Eq. (14a) for $\underline{D}(\underline{v})$ into Eq. (68) we have

$$\frac{\partial \text{K.E.}}{\partial t} = - \frac{e^2 n}{m_e} \sum_\nu \text{Re} \int \frac{d\underline{k}}{(2\pi)^3} \ I_\nu(\underline{k}) \int d\underline{v} \int_0^\infty dt \hat{\underline{k}} \cdot \underline{v}$$

$$\text{x} \quad \hat{\underline{k}} \cdot \frac{\partial \langle F_e \rangle}{\partial \underline{v}} \ \exp[- i(\omega - \underline{k} \cdot \underline{v})t - \frac{1}{2} \langle [\underline{k} \ \delta\underline{r}(- t)]^2 \rangle] \ . \qquad (69)$$

But the main contribution to the $\underline{v}$ integration comes from $\underline{k} \cdot \underline{v} \approx \omega_L$ so that,
ignoring the acoustic energy $I_a(k)$, Eq. (69) becomes

$$\frac{\partial \text{K.E.}}{\partial t} = - \frac{e^2 n}{m_e} \ \text{Re} \int \frac{d\underline{k}}{(2\pi)^3} \ \frac{I(\underline{k})}{k^2} \ \omega_L \int d\underline{v} \int_0^\infty dt \ \underline{k} \cdot \frac{\partial \langle F_e \rangle}{\partial \underline{v}}$$

$$\text{x} \quad \exp[- i(\omega - \underline{k} \cdot \underline{v})t - \frac{1}{2} \langle [\underline{k} \cdot \delta\underline{r}(- t)]^2 \rangle] \qquad (70)$$

If we now substitute the imaginary part of Eq. (8) into Eq. (70) we have

$$\frac{\partial \text{K.E.}}{\partial t} = \int \frac{d\underline{k}}{(2\pi)^3} \ \frac{I(\underline{k})}{4\pi} \ \omega_L \ I_m \ \chi_e^{NL}(\underline{k}, \omega_L) \ , \qquad (71)$$

and, with Eqs. (6), (7), and (47)

$$I_m \ \chi_e^{NL}(\underline{k}, \omega_L) = 2(\gamma_L^W + \underline{\nu})/\omega_L$$

$$= 2[\gamma_L \text{Pf}(k) \ x^2 - \nu]/\omega_L$$

so that Eq. (71) becomes

$$\frac{\partial \text{K.E.}}{\partial t} = 2 \int \frac{d\underline{k}}{(2\pi)^3} \ \frac{I(\underline{k})}{4\pi} \ [\gamma_L \text{Pf}(k) \ x^2 - \nu] \qquad (72)$$

A29

$$\frac{\partial K.E.}{\partial t} \approx 2 \int_0^1 \frac{dx}{2\pi} I(x) [\gamma_L Px^2 - \nu] \, , \; Px^2 \geq 1 \, , \tag{73}$$

for the many cases in which $I(k)$ is narrower in k than $f(k)$. It is now seen that the heating rate is affected by the angular spread of the spectrum. The (angular) integral over x with $I(x)$ given by Eq. (50) is tabulated and can be easily performed. However, it is useful to express the resulting integral in terms of the total wave energy density $\langle |\delta E|^2 \rangle$ given by Eq. (52). This can be approximately done for $(1 + r)P \gg r$ to yield

$$\frac{\partial K.E.}{\partial t} \approx \frac{2}{3} \alpha \gamma_L P \frac{\langle |\delta E|^2 \rangle}{4\pi} \, , \tag{74a}$$

where $\langle |\delta E|^2 \rangle$ is given by (52), and $\alpha$ is given by

$$\alpha = 1 + (1 - P^{-3/2}) \frac{6}{3 + \ln[(1+r)P]} \, . \tag{74b}$$

The quantity $\alpha$, which comes from the angular dependence of $I(x)$, varies slowly between 1 and about 2. If we define the net dissipation rate, or enhanced collision frequency, $\nu^*$ by

$$\frac{\partial K.E.}{\partial t} \equiv \frac{\nu^* E_o^2}{8\pi} \tag{75}$$

then we have with (74), (52), and (4a)

$$\nu^* = \alpha \frac{\omega_L}{12} \frac{\langle \delta E^2 \rangle}{4\pi n\theta} \tag{76a}$$

$$= \alpha \frac{\omega_L}{12} \frac{27/4}{(k_D^2/k_m^2 + 9/2)^2} \left\{ \left( \log[(1+r)P] \right)^2 - 4 \left( \log[(1+r)P] - 2 \right) \right.$$

$$\left. - \frac{8}{\sqrt{(1+r)P}} \right\} \tag{76b}$$

A30

It is important to note that the dissipation rate $\nu^*$ has precisely the same form as that proposed by Kruer and Dawson to describe their determination of $\nu^*$ by simulation.[1] In place of $\gamma_L P$ Kruer and Dawson have the maximum growth rate $\gamma^{growth}$ which here is equal to $\gamma_L P$. Two qualitative features of this formula have been observed by experiment or by simulation. In particular, $\nu^*$ increases very slowly with P for large P. This result may be viewed as a "saturation" of the enhancement of the collision frequency. Such a "saturation" for $\nu^*$ has been experimentally observed by Ingraham;[4] secondly, $\nu^*$ is proportional to the maximum growth rate, approximately given here by $\gamma_L P$. This behavior has been observed by computer simulation. Quantitatively, the value of $\nu^*$ observed in computer simulations[1] is found to be in agreement with Eq. (76).

## V. TOTAL WAVE ENERGY--EXAMPLES

### A. Ionosphere

It is useful to consider the total energy of waves for some specific cases since, generally speaking, transport phenomena depend on the total energy. In Table 1 we show numerical results for the total energy density of waves given by Eq. (52) as compared with $n\theta_e$. Three matching wave numbers are considered corresponding to the Landau damped regime, the collisionally damped regime and the region of transition between the two. In this illustration of Eq. (52) we use conditions relevant to the F region of the ionosphere where parametrically excited waves have been observed,[2] viz., $\nu_c/\omega_{pe} \approx 2 \times 10^{-5}$, $k_D \approx 3$ cm$^{-1}$. We note that the total wave energy density is very sensitive to $k_D/k_m$ in the neighborhood of $r = 1$, corresponding to $k_D/k_m \approx 5$. Indeed, the energy changes by at least an order of magnitude for $k_D/k_m = 4.5$ to $k_D/k_m = 6.5$. The saturation is quite strong for $r \ll 1$, and is much weaker for $r \gg 1$.

### B. Computer Simulations

It has already been verified[8] that the total saturated wave energy predicted by perturbed orbit theory is in good agreement with computer simulations.[1] For the sake of completeness it is useful to make a typical comparison, here, between Eq. (52) and the total wave energy found in computer simulation. [Computer simulations are often dominated by the oscillating two-stream instability. However, it can be proven that (52), although derived here for the decay instability, also applies to the oscillating two-stream instability for $T_e \gg T_i$ as well as at $T_e \approx T_i$. This is indicated by the results of Ref. 8.] Consider, then the case $E_o/\sqrt{(4\pi n\theta_e)} = 0.5$ given by Kruer and Dawson.[1] In this case $(1+r)P$ may lie between 100 and 200, and $k_D/k_m \approx 0.25$. Substituting these values into Eq. (52) we easily find that

A32

$$\frac{\langle \delta E^2 \rangle}{4\pi n \theta_e} = \begin{cases} 0.17 \text{ for } (1+r)P=100 \\ 0.23 \text{ for } (1+r)P=200 \end{cases}$$

This is in clear agreement with the simulation value of $\langle \delta E^2 \rangle (4\pi n \theta)^{-1} = 0.2$. [We caution the reader to note that acoustic waves are excited in the simulations of Kruer and Dawson for $E_0 / \sqrt{4\pi n \theta_e} < 0.4$ and will contribute to saturation. This contribution has not been included here, since $T_e \approx T_i$, but was included in Ref. 8, and found to decrease $\langle \delta E^2 \rangle / 4\pi n \theta_e$ by about an order of magnitude below Eq. (52).]

## C.  Comparison of Saturation Mechanisms

To obtain a clear idea of the relative strengths of the saturation by perturbed orbits compared to induced scatter off ions for the parametric instability we consider the total wave energy predicted by the two mechanisms. In Table 2 we show the total wave energy for various values of $P_c = E_0^2 / E_{thc}^2$, where $E_{thc}^2$ is the threshold field in the collision damped region. The values in parentheses are the total energy as predicted by the mechanism of induced scattering off ions.[17] It is apparent that the perturbed orbit mechanism is dominant for $r \lesssim 1$. On the other hand, for $r \gg 1$ the perturbed orbit mechanism predicts larger energies than the mechanism of induced scattering from ions. Hence the transition between the two regions of linear damping establishes a simple demarcation between the regions where the saturation by perturbed orbits is dominant or not.

| P | $k_m/k_D = 0.22$, $r \ll 1$ | $k_m/k_D = 0.19$, $r = 1$ | $k_m/k_D = 0.15$, $r \gg 1$ |
|---|---|---|---|
| 5 | 0.0062 | 0.011 | 0.14 |
| 10 | 0.017 | 0.022 | 0.18 |
| 20 | 0.035 | 0.038 | 0.21 |
| 30 | 0.049 | 0.05 | 0.23 |

Table 1.  Total wave energy  $\langle \delta E^2 \rangle (4\pi)^{-1}$ in units of $n\theta_e$ for range of pump intensity P and matched wave number $k_m$ as predicted by perturbed orbit saturation for $\nu_c/\omega_{pe} = 2 \times 10^{-5}$.

| $P_c$ | $k_m/k_D = 0.21$, $r = 1.6$ | $k_m/k_D = 0.23$, $r = 0.3$ | $k_m/k_D = 0.25$, $r = 0.1$ |
|---|---|---|---|
| 10 | .023 (.024) | .0028 (.007) | $\sim 0$ ($\sim 0$) |
| 20 | .043 (.110) | .010 (.076) | .001 (.004) |
| 40 | .070 (.290) | .024 (.279) | .006 (.160) |

Table 2.  Total wave energy  $\langle \delta E^2 \rangle (4\pi)^{-1}$ in unites of $n\theta_e$ for range of pump intensity $P_c$ and matched wave number $k_m$ as predicted by perturbed orbit (induced scattering from ions) saturation for $\nu_c/\omega_{pe} = 3 \times 10^{-4}$.

## VI. SUMMARY AND CONCLUSIONS

A. The primary aim of this work was to determine the saturated spectrum of the parametric decay instability and to show that this spectrum is broad in angle. The nonlinear mechanism responsible for this spectrum was the scattering and heating of electrons by Langmuir waves (perturbed electron orbits). An analytical solution is found for the angular spectrum in Sec. III-A and is given by Eq. (50).

B. The width of the spectrum in k is determined in Sec. III-C, where the spectral half-width is found to be proportional to the half-width of the linear growth rate. The total saturated wave energy density is given by Eq. (52) and is in agreement with computer simulations.[1]

C. The anomalous collision frequency $\nu^*$, which describes the dissipation rate of the pump, is given, in Sec. V, by (76). It is pointed out that the enhancement of $\nu^*$ appears to saturate for large pump intensities and that $\nu^*$ is proportional to the linear growth rate of the fastest growing mode. This behavior has been confirmed by experimental observations of Ingraham[4] and simulations.[1] The latter observations are in quantitative agreement with Eq. (76).

D. The angular dependence of the nonlinear damping rate of Langmuir waves, denoted by $\gamma_L^W$, has been analytically obtained, and is given by Eq. (41). This is the first time (to our knowledge) that $\gamma_L^W$ has been calculated fo the nonlinear mechanism in which Langmuir waves deflect electrons (perturbed orbits). To obtain the variation of $\gamma_L^W$ with angle it was necessary to consider deflections of electrons by nonresonant as well as resonant Langmuir waves.

E. A comparison is made between the present results of saturation by perturbed orbits and the results of nonlinear Landau damping. This is described in Sec. V-C.

A35

# APPENDIX A-1

To obtain $\gamma_p^{NL}$ we consider the nonlinear dielectric function in the presence of the pump for the decay branch of the parametric instability. The decay branch may be treated separately since linearly the oscillating two-stream instability and the decay instability occur in disjoint regions of k space corresponding to $\delta \gtrless o$, where $\delta = \omega_o - \omega_L(k)$, and nonlinearly the orbit perturbations do not result in any transfer between these regions. The decay branch of the parametric instability is described by the dielectric function[13]

$$\epsilon_{\text{Pump}}(\underline{k},\omega) = \epsilon(\underline{k},\omega) - \left\{ \frac{\Lambda_e}{2} \left[ \chi_e(\underline{k},\omega) - \chi_e(\underline{k},\omega-\omega_o) \right] \right\}^2 \frac{1}{\epsilon(\underline{k},\omega-\omega_o)} \quad , \qquad \text{(A1)}$$

where $\quad \Lambda_e = \left( \frac{\omega_{pe}}{\omega_o} \right)^2 \left( \frac{k}{k_D} \right) \cdot \sqrt{\frac{(\hat{k}\cdot E_o)^2}{4\pi n \theta_e}} .$

Here $\epsilon_{\text{Pump}}$ denotes the dielectric function of the plasma in the presence of a pump $E_o \sin \omega_o t$, where $\epsilon$ is the usual linear dielectric function in the absence of the pump, $\epsilon = 1 + \sum_s \chi_s$, with $\chi_s$ as the linear susceptibility for species s. The zeros of $\epsilon_{\text{Pump}}$ determine the frequencies and growth rates of plasma modes made unstable by the external pump.

It has been demonstrated in a previous publication that the nonlinear dielectric function with the inclusion of particle-orbit perturbations due to finite amplitude unstable waves has precisely the same form as Eq. (A1) with the linear susceptibilities $\chi_s$ everywhere replaced by nonlinear susceptibilities $\chi_s^{NL}$, that is,

$$\epsilon_{\text{Pump}}^{NL}(\underline{k},\omega) = \epsilon^{NL}(\underline{k},\omega) - \left\{ \frac{\Lambda_e}{2} \left( \chi_e^{NL}(\underline{k},\omega) - \chi_e^{NL}(\underline{k},\omega-\omega_o) \right) \right\}^2 \frac{1}{\epsilon^{NL}(\underline{k},\omega-\omega_o)} \quad , \qquad \text{(A2)}$$

where

$$\epsilon^{NL}(\underline{k},\omega) = 1 + \sum_s \chi_s^{NL}, \qquad \text{(A3)}$$

A36

and

$$\chi_s^{NL}(\underline{k},\omega) = -i\,\frac{\omega_{os}^2}{k^2}\int_0^\infty d\tau \int d^3v\; e^{i(\omega - \underline{k}\cdot\underline{v})\tau}\;\langle e^{-i\underline{k}\cdot\delta\underline{r}_s(-\tau)}\rangle\underline{k}\cdot\frac{\partial\langle F_s\rangle}{\partial\underline{v}}\;,$$

with $\delta\underline{r}_s(\tau)$ the wave perturbation of the particle orbit as given by Eq. (9).

To calculate $\gamma_p^{NL}$ we note from Appendix B that, for $(\omega_d(o)/kV_e)^2 \ll 1$,

$$\text{Re }\chi_e^{NL} \sim \text{Re }\chi$$

so that, in (A2),

$$\{\chi_e^{NL}(\underline{k},\omega) - \chi_e^{NL}(\underline{k},\omega-\omega_o)\}^2 \sim \left\{\frac{k_D^2}{k^2}\right\}^2$$

and, hence, (A2) becomes

$$\epsilon_{PUMP}^{NL}(\underline{k},\omega) = \epsilon^{NL}(\underline{k},\omega) - \frac{k_D^2/4k^2\,\Lambda^2\,x^2}{\epsilon^{NL}(\underline{k},\omega-\omega_o)} \tag{A4}$$

where $\Lambda^2 \equiv (\omega_{pe}/\omega_o)^4\,E_o^2\,(4\pi n\theta_e)^{-1}$ and $x \equiv (\hat{\underline{k}}\cdot\hat{\underline{e}}_o)$. Equation (A4) accounts for nonlinearities in unstable wave fluctuations through the perturbed orbit $\delta\underline{r}(-\tau)$. The nonlinear mode frequencies and growth rates, of the parametric instability, in the presence of finite amplitude wave fluctuations are determined by setting

$$\epsilon_{PUMP}^{NL}(\underline{k},\omega) = 0\quad,$$

with complex solution

$$\omega = \omega_p^{NL} - i\gamma_P^{NL}$$

where $\omega_p^{NL}$ is the nonlinear frequency and $\gamma_p^{NL}$ is the desired nonlinear growth rate. The problem, now, is to carry out this solution so as to obtain $\gamma_p^{NL}$. As one might expect, the solution of (A4) for $\gamma_p^{NL}$ is similar to the solution, given in Ref. 13 of (A1) for the linear parametric growth rate $\gamma_p^L$. We repeat the main steps as they apply to (A4). The solution of (A4) for the zero of

$\epsilon^{NL}_{PUMP}$ is given in terms of the zeros of $\epsilon^{NL}(\underline{k},\omega)$ and $\epsilon^{NL}(\underline{k},\omega-\omega_o)$. These zeros are the nonlinear high and low frequency modes that are coupled by the pump. The zeros of $\epsilon^{NL}(\underline{k},\omega)$ and $\epsilon^{NL}(\underline{k},\omega-\omega_o)$ are the high (Langmuir) and low (acoustic) frequency modes denoted by

$$\omega_{HIGH} = \omega_L^{NL} - i\gamma_L^{NL} \ ,$$

and

$$\omega_{LOW} = \omega_a^{NL} - i\gamma_a^{NL} \ .$$

Indeed, the calculation of $\omega_L^{NL}$ and $\gamma_L^{NL}$ is the subject of Sections II and III of this paper. In the neighborhoods of the zeros of $\epsilon^{NL}$ we have

$$\epsilon^{NL}(\underline{k}, \pm\omega) \sim \frac{1}{2} \ [\omega - (\pm\omega_L^{NL} - i\gamma_L^{NL})]/\omega_L^{NL}$$

$$\epsilon^{NL}(\underline{k},\pm(\omega-\omega_o)) \sim \frac{1}{2}\left(\frac{k_D}{k}\right)^2 \ [\omega-\omega_o - (\pm\omega_a^{NL} - i\gamma_a^{NL})]/\omega_a^{NL} \qquad (A5)$$

Hence if $\omega \sim \omega_L^{NL}$ and if $\omega_o$ is chosen such that $\omega-\omega_o \sim \omega_a^{NL}$ then (A4) becomes

$$\epsilon^{NL}_{PUMP}(\omega) \sim \frac{\omega - \omega_L^{NL} + i\gamma_L^{NL}}{1/2 \ \omega_L^{NL}} + \frac{1}{2} \ \frac{\omega_a^{NL} \Lambda^2 x^2}{\omega-\omega_o + \omega_a^{NL} + i\gamma_a^{NL}} \qquad (A6)$$

If we now solve this for the imaginary part of $\omega$ we obtain

$$\gamma_p^{NL} \equiv I_m \ \omega = \gamma_L^{NL} - \frac{1}{15} \ \frac{\omega_a^{NL} \ \omega_L^{NL} \ \Lambda^2 \ (\gamma_a^{NL} - \gamma_p^{NL}) \ x^2}{(\Delta\omega)^2 + (\gamma_a^{NL} - \gamma_p^{NL})^2} \qquad (A7)$$

where

$$\Delta\omega \equiv \omega_L^{NL} + \omega_a^{NL} - \omega_o \qquad (A8)$$

is a nonlinear generalization of the "frequency mismatch".[14] Finally, with $\gamma_a^{NL} \gg \gamma_p^{NL}$ (at saturation $\gamma_p^{NL} \sim o$), Eq. (A7) becomes

A38

$$\gamma_p^{NL} = \gamma_L^{NL} - \gamma_L \left( \frac{\omega_L^{NL}}{\omega_L} \right) \left( \frac{\gamma_a/\omega_a}{\gamma_a^{NL}/\omega_a^{NL}} \right) P \, f \, \chi^2$$

$$f \equiv [1 + (\Delta\omega / \gamma_a^{NL})^2]^{-1}$$

$$P \equiv \frac{1}{16} \Lambda^2 \frac{\omega_a \, \omega_L}{\gamma_a \, \gamma_L} \tag{A9}$$

so that $P$ will be recognized as the <u>pump ratio</u>, i.e., the ratio of the pump intensity to the linear threshold value of the pump intensity. Equation (A9) expresses the nonlinear growth rate of the parametric decay instability in terms of the nonlinear damping rates of Langmuir and acoustic waves, $\gamma_L^{NL}$ and $\gamma_a^{NL}$. These damping rates are, of course, determined by $\epsilon^{NL}(\underline{k},\omega)$ as, (e.g., see (A5))

$$\gamma_L^{NL} = \left[ \frac{\partial}{\partial\omega} \text{Re } \epsilon^{NL}(\omega_L) \right]^{-1} \text{Im } \epsilon^{NL}(\omega_L)$$

In deriving (A9) we have temporarily ignored the effects of collisional damping. To recover collision damping we note that in the presence of collisions

$$\gamma_L^{NL} = \nu_c + \left[ \frac{\partial}{\partial\omega} \text{Re } \epsilon^{NL}(\omega_L) \right]^{-1} \text{Im } \epsilon^{NL}(\omega_L)$$

$$\gamma_L = \nu_c + \gamma_{\mathscr{L}} \tag{A10}$$

where $\nu_c$ is the collisional damping decrement and $\gamma_{\mathscr{L}} \equiv \gamma_{\mathscr{L}}(k)$ is the Landau damping decrement. Substituting (A10) into (A9) we thus have

$$\gamma_p^{NL} = (\frac{\partial}{\partial\omega} \text{Re } \epsilon^{NL})^{-1} \text{Im } \epsilon^{NL}(\omega_L) + \nu_c - \gamma_L \left( \frac{\omega_L^{NL}}{\omega_L} \right) \left( \frac{\gamma_a/\omega_a}{\gamma_a^{NL}/\omega_a^{NL}} \right) Pf \; \chi^2 \; , \tag{A11}$$

A39

For the special case $\gamma_a/\omega_a \simeq \gamma_a^{NL}/\omega_a^{NL} \simeq 1$, corresponding to $T_e \gtrsim T_i$ and $\omega_L^{NL}/\omega_L \simeq 1$, we write for Eq. (A11)

$$\gamma_p^{NL} = \gamma_L^W + \gamma_L - \gamma_L P \, f \, x^2 ,$$

$$\gamma_L^W + \gamma_L \doteq \left[ \frac{\partial}{\partial \omega} \, \text{Re} \,\, \epsilon^{NL}(\omega_L) \right]^{-1} \text{Im} \,\, \epsilon^{NL}(\omega_L) , \qquad (A12)$$

which is Eq. (4).

One final comment should be made with regard to Eq. (A12). The derivation of Eq. (A9) resulted in a resonance function $f(k)$ which is valid only for $\Delta\omega \ll \gamma_a$ , i.e., very close to $k_m$.[9] More generally we use

$$f(k) = \left[ 1 + \left( \frac{\Delta\omega}{2\gamma_a} \right)^2 (\omega_a + \delta)^2/\omega_a \delta \right]^{-1} ; \quad k < k_c$$

$$= 0 \qquad\qquad\qquad\qquad\qquad ; \quad k > k_c \qquad (A13)$$

where $k_c$ satisfies $\delta(k_c) = 0$, and separates the decay instability from the oscillating two-stream instability. Clearly for $\Delta\omega \ll \gamma_a$ Eq. (A13) reduces to the previous form, while more generally it provides the necessary cutoff between the two branches of the instability.

## APPENDIX

The real part of the susceptibility is given by Eq. (21) as

$$\text{Re } \chi_s^{NL}(\underline{k},\omega) = \frac{\omega_{ps}^2}{k^2} \int d^3v \; \underline{k} \cdot \frac{\partial \langle F_s \rangle}{\partial \underline{v}} \int_0^\infty dt \text{ Re } \exp\{i(\omega - \underline{k} \cdot \underline{v})t$$

$$- \frac{1}{3} \underline{k} \cdot \underline{D}(\underline{v}) \cdot \underline{k} \; t^3 - \frac{1}{2}[\omega_d^{nr}(v)]^2 \; t^2\} \tag{B1}$$

However, the main contribution to the $\underline{v}$ integration in (B1) comes from $v \leqslant v_s$. This is because the t integral is a slowly varying function of $v$. (Note that this is not the case for $I_m \chi_s^{NL}$ since, then, the time integral is sharply peaked about $v = v_p \gg v_s$.) Hence, from Eq. (14a), $D(\underline{v})$ will be very close to zero so that (B1) reduces to

$$\text{Re } \chi_s^{NL}(\underline{k},\omega) = \frac{\omega_{ps}^2}{k^2} \int d^3v \; \underline{k} \cdot \frac{\partial \langle F_s \rangle}{\partial \underline{v}} \int_0^\infty dt \text{ Re } \exp\{i(\omega - \underline{k} \cdot \underline{v})t$$

$$- \frac{1}{3} \underline{k} \cdot \underline{D}(\underline{v}) \cdot \underline{k} \; t^3 - \frac{1}{2}[\omega_d^{nr}(v)]^2 \; t^2\}$$

$$= \frac{\omega_{ps}^2}{k^2} \int d^3v \; \underline{k} \cdot \frac{\partial \langle F_s \rangle}{\partial \underline{v}} \frac{(\omega - \underline{k} \cdot \underline{v})}{\omega_d^2(v)} \; Y\left(\frac{\omega - \underline{k} \cdot \underline{v}}{\sqrt{2} \; \omega_d(v)}\right) , \tag{B2}$$

where $Y(\alpha) \equiv \alpha^{-1} \exp(-\alpha^2) \int_0^\alpha dt \exp(t^2)$ , a function discussed in Ref. 18. Since the integral is dominated by $\underline{v}$'s which satisfy $v \leqslant v_s$, so that $\omega = \omega_L \gg \underline{k} \cdot \underline{v}$, we use the asymptotic expansion for small $\underline{k} \cdot \underline{v}/\omega$ in (B2) to obtain

$$\text{Re } \chi_s^{NL} = -\frac{\omega_{ps}^2}{\omega^2} \left(1 + \frac{3v_s^2}{v_p^2}\left[1 + \frac{v_p^2}{v_s^2} \; \frac{\omega_d^2(o)}{\omega^2}\right]\right) \tag{B3}$$

where $\omega_d(o) \equiv \omega_d(\underline{v})$ at $\underline{v} = o$. From (14), we see that

A41

$$\omega_d^2(o) = \frac{e^2 \, k^2}{m_e^2} \int \frac{d^3 \, k'}{(2\pi)^3} \, (\hat{\underline{k}} \cdot \hat{\underline{k}}')^2 \, I(\underline{k}')$$

$$\sim \frac{1}{2} \left( x^2 + \frac{1}{3} \right) \omega_{pe}^2 \, \frac{v_e^2}{v_p^2} \, \frac{\langle \delta E^2 \rangle}{4\pi n \theta_e} \tag{B4}$$

Therefore, (B3) for electrons can be written

$$\text{Re } \chi_e^{NL} = - \frac{\omega_{pe}^2}{\omega^2} \left( 1 + \frac{3 v_e^2}{v_p^2} \left[ 1 + \frac{1}{2} (x^2 + \frac{1}{3}) \, \frac{\langle \delta E^2 \rangle}{4\pi n \theta_e} \right] \right) \tag{B5}$$

Correspondingly, the Langmuir frequency is shifted by the fluctuating waves to

$$(\omega_L^{NL})^2 = \omega_{pe}^2 \left( 1 + \frac{3 k^2}{k_D^2} \left[ 1 + \frac{1}{2} (x^2 + \frac{1}{3}) \, \frac{\langle \delta E^2 \rangle}{4\pi n \theta_e} \right] \right) \tag{B6}$$

Hence, we explicitly have a turbulence correction to the Langmuir frequency. This turbulence correction appears as an <u>effective temperature</u> increase given by

$$v_e^2 \rightarrow v_e^2 \left( 1 + \frac{1}{2} (x^2 + \frac{1}{3}) \, \frac{\langle \delta E^2 \rangle}{4\pi n \theta_e} \right)$$

Furthermore, with (L5) and the matching condition,

$$\omega_o \simeq \omega_L^{NL} (k) \, ,$$

it is clear that increasing turbulence will result in the excited waves occuring at longer wavelengths. This prediction has been observed in recent computer simulations.[1] In these simulations, however, the transition to larger wavelengths is directly correlated with electron heating.

A42

Equation (B3) gives Re $\chi_s^{NL}(\underline{k}, \omega - \omega_0)$ in the neighborhood of $\omega - \omega_0 \cdot \omega_n$. We can evaluate $\chi_s^{NL}(\underline{k}, \omega_a)$ in the same manner as above. For present purposes we need only use the result that for $\langle \delta E^2 \rangle / 4\pi n \theta_e \ll 1$ we have

$$\text{Re } \chi_s^{NL}(\underline{k}, \omega_a) \approx \text{Re } \chi_s(\underline{k}, \omega_a), \quad \frac{\langle \delta E^2 \rangle}{4\pi n \theta_e} \ll 1 \tag{B7}$$

We wish to show that

$$\omega_d^r(\underline{v}) < \omega_d^{nr}(\underline{v}), \quad \text{when} \quad \frac{\langle \delta E^2 \rangle}{4\pi n \theta_e} \gtrsim \left(\frac{k}{k_D}\right)^4 \tag{C1}$$

We are only interested in $\underline{v} \approx \hat{\underline{k}} v_c$ since, as is evident from (27), only this neighborhood of $\underline{v}$ contributes to $\text{Im} \, \chi^{NL}$ and damping. The quantity $\omega_d^r$ is defined by $(\omega_d^r)^3 = (2/3) \, \underline{k} \cdot \underline{D} \cdot \underline{k}$ with $\underline{D}$ given by (14a). The t' integral in (14a) is approximately given by

$$\text{Re} \int_0^\infty dt' \, \exp\left\{- i(\omega_L - \underline{k}' \cdot \underline{v})t' - \frac{1}{2}\langle [\underline{k}' \cdot \delta \underline{r}(-t')]^2 \rangle\right\}$$

$$\approx \begin{cases} \sqrt{\pi/2} \; \omega_d^{-1} \;, & |\omega_L - \underline{k}' \cdot \underline{v}| \le \sqrt{2} \, \omega_d \\ 0 & , \quad |\omega_L - \underline{k}' \cdot \underline{v}| > \sqrt{2} \, \omega_d \;, \end{cases} \tag{C2}$$

and combining (C2), (14a) and (18) we have

$$(\omega_d^r)^3 \approx \sqrt{\frac{\pi}{2}} \, \frac{2e^2 k^2}{3m^2} \int \frac{d\underline{k}'}{(2\pi)^3} \; \frac{(\hat{\underline{k}} \cdot \hat{\underline{k}}')^2 \, I_L \, (\underline{k}')}{\omega_d} \, H\{\sqrt{2} \, \omega_d - |\omega_L - \underline{k}' \cdot \underline{v}|\}, \; \underline{v} = v_c \hat{\underline{k}} \tag{C3}$$

where $H\{M\}$ is the Heavyside step function defined by

$$H\{M\} \equiv \begin{cases} 1, & M \ge 0 \\ 0, & M < \end{cases} \tag{C4}$$

Since we are only interested in $\omega_d^r \equiv \omega_d^r(\underline{v})$ for $\underline{v}$ in the neighborhood of $\hat{\underline{k}} v_c$ we have, in (C3),

$$\omega_L - \underline{k}' \cdot \underline{v} = \omega_L [1 - \underline{k}' \cdot \hat{\underline{k}} \, v_c / \omega_L]$$

$$= \omega_L [1 - \frac{k'}{k} z_c (xx' + \sqrt{1 - x^2} \sqrt{1 - x'^2} \, \cos \phi')] \tag{C5}$$

and

$$(\underline{k}\cdot\hat{\underline{k}}')^2 = k^2(xx' + \sqrt{1 - x^2}\sqrt{1 - x'^2}\cos\phi')^2, \qquad (C6)$$

where we have used the notation of (33) in which $x$ and $x'$ denote the cosine of the angle that $\underline{k}$ and $\underline{k}'$, respectively, make with the pump direction, and $\phi'$ denotes the azimuthal angle between $\underline{k}'$ and the pump direction. Substituting (C5) and (C6) in (C3) and dividing by $\omega_L^3$, we have

$$\frac{(\omega_d^r)^3}{\omega_L^3} = \frac{2}{3}\sqrt{\frac{\pi}{2}}\,\frac{k^2}{k_D^2}\int_0^\infty \frac{k'^2 dk'}{2\pi}\int_0^1 \frac{dx'}{2\pi}\int_0^{2\pi}\frac{d\phi'}{2\pi}\,\frac{I(k',x')}{4\pi n\theta}\,[xx' + \sqrt{1-x^2}\sqrt{1-x'^2}\cos\phi']^2$$

$$\times\,\frac{\omega_L}{\omega_d}\,H\left\{\sqrt{2}\,\frac{\omega_d}{\omega_L} - \left|1 - \frac{k'}{k}\,z_c(xx' + \sqrt{1-x^2}\sqrt{1-x'^2}\cos\phi)\right|\right\} \qquad (C7)$$

In arriving at (C7) we have used the polar coordinate description as in (33) $\int d\underline{k}' \equiv \int k'^2\,dk'\,dx'\,d\phi'$. Consider first the $k'$ integral in (C7). This is governed by the $k'$ dependence of $I(k',x')$. It is seen in Sec. IIIC that $I(k',x')$ is zero except for a very narrow region of $k'$. That is

$$I(k',x') = 0, \quad k' \le k_p, \quad k' \ge k_p - \Delta k \qquad (C8)$$

where $k_p$ is the value of $k'$ at which $I(k',x')$ is a maximum, and $\Delta k \ll k_p$ so that

$$1 - \frac{\Delta k}{k_p} \le \frac{k'}{k_p} \le 1\,, \quad \text{for}\quad I(k',x') \ne 0 \qquad (C9)$$

Hence, if $k = k_p$ then $k'/k$ in (C7) is unity or slightly less than unity and (C7) becomes at $k = k_p$

$$\left(\frac{\omega_d^r}{\omega_L}\right)^3 = \frac{2}{3}\sqrt{\frac{\pi}{2}}\,\frac{k^2}{k_D^2}\int_0^1 dx'\int_0^{2\pi}\frac{d\phi'}{2\pi}\,\frac{I(x')}{4\pi n\theta_c}\,[xx' + \sqrt{1-x^2}\sqrt{1-x'^2}\cos\phi']^2$$

$$\times\,\frac{\omega_L}{\omega_d}\,H\left\{\sqrt{2}\,\frac{\omega_d}{\omega_L} - \left|1 - z_c(xx' + \sqrt{1-x^2}\sqrt{1-x'^2}\cos\phi'|\right\}\,,\quad k = k_p \qquad (C10)$$

A45

To obtain (C10) we have integrated over $k'$ taking advantage of the narrowness of $I(k',x')$ in $k'$ to set $k' = k_p$ in the integrand, and we have used the definition $(2\pi)^{-2}\int d'^2 dk' \, I(k',x') \equiv I(x')$. We have evaluated $(\omega_d^r/\omega_L)^3$, in (C10), at $k = k_p$ since it is near $k = k_p$ that the spectrum is large. To complete the evaluation of (C10) we first consider the case of $x = 1$ to obtain

$$\left(\frac{\omega_d^r}{\omega_L}\right)_{x=1}^3 \approx \frac{2}{3}\sqrt{\frac{\pi}{2}}\,\frac{k^2}{k_D^2}\int_0^1 dx'\,\frac{I(x')}{4\pi n\theta_e}\,x'^2\,\frac{\omega_L}{\omega_d}\,H\left\{\frac{\sqrt{2}\,\omega_d}{\omega_L} - 1 + z_c x'\right\} \qquad (C11)$$

since the integrand of (C10) is independent of $\phi'$ when $x = 1$. We normalize $\omega_d^r$ to $\omega_d$ by substituting (40b) into (C11), with $v_e/v_p = k/k_D$, to obtain

$$\left(\frac{\omega_d^r}{\omega_d}\right)_{x=1}^3 \approx \left(\frac{2}{3}\right)^3\sqrt{\frac{\pi}{2}}\left(\frac{k_D}{k}\right)^2\int_0^1 dx'\,\frac{I(x')}{I(1)}\,\frac{\omega_d(1)}{\omega_d(x')}\,x'^2\,H\left\{\sqrt{2}\,\frac{\omega_d}{\omega_L} - 1 + z_c x'\right\}, \qquad (C12)$$

Our object, now, will be to determine under what conditions $\omega_d^r/\omega_d <<< 1$. From (C12), and the definition of H, it is seen that $\omega_d^r/\omega_d \approx 0$ when

$$\sqrt{2}\,\frac{\omega_d}{\omega_L} - 1 + z_c\,x' < 0,\quad \text{all } x' \qquad (C13)$$

Substituting (38a) for $(1-z_c)$ and (40b) for $\omega_d/\omega_L$ into (C13) we have

$$\sqrt{2}\,\frac{\omega_d}{\omega_L} - 1 + z_c x' = \sqrt{2}\,\frac{\omega_d}{\omega_L} - (1-z_c)\,x' - (1-x')$$

$$= \sqrt{2}\left(\frac{3}{2}\right)^{1/4}\left(\frac{k}{k_D}\right)\left(\frac{I(x')}{4\pi n\theta_e}\right)^{1/4} - x'\sqrt{\frac{2}{3}}\left(\frac{I(x')}{4\pi n\theta_e}\right)^{1/2} - (1-x')$$

$$< 0\quad,\quad \text{all } x'\,. \qquad (C14)$$

This inequality is satisfied for all $x'$ when

$$1 > \frac{I(1)}{4\pi n\theta_e} > \frac{27}{2}\left(\frac{k}{k_D}\right)^4\,, \qquad (C15)$$

A46

lience, (C15) is satisfied and

$$H\left\{\sqrt{2}\,\frac{\omega_d}{\omega_L} - 1 + z_c x'\right\} = 0, \quad \text{all } x' \tag{C16}$$

when $I(1)\,(4\pi n\theta)^{-1} > (27/2)\,(k/k_D)^4$. Substituting (C16) into (C12) we thus have

$$\left(\frac{\omega_d^r}{\omega_d}\right)_{x=1} \approx 0, \quad \text{when } \frac{I(1)}{4\pi n\theta_e} > \frac{27}{2}\left(\frac{k}{k_D}\right)^4 \tag{C17}$$

Furthermore, when $\omega_d^r \approx 0$, then $\omega_d \approx \omega_d^{nr}$, so that (C17) becomes

$$\left(\frac{\omega_d^r}{\omega_d^{nr}}\right)_{x=1} \approx 0, \quad \text{when } \frac{I(1)}{4\pi n\theta_e} > \frac{27}{2}\left(\frac{k}{k_D}\right)^4 \quad . \tag{C18}$$

Although (C18) is limited to $x = 1$, it can also be proven to hold for all $x$. To see this we note that if the argument of H in (C10) is negative for $x = 1$, then the argument of H is negative for all $x$. Consequently, if (C18) is true for $x = 1$ then it is true for all $x$ that

$$\left(\frac{\omega_d^r}{\omega_d^{nr}}\right) \approx 0 \quad \text{when } \frac{I(1)}{4\pi n\theta_e} > \frac{27}{2}\left(\frac{k}{k_D}\right)^4 \quad . \tag{C19}$$

Roughly speaking, it follows from (C19), (50b), and (52) that

$$\omega_d^r \ll \omega_d^{nr} \quad , \quad \text{when } \frac{\langle \delta E^2\rangle}{4\pi n\theta_e} > \left(\frac{k}{k_D}\right)^4 \quad , \tag{C20}$$

since when $I(1)\,(4\pi n\theta)^{-1} = (27/2)\,(k/k_D)^4$ then it is found from (50b) and (52) that $\langle \delta E^2\rangle\,(4\pi n\theta)^{-1} \approx 2(k/k_D)^4$. The precise value of $\langle \delta E^2\rangle$ at which $\omega_d^r = \omega_d^{nr}$ is rather complex to determine.

## APPENDIX A-4

To derive (31) we first substitute (14a) and (14b) into (23b), and drop the sum on $\nu$ since $I_L(\underline{k}') \gg I_a(\underline{k}')$, to obtain

$$\omega_d^2(\underline{v}) = \frac{e^2 R_e}{m^2 (2\pi)^3} \int d\underline{k}' \ (\underline{k} \cdot \hat{\underline{k}}')^2 \ I_L(\underline{k}') \int_0^\infty dt' \left( \frac{2^{\frac{3}{2}}}{3\omega_d} - t' \right)$$

$$\times \exp\{- i(\omega_L - \underline{k}' \cdot \underline{v})t' - \tfrac{1}{2}\langle [\underline{k}' \cdot \delta \underline{r}(-t)]^2 \rangle\} \tag{D1}$$

In arriving at (D1) we have assumed that $\omega_d$ varies slowly with $\underline{k}$, compared to the variation of $I_L(\underline{k})$ with $\underline{k}$. The quantity $\langle [\underline{k}' \cdot \delta \underline{r}(-t)]^2 \rangle$ is given by (19) and to perform the $t'$ integrations in (D1) we shall use the fact that the orbit function $\exp\{- \tfrac{1}{2}\langle [\underline{k}' \cdot \delta \underline{r}(-t)]^2 \rangle\}$ approaches zero very rapidly with $t'$ for $t' > \omega_d^{-1}$. The $t'$ integration can be divided into two parts according to whether $\underline{k}'$ satisfies

$$|\omega - \underline{k}' \cdot \underline{v}| \geq \sqrt{2} \ \omega_d \ , \quad \underline{k}' \epsilon V_1 \tag{D2}$$

$$|\omega - \underline{k}' \cdot \underline{v}| < \sqrt{2} \ \omega_d \ , \quad \underline{k}' \epsilon V_2 \tag{D3}$$

For convenience of notation we denote the regions of $\underline{k}'$ space for which either (D2) or (D3) obtain by $V_1$ and $V_2$, respectively. In the region $\underline{k}' \epsilon V_1$, we have

$$\text{Re} \int_0^\infty dt' \left( \frac{2^{3/2}}{3\omega_d} - t' \right) \exp\{-i(\omega - \underline{k}' \cdot \underline{v})t' - \tfrac{1}{2}\langle [\underline{k}' \cdot \delta \underline{r} \ t')]^2 \rangle\}$$

$$\approx 0 \left( \frac{2^{\frac{3}{2}}}{3\omega_d} \ \frac{\sqrt{\pi/2}}{\omega_d} \ \exp\left[ - \frac{(\omega - \underline{k}' \cdot \underline{v})^2}{2\omega_d^2} \right] \right)$$

$$+ \frac{(\omega - \underline{k}' \cdot \underline{v})^2 - (9/5)\omega_d^2}{[(\omega - \underline{k}' \cdot \underline{v})^2 - \omega_d^2]^2} \quad , \quad \underline{k}' \in V_1$$

$$\approx \frac{(\omega - \underline{k}' \cdot \underline{v})^2 - (9/5)\omega_d^2}{[(\omega - \underline{k}' \cdot \underline{v})^2 - \omega_d^2]^2} \quad , \quad \underline{k}' \in V_1 \tag{D4}$$

where $O(F)$ mean less than $F$. This result is exact in the asymptotic limit of large $(\omega - \underline{k}' \cdot \underline{v})^2$, and is a good approximation for any conceivable orbit function for all $\underline{k}' \in V_1$, that is, for $|\omega - \underline{k}' \cdot \underline{v}| \geq \sqrt{2}\,\omega_r$. Note that the number $(9/5)$ in (D4) reflects the fact that when $\exp\{-\frac{1}{2}\langle[\underline{k}' \cdot \delta\underline{r}(-t)]^2\rangle\}$ is Gaussian in $(\omega_d t')$ then the second integral in (D4) vanishes for $(\omega - \underline{k}' \cdot \underline{v})^2 \approx (9/5)\omega_d^2$. To perform the integration in (D4) we have used the fact that the orbit function approaches zero very rapidly with $t'$ for $t' > \omega_d^{-1}$. This integration does not vary much with the precise form of the orbit function providing $\underline{k}' \in V_1$ and the orbit function approaches zero rapidly with $t'$ on the time scale $\omega_d^{-1}$. Note that the surviving contribution to the $t'$ integration in (D4) comes from the $\omega^{nr}$ term. The contribution from $\underline{k} \cdot \underline{D} \cdot \underline{k}$ for $\underline{k}' \in V_1$ is negligible.

For the $\underline{k}'$ region $|\omega - \underline{k}' \cdot \underline{v}| < \sqrt{2}\,\omega_d$, the $t'$ integration in (D1) is, approximately,

$$\mathrm{Re}\int_0^\infty dt' \left(\frac{2^{\frac{3}{2}}}{3\omega_d} - t'\right) \exp\{- i(\omega - \underline{k}' \cdot \underline{v})t' - \frac{1}{2}\langle[\underline{k}' \cdot \delta\underline{r}(- t')^2\rangle\}$$

$$\approx \frac{2^{-1/6}\,\Gamma(7/3)}{\omega_d^2}\, \exp\left[- \frac{(\omega - \underline{k}' \cdot \underline{v})^2}{2\omega_d^2}\right]$$

$$- \frac{2^{-1/3}\,\Gamma(5/3)}{\omega_d^2}\left[1 - \frac{(\omega - \underline{k}' \cdot \underline{v})^2}{2\omega_d^2}\right] \quad , \quad \underline{k}' \in V_2 \tag{D5}$$

A49

To arrive at (D5) we have used the fact that the orbit function approaches zero very rapidly for $t' > \omega_d^{-1}$. We have, in fact, used $\exp\{-\frac{1}{2}\langle[\underline{k}'\cdot\delta\underline{r}(-t')]^2\rangle\} \approx \exp(-\frac{1}{2}\omega_d^3 t^3)$. This form for the orbit function is adequate in (D5) for the $\underline{k}'$ region $|\omega - \underline{k}'\cdot\underline{v}| \leq \sqrt{2}\,\omega_d$. For this region (D5) does not vary much with the precise form of the orbit function providing the orbit function rapidly approaches zero on the time scale $\omega_d^{-1}$. It is of some interest that both $\underline{k}\cdot\underline{D}\cdot\underline{k}$ and $(\omega_d^{nr})^2$ contribute to (D5), and that the contribution from $(\omega_d^{nr})^2$ can be seen to be negative and thus tends to oppose and weaken $\underline{k}\cdot\underline{D}\cdot\underline{k}$ when $|\omega - \underline{k}'\cdot\underline{v}| < \sqrt{2}\,\omega_d$. Note, too, that the contribution from $(\omega_d^{nr})^2$ vanishes for $(\omega - \underline{k}'\cdot\underline{v}) \approx \sqrt{2}\,\omega_d$.

Substituting (D4) and (D5) into (D1) we obtain $\omega_d$ as

$$\omega_d^2(\underline{v}) = \frac{e^2}{m^2}\,\frac{\text{Re}}{(2\pi)^3}\left\{\int\!\!\int_{\underline{k}'\in V_1}d\underline{k}'\;(\underline{k}\cdot\hat{\underline{k}}')^2\,I_L(\underline{k}')\;\frac{(\omega - \underline{k}'\cdot\underline{v})^2 - (9/5)\omega_d^2}{[(\omega - \underline{k}'\cdot\underline{v})^2 - \omega_d^2]^2}\right.$$

$$+\int_{\underline{k}'\in V_2}d\underline{k}'\;(\underline{k}\cdot\hat{\underline{k}}')^2\,I_L(\underline{k}')\left(\frac{2^{-1/6}\,\Gamma(7/3)}{\omega_d^2}\,\exp\left[-\frac{(\omega - \underline{k}'\cdot\underline{v})^2}{2\omega_d^2}\right]\right.$$

$$\left.\left.-\;\frac{2^{-1/3}\,\Gamma(5/3)}{\omega_d^2}\left[1 - \frac{(\omega - \underline{k}'\cdot\underline{v})^2}{2\omega_d^2}\right]\right)\right\} \qquad\text{(D6)}$$

But, for $\underline{k}'\in V_2$ the following is a good approximation

$$\frac{2^{-1/6}\,\Gamma(7/3)}{\omega_d^2}\,\exp\left[-\frac{(\omega - \underline{k}'\cdot\underline{v})^2}{2\omega_d^2}\right] - \frac{2^{-1/3}\,\Gamma(5/3)}{\omega_d^2}\left[1 - \frac{(\omega - \underline{k}'\cdot\underline{v})^2}{2\omega_d^2}\right]$$

$$\approx \frac{1}{(\omega - \underline{k}'\cdot\underline{v})^2 + 3\omega_d^2}\;;\quad \underline{k}'\in V_2 \qquad\text{(D7)}$$

This approximation is correct to within 5% for $(\omega - \underline{k}' \cdot \underline{v}) = 0$ and, at worst, is correct to within a factor of 2 for $(\omega - \underline{k}' \cdot \underline{v}) = \sqrt{2}\,\omega_d$. In addition, for $|\omega - \underline{k}' \cdot \underline{v}| > \sqrt{2}\,\omega_d$ the following is a good approximation.

$$\frac{(\omega - \underline{k}' \cdot \underline{v})^2 - (9/5)\omega_d^2}{[(\omega - \underline{k}' \cdot \underline{v})^2 - \omega_d^2]^2} \approx \frac{1}{(\omega - \underline{k}' \cdot \underline{v})^2 + 3\omega_d^2} \quad , \quad \underline{k}' \epsilon\, V_1 \tag{D8}$$

This is asymptotically exact for large $(\omega - \underline{k}' \cdot \underline{v})$ and is correct to within a factor of 2 for the worst case of $(\omega - \underline{k}' \cdot \underline{v}) = \sqrt{2}\,\omega_d$. Finally, we substitute the approximations (A7) and (A8) and use

$$\int_{\underline{k}' \epsilon\, V_1} d\underline{k}' \quad + \quad \int_{\underline{k}' \epsilon\, V_2} d\underline{k}' \quad \equiv \quad \int d\underline{k}'$$

to obtain the desired result for $\omega_d$

$$\omega_d^2(\underline{v}) = \frac{e^2}{m^2\,(2\pi)^3} \int d\underline{k}' \; \frac{(\underline{k} \cdot \hat{\underline{k}}')^2 \, I_L(\underline{k}')}{(\omega - \underline{k}' \cdot \underline{v})^2 + 3\omega_d^2} \quad , \tag{D9}$$

where, as has been shown, the integrand of (D9) is very close to the integrand of (D6) except for $\underline{k}'$ in the vicinity $(\omega - \underline{k}' \cdot \underline{v})^2 \approx 2\omega_d^2$ where they agree to within a factor of 2.

Fig. 1 Plot of $(\log_e Px^2)^2$, $(\log_e Px^2)^2 (1+F)^{-1}$, and $F$ for $P = 10$ and $k_m \lambda_D = 0.21$

$(\log_e Px^2)^2 (1+F)^{-1}$

$$\frac{I}{4\pi n\theta_e} = 4.57 \times 10^{-3} (\log_e Px^2)^2 (1+F)^{-1}$$

$(\log_e Px^2)^2$

$F$

A52
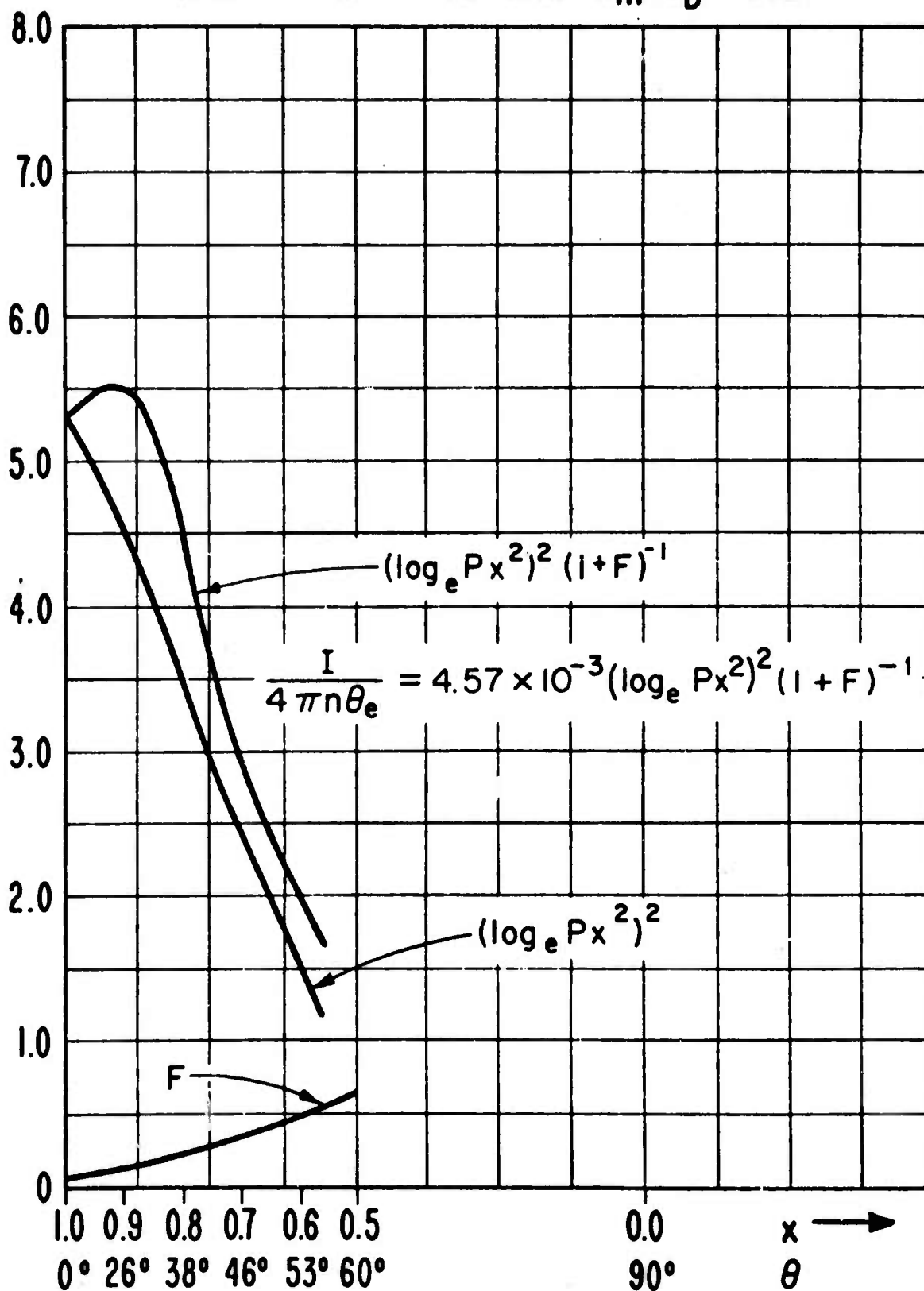
# REFERENCES

1. W. L. Kruer and J. M. Dawson, Phys. Fluids $\underline{15}$, 446 (1972); J. S. DeGroot and J. I. Katz (private communication).

2. A. Y. Wong and R. J. Taylor, Phys. Rev. Letters $\underline{27}$, 644 (1971).

3. M. A. Biondi, D. P. Sipler, and R. D. Hake, Jr., J. Geophys. Res. $\underline{75}$, 6421 (1970).

4. H. Dreicer, D. Henderson, and J. Ingraham, Phys. Rev. Letters $\underline{26}$, 1616 (1971); A. Wong, and R. Stenzel, Phys. Rev. Letters $\underline{28}$, 274 (1972); T. K. Chu and H. W. Hendel (private communication); J. Ingraham (private communication).

5. V. V. Pustovalov and V. P. Silin, Zh. E.T.F. $\underline{59}$, 2215 (1970).

6. D. F. DuBois and M. V. Goldman, Phys. Fluids $\underline{15}$, 919 (1972).

7. E. Valeo, C. Oberman, and F. W. Perkins, Phys. Rev. Letters $\underline{28}$, 340 (1972).

8. B. Bezzerides and J. Weinstock, Phys. Rev. Letters $\underline{28}$, 481 (1972).

9. D. F. DuBois and M. V. Goldman, Phys. Rev. Letters $\underline{28}$, 218 (1972).

10. J. Weinstock, Phys. Fluids $\underline{11}$, 1977 (1968).

11. T. H. Dupree, Phys. Fluids $\underline{9}$, 1773 (1966).

12. J. Weinstock, Phys. Fluids $\underline{12}$, 1045 (1969).

13. $\omega_d$ resembles the bounce frequency $\omega_B$. $\omega_d$ describes the effects of a broad wave spectrum as well as a single wave upon the particle whereas $\omega_B$ only refers to a single wave. Numerically, it can be gleaned from Eqs. (12) and (13) that $\omega_d$ is of the order of but less than the bounce frequency of a particle in a single wave whose amplitude is the R.M.S. amplitude of the actual spectrum of waves.

14. D. F. DuBois and M. V. Goldman, Phys. Rev. $\underline{164}$, 207 (1967).

15. D. Biskamp and R. Chodura, Phys. Rev. Letters 27, 1553 (1971).

16. A. Sleeper, J. Weinstock, and B. Bezzerides, Phys. Rev. Letters, 29, 343 (1972).

17. D. F. DuBois and M. V. Goldman (private communication).

18. B. Fried and S. Conte, "The Plasma Dispersion Function", Academic Press, New York, 1961.

## ACKNOWLEDGMENTS

CRITICAL FLUCTUATION LEVEL FOR THE

PURELY GROWING PARAMETRIC INSTABILITY

D.F. DuBois

B. Bezzerides

# CRITICAL FLUCTUATION LEVEL FOR THE
# PURELY GROWING PARAMETRIC INSTABILITY

## I. Introduction

Recent detailed calculations of Harker[1], Meltz[2] and Perkins[3] have led to the conclusion that the observed incoherent backscatter spectrum at Arecibo from the modified ionosphere can be explained in terms of pump-enhanced critical fluctuation theory. This theory was first developed by DuBois and Goldman[4] who calculated the steady-state wave-fluctuation spectrum for a pump, near but below the threshold for the parametric decay instability. It appears that the Arecibo experiments have been carried out with local pump amplitudes just at or slightly below threshold for plasma waves propagating in the pump direction with the wave number observed in the backscatter. Therefore in the geometry at Arecibo the waves observed in the backscatter, which propagate at an angle of about $40^\circ$ from the pump polarization ($\cos^2\theta \simeq \frac{1}{2}$), have a threshold about twice that of the pump.

The considerable detail of the Arecibo backscatter spectrum presents many spectral features to be explained by theory. The critical fluctuation theory predicts a ratio of peak intensity of the enhanced decay line (i.e. the Stokes or downshifted component of the plasma line) to the ion line which is in agreement with experiment[5]. Likewise, the ratio of the anti-Stokes component of the plasma line is consistent with experiment[6]. A spectral peak shifted by exactly the heater frequency has been identified[6] as the high-frequency component of the purely growing parametric instability which is a different branch of the dispersion relation.

In this note we compute the critical fluctuation level for the purely growing instability. Then assuming values for the pump which appear to

B1

explain the features of the decay instability[1,2,3] we compute the ratio of the purely growing line to the decay line (Stokes line). While this report was in preparation we became aware of the results for a homogeneous plasma which have recently been computed numerically in detail for equal electron and ion temperators by Hagsfors and Gieraltowski who used the complete plasma dispersion function. The approximate analytic result given here seems to agree with the more complete numerical results and allow us to take into account the altitude integration of the backscattered signal.

## II. Critical Fluctuation Theory

A general discussion of the parametrically excited wave-fluctuation spectrum has been given elsewhere[7,4].

$$I(k,\omega - n\omega_o) \equiv \lim_{T,V\to\infty} \frac{\left\langle |E(k,\omega - n\omega_o)|^2 \right\rangle}{TV}$$

$$= \frac{(4\pi)^2}{k^2} \sum_m \frac{|C_{nm}|^2}{|D(k,\omega)|^2} \; N(k,\omega - m\omega_o) \tag{2.1}$$

where $C_{nm}$ is the cofactor of the parametric coupling matrix $M_{nm}$ and $D(k,\omega) = \det(M_{nm})$. The source term $N(k,\omega)$ is the spectral density of the fluctuating densities

$$N(k,\omega) = \lim_{T,V\to\infty} \frac{\left\langle |\delta\rho(k,\omega)|^2 \right\rangle}{TV} = \frac{1}{2\pi} \sum_s \frac{\Theta_s}{\omega} \; \mathrm{Im}\, \chi^s(k,\omega) \tag{2.2}$$

where we have used the fluctuation-dissipation theorem to relate this to the imaginary part of the electrostatic susceptibility arising from particle species $s$ with temperature $\Theta_s$[7]. In deriving this expression it is assumed

B2

that the off-diagonal components of $M_{nm}$ are real so that no mixed correlation terms of the form $\langle \delta p(k, \omega - n\omega_o) \delta p^*(k, \omega - n'\omega_o) \rangle$ occur for $n \neq n'$.

To treat the purely growing mode it is well-known[8] that the three Fourier components at $\omega$, $\omega - \omega_o$, and $\omega - 2\omega_o$ are coupled. The matrix $M_{nm}$ in this case has been shown to be[9,7]

$$M = \begin{bmatrix} \epsilon(k,\omega) + \overline{\Lambda}^2 & -\overline{\Lambda}(k_D/k) & -\overline{\Lambda}^2 \\ -\overline{\Lambda}(k_D/k) & \epsilon(k,\omega - \omega_o) - 2\overline{\Lambda}^2 & \overline{\Lambda}(k_D/k) \\ -\overline{\Lambda}^2 & \overline{\Lambda}(k_D/k) & \epsilon(k,\omega - 2\omega_o) + \overline{\Lambda}^2 \end{bmatrix} \tag{2.3}$$

where $\overline{\Lambda}^2 = \frac{1}{4}\Lambda^2\mu^2$; $\Lambda^2 = \dfrac{E_o^2}{4\pi n\theta_e}$; $\mu = \cos\theta$ 

(2.4)

Here $E_o$ is the pump amplitude and $\mu$ is the cosine of the angle between $\overline{E}_o$ and $\overline{k}$. We assume that $\Lambda(k/k_D)\mu \ll 1$ so that the Bessel functions which appear in the general expression for $M_{nm}$ can be Taylor expanded[7]. If we use this explicit form for $M_{nm}$ we can evaluate (2.1) to obtain

$$I(k,\omega) = \frac{(4\pi)^2}{k^2} \frac{1}{|D(k,\omega)|^2} \left[ \left(\frac{k_D}{k}\right)^4 |\overline{J}_1\overline{J}_A - \overline{\Lambda}^2|^2 N(k,\omega) \right. \tag{2.5}$$

$$\left. + \left(\frac{k_D}{k}\right)^2 |J_A|^2 \overline{\Lambda}^2 N(k,\omega - \omega_o) + \left(\frac{k_D}{k}\right)^4 |J_1 - 1|^2 \overline{\Lambda}^4 N(k,\omega - 2\omega_o) \right]$$

where

$$\begin{aligned} J_S &= \epsilon(k,\omega) & ; \quad \overline{J}_S &= J_S + \overline{\Lambda}^2 \\ J_A &= \epsilon(k,\omega - 2\omega_o) & ; \quad \overline{J}_A &= J_A + \overline{\Lambda}^2 \\ J_1 &= \frac{k^2}{k_{D_e}^2}\epsilon(k,\omega - \omega_o) & & \end{aligned} \tag{2.6}$$

B3

In this notation the determinant is[7]

$$D(k,\omega) = \frac{k_D^2}{k^2} \left[ J_S J_A J_i + \overline{\Lambda}^2 (J_i - 1)(J_S + J_A) + 0(\frac{k^2}{k_D^2} \Lambda^4) \right] \qquad (2.7)$$

For both instabilities the high frequency waves are near enough to the Langmuir frequencies $\omega_L(k)$ to use the expansions

$$J_S = \frac{2}{\omega_L} (\omega - \omega_L + i\gamma_L)$$

$$\qquad (2.8)$$

$$J_A = - \frac{2}{\omega_L} (\omega - 2\omega_o + \omega_L + i\gamma_L)$$

We must be more careful in treating $J_i$ as we will show. We will chose $\omega$ to be near $\omega_L$. The dominant noise source in this case is $N(k, \omega - \omega_o)$ which is predominantly ion Cerenkov emission. If we use the relation

$$\gamma_\nu = (\partial \epsilon_1 / \partial \omega_\nu)^{-1} \sum_s \text{Im } \chi^s(k, \omega_\nu)$$

for the damping of a longitudinal wave of frequency $\omega_\nu$ we can compute the ratios

$$\frac{N(k, \omega - \omega_o)}{N(k, \omega)} \simeq \frac{N(k, \omega - \omega_o)}{N(k, \omega - 2\omega_o)} \simeq \frac{k_D^2}{k^2} \frac{\gamma_a}{\gamma_L} \frac{\omega_L^2}{\omega_a^2} \qquad (2.9)$$

For $\theta_e = \theta_i$, we have $\gamma_a \simeq \omega_a$ and this ratio is $(k_D^2/k^2)(\omega_L/\gamma_L)(\omega_L/\omega_a)$. With

$$\overline{\Lambda}^2 \le \frac{1}{4}\Lambda c^2 = \frac{4\gamma_L}{\omega_L}$$

and $J_i \simeq 1$, we see that the second term exceeds the first term by the large factor $\omega_L/\omega_a$. The last term is similarly small.

B4

## III. Decay Instability

Under the conditions $\omega_a \gg \gamma_L$ it is readily seen that $J_A \gg J_S$ and the dispersion $D(k,\omega) = 0$ reduces to

$$D(k,\omega) = \frac{k_D^2}{k^2} \; J_A \; \left[ J_S J_i + \bar{\Lambda}^2 \; (J_i - 1) \right] = 0 \tag{3.1}$$

In this case it is valid to assume $J_i$ is near one of its zeros and approximate[10]

$$J_i \simeq \frac{-2(\omega - \omega_o + \omega_a + i\gamma_a)}{\omega_a} \tag{3.2}$$

where $\omega_a$ and $\gamma_a$ are the frequency and damping of an ion acoustic wave. The dispersion relation is then a quadratic in $\omega$ with the solutions (provided $\Lambda^2 \ll 1$)[4,7]

$$\omega_+ - \omega_o \equiv -\Omega_+ = \omega_L - \omega_o - i\gamma_L \left( 1 - \frac{\Lambda^2}{\Lambda_T^2} \right) \tag{3.3}$$

$$\omega_- - \omega_o \equiv -\Omega_- = \omega_a - i\gamma_a \tag{3.4}$$

where it has been assumed that $\Lambda^2 \ll 1$, $\gamma_L \ll \gamma_a$ and $(\Lambda^2/\Lambda_c^2)(\gamma_L/\gamma_a) \ll 1$. The threshold value of $\Lambda_c^2$ for the decay instability in this case is

$$\Lambda_T^2 = \frac{\Lambda_c^2}{f(\Delta\omega)\mu^2} \; ; \quad \Lambda_c^2 = 16 \frac{\gamma_L}{\omega_L} \frac{\gamma_a}{\omega_a} \tag{3.5}$$

$$f(\Delta\omega) \simeq \frac{\gamma_a^2}{(\Delta\omega)^2 + \gamma_a^2} \; ; \quad \Delta\omega = \omega_o - \omega_L - \omega_a \tag{3.6}$$

B5

Then if we define $\Omega = \omega_o - \omega$ we can combine these results to write

$$D(k,\omega) = D(k,\omega_o - \Omega) = -\frac{k_D^2}{k^2} J_A \frac{4}{\omega_L \omega_a} (\Omega - \Omega_+)(\Omega - \Omega_-) \qquad (3.7)$$

Substitution of this result into (2.5) yields

$$I(\omega_o - \Omega) = \frac{(4\pi)^2}{k_D^2} \frac{\bar{\Lambda}^2}{16} \frac{\omega_L^2 \omega_a^2}{(\Omega - \omega_o + \omega_L)^2 + \gamma_L^2\left(1 - \frac{\Lambda^2}{\Lambda_T^2}\right)^2} \frac{N(k,\Omega)}{(\Omega - \omega_a)^2 + \gamma_a^2} \qquad (3.8)$$

Since $\gamma_L \ll \gamma_a$ the first $\Omega$ dependent denominator is sharply peaked at $\Omega = \omega_o - \omega_L$ (especially near threshold) and we can write approximately

$$I(\omega_L) = \frac{(4\pi)^2}{k_D^2} \frac{\bar{\Lambda}^2}{16} \frac{\omega_L^2}{\gamma_L(1 - \Lambda^2/\Lambda_T^2)} \frac{\omega_a^2}{\gamma_a^2} f(\Delta\omega) N(k,\omega_o - \omega_L) \pi\delta(\Omega - \omega_o + \omega_L)$$

These are the familiar results for the decay instability.[4]

## IV. Purely Growing Instability

Using the definitions (2.6) and the approximations (2.8) we can write the dispersion relation as

$$\frac{k^2}{k_D^2} D(k,\omega_o - \Omega) = \frac{\delta^2 - (\Omega - i\gamma_L)^2}{(\omega_L^2/4)} J_1 + \bar{\Lambda}^2(J_1 - 1) \frac{4\delta}{\omega_L} \qquad (4.1)$$

where $\qquad \delta \equiv \omega_o - \omega_L \qquad (4.2)$

B6

Next we assume that $|\Omega| \ll k v_1$ when $v_1$ is the ion thermal velocity. Then it can be shown that we can write approximately

$$J_1 = \frac{k^2}{k_{D_e}^2} \varepsilon(k,-\Omega) \simeq \frac{k^2}{k_{D_e}^2} \varepsilon(k,0) = 1 + \frac{k_{D_1}^2}{k_{D_e}^2} + 0(\frac{k^2}{k_{D_e}^2}) \qquad (4.3)$$

Then we can write

$$J_1 = 1 + \frac{1}{\beta} \qquad (4.4)$$

where $\beta$ is the ion to electron temperature ratio

$$\beta \equiv \frac{\Theta_1}{\Theta_e} \qquad (4.5)$$

With this approximation, the determinant is again quadratic in $\Omega$ and can be factored into its roots

$$-\frac{k^2}{k_{D_e}^2} D(k,\omega_0 - \Omega) = \frac{-4}{\omega_L^2} \frac{\beta+1}{\beta} (\Omega - \Omega_+)(\Omega - \Omega_-) \qquad (4.6)$$

where

$$\Omega_{\pm} = i\gamma_L \pm i\delta \sqrt{\frac{2\gamma_L}{(-\delta)} \frac{\Lambda^2}{\Lambda_g^2} - 1} \qquad (4.7)$$

and where

$$\Lambda_g^2 = \frac{8(1+\beta)}{\mu^2} \frac{\gamma_L}{\omega_L} = \frac{(1+\beta)}{2} \frac{\omega_a}{\gamma_a} \frac{\Lambda_c^2}{\mu^2} \qquad (4.8)$$

The root $\Omega_+$ attains a zero imaginary part for the minimum value of $\Lambda^2 \mu^2$ when $\delta = -\gamma_L$ and this minimum threshold is just $\Lambda_g^2$. No instability is possible unless $\delta < 0$ i.e. $\omega_0 < \omega_L(k)$. These results agree with those of Nishikawa[8] and Sanmartin[10].

Inserting eqn. (4.7) into (4.6) we find for the spectral contribution of the growing mode (for $\delta < 0$)

$$I(\omega_o - \Omega) = \frac{(4\pi)^2}{k_D^2} \frac{\bar{\Lambda}^2}{16} \frac{\beta^2}{(1+\beta)^2} \frac{4\omega_L^2(\delta^2 + \gamma_L^2)}{\left[\Omega^2 + (\gamma_L - \delta S)^2\right]\left[\Omega^2 + (\gamma_L + \delta S)^2\right]} N(k, \Omega) \qquad (4.9)$$

where

$$S = \sqrt{\frac{2\gamma_L}{(-\delta)} \frac{\Lambda^2}{\Lambda_g^2} - 1} \qquad (4.10)$$

where we have replaced $|J_A(\Omega)|^2$ by $|J_A(0)|^2 = \frac{4}{\omega_L^2}(\delta^2 + \gamma_L^2)$ since the other factors peak at $\Omega = 0$.

This function peaks at $\Omega = 0$ with the peak value

$$I(\omega_o) = \frac{(4\pi)^2}{k_D^2} \frac{\bar{\Lambda}^2}{16} \frac{\beta^2}{(1+\beta)^2} \left[\frac{4\omega_L^2(\delta^2 + \gamma_L^2)}{(\gamma_L^2 - \delta^2 S^2)^2}\right] N(k, 0) \qquad (4.11)$$

Defining $\bar{\delta} = \delta/\gamma_L$ we can rewrite this using (4.10) as

$$I(\omega_o) = \frac{(4\pi)^2}{k_D^2} \frac{\bar{\Lambda}^2}{16} \frac{\beta^2}{(1+\beta)^2} \frac{4\omega_L^2}{\gamma_L^2} \left[\frac{1+\bar{\delta}^2}{(1+\bar{\delta}^2 + 2\bar{\delta}P_g)^2}\right] N(k, 0) \qquad (4.12)$$

where $P_g \equiv \Lambda^2/\Lambda_g^2$.

The factor in square brackets is a maximum at $\delta^2 = \gamma_L^2$ for $P_g = 1$. The width of this function is $\Delta\bar{\delta} \sim 1$ (or $\Delta\delta = \gamma_L$). Assuming $\beta = 1$ we have $\Lambda_g^2 = \Lambda_c^2$. If the modes propagating in the $\mu = 1$ direction are taken to be just at threshold then $\Lambda^2 = \Lambda_c^2$. For $\mu^2 = \frac{1}{2}$ ($\theta \approx 40^o$) the factor in square brackets reaches a maximum at

$$\bar{\delta} \simeq -.68 \qquad \text{(for } P_g = \frac{1}{2}) \qquad (4.13)$$

and $I(\omega_o)$ has the maximum value

$$I(\omega_o) = \frac{(4\pi)^2}{k_D^2} \frac{\overline{\Lambda}^2}{16} \frac{\omega_L^2}{\gamma_L^2} (2.4) \ N(k,0) \ \frac{4\beta^2}{(1+\beta)^2} \tag{4.14}$$

## V. Comparison with Experiment

The ratio of the maximum decay line to the maximum of the purely growing line for a homogeneous plasma with $\Lambda^2 \mu^2 / \Lambda_c^2 = \frac{1}{2}$ and $\beta = 1$ is then (for $\Theta_e = \Theta_i$ we take $\gamma_a = \omega_a$)

$$\frac{I(k,\omega_o)}{I(k,\omega_L(k))} = \frac{(2.4)}{4} \frac{N(k,0)}{N(k,\omega_o - \omega_L(k))} \tag{5.1}$$

The ratio of the ion fluctuation factors is

$$\frac{N(k,0)}{N(k,\omega_o - \omega_L(k))} = e^{+\frac{(\omega_o - \omega_L(k))^2}{2k^2 V_i^2}} \tag{5.2}$$

where $V_i^2 = \Theta_i / m_i$. At the spectral peak considered here $\omega_o - \omega_L(k) = C_a k$. Using[7] $C_a = 1.6 (\Theta_e/m_i)^{\frac{1}{2}}$ for $\Theta_e = \Theta_i$ we have (assuming $\sqrt{m_e/m_i} \ll 1$)

$$\frac{N(k,0)}{N(k,\omega_o - \omega_L(k))} = e^{\frac{\Theta_e}{\Theta_i}(1.28)} \tag{5.3}$$

$$= 3.6 \qquad \text{for } \Theta_e = \Theta_i \qquad (\beta = 1)$$

Therefore for equal electron and ion temperatures

$$\frac{I(k,\omega_o)}{I(k,\omega_L(k))} \approx 2.2 \tag{5.4}$$

B9

The actual backscattered signal observed at Arecibo is proportional to the integral of I over a range of altitudes[1,2,3]. In the case of the decay line we find from (3.9) that I is proportional to $\delta(\Omega - [\omega_o - \omega_L(k,z)])$ where

$$\omega_L(k,z) = \sqrt{\omega_p^2(z) + 3k^2 Ve^2}$$

so that a given frequency arises from a definite altitude. Assuming that the pump amplitude is constant over the altitude range in question the maximum frequency return arises for the altitude $z_d$ where $\Delta\omega = 0$

$$\omega_o = \omega_L(k,z_d) + \omega_a(k)$$

In this case we have

$$\int dz \ I(\omega_L, z) = \frac{(4\pi)^2}{k_D^2} \frac{\overline{\Lambda}^2(z_o)}{16} \frac{\omega_L^2(z_d)}{\gamma_L(z_d)(1-P_d)} N(k, \omega_a(k)) \frac{\pi 2H}{\omega_p(z_d)} \qquad (5.5)$$

where $P_d = \Lambda^2 \mu^2 / \Lambda_c^2$ - the pump ratio relative to the minimum decay instability threshold and where we have taken

$$\frac{d}{dz} \omega_L(k,z) \simeq \frac{\omega_p(z_d)}{2H}$$

where H is the density gradient scale height.

In the case of the zero frequency mode the scattered return from each altitude is centered at a shifted frequency of $\omega_o$. The most sensitive altitude dependent quantity in (4.12) is

B10

$$\bar{\delta}(z) = \frac{\omega_o - \omega_L(k,z)}{\gamma_L} \cong -1 - (z-z_q) \frac{\omega_p(z_g)}{2H\gamma_L} \tag{5.6}$$

where we have taken $z_g$ to be the altitude of best matching for which

$$\omega_o - \omega_L(k,z_g) = -\gamma_L. \tag{5.7}$$

The altitude integrated spectrum is then

$$\int dz \ I(\omega_o,z) = \frac{(4\pi)^2}{k_D^2} \frac{\bar{\Lambda}^2}{16} \frac{\beta^2}{(1+\beta)^2} \frac{4\omega_L^2(z_o)}{\gamma_L^2(z_o)} \int_0^\infty dz \frac{[1+\bar{\delta}^2(z)]N(k,0)}{[1+\bar{\delta}^2(z)+2\bar{\delta}(z)P_g]^2} \tag{5.8}$$
$$(\bar{\delta}<0)$$

$$= \frac{(4\pi)^2}{k_D^2} \frac{\bar{\Lambda}^2}{16} \frac{\beta^2}{(1+\beta)^2} \frac{4\omega_L^2(z_o)}{\gamma_L^2(z_o)} \cdot \frac{2H\gamma_L}{\omega_p(z_o)} \tag{5.9}$$

$$\times \left[ \frac{P_g^2}{(1-P_g^2)} + \frac{1}{(1-P_g^2)^{3/2}} \left( \pi/2 + \tan^{-1} \frac{P_g}{\sqrt{1-P_g^2}} \right) \right]$$

where $P_g = \Lambda^2\mu^2/\Lambda_g^2$.

We then obtain the ratio of maximum backscattering cross sections

$$\frac{\mathrm{Max}(d\sigma/d\omega)\mathrm{growing}}{\mathrm{Max}(d\sigma/d\omega)\mathrm{decay}} = \frac{\int dz \ I(\omega_o,z)}{\int dz \ I(\omega_L,z)} = \frac{4}{\pi} \frac{\Lambda^2(z_g)}{\Lambda^2(z_d)} \frac{\beta^2}{(1+\beta)^2}$$

$$\times \left[ \frac{1-P_d}{1-P_g^2} \right] \left[ P_g + \frac{1}{\sqrt{1-P_g^2}} \left( \pi/2 + \tan^{-1} \frac{P_g}{\sqrt{1-P_g}} \right) \frac{N(k,0)}{N(k,\omega_a)} \right] \tag{5.10}$$

B11

With our assumption $P_g = P_d = \frac{1}{2}$ for the observed waves and assuming $\Lambda^2 (z_g) = \Lambda^2(z_d)$ this ratio turns out to be (for $\beta = 1$)

$$\frac{\text{Max}(d\sigma/d\omega)\text{growing}}{\text{Max}(d\sigma/d\omega)\text{decay}} \simeq 2.16 \tag{5.11}$$

This ratio is larger by a factor of 2 or 3 than those observed at Arecibo. A factor of 2 or so could arise from the crudeness of our approximations. In particular our treatment of the decay instability suffers when $\Theta_e = \Theta_i$ because the ion acoustic mode is poorly defined. The theory does clearly indicate that the decay line peak and the growing line peak should be of comparable order of magnitude as observed.

In the calculation above we assumed that the pump amplitude was the same at the altitudes $z_d$ and at $z_g$. The altitudes are defined respectively by

$$\omega_o + \gamma_L = \omega_L(k, z_g) = \omega_L(k,0) - z_g \frac{\omega_p}{2H} \tag{5.12}$$

$$\omega_o - \omega_a(k) = \omega_L(k, z_d) = \omega_L(k,0) - z_d \frac{\omega_p}{2H} \tag{5.13}$$

so that

$$\Delta z = z_d - z_g = \left[\gamma_L + \omega_a(k)\right] \frac{2H}{\omega_p} \simeq \frac{2\gamma_L H}{\omega_p} \tag{5.14}$$

For the parameters at Arecibo

$$\frac{\Delta z}{H} \simeq 1.2 \times 10^{-3} \tag{5.15}$$

B12

This small range justifies our approximation of using constant values of $\gamma_L$ in our calculations.

The spacing of the Airy function maxima of the pump field is given by

$$\frac{\Delta z}{H} \max \;\tilde{=}\; 2 \cdot \left(\frac{H\omega}{c}\right)^{1/3} \frac{c}{\omega H} \tag{5.16}$$

For a scale height of $H = 100$ km and $c/\omega \sim 10$m this is

$$\frac{\Delta z}{H} \max \;\tilde{=}\; 4.10^{-3} \tag{5.17}$$

Because of this the assumption that $\Lambda^2(z_d) = \Lambda^2(z_g)$ may not be valid. The ratio is reduced if we assume $\Lambda^2(z_g) < \Lambda^2(z_d)$, i.e. the altitude at which the observed growing mode is excited is at a <u>lower</u> point on the Airy pattern than the altitude $z_d$ at which the observed decay mode is excited. This implies that a variability in this ratio should be observed with changing scale height $H$ and changing modifier frequency $\omega_o$.

# References

1. K. J. Harker, "Cross-Section Calculations and Wave-Wave Interactions." _Summary of Theoretical Meeting of 17 November 1972_, Battelle-Columbus Laboratories, p. 109.

2. G. Meltz and N. M. Tomljanovich, "A Comparison of Plasma Line Measurements with Decay Instability Saturation Theory." op cit. p. 258.

3. F. W. Perkins, "Parametric Instabilities in the Ionosphere." op cit. p. 204.

4. D. F. DuBois and M. V. Goldman, _Phys. Rev._ $\underline{164}$, 207 (1967).

5. D. F. DuBois and M. V. Goldman, _Phys. Fluids_ $\underline{15}$, 919 (1972).

6. I. J. Kantor, Thesis "Plasma Waves Induced by H. F. Radio Waves." Rice University, Houston, Texas (1972).

7. D. F. DuBois, in _Statistical Physics of Charged Particle Systems_, edited by R. Kubo and T. Kihara (Syokabo, Tokyo, 1969).

8. K. Nishikawa, _J. of Phys. Soc. Japan_ $\underline{24}$, 916, 1152 (1968).

9. D. F. DuBois and M. V. Goldman, _Phys. Rev. Letters_ $\underline{19}$, 1105 (1967).

10. J. R. Sanmartin, _Phys. Fluids_ $\underline{13}$, 1533 (1970).

APPENDIX C:

# NONLINEAR WAVE OPTICS OF PARAMETRIC PUMP RADIATION
## IN AN INHOMOGENEOUS PLASMA

Donald F. DuBois, Martin V. Goldman
Dean McKinnis

## I. Introduction

Intense electromagnetic radiation incident on a plasma can excite parametrically unstable electrostatic plasma waves.[1] This flow of energy from electromagnetic to electrostatic waves can be described as an anomalous absorption of the electromagnetic wave. Recent calculations[2,3] of the anomalous absorptive conductivity (or equivalently the nonlinear resistivity) based on a theory of saturation of the electron-ion decay instability indicate a conductivity which is linear in the radiation power when the latter exceeds the instability threshold. In this paper we extend this calculation and find that when the radiation intensity sufficiently exceeds threshold the nonlinear conductivity saturates at a constant value. This model of the nonlinear conductivity is added to the linear conductivity, arising from electron-ion collisions, in the wave equation for the radiation as it propagates into a plane-layered inhomogeneous plasma.[4] We compute the effects of anomalous absorp-tion on the reflectivity and the spatial distribution of the radiation field, flux, energy density and force density. The nonlinear resis-tivity is scaled with a variable multiplicative parameter, $\eta$, to enable comparisons with various more detailed theories.[4,5] This form of resistivity may also be of some interest in other contexts. For example, numerical simulations in other parameter regimes (e.g., unequal temper-atures) are often interpreted using similar forms for the resistivity, based on different saturation arguments.

In Section 2 we review the results of the theory of nonlinear con-ductivity plus the necessary approximations. The geometry and para-meters associated with the radiation wave equations are set forth.

C1

In Section 3, some of the approximations of previous theory are relaxed and the nonlinear resistivity is generalized.

Section 4 describes the method of integration of the radiation wave equation.

Section 5 is devoted to applications of the theory to ionospheric modification experiments.[7,8] We conclude that anomalous absorption of $\sim 6$ Mhz radio waves with vacuum intensity $\sim 50$ $\mu$ W/m$^2$ at the F-layer of the ionosphere (200–300km) is on the order of 10% – 20%.

## II. Review of Theory

It has been shown recently[2,3] how to relate the high-frequency electron resistivity to the spectrum of enhanced Langmuir waves, driven parametrically unstable by incident radiation and saturated by induced scattering off ions. The conditions for validity of the calculation were

a) The electron and ion temperatures do not differ significantly (e.g., by more than a factor of two).

b) The total Langmuir wave energy density must be less than the electron particle energy density.

c) The radiation field must sufficiently exceed the linear parametric decay instability threshold.

The power flows from the radiation into the Langmuir waves and finally into the particles. The first condition guarantees that the acoustic waves are insignificantly enhanced relative to the Langmuir waves and therefore play no role in the enhancement of the resistivity. The high-frequency resistivity formula obtained in Reference 2 thus differs from the usual Dawson-Oberman enhancement formula.[9] The second condition was necessary to justify the application of weak turbulence theory[4] to the saturation of the Langmuir wave intensity spectrum. The third condition guarantees that spontaneous emission plays no large role in the energy balance considerations. The result obtained in Reference 2 for the dissipative part of the high-frequency electromagnetic (transverse) conductivity, $\sigma_T^{NL}$, is

$$\sigma_T^{NL} \cdot |E_o|^2 = \frac{1}{\pi} \int \frac{d^3k}{(2\pi)^3} \; \gamma(k) \; I_1(\underline{k}) \tag{1}$$

where $E_o$ is the local radiation field, $I_1(\underline{k})$ is the spectrum of electrostatic field fluctuations integrated over frequencies near the Langmuir frequency, and $\gamma(k)$ is the total linear damping rate of electrostatic waves of wave number k.

The theory developed[2,4] for the spectrum $I_1(k)$ required the constraints a), b), and c) above; in addition, neglected the zero-frequency (or oscillating two-stream) instability of Nishikawa[10]; and, finally, was valid only in a certain region of $\underline{k}$-space to be described below. The spectrum was found to be highly peaked in angle about the pump polarization direction for wave numbers which were not too small. As a function of wave number, it was found to cut-off sharply for wave numbers larger than the frequency-matched wave number, $k_m$, determined by

$$\omega_o = \omega_p(1 + 3k_m^2)^{\frac{1}{2}} + \alpha \; k_m \; \omega_p, \tag{2}$$

where $\omega_o$ is the pump frequency, $\omega_p$ the plasma frequency, $\alpha = (m_e/m_1)^{\frac{1}{2}}$, and k is measured in units of the Debye wave number. The analytic expression found in Reference 2 for the angle-averaged spectrum was

$$\overline{I}_1(k) \equiv \frac{1}{4\pi} \quad d\Omega I_1(\underline{k}) = \frac{\theta}{6dk^2} \int_k^{k_c} \left( Pf(\overline{k}) - 1 \right) d\overline{k} \tag{3}$$

Here $\theta$ is the electron temperature in energy units, $d = 2 \times 10^{-3} \alpha^2$, $k_c$ is the critical wave number separating the decay from the zero-frequency instabilities,

C4

$$\omega_o = \omega_p (1 + 3k_c^2)^{\frac{1}{2}} \qquad (4)$$

and $f$ is the frequency-matching resonance function given in Reference 2 which peaks at $k_m$, is zero at $k_c$ and tends to zero as $K$ decreases away from $k_m$. $P$ is the square of the ratio of the pump field to the minimum threshold field for the equal temperature three-mode decay instability:

$$P = E_o^2 / E_{Th}^2 \qquad (5)$$

$$\frac{E_{Th}^2}{4\pi n \theta} = \frac{16\gamma(k_m)}{\omega_p} \qquad (6)$$

The spectrum given in Eq. (3) spreads towards lower wave numbers with a width given roughly by

$$k_c - k_{min} \simeq \frac{2}{3} P\alpha \quad \text{for } k_{min} > 0. \qquad (7)$$

Formula (3) for the spectrum $\overline{I}_1(k)$ is valid only for $P \gg 1$, for $k_m$ in the collision-damped regime rather than the Landau-damped regime, and for wave numbers such that $\alpha k > \gamma(k)$. When this last condition is violated, a second (antistokes) Langmuir wave upshifted from the pump frequency is dragged in and increases the linear decay instability threshold, thereby reducing the spectral intensity.

Under the above conditions, and under the further condition that the spectrum not be spread to zero in wave number (i.e., $(2/3)Pa < k_c$), expressions for the total energy and dissipative nonlinear conductivity were obtained in Reference 2:

$$\overline{E} \equiv \frac{k_D^3}{8\pi^3} \int_{k_{min}}^{k_c} dk \; k^2 \; \overline{I}_1(k) \simeq \frac{2}{3} \; \frac{\gamma}{\omega_p} \; P^2 \; n\theta \tag{8}$$

$$4\pi \; \sigma_T^{NL} \simeq \frac{1}{6} \; P\gamma \tag{9}$$

In the course of the present paper, it will be found necessary to lift all of the above restrictions, with the exception of a), b), and c) above and the neglect of the zero-frequency instability.[10a]

In an inhomogeneous plasma, we cannot regard the pump field as explicitly known locally near the reflection point without solving Maxwell's equation for the pump field and including any nonlinear contributions to the conductivity such as that of Eqs. (1) or (9). If we adopt the plane geometry illustrated in Fig. 1, we must solve the following second-order nonlinear equation for the (complex) pump field $E = E_o \; e^{-i\varphi}$ in the presence of the absorptive part of the transverse conductivity, $\sigma_T$:

$$\frac{\partial^2 E}{\partial z^2} + \left[ 1 - \frac{\omega_p^2(z)}{\omega_o^2} + \frac{4\pi\sigma_T \; (E_o, z) \; i}{\omega_o} \right] \; E = 0 \tag{10}$$

Here the spatial coordinate z has been made dimensionless by scaling it in units of $c/\omega_o$ , the free-space wavelength over $2\pi$. z is measured from the reflection point towards lower densities. For the linear density profile we are considering in the present paper,

C6

$$\frac{\omega_p^2}{\omega_o^2} = 1 - \frac{z}{z_o} \tag{11}$$

where $z_o$ is a dimensionless density scale length, related to the customary scale length L by

$$z_o = \frac{\omega_o L}{c} \tag{12}$$

In the absence of any dissipation ($\sigma_T = 0$) the solution to Eq. (10) which is damped on the overdense side of the reflection point is the well-known Airy function, sketched in Fig. 2. Notice the first maximum occurs at $z = z_o^{1/3}$ and represents an enhancement over the incident power by a (swelling) factor, $3.8\, z_o^{1/3}$. A value of $z_o = 1000$ corresponds, for the Nd-laser value of $c/\omega_o = 0.1\mu$, to a density scale length $L = 100\,\mu = 0.1$ mm. For comparison, in radio-wave ionospheric experiments, $c/\omega_o$ is ~10 meters, and a $z_o$ of 1000 yields $L = 10^4$ meters, compared to measured scale lengths of $10^4 - 10^5$ meters.

The dissipative conductivity contained in Eq. (10) consists of the linear conductivity plus a nonlinear contribution suitably evaluated in the inhomogeneous plasma. Perkins and Flick[11] have shown that the linear stability analysis for an inhomogeneous plasma in the geometry we are considering is unchanged from the analysis of an infinite homogeneous plasma usually considered, provided the density scale length exceeds the electron mean free path. We shall consider only such cases here and assume that $\sigma_T^{NL}$ can be obtained from the Eqs. (5) (6) and (19) by using local values of n, $\theta$, and $E_o$. The evaluation of $\sigma_T^{NL}$ at a given position in the inhomogeneous plasma from Eq. (1) requires a knowledge of the angle-averaged spectrum

C7

$I_1$ (k) for the appropriate frequency-matched wave number, $k_m$. From Eqs. (2) and (11) it is easy to see that when $k_m \ll 1$, it is (in units of the Debye wavenumber) given by approximately

$$k_m^2 \simeq \frac{1}{3} \frac{z}{z_o} \ll 1 \qquad (13)$$

Thus, as the pump wave propagates inwards towards the reflection point, it first drives Langmuir waves with $k_m$ in the Landau-damped regime, then in the collision-damped regime, and finally it encounters the range very close to the reflection point where four-mode effects raise the threshold ($k_m \leq \gamma_c/\omega_p a$). In order to evaluate the resistivity in all these regions, the results of Reference 2 must be generalized to deal with Landau damping, four-mode effects, and extreme broadening of the spectrum. These effects will be considered next.

## III. Generalization of the Nonlinear Resistivity

In this section we shall discuss the qualititave and quantitative implications of Landau damping, four-mode effects, and spectrum k-broadening for the nonlinear resistivity derived in Reference 2 and described in Section II.

As we shall soon see, the shape of the pump amplitude squared obtained from solving the nonlinear equation (10) will not differ in quality substantially from the Airy function solution illustrated in Fig. 2. That is, the pump amplitude squared will generally have a peak at $z = z_o^{1/3}$, and lower peaks near $3z_o^{1/3}$, $5z_o^{1/3}$, etc. Four-mode effects are important when $ak \leq [\gamma + \gamma^{NL}(k)]/\omega_p$. Whenever they are important, $\gamma^{NL}$ is reduced, so we may qualitatively look for the solution to

$$\alpha \, k_4 = \frac{\gamma(k_4)}{\omega_p} \qquad (14)$$

to determine the wave number $k_4$ at which four-mode effects are important. In the small k limit $\gamma(k)$ is the collision-damping rate $\gamma_c$, and independent of k, so one solution of Eq. (14) is

$$k_4 = \frac{\gamma_c}{\omega_p} \quad \frac{1}{\alpha} \qquad (15)$$

We shall take $\gamma_c/\omega_p$ to be of the order $4 \times 10^{-6}$ for the ionospheric F-layer at $n_e = 5 \times 10^5 \, C_m$ and $\Theta_e \approx 0.2$ eV ($2319^{\circ}$k) and of the order $3 \times 10^{-4}$ for a laser-produced plasma at $n_e \approx 10^{21}$ and $\Theta_e \approx 1$ keV, using[12]

$$\gamma_c/\omega_p = \frac{(k_D{}^3/n) \, \ln \dfrac{\Theta}{\omega_p}}{48} \qquad (16)$$

For the ionosphere the ions at the F-layer are mainly oxygen, so $\alpha = 5.83 \times 10^{-3}$, whereas for laser applications, $\alpha = .0234$ (for hydrogen). Four-mode effects are important, therefore, for $k \leq k_4$, where, for the two cases,

$$k_4^{\text{Ionosphere}} = 6.86 \times 10^{-4}, \quad k_4^{\text{laser}} = .0129 \qquad (17)$$

If we use Eq. (13) to relate this frequency-matched wave number to a distance from the reflection point, we obtain

$$z_4^{\text{Ionosphere}} \approx 1.4 \times 10^{-6} z_o, z_4^{\text{laser}} = 5 \times 10^{-4} z_o \qquad (18)$$

For a typical ionospheric scale height, $z_o = 5 \times 10^3$, whereas for a typical laser-produced plasma, $z_o = 10^3$, so

$$z_4^{\text{Ionosphere}} = 7 \times 10^{-3}, \quad z_4^{\text{laser}} = .5 \qquad (19)$$

which are both on the low pump-field side of the first maximum. The situation
is illustrated in Fig. 3. In this region the nonlinear conductivity will
usually not be very effective in the nonlinear Maxwell equation since the
pump field is far below its first maximum. Another solution to Eq. (14)
is in the Landau-damped region where $\gamma(k_4)$ becomes large as $k_4$ increases.
In this region, Eq. (14) becomes

$$\alpha k_4 = \sqrt{\frac{\pi}{8}} \; \frac{1}{k_4^3} \; e^{-3/2} \; e^{-1/2 k_4^2} \qquad (20)$$

which, for $\alpha = 5.83 \times 10^{-3}$ has the approximate solution $k_4^{\text{Ionosphere}} = .240$,
and for $\alpha = .0233$ has the approximate solution $k_4^{\text{laser}} = .265$. Four-mode
effects therefore again begin to be important for wave numbers exceeding
.24 to .265 in the Landau-damping region. Spatially, this wave number
corresponds to a distance from the reflection point found from Eq. (13)
to be

$$z_4 = 210$$

for a scale length of $z_o = 10^3$. At this point the modified Airy pattern
will have undergone over 10 oscillations and decreased in amplitude at
the peaks. We shall soon see how Landau damping reduces nonlinear
resistivity in this region even more drastically. Thus, we conclude
that four-mode effects are of marginal importance.

For frequency-matched wave numbers $k_m$ in the collision-damped
regime and sufficiently large pumping power, P, the expressions in
Eqs. (8) and (9) for the total wave energy and the resistivity should be
modified to be consistent with a spectrum that has broadened all the way
down to zero wave number. The approximate expression for the angle-
averaged spectrum $\overline{I}_1(k)$ in Eq. (3) is still valid. From Eq. (7) we see
that for pump power P exceeding P*, where,

$$P^* = \frac{3k_c}{2\alpha} \tag{21}$$

the spectrum will be totally broadened. The total energy $\bar{E}$ can generally be found from the approximate spectrum of Eq. (3) as follows:

$$\bar{E} = \frac{k_D^3}{8\pi^3} \int_{k_{min}}^{k_c} dk\, k^2\, \bar{I}_1(k) = \frac{k_D^3\, \theta}{48\pi^3 d} \int_{k_{min}}^{k_c} dk \int_k^{k_c} (Pf(k')-1)\, dk' \tag{22}$$

Integrating by parts and noticing that the boundary terms are negligible if the spectrum is small at $k_c$ and $k_{min}$ or, in the case of $k_{min} = 0$, $\bar{I}_1$ may even diverge, provided

$$\lim_{k \to 0} k^3 \bar{I}_1(k) = 0$$

Then

$$\bar{E} = \frac{k_D^3 \theta}{48\pi^3 d} \int_{k_{min}}^{k_c} dk\, k(P\, f(k) - 1) \tag{23}$$

Using the peakedness of $f(k)$ at $k_m$, and the approximate result that the integral of $f(k) = 2\alpha/3$, we obtain

$$\bar{E} = \frac{k_D^3 \theta}{48\pi^3 d} \left[ k_m\, P\, \frac{2}{3}\, \alpha - k_c(k_c - k_{min}) + \frac{(k_c - k_{min})^2}{2} \right] \tag{24}$$

It is easy to show that $k_c - k_m \approx \alpha/6$. The exact expression for d is[4a] $d = (\alpha^2/432\pi^2)\, (k_D^3/n)\, (\omega_p/\gamma)$. We thus obtain from Eq. (24) two expressions for the energy $\bar{E}$. For the case $k_{min} > 0$, $k_c - k_{min} \sim P(2/3)\alpha$ and the expression in Eq. (8) results when $P \gg 1$. For the case $k_{min} = 0$, or $(2/3\, P\alpha > k_c$, we obtain

$$\bar{E} \simeq n\theta \, \frac{6}{\pi} \, \frac{\gamma}{\omega_p} \, \frac{k_m}{\alpha} \left[ P - \frac{3k_m}{4\alpha} \right], \text{ for } P > \frac{3}{2} \frac{k_m}{\alpha} \qquad (25)$$

For sufficiently large P, therefore the total energy goes as P rather than $P^2$ and the corresponding conductivity is eventually independent of the pump power. From Eqs. (1) and (25), in the collision-damped region for $k_m$,

$$4\pi\sigma_T^{NL} = \frac{16\pi\gamma\bar{E}}{E_o^2} \simeq \frac{3\gamma}{2\pi} \, \frac{k_m}{\alpha} \, (1 - \frac{3k_m}{4\alpha P}), \quad P \geq \frac{3}{2} \, \frac{k_m}{\alpha} \gg 1 \qquad (26)$$

Another effect not included in the above analysis but of possible importance at low wave numbers and high P is the inception of mode-coupling of Langmuir and acoustic waves as a stronger saturation mechanism than induced scattering of Langmuir waves into Langmuir waves. Mode-coupling is discussed in Reference 4a, Eqs. (25) through (28), where it is concluded that it is relatively weak except at small wave numbers. When it dominates, the spectrum can be shown to be rigorously isotropic in angle as a consequence of the balance between spontaneous emission and mode-coupling damping. The spectrum can then be shown to be about one-third as wide in k as the narrow spectrum discussed above in the absence of mode-coupling and the total wave energy is doubled. The ratio of the Langmuir wave nonlinear mode-coupling to induced scattering damping rates at $k_m$ can be shown from the spectral form to be

$$\frac{\gamma^{MC}}{\gamma^{SP}} \simeq \frac{2}{5} \, \frac{P}{k_m^2} \, \frac{\gamma}{\omega_p} \qquad (27)$$

When this ratio is large compared to one, the total wave energy and, hence, the conductivity is multiplied by a factor 2 in comparison with its

C12

value in the absence of mode-coupling. Since the isotropic spectrum does not spread to zero wave number until P is three times larger than before, the total wave energy remains proportional to $P^2$ for higher values of P than previously. All of these features increase the resistivity for those values of P and $k_m$ for which $\gamma^{MC}/\gamma^{SP}$ is large compared to one.

Next, we explore the effects of linear Landau damping on the spectrum and resistivity for the case of $k_m$ exceeding about 0.2. A complete treatment of saturation in the Landau-damped region requires the addition of particle orbit perturbation corrections[13] as well as the induced-scattering saturation mechanisms we have included. If we ignore the orbit perturbation corrections (which may be weaker), then a linear Landau-damping term must be added to $\gamma_p^{NL}$ in the equation (4) of Reference 2. This leads to an approximation for the angle-average spectrum which is of the following form:

$$\bar{I}_1(k) = \frac{\theta}{6dk^2} \left[ \int_k^{kc} dk' \ (P_c f(k') - 1 - \Gamma(k')) \right] \tag{28}$$

$P_c$ in this expression is defined in accordance with Eqs. (5) and (6), but with $\gamma$ in Eq. (6) redefined to be the collision damping rate $\gamma_c$ cited in Eq. (16). $\Gamma(k)$ is the ratio of the Landau damping rate to the collision-damping rate,

$$\Gamma(k) \equiv \frac{\omega_p}{\gamma_c} \ \sqrt{\frac{\pi}{8}} \ e^{-3/2} \frac{1}{k^3} \ e^{-1/2 \ k^2} \tag{29}$$

C13

The integral over $\Gamma(k')$ is trivial, leading to

$$\bar{I}_1(k) = \frac{\theta}{6dk^2}\left[\int_k^{k_c} dk' \; (P_c f(k') - 1) - k_c^3 \; \Gamma(k_c) + k^3 \; \Gamma(k)\right] \quad (30)$$

The width of the spectrum is now given by

$$k_c - k_{min} \approx P_c \frac{2}{3} \alpha - k_c^3 \; \Gamma(k_c) + k_{min}^3 \; \Gamma(k_{min}) \quad (31)$$

Unlike the result in the collision-damped regime, this width depends on $k_c$ and is narrower than before. The pump power $P_c$ at which the spectrum is just spread from $k_c$ to $k = 0$ is given by the solution to the transcental equation (31) with $k_{min} = 0$. For $\alpha = 1/42$ and $\gamma_c/\omega_p = 3 \times 10^{-4}$ some solutions are given in Table 2. From the values of $\Gamma(k_c)$ we see that Landau damping is just equal to collision damping for $k \sim 0.215$. This result is not changed very much for the ionosphere. For smaller $k_c$, $P_c$ remains about 14. In Figs. 4 through 8, the spectrum of Eq. (30) is plotted numerically and integrated to obtain the total energy, for $\alpha = 1/42$ and $\gamma_c/\omega_p = 3 \times 10^{-4}$. In Figs 4 and 5, $P_c$ is kept fixed at 10 and the matched wave number is increased from .21 where Landau damping is just becoming important to .25 where it is very strong. In agreement with Table 1, the spectrum has not spread to zero for $P_c = 10$. As $k_m$ increases, the spectrum is seen to narrow and diminish in intensity until it is flat at zero for $k_m = 0.25$ (not shown). In spatial terms the spectrum diminuation occurs over one or two cycles of the modified Airy pattern in the region where the field peaks are already diminished. In Figs. 6 through 8, $P_c$ is fixed at 20 and the matched wave number is again increased from .21 to .25. At $k_m = 0.21$ and 0.23

C14

the spectrum has broadened to zero, in agreement with Table 1, whereas for $k_m = 0.25$ the spectrum has narrowed and diminished in intensity considerably due to heavy Landau damping. The cross-marks in Figs. 6 and 7 are values of $k^2 \bar{I}_1(k)$, which is seen to go to zero as $k \to 0$. Thus, there is no large contribution to the total energy from small wave numbers (where four-mode effects should really be included anyway). In Table 2 the total energy is integrated numerically from the spectra of Figs. 4 through 8 and also for the case $P_c = 40$. Except for $P_c$ values of the order of 40 or more, the total energy of waves decreases sharply in the Landau-damped region. For $P_c$ values less than ~40, the contributions to the resistivity in the Landau-damped region are also decreasing with larger $k_m$ (farther from the reflection point) and we shall adopt the point of view that a crude interpolation of the resistivity from the collision-damped value to zero deep in the Landau-damped region is adequate at these $P_c$ values.

To conclude this discussion of generalization of the nonlinear resistivity we next examine modifications due to the new findings of more exact theories[4,5,5a]. Numerical integrations of the time-dependent 1-dimensionalized nonlinear plasma wave kinetic equations[4,5] yield total plasma wave energies from 2 to 3 times larger than the values obtained from the approximate analytic theories (e.g., eqn. 8). 2-dimensional integrations have also been performed recently[5a] but the resulting total energy has not yet been given. In all of these integrations the form used for the resonant mismatch factor $f(k)$ also can vary the coefficient of the total energy by a factor of 2 or 3. DuBois and Goldman[4] use a form of $f(k)$ based on a resonance approximation for the ion-acoustic dielectric function

which, however, is truncated to zero beyond $k_c$, the critical wave number separating the decay from the zero-frequency instability ($k_c$ is defined in equation 4 of the present paper). In references 3,5 and 5a, the exact equal-temperature ion-acoustic dielectric function is used, but no truncation at $k_c$ is included. The treatment of Reference 3 appears to yield a total energy about 9/4 times larger than that of Reference 4, due to the different choice for $f(k)$.

In view of the fact that the total wave energy (and hence the nonlinear absorptive conductivity which is proportional to the total wave energy) are known only to within a constant which may vary by as much as an order of magnitude, we shall use a variable multiplicative parameter $\eta$ defined in terms of the total plasma wave energy $\bar{E}$ as follows:

$$\bar{E} = 4\eta \frac{\gamma_c}{\omega_p} P^2 n\theta, \qquad P \leq \frac{3}{2} \frac{k_m}{\alpha}$$

$$\bar{E} = 4\eta\, 3 \frac{\gamma_c}{\omega_p} \frac{k_m}{\alpha} \left[ P - \frac{3k_m}{4\alpha} \right] n\theta, \qquad P \geq \frac{3}{2} \frac{k_m}{\alpha} \tag{32}$$

Comparing with eqns. (8) and (25) we see that $\eta = \frac{1}{6}$ for the theory upon which those equations rest. In table 3 we indicate values of $\eta$ which may arise from various theories.

In accordance with the above discussion, the absorptive conductivity we shall use in the integrations of the radiation wave equation (10) is

$$\frac{4\pi\sigma_T}{\omega_0} = \frac{\omega_p^2}{\omega_0^2}\frac{\nu_{ei}}{\omega_0} + \eta\left|\frac{E}{E_{th}}\right|^2\frac{\gamma_c}{\omega_0} W(E) \tag{33}$$

The first term on the right side is the linear collisional damping term. $\nu_{ei}$ is the electron-ion collision frequency, which we take to be $2\gamma_c$ where $\gamma_c$ is defined in equation (16). The second term on the right side is the nonlinear contribution to the absorptive conductivity which includes four-mode effects, an interpolation from the collision-damped region into the heavily Landau-damped region, and broad-spectrum effects, as well as the scaling factor $\eta$ defined in equations (32) and Table 3. The various quantities appearing in $\sigma_T^{NL}$ are defined below:

$$E_{th}^2 = 64\pi n(z)\theta\frac{\gamma(k_m)}{\omega_p}\left[1 + \frac{4\sqrt{3}}{9}\frac{\gamma(k_m)}{\omega_a}\right] \tag{34}$$

Here $\gamma(k_m)$ is the total damping rate, including collision-damping plus Landau-damping when significant. $\gamma(k_m)$ assures that the conductivity decreases in the Landau-damped region. The factor in square brackets in eqn (34) guarantees the increase in threshold associated with the onset of four-mode effects, although it is quantitatively correct only for electrons not compared to ions and then more precisely should involve $\gamma^{NL}$, as described above in eqn (14). The reduction of the conductivity in the Landau-damped regime is likewise only a quantitative interpolation.

The factor $W(E)$ accounts for the broad spectrum effects described by equations (8), (25), and (32):

$$W(E) = \begin{cases} 1, & P \leqslant \frac{3}{2}\frac{k_m}{\alpha} \\[4mm] \dfrac{2}{(2/3)\frac{\alpha P}{k_m}} - \dfrac{1}{\left[(2/3)\frac{\alpha P}{k_m}\right]^2}, & P \geqslant \frac{3}{2}\frac{k_m}{\alpha} \gg 1 \end{cases} \qquad (35)$$

where P is defined in Eq. (5).

## IV. Integration of the Nonlinear Wave Equation for the Pump Field in a Linear Density Profile

Here our object is to integrate the wave equation (10) for the radiation field in a linear density profile, building into the nonlinear conductivity the effects described by equation (33) of the last section.

Even in the presence of linear and nonlinear damping the wave equation generally has a solution which grows in the overdense region in the direction of higher densities and one which decays. We begin our numerical integration with an arbitrary boundary value of E deep in the overdense region and integrate towards lower densities. In this direction the unphysical and therefore unwanted "growing solution" decays spatially and we have verified it is negligible by the time it reaches the oscillatory region ($z > 0$).

At $z = z_0$ the density vanishes and E consists of an incident and reflected plane wave:

$$E \simeq a\,e^{i(z_0-z)} + b\,e^{-i(z_0-z)} = E_{inc.}(z) + E_{refl.}(z) \qquad (36)$$

Since we are assuming time-dependence as $e^{-i\omega t}$ and decreasing z is increasing density, $|a|$ is the amplitude of the incident wave and $|b|$ is the amplitude of the reflected wave. The reflection coefficient

$$R = |\frac{b}{a}|^2 \qquad (37)$$

is then extracted at $z_0$ along with the incident intensity at $z_0$, both corresponding to the chosen boundary value for E in the deep overdense region. Let us separate

C18

the field E into its real and imaginary parts,

$$E = E_{real}(z) + i\, E_{imag.}(z) \tag{38}$$

The wave equation (10) with the appropriate $\sigma_T^{NL}$ is then integrated from the deep overdense boundary value at $z_{initial} < 0$ towards positive z by a Runge-Kutta method with error control. When $E_{real}$ and $E_{imag.}$ near $z_o$ are known from the numerical integration which started at $z_{initial} < 0$, the reflection coefficient at $z = z_o$ is determined as follows: Take the derivative of Eqs. (36) and (38)

$$\left.\frac{\partial E}{\partial z}\right|_{z_o} = i\, a + i\, b = E'_{real} + E'_{imag.} \tag{39}$$

Equations (36) - (39) are now algebraic equations which may be solved for a and b in terms of $E_{real}(z_o)$, $E_{imag.}(z_o)$ and their first derivatives at $z_o$. The reflection coefficient is then:

$$R = |\frac{b}{a}|^2 = \left[\frac{(E_{real}(z_o) + E'_{imag.}(z_o))^2 + (E_{imag.}(z_o) - E'_{real}(z_o))^2}{(E_{real}(z_o) - E'_{imag.}(z_o))^2 + (E_{imag.}(z_o) + E'_{real}(z_o))^2}\right] \tag{40}$$

To understand the radiation field patterns produced by this nonlinear resistivity, we first examine the zero-resistivity ($\sigma = 0$) Airy function pattern. As a function of position and time, the electric field may be written as

$$E(z) = |A(z)|\, \cos(\phi(z) + \omega t), \tag{41}$$

where $A(z)$ is an Airy function solution. The Airy function solution $A(z)$ normally oscillates both positive and negative, and the phase $\phi$ is constant, so $E(z)$ is a standing wave. We have instead chosen to use the absolute value $|A(z)|$ and represent the negative and positive character of A by allowing the

C19

phase $\phi$ to change discontinuously by $\pi$ at the nodes of $A(z)$ for reasons to become evident. Equation (41) of course still represents a standing wave and with the choice of zero phase at $z = 0$ is identical with $A(z) \cos \omega t$. The phase $\phi(z)$ and amplitude squared $A^2$ are plotted in Fig. 9, with A normalized to an incident wave of unit amplitude.

In the following sections we consider ionospheric and laser cases of nonlinear absorption. For each set of values of $\eta$, the incident intensity,

$$I_{inc} = \frac{cE^2_{inc}}{8\pi},$$

and the scale length $z_c$, we have obtained a value for the reflectivity and plots of the radiation amplitude $|A(z)|^2$ (in units of the incident intensity) and the phase $\phi(z)$, defined by equation (41). The amplitude maxima will be seen to exhibit a reduced swelling factor, due to the absorption, but otherwise show the characteristic oscillatory structure of Figure 9. The reduction of the relative intensity at the maxima is an example of the saturation mechanism we have called pump depletion, and which is the analog of bump-on-tail flattening in quasilinear theories, such as the gentle bump plasma instability. That is, the unstable plasma waves are reacting back on their source of energy (in this case the pump), tending (through absorption) to reduce its effectiveness in driving the waves unstable. Also, the amplitude minima lift from zero and the phase in their vicinity will show smoothing from the step-like behavior of Figure 9, so the wave begins to show some of the character of a travelling wave rather than a standing wave. (Note a perfect travelling plane wave would have a linear phase and constant amplitude.)

These effects are more pronounced closer to the incidence point $z_o$ rather than the reflection point $z = 0$. The reason is as follows:

One half of the absorption of a wave reflecting off an overdense plasma occurs on the return trip. Even in a case of total absorption, the wave patterns very near the reflection point would not look like a travelling wave because the reflected wave has not damped to zero until it returns all the way back to $z_o$. Thus, even for cases of strong linear or nonlinear absorption the oscillatory structure of the radiation wave pattern near the reflection point is preserved. It is only after several oscillations (at least 12% $z_o$) away from the reflection point that the nonlinear absorption will have had its full effect. Geometric optics approximations[14] which only contain the envelope of the wave pattern are inherently inaccurate. Although they can be scaled to give reasonably good reflectivities, they cannot show the large variations in pump field and consequently in plasma wave energy near the reflection point. This structure is of interest in the ionospheric and laser applications, in the former case, because of scattering measurements from specific altitudes near the reflection height, and in the latter case because of possible pondermotive-force-induced motions of the density profile.

These quantities associated with the solution to the nonlinear pump radiation wave equation which are of interest to us are the Poynting flux, the energy density, and the pondermotive force. In our geometry and units, with a plane polarized pump field, the time-average Poynting flux is

$$J_z \equiv \frac{c}{4\pi} \ \frac{\omega}{2\pi} \int_0^{2\pi/\omega} dt \quad |\underline{E}(z,t) \times \underline{B}(z,t)|$$

$$= - \frac{c}{8\pi} \ E_o^2 \ \frac{\partial \phi}{\partial z} \tag{42}$$

where $E(z) = E_o e^{-i\phi}$, and z is in units of $c/\omega$, as before. By plotting $-J_z$ we can get some idea of where the absorption is occurring, since the loss

C21

term in the conservation equation is proportional to $-\partial J_z/\partial_z$. With this definition of $J_z$ as the <u>total</u> Poynting flux it must vanish for the case of total reflection. This is evident from equation (42) and Figure 9, since the Airy function solution has steps in $\phi$ only at the nodes of $E_o$.

The time-average energy density of the radiation in the plasma is given by

$$U \equiv \frac{1}{16\pi} \left[ |B|^2 + |E|^2 \left(1 + \frac{\omega_p^2}{\omega^2}\right) \right]$$

$$= \frac{1}{16\pi} \left[ \left|\frac{\partial E_o}{\partial z}\right|^2 + E_o^2 \left(\left|\frac{\partial \phi}{\partial z}\right|^2 + 1 + \frac{\omega_p^2}{\omega^2}\right) \right] \tag{43}$$

This expression includes magnetic, electric and coherent particle kinetic energy densities[15].

## V. Nonlinear Absorption of Ionosphere-Modifying Radio Waves

In recent experiments[8] low frequency (5-10 Mhz) ordinary radio waves with local vacuum intensities of up to 50 $\mu\omega/m^2$ are reflected from the F-layer of the ionosphere (200-300 km altitudes). The electric field of these waves near the reflection point should be approximately plane-polarized along the direction of the geomagnetic field and is believed at its peak to exceed the threshold for excitation of parametric instability.[7] Ionospheric measurements show the reflectivity of lower intensity diagnostic radiation in the same frequency range drops within seconds when the high-intensity radiation pump is turned on and comes back up again within seconds when the pump is turned off. Since the growth time for the decay parametric instability is on the order of tens of milliseconds this behavior may be due to scattering from associated slow hydrodynamic instabilities rather than from anomalous absorption or scattering off enhanced Langmuir or ion-acoustic waves. However, the issue is still not resolved.

Incoherent back-scattering experiments performed at Arecibo,[16] using 430 Mhz radio waves, have probed approximately vertically propagating Langmuir and ion-acoustic waves of wave number $k = \dfrac{4\pi f_1}{c} \approx .05\, k_D$ (for $\theta_e \approx 0.2$ eV). According to equation (13), this corresponds to scattering from an altitude $z/z_0 = 7.5 \times 10^{-3}$, neglecting geomagnetic field effects. At present, there is some question as to whether the scattering is from nonlinearly saturated plasma waves or from the pump wave beating with ion-acoustic fluctuations[1] to produce Langmuir fluctuations below the parametric instability threshold.

Against the background of these experiments it is especially important to determine the extent of pump nonlinear absorption and the spatial behavior of the pump electric field. The existence of significant nonlinear

C23

absorption bears on reflectivity experiments for the pump or a secondary diagnostic wave, as well as the entire question of anomalous heating and possibly airglow production. The local values of the pump electric field and its modified swelling pattern are needed to understand the scattering experiments.

The first set of computer runs have been performed using the following set of parameters:

$$n_0 = 5 \times 10^5 \text{ cm}^{-3}$$

$$\theta_{\substack{e \\ i}} = 0.2 \text{ eV} = 2319^\circ\text{K} \text{ (daytime)}$$

$$\alpha \equiv (m_e/m_i)^{1/3} = .00583 \text{ (oxygen)}$$

$$\omega_0/2\pi = \text{modifier (pump) frequency} = 6.35 \text{ Mhz}$$

(44)

Derived quantities based on the above parameters are:

$$\omega_{pe_0} = 4 \times 10^7 \text{ radians/sec}$$

$$\nu_{ei_0} = 2\gamma_{co} = 350 \text{ Hz}$$

$$\Lambda_{th}^2 \equiv \frac{E_{o_{th}}^2}{4\pi n_0 \theta_e} = 16 \frac{\gamma_{co}}{\omega_p} = 7 \times 10^{-5}$$

$$I_{th} = \frac{c}{8\pi} E_{o_{th}}^2 = 168 \mu\text{W/m}^2 \text{ (locally)}$$

(45)

C24

The peak plasma frequency, $\omega_{pe_0}$ is equal to the pump frequency, $\omega_0$. $\gamma_{co}$ is computed using equation (16). The threshold for the parametric instability is indicated as $I_{th}$, and should be understood as the value which $\dfrac{cE_c^2}{8\pi}$ (including swelling due to inhomogeneity) must exceed locally to excite the parametric decay instability. We consider two scale heights: $H = 37.5$ km ($z_0 \equiv \dfrac{\omega_0}{c} H = 5000$) and $H = 75$ km ($z_0 \equiv \dfrac{\omega_0 H}{c} = 10^4$).

The integrated total absorption is numerically measured by the quantity $1 - R$, where $R = |E_{ref}/E_{inc}|^2$ is the power reflection coefficient at the "source point" $z = z_0$. We also compute for each case the integrated purely linear reflectivity $R_{lin}$, obtained by integrating the wave equation (10) using only the linear dissipative conductivity (first term on right side of equation (33)). These results compare favorably (within 50%) with the value of $R_{lin}$ calculated from geometric optics.

$$R_{lin} = e^{-\frac{8}{3} \frac{\nu_{ei}}{\omega_0} z_0} \tag{46}$$

The quantity $R_{lin} - R = (1 - R) - (1 - R_{lin})$ is a measure of the anomalous absorption (excess beyond linear).

In Figure 10 both $1 - R$ (left axis) and $R_{lin} - R$ (right axis) are shown for an incident vacuum intensity of $50\mu w/m^2$, which is about the maximum presently available at the Platteville transmitter[8] in Colorado. (Approximately one half this value is attainable at Arecibo, Puerto Rico.)

The absorption is plotted as a function of the multiplicative scaling parameter, $\eta$, defined in equation (33) and Table 3. As explained in Table 3, the results of the best available theories indicate $\eta$-values between $\frac{1}{2}$ and $3/4$. The recent results of Fejer and Kuo[5a] indicate a saturated spectrum of plasma waves which has some angular extent, although they do not compute the total plasma wave energy or conductivity. The isotropic angle spectrum approximation of Goldman and DuBois[4,4a] predicts a rough doubling of the total plasma wave energy as compared to the extreme anisotropic spectrum solution, so we also look at $\eta$ values as high as 2.

For a scale height of 37.5 km, the linear absorption $1 - R = 9\%$ for the parameters of (44) and (45). (Equation (46) gives 12%.) The excess nonlinear (anomalous) absorption $R_{lin} - R$ is between 9% and 23% depending on $\eta$. The behavior of $R_{lin} - R$ with $\eta$ is roughly linear.

For a scale height of 75 km, the linear absorption is $1 - R_{lin} = 17\%$ for the parameters of (44) and (45). (Equation (46) gives 23%.) The excess nonlinear absorption $R_{lin} - R$ is between 14% and 33%, depending on $\eta$. Longer density scale lengths are therefore seen to lead to stronger absorption. The physical reason is that the absorption region is "stretched", although from the above results it appears that this is a stronger effect for the linear absorption than the nonlinear contribution (presumably because the nonlinear absorption region is thinner spatially).

The above results are for relatively high daytime electron temperatures. Strictly speaking, the effects of photoelectrons on the plasma wave damping should be included for daytime parameters. We have crudely estimated the effects of photoelectrons in a separate data run by adjusting the Landau damping to be three times larger than the collisional damping of the Langmuir waves at a matched wave number of $k_m \simeq 0.1 k_D$. (Ordinarily

the Landau damping is much smaller than the collision damping.) The factor 3 was chosen as an average. At this density and temperature downward propagating plasma waves have a photoelectron damping rate equal to the collisional damping rate and upward propagating plasma waves have photoelectron damping five times collisional damping. (The photoelectrons originate mainly at lower altitudes.) Also, there should not be many photoelectrons at energies beyond $\frac{m}{2} (\frac{\omega_p}{k})^2 \approx 20eV$. This has the effect of raising the threshold for parametric instability by a factor of ~4 at altitudes in the vicinity of $z/z_o = .03$ and by more below. It does not alter the nonlinear conductivity at higher altitudes because the phase velocities at the correspondingly smaller matched wave numbers are too high to allow wave resonance with photoelectrons. The net effect is to condense the spatial region of nonlinear absorption. For all parameters the same as in Figure 10, but photoelectrons included in the above manner, and a scale height of 75 km, we find for $\eta = 2/3$, $R_{lin} - R = 11\%$ anomalous absorption compared to 14% anomalous absorption without photoelectrons; and for $\eta = 2$, $R_{lin} - R = 27\%$ anomalous absorption, compared to 33% anomalous absorption, without photoelectrons. Photoelectrons thus appear to reduce the percent of anomalous absorption by a factor of about 20%. When photo-electron damping of Langmuir waves is a strong effect, or, indeed even if the normal Landau damping region is to be treated properly, the absorptive conductivity arising from orbit perturbation saturation[13] must be used rather than the conductivity associated with weak turbulence saturation, which we have been using here. We are presently putting into effect a program for doing this.

We have also made some runs at lower electron temperature (.13eV = 1500°K). Since the linear absorptive conductivity goes as $\nu_{ei}$ and hence as $\theta_e^{-3/2}$, the linear absorption should and did increase. The nonlinear

C27

absorption also increased, although not as strongly as the linear absorption
Making some numerical comparisons for the H = 75 km shown in Figure 10, but
with all other parameters except temperature the same, we find the linear
absorption $1 - R_{lin}$ increased from 17% to 28% as $\theta_e$ is decreased from
$2320^\circ$K to $1500^\circ$K, whereas the anomalous absorption $R_{lin} - R$ increased
from 14% (.2eV) to 19% (.13eV) for $\eta = 2/3$ and from 33% (.2eV) to 39%
(.13eV). Nighttime anomalous absorption would thus appear to be stronger
than daytime anomalous absorption, although orbit perturbation effects[13]
must be included to really determine whether this is true. Daytime neutral
collisional absorption of the modifier (pump) at lower altitudes (D-region)
would make daytime anomalous absorption still weaker.

In Figures 11 and 12 we have plotted the absorption $1 - R$ as a
function of incident intensity for the two scale heights H = 37.5 km and
75 km using the same $\eta$-values and other, fixed parameters as in Figure 10.
The absorption goes up somewhat more slowly than linear.

In Figures 13 and 14 we plot the pump radiation electric field
amplitude squared versus altitude. The pump amplitude is normalized to
the incident amplitude and the altitude is in units of $c/\omega_o$. For the
parameters of (44) and (45) this distance is 7.5 meters. The spatial wave
patterns are plotted for an incident vacuum intensity of 50 $\mu$w/m$^2$, a scale
height of 75 km ($z_o = 10^4$), and a nonlinear scaling parameter $\eta = 2$.
The density is $5 \times 10^5$ cm$^{-3}$ and the temperature is 0.2eV. Results are
shown both for a purely linear absorptive conductivity and for the linear
plus nonlinear absorptive conductivity of equation (33). The peak of the
Airy function swelling pattern is indicated by X for comparison. The effect
of pump depletion discussed in section IV is evident. The peak swelling
factor at the first maximum is reduced from 82 with no absorption to 71

C28

with linear absorption, to 56 with linear plus nonlinear absorption. The amplitudes at all the maxima are reduced by somewhat smaller percentages. For the case shown we are not very far above threshold even at the first maxima of the field pattern. Based on the actual swelling at the first maximum of the curve which incudes linear plus nonlinear absorption we find $P = 17$. If we had used the Airy function swelling factor this number would have come out to be $P \sim 24$.

For comparisons with scattering experiments, $z$ must be multiplied by 7.5 meters to convert it into distance below the reflection point. If the scattering experiment measures a wave number $k_m/k_D = .05$, this would correspond to $z = 75$ in Figure 13. Since the density scale height is never known precisely and since we have left out effects of the geomagnetic field, this information is not enough to determine whether the pump field is at a trough or a peak for the measured plasma waves. (Also, incident intensities of order $25\mu W/m^2$ should be used for Arecibo scattering experiments.) Pump depletion is seen to reduce the magnitude of the peaks from the values they would otherwise have had from linear swelling and linear absorption alone. Note, the pump field amplitude still shows the nodes characteristic of a standing wave pattern, in accordance with the discussion at the end of Section IV, due to reflection over short distances from the reflection point $z = o$.

Figure 14 shows the pump field amplitude squared down at lower altitudes. The node-lifting associated with the increased absorption and partial conversion from a standing wave to a travelling wave is apparent here.

Figure 15 shows the pump phase versus distance for the same parameters and distance range of Figure 14. The phase $\Phi$ is defined by

$E = E_o(z) \cos(\phi(z) + \omega t)$, where the amplitude $E_o(z)$ is defined to be positive. Figure 8 shows the phase in the absence of absorption for $z_o = 10^3$. The smoothing of the corners of the step like phase is also indicative of the transition from a standing wave to a travelling wave.

In Figure 16 we have plotted the negative of the total Poynting flux in units of the incident flux for the same parameters as in Figure 13. The total Poynting flux is defined in equation (42). In the absence of any absorption this net flux must vanish. The lower curve in Figure 16 includes only linear absorption. The upper curve includes both linear and nonlinear absorption. The steeper regions of the oscillating flux are the regions where the absorption is strongest, and correspond to the maxima of $E_o(z)$. The curve including both linear and nonlinear absorption shows stronger oscillations than the curve including only linear absorption because $\partial J/\partial z \propto \sigma^{NL} E_o^2 \propto E_o^4$. Also, the curve including both linear and nonlinear absorption rises to a higher value at $z = z_o$ than the curve with linear absorption alone because the smaller the reflected wave at that point, the higher the net Poynting flux.

Figure 17 is another plot of the pump radiation electric field amplitude squared versus distance z, with all parameters the same as in Figure 13, except for a value of the nonlinear scaling parameter $\eta = 2/3$ (compared to $\eta = 2$ in Figure 13). Again, the points around $z = 50$ to $100$ are where the incoherent scatter return from a 430 Mhz diagnostic might be expected to originate since these altitudes correspond to the frequency matched wave number.

C30

# IV. Conclusion

The nonlinear transverse absorptive conductivity $\sigma_T^{NL}$ which is associated with the steady state flow of energy from an electromagnetic pump wave to parametrically excited electrostatic Langmuir waves has been generalized beyond previous 1-dimensional saturation calculations. New effects which have been built into $\sigma_T^{NL}$ include:

a) Effects of a broad spectrum in $|\underline{k}|$ at high pump powers. This changes the dependence of $\sigma_T^{NL}$ from linear in the pump power to independent of the pump power.

b) Four mode effects which decrease $\sigma_T^{NL}$ for very small $k_m$ and for $k_m$ in the Landau-damped region.

c) Qualitative decrease of $\sigma_T^{NL}$ when $k_m$ is in the Landau-damped region.

d) Qualitative effects of more exact 1-D and 2-D theories are included through a multiplicative scaling parameter $\eta$, to which $\sigma_T^{NL}$ is proportional.

The resulting expression for $\sigma_T^{NL}$ is added to the linear conductivity in the wave equation for the pump radiation as it propagates towards its reflection point in a plane-layered inhomogeneous plasma. The pump wave equation has been integrated to find the total absorption (or reflectivity) at various incident power levels and frequencies, and various density scale lengths, temperatures, and $\eta$-values. In addition, the spatial pattern of the pump amplitude and phase has been displayed, and the local total Poynting flux has been plotted as a function of position for the various runs. The method used does not rely in any essential way on a linear density gradient and can be generalized in future computations.

For the ionospheric cases run, the effects (a) and (b) above do not matter in $\sigma_T^{NL}$ because the power levels are so low (typically no more than 20 times the parametric instability threshold power). Anomalous absorption

is defined as total absorption minus linear absorption. For the current
maximum available vacuum pump power of 50 $\mu\omega/m^2$ at 200-300 km in the 5-10
Mhz radio-wave range in no case do we find anomalous absorption of more than
40%. Without the effects of orbit perturbation built into $\sigma_T^{NL}$, nighttime
anomalous absorption is stronger than daytime anomalous absorption. Typical
daytime anomalous absorption (with photoelectron effects built in very crudely
as a limitation on the spatial extent of the nonlinear region) is 10-25%
at 50 $\mu\omega/m^2$. At night it is 20-40%. These values correspond to a scale
height of 75 km. The absorption which occurs at higher pump powers is
computed and may be of interest if self-focusing effects[18] can intensify the
local pump power.

An interesting feature of the pump radiation field as a function of
position is that it is essentially a standing wave at altitudes within a
few percent of the density scale height below the reflection point even
when there is strong anomalous absorption. This kind of behavior appears to
have been born out by incoherent scatter measurements.[17] We find it leads
to strong oscillations in the Poynting flux pattern and hence to bands of
altitudes at which local anomalous heating would be strongest. In general,
the maxima of the pump amplitude oscillations are lower than they would be
with no absorption or with linear absorption alone. This phenomenon of
pump depletion[4] is evidence of the transfer of energy from the pump to the
plasma waves.

## Acknowledgements

## Table 1.

Pump Power Ratio $P_c$ for Spreading Spectrum to $k = 0$ as a Function of $k_c$. ($a = 1/42$ and $\gamma_c/\omega_p = 3 \times 10^{-4}$).

| $k_c$ | $\Gamma(k_c)$ | $P_c$ for spreading to zero k |
|-------|---------------|-------------------------------|
| .21   | .70           | 14                            |
| .23   | 2:83          | 16                            |
| .25   | 8.95          | 25                            |

## Table

Values of the wave energy $\overline{E}$ in units of $n\theta$

for $a = 1/42$, $\gamma_c / \omega_p = 3 \times 10^{-4}$

|            | $k_m = 0.21$ | $k_m = 0.23$ | $k_m = 0.25$ |
|------------|--------------|--------------|--------------|
| $P_c = 10$ | .024         | .007         | ~0           |
| $P_c = 20$ | .110         | .076         | .004         |
| $P_c = 40$ | .290         | .279         | .160         |

C35

## Table 3

Values of the scaling parameter $\eta$ appearing in the total plasma wave energy $E$ or, equivalently, the absorptive nonlinear conductivity $\sigma_T^{NL}$.

| $\eta$ | Theory |
|---|---|
| $\frac{1}{6}$ | Resonant approx. for $f(k)$, cutoff at $k_c$. Analytic saturated theory of Ref. 2, 4a |
| $\frac{3}{8}$ | Resonant approx. for $f(k)$ no cutoff at $k_c$. Analytic saturated theory of Ref. 3 |
| $\frac{1}{2}$ | Resonant approx. for $f(k)$, cutoff at $k_c$. Time-dependent numerical integration (B. Godfrey, D.F. DuBois, M.V. Goldman[4]) |
| $\frac{3}{4}$ | Exact $f(k)$. No cutoff at $k_c$. Time-dependent 1-D numerical integration. W. Kruer, E. Valeo[5] |
| ? | Exact $f(k)$. No cutoff at $k_c$. Time-dependent 2-D numerical integration. J. Fejer, Y.Y. Kuo[5a] |
| 2 | Value used by F. Perkins and by G. Meltz and N. Tomljamovich in recent geometric optics approximations[14] to the nonlinear absorption problem. |

## Figure Captions

### Figure 1

Geometry for normal incidence of electromagnetic wave on a plane-layered inhomogeneous plasma. The spatial coordinate $z$ is in the dimensionless units of $c/\omega_o$, the free-space wavelength over $2\pi$.

### Figure 2

Airy function solution (zero resistivity) for field amplitude squared in units of incident field amplitude squared. $z_o$ is the dimensionless density scale length (in units of $c/\omega_o$).

### Figure 3

Frequency-matched wave number $k_m$ (in units of $k_D$) as a function of spatial position $z$ (in units of $\omega_o/c$), illustrating the regions of low and high resistivity corresponding, respectively, to low and high Langmuir-wave intensity.

### Figure 4

Angle-averaged intensity of the Langmuir spectrum versus wave number for $P_c = 10$ and matched wave number $k_m = 0.21$. Wave number is in units of the Debye wave number.

### Figure 5

Angle-averaged intensity of the Langmuir spectrum versus wave number for $P_c = 10$ and matched wave number $k_m = 0.23$. Wave number is in units of the Debye wave number.

## Figure 6

Angle-averaged intensity of the Langmuir spectrum versus wave number for $P_c = 20$ and matched wave number $k_m = 0.21$. Wave number is in units of the Debye wave number.

## Figure 7

Angle-averaged intensity of the Langmuir spectrum versus wave number for $P_c = 20$ and matched wave number $k_m = 0.23$. Wave number is in units of the Debye wave number.

## Figure 8

Angle-averaged intensity of the Langmuir spectrum versus wave number for $P_c = 20$ and matched wave number $k_m = 0.25$. Wave number is in units of the Debye wave number.

## Figure 9

Amplitude squared and phase of the Airy function (zero resistivity) solution, $E(z) = |A(z)| \cos(\phi(z) + \omega T)$. The sign of the Airy function $A(z)$ is represented as $\pi$ phase changes at nodes of $A(z)$. The amplitude is normalized to incident intensity unity; $z_o = 10^3$.

## Figure 10

Integrated absorption $1 - R$, $R = |E_{refl}/E_{inc}|^2$, for incident intensity $I_{inc} = cE_{inc}^2/8\pi = 50\mu W/m^2$ ($\pm 2\%$) and various values of the nonlinear scaling parameter $\eta$ defined in equation (33) and Table 3. Both linear and nonlinear absorption are included and the following parameters are used: $n = 5 \times 10^5 \, cm^{-3}$, $\theta_e = 0.2eV$ ($2319^\circ K$), $f_{modifier} = 6.35$ mhz, $\nu_{ei} = 350$ Hz. The ions are assumed to be oxygen. Scale heights of $37.5$ km ($z_o = 5000$) and $75$ km $1z_o = 10^4$) are used. The right side scale on each plot is $R - R_{linear}$, which is a measure of the relative percent of nonlinear absorption.

## Figure 11

Integrated linear and nonlinear absorption, $1 - R$, $R = |E_{refl}|^2/|E_{inc}|^2$ as a function of incident intensity, $I_{inc} = cE_{inc}^2/8\pi$. The nonlinear scaling parameter $\eta$ is defined in equation (33) and Table 3. The scale height is $H = 37.5$ km and the integrated linear absorption is shown as well.

## Figure 12

Integrated linear and nonlinear absorption, $1 - R$, $R = |E_{refl}|^2/|E_{inc}|^2$ as a function of incident intensity, $I_{inc} = cE_{inc}^2/8\pi$. The nonlinear scaling parameter $\eta$ is defined in equation (33) and Table 3. The scale height is $H = 75$ km and the integrated linear absorption is shown as well.

C39

## Figure 13

Pump radiation electric field amplitude squared (in units of incident amplitude squared) versus altitude (in units of $c/\omega = 7.5$ meters). Lower altitudes are towards the right and the lowest altitude shown is ~1 km below the reflection height. Linear and linear plus nonlinear cases are plotted for an incident vacuum intensity of $50 \mu W/m^2$, a scale height of $H = 75$ km ($z_o = 10^4$), and a nonlinear scaling parameter $\eta = 2$ (see equation (33) and Table 3). The density is $5 \times 10^5 cm^{-3}$ and the temperature is 0.2eV. The peak of the Airy function swelling factor is shown by X for comparison. The integrated linear absorption is $1 - R = 17\%$, whereas the integrated linear and nonlinear absorption is an additional 33%.

## Figure 14

Radiation amplitude squared versus distance for the same parameters as in Figure 12, but at lower altitudes (in the vicinity of 3 km below the reflection point). Node lifting is beginning to become apparent here.

## Figure 15

Radiation phase versus distance for the same parameters and distance range of Figure 13. The phase, $\phi$, is defined by $E = E_o(z) \cos (\phi(z) + \omega t)$, where the amplitude $E_o$ is defined to be positive. Figure 8 shows the phase in the absence of absorption for $z_o = 10^3$.

C40

## Figure 16

Negative of Poynting flux in units of incident flux for parameters of Figure 12.


## Figure 17

Radiation amplitude squared (in units of incident amplitude squared) versus distance (in units of $c/w = 7.5$ meters). The incident intensity is $50 \mu w/m^2$, the scale height is 75 km, and the nonlinear scaling parameter $\eta = 2/3$ (see equation (33) and Table 3). The density is $5 \times 10^5$ $cm^{-3}$ and the temperature is 0.2 eV. The peak of the Airy function swelling factor is shown by X for comparison.
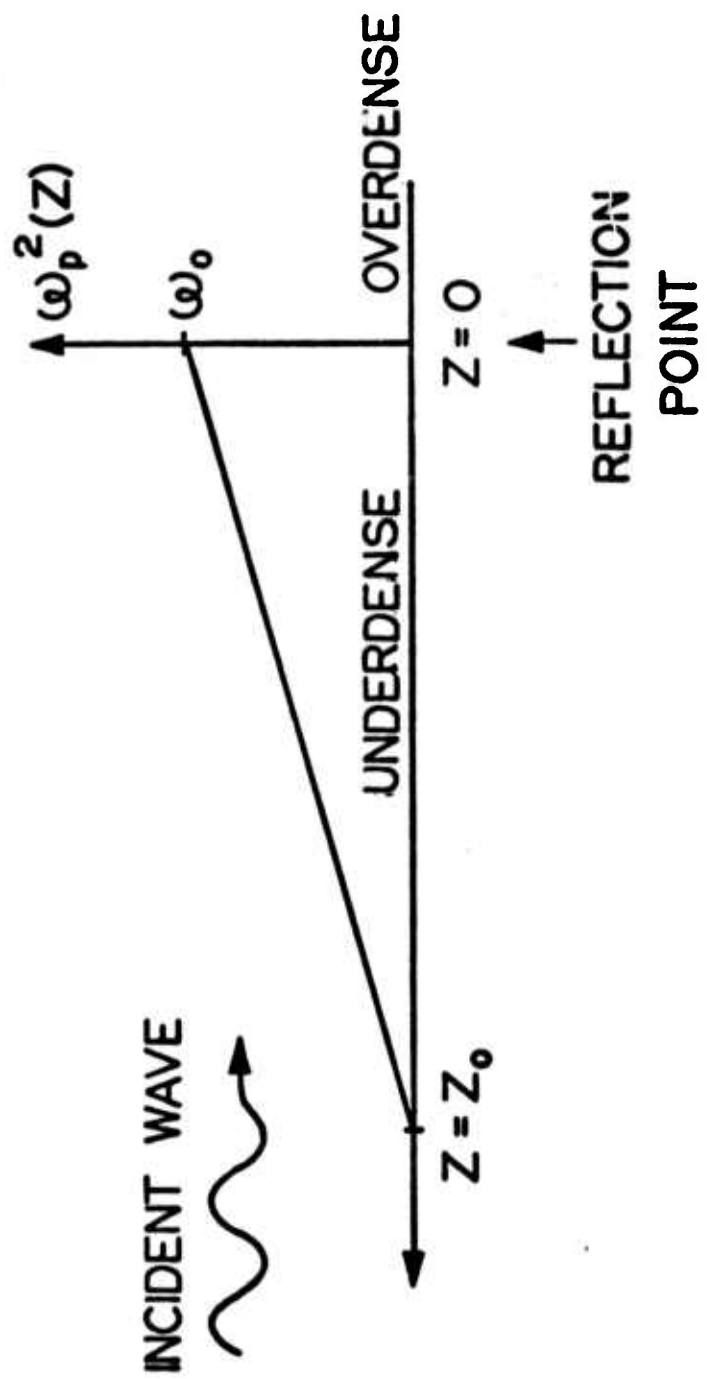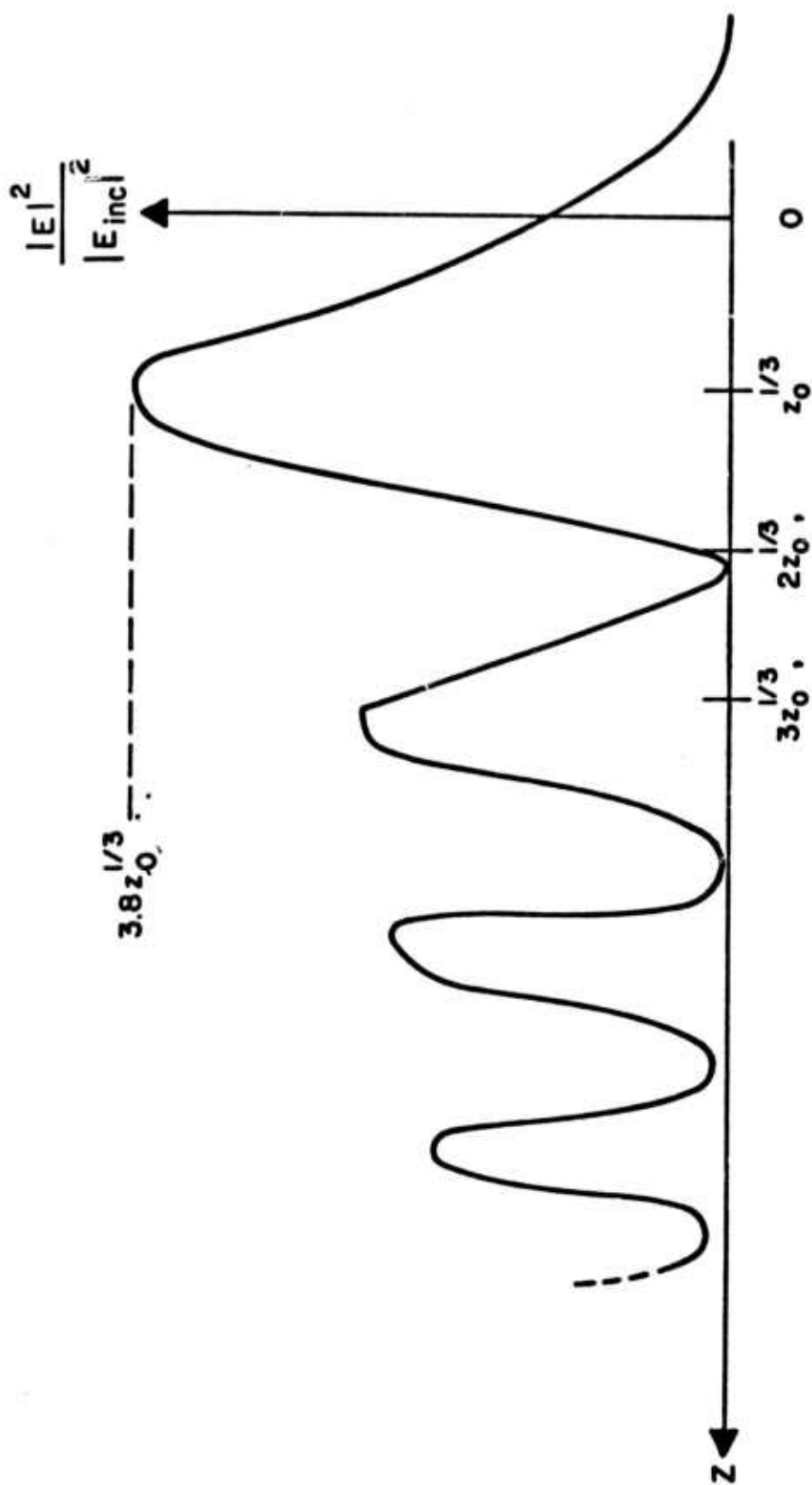
FIGURE 1

FIGURE 2

$\dfrac{k_M}{k_0}$
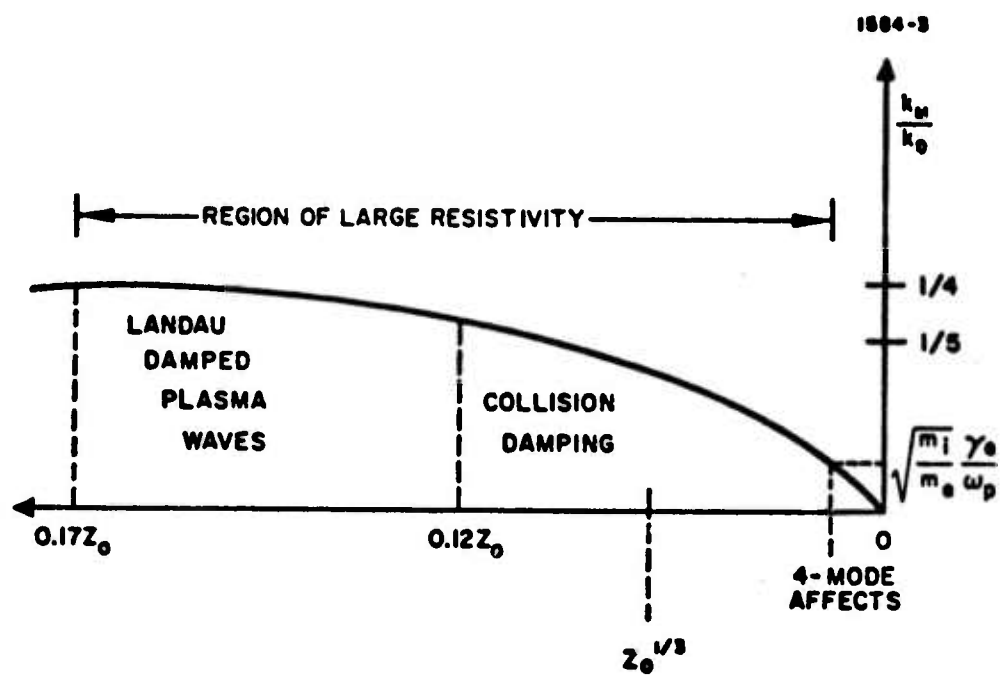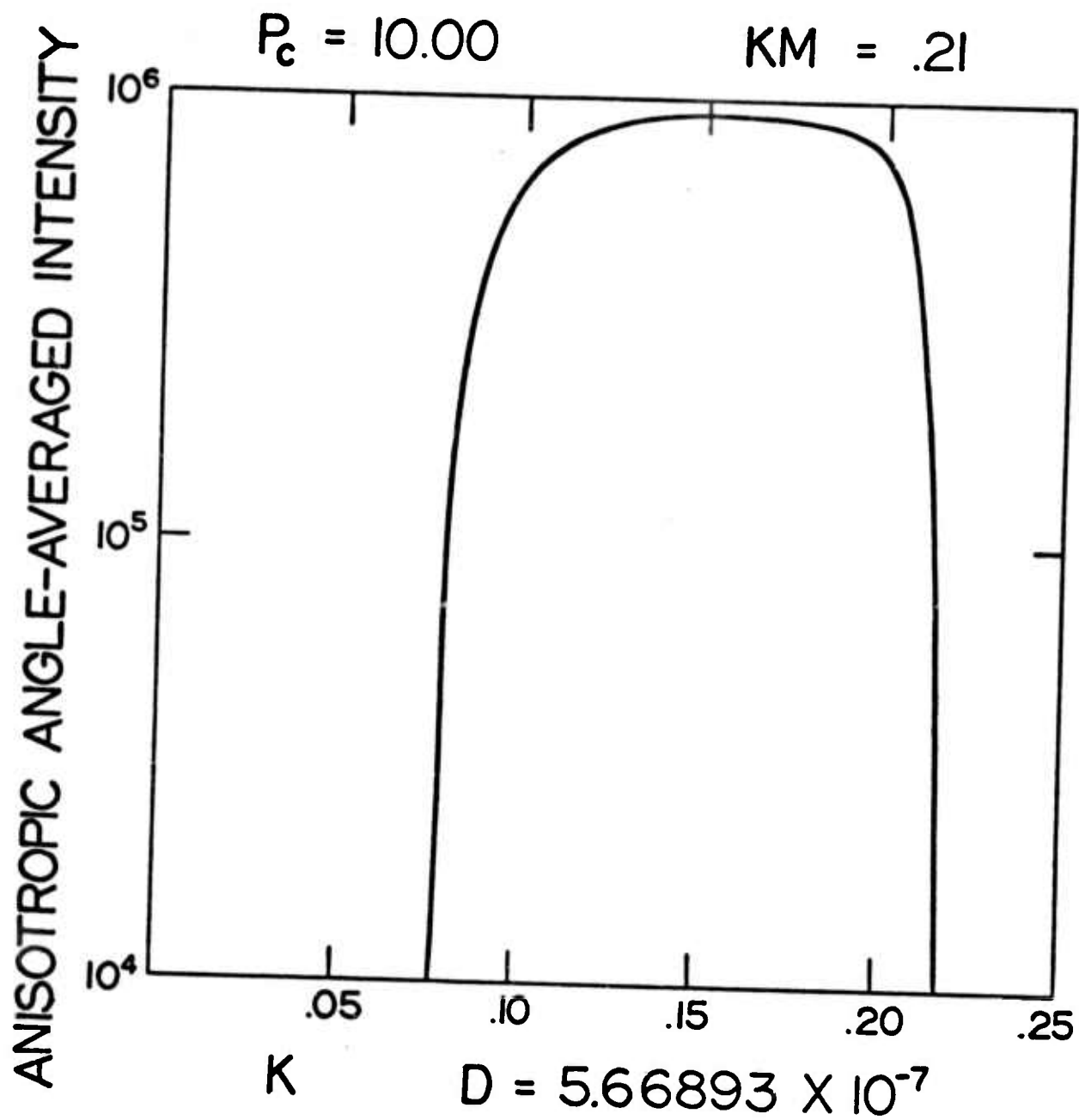
REGION OF LARGE RESISTIVITY

1/4

1/5

LANDAU
DAMPED
PLASMA
WAVES

COLLISION
DAMPING

$\sqrt{\dfrac{m_i}{m_e}}\dfrac{\gamma_e}{\omega_p}$

0.17$Z_0$

0.12$Z_0$

0

4-MODE
AFFECTS

$Z_0^{1/3}$

FIGURE 3

C44

FIGURE 4

C45

FIGURE 5

C46

FIGURE 6

C47

$P_c = 20.00$    KM $= .23$

ANISOTROPIC ANGLE-AVERAGED INTENSITY

K    $D = 5.66893 \times 10^{-7}$

FIGURE 7

C48

$P_c = 20.00 \qquad KM = .25$

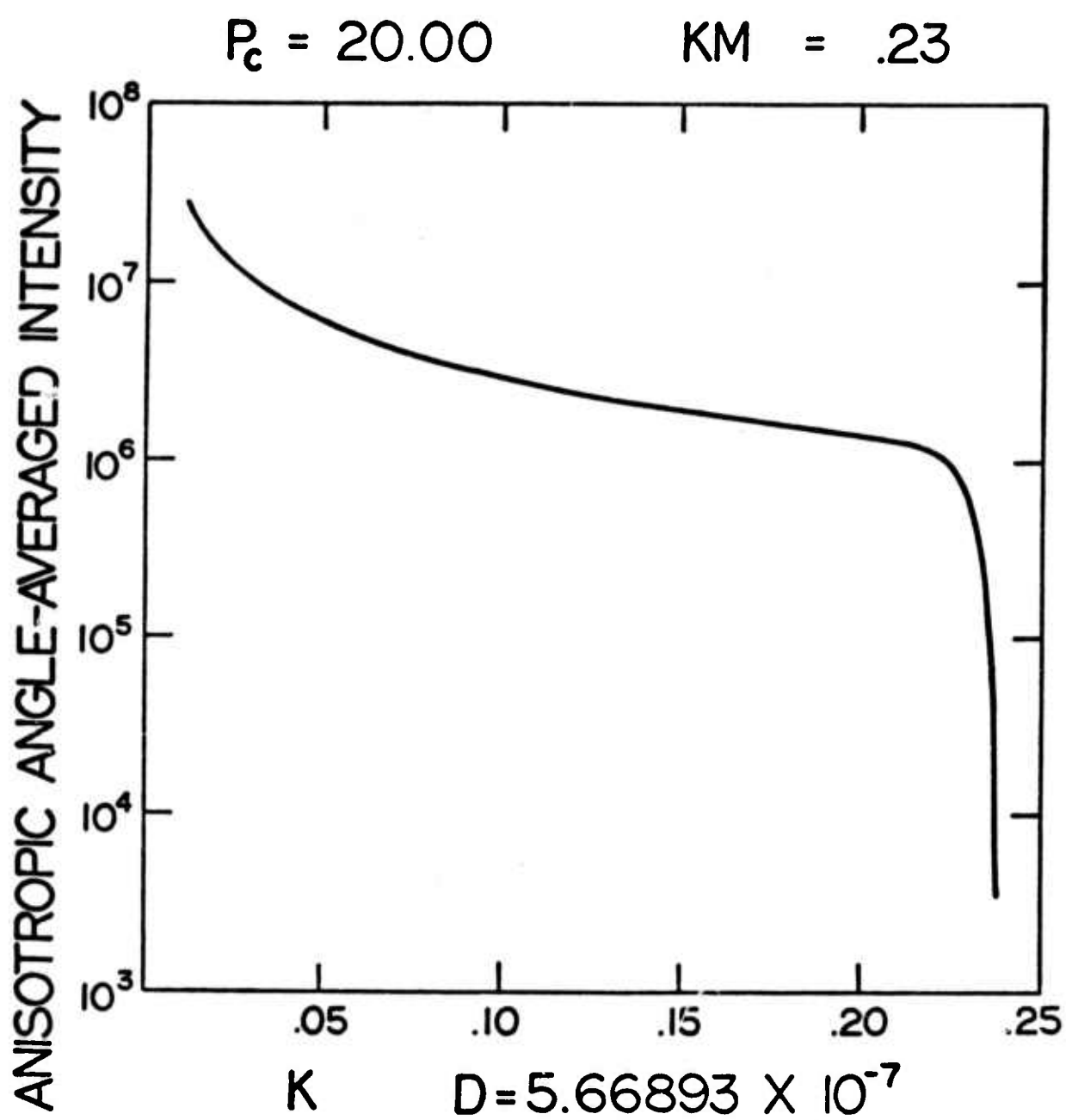ANISOTROPIC ANGLE–AVERAGED INTENSITY

K      $D = 5.66893 \times 10^{-7}$

FIGURE 8

C49
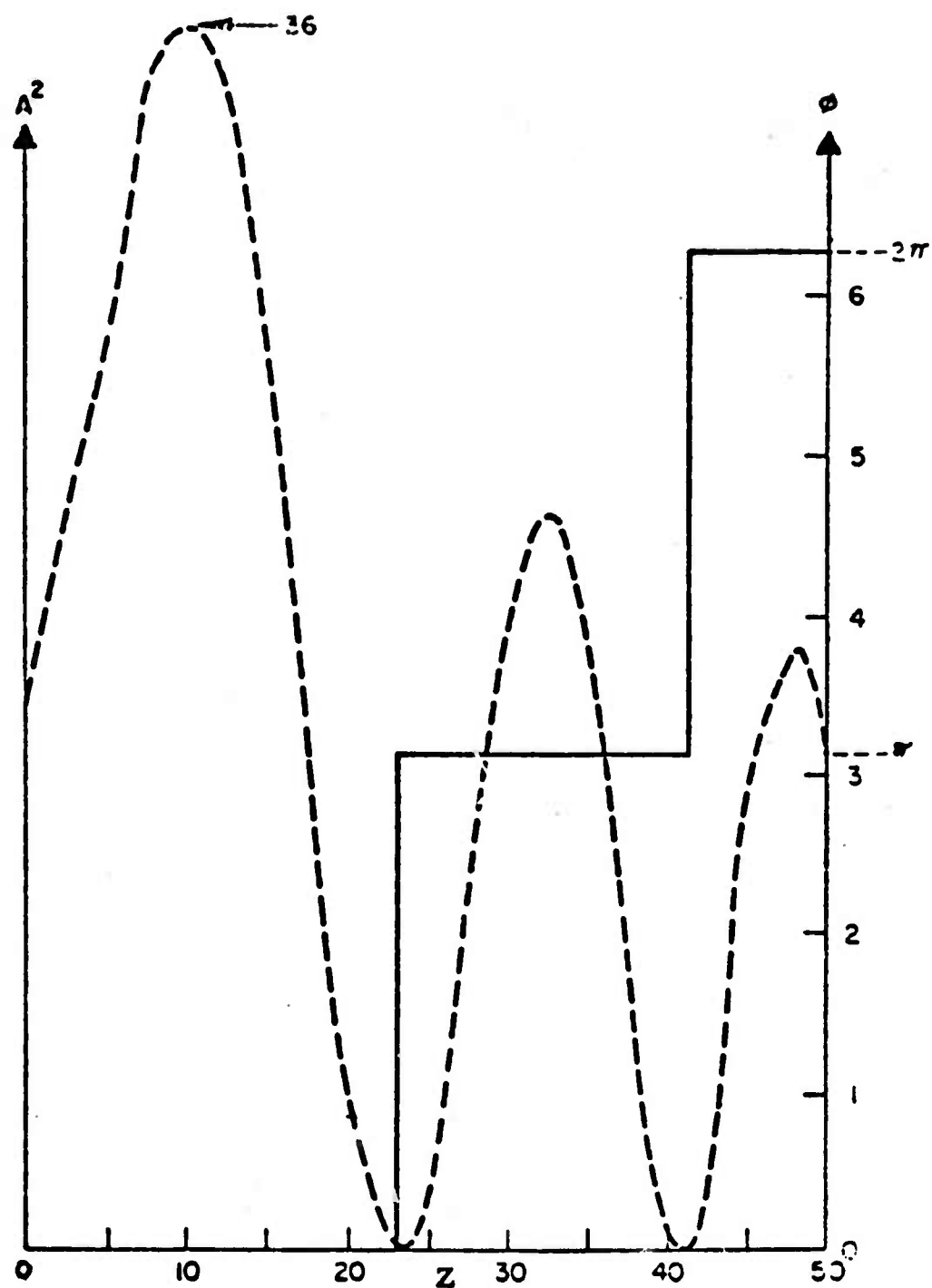
FIGURE 9

C50
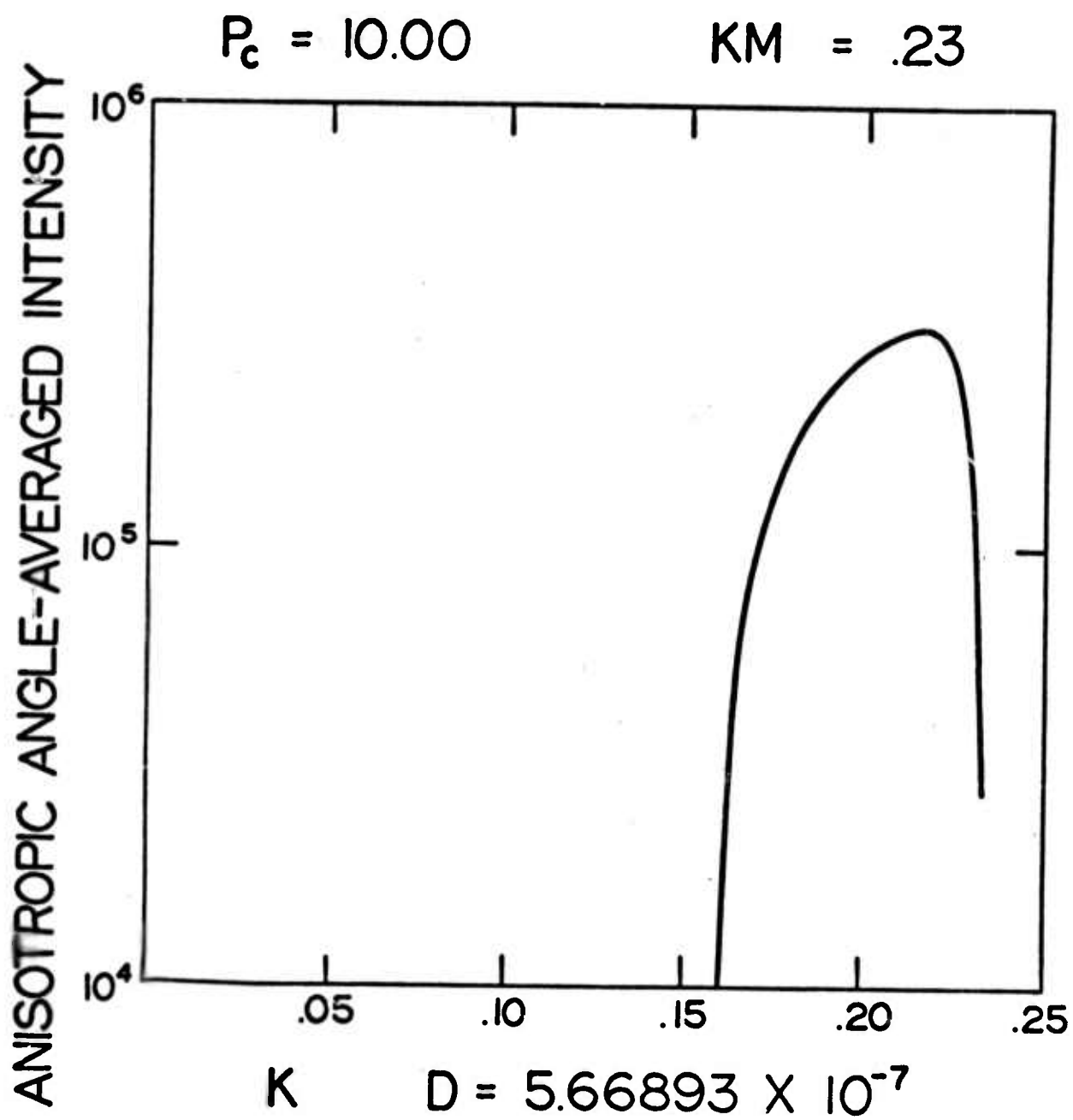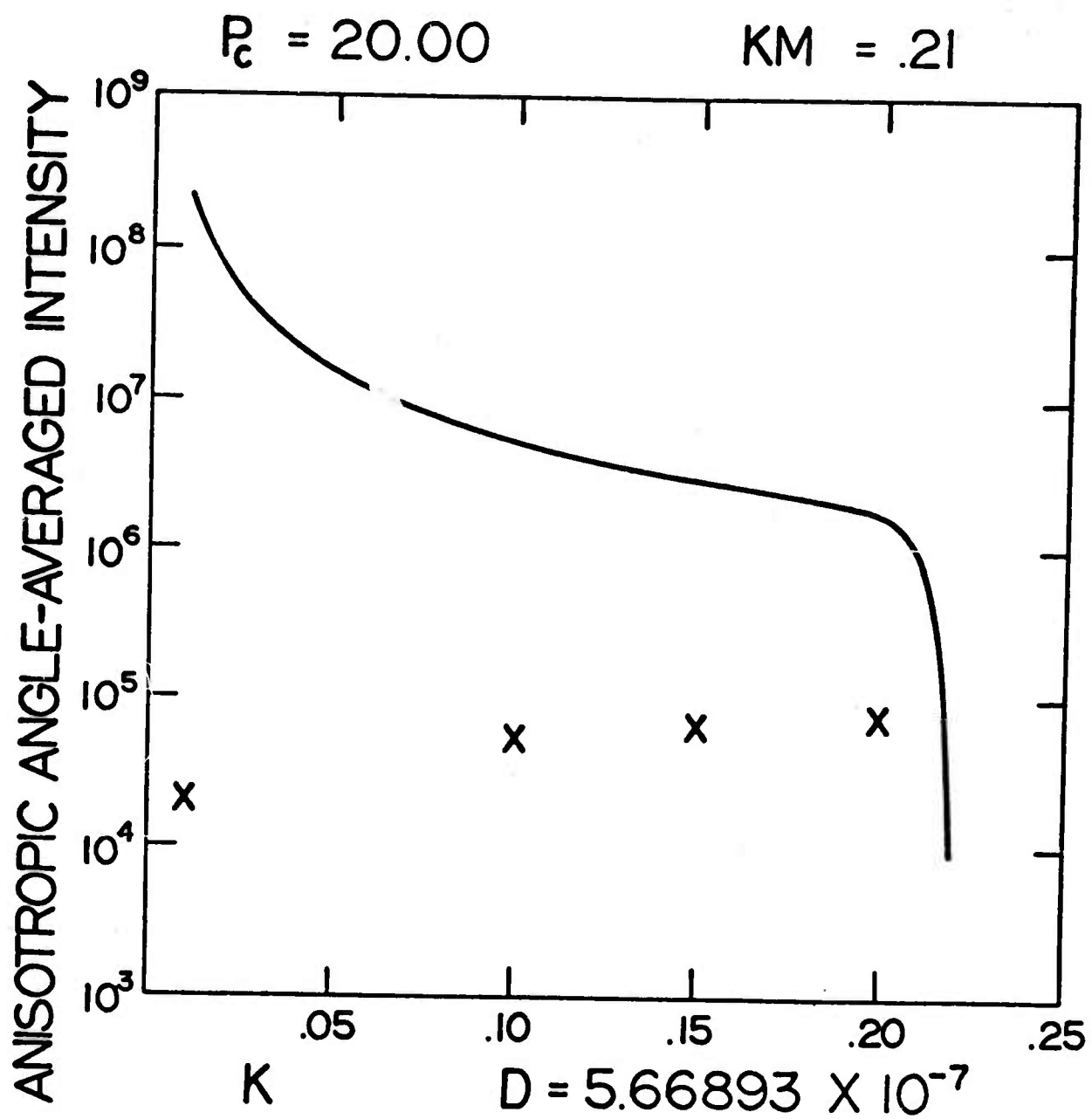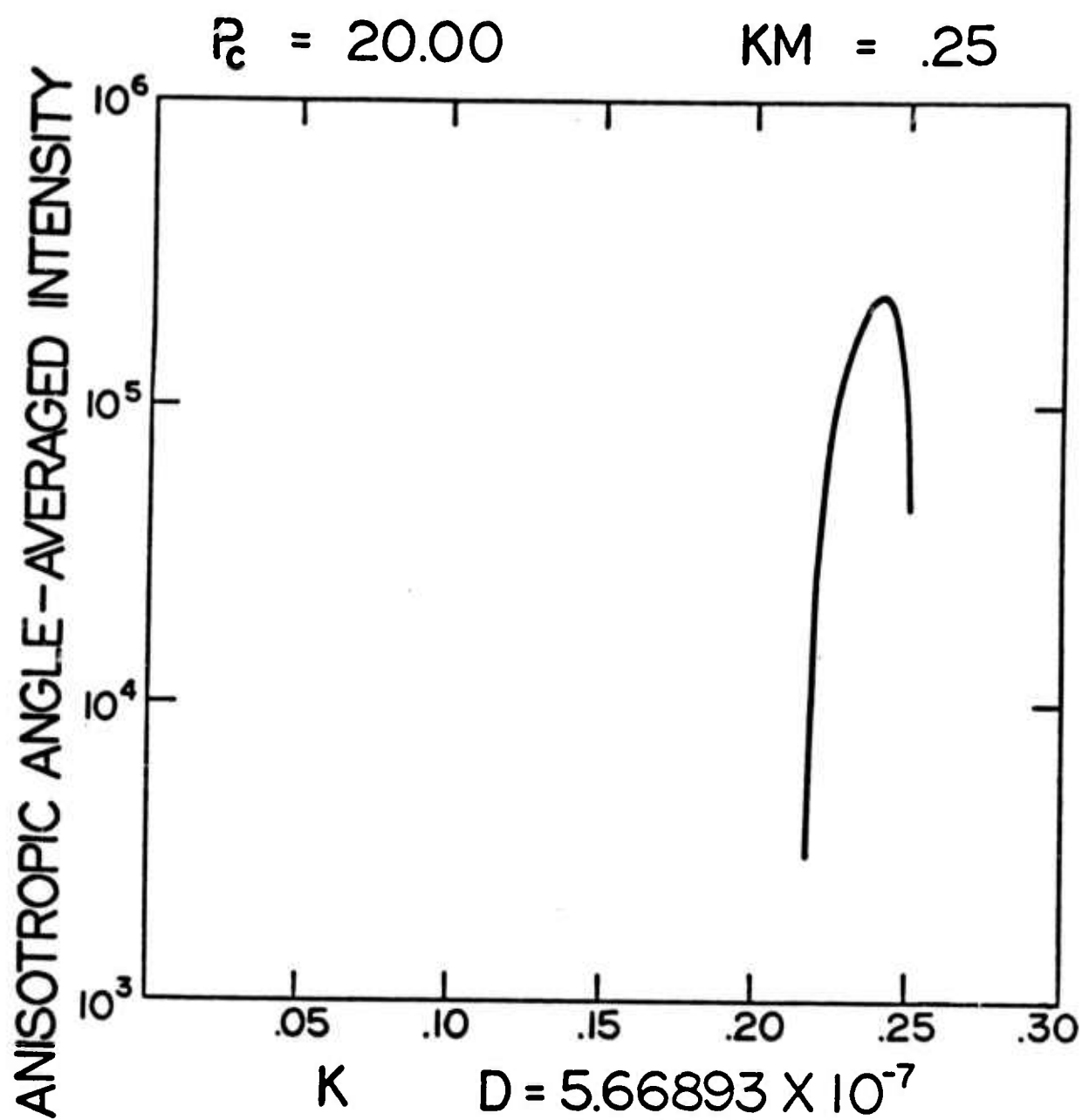
$I_{inc} = 50 \mu W/m^2$

FIGURE 10

C51

**FIGURE 11**

C52
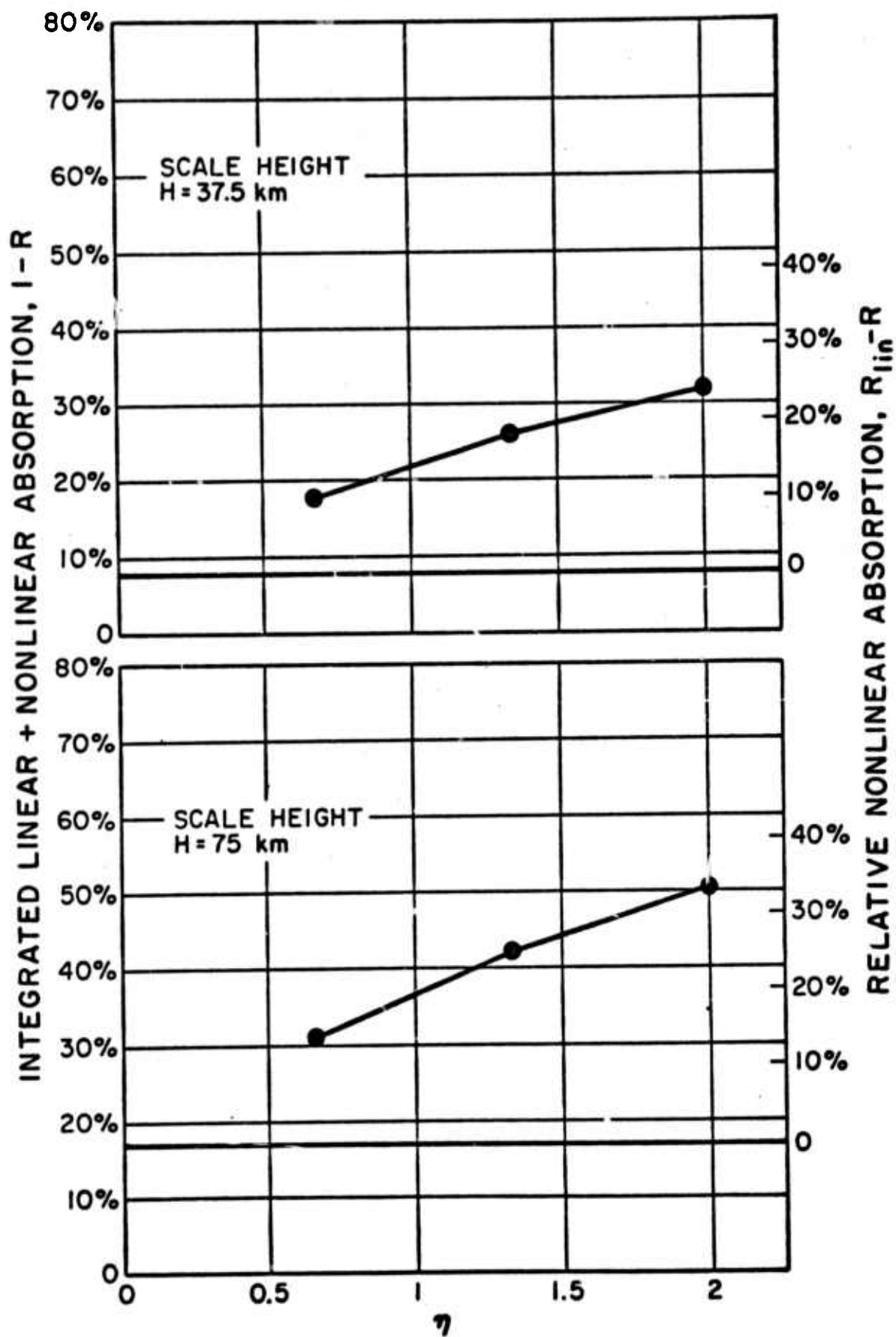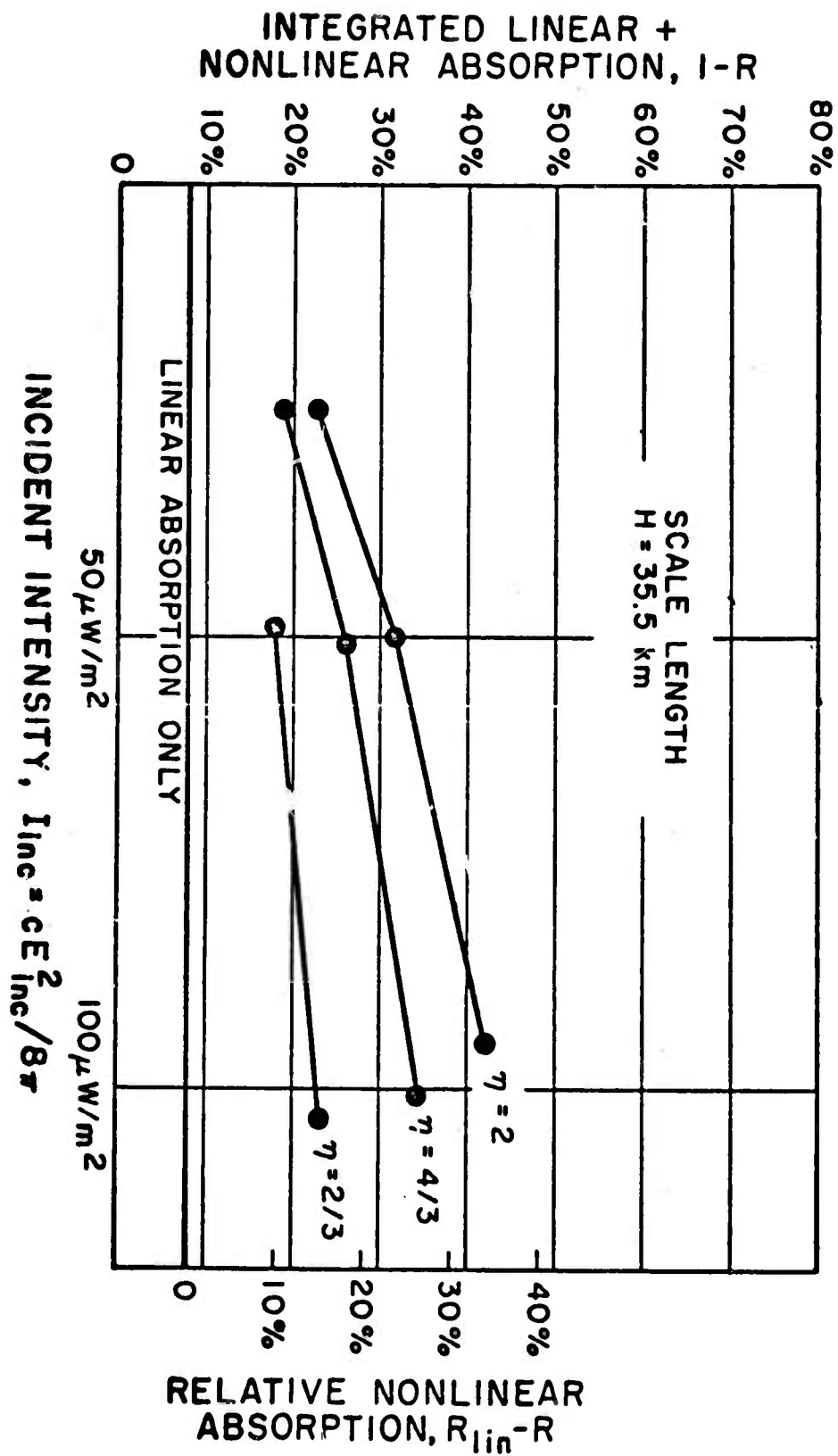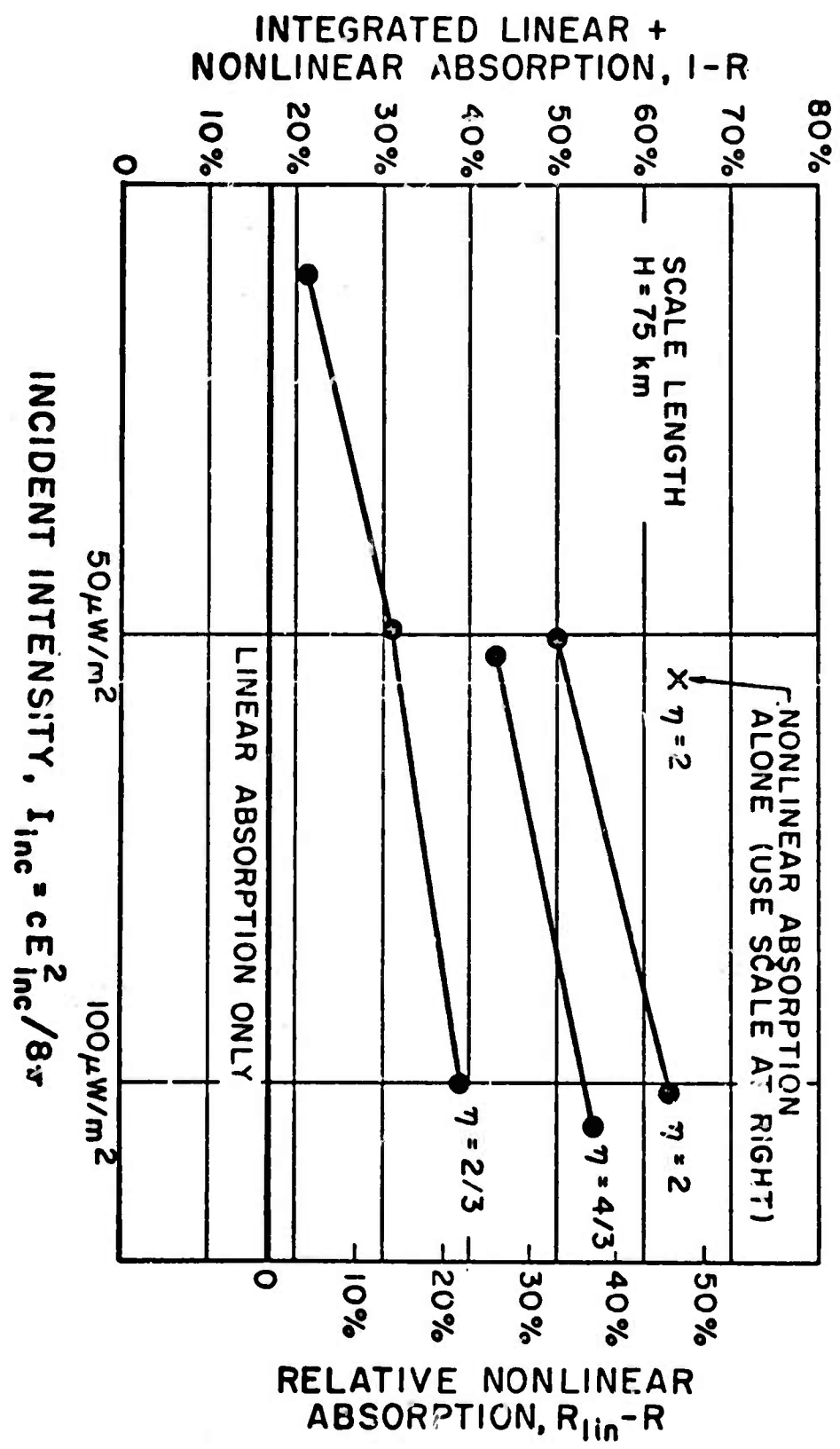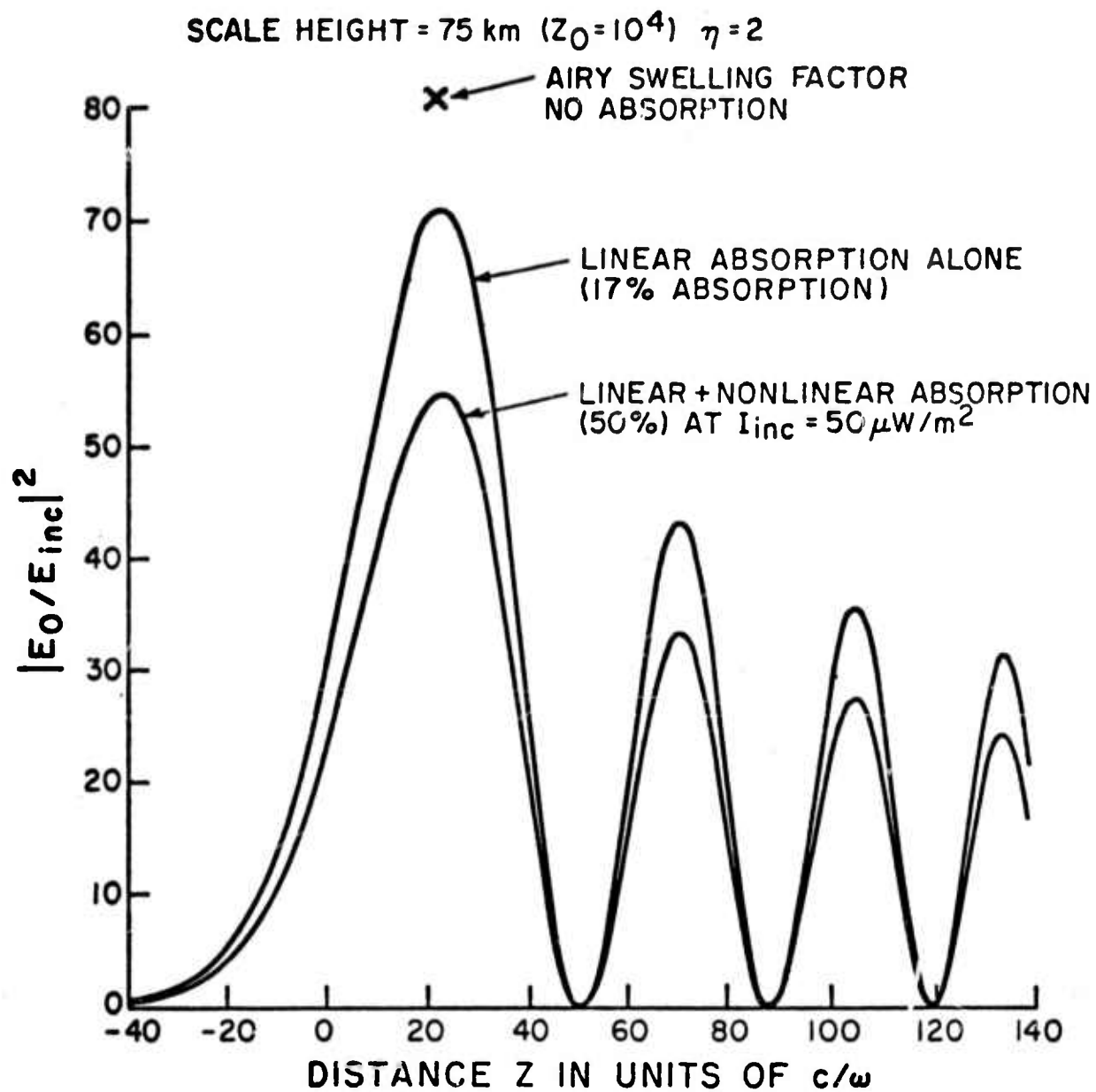
FIGURE 12

SCALE HEIGHT = 75 km $(Z_0 = 10^4)$ $\eta = 2$

FIGURE 13

C54
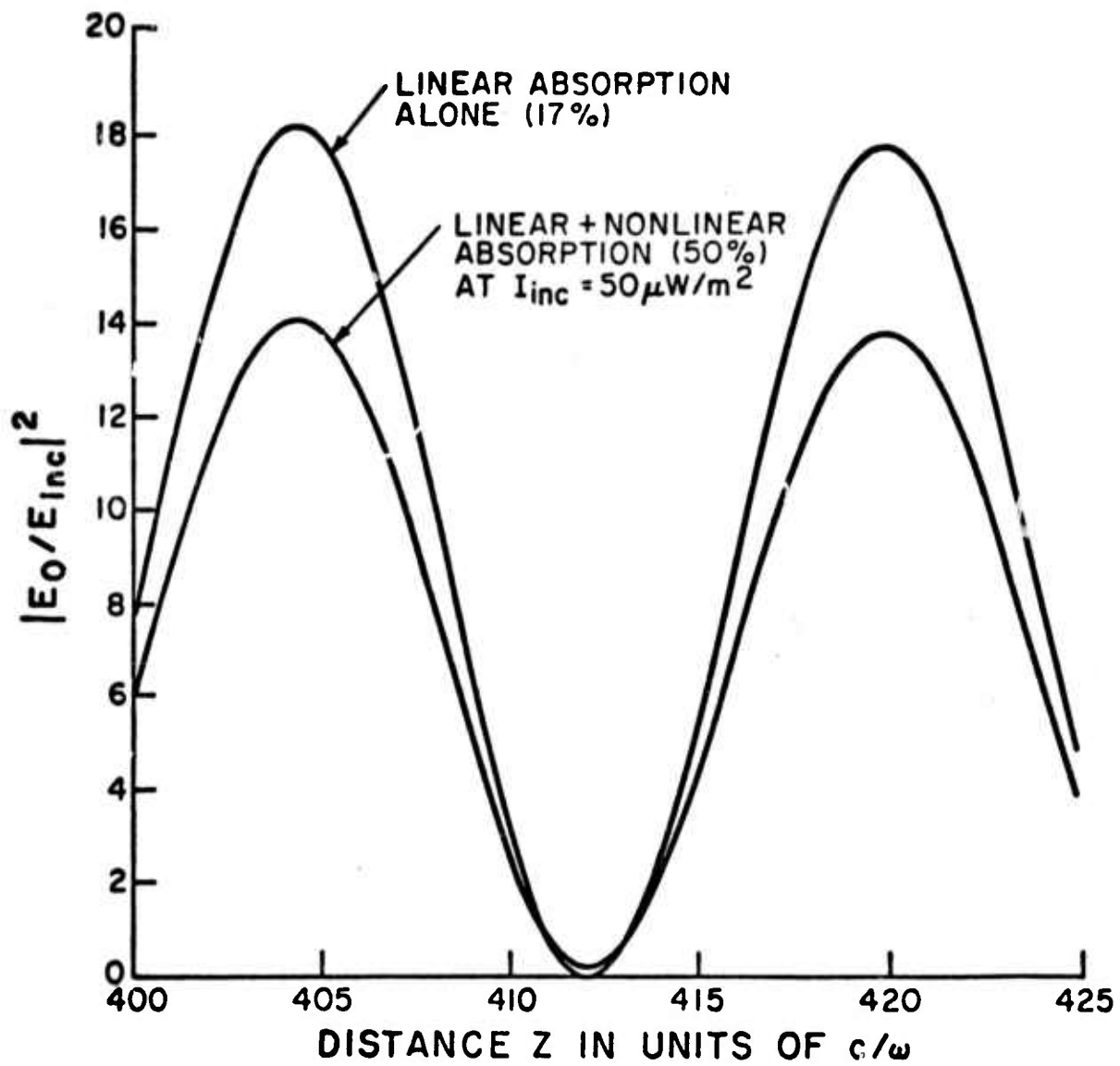
FIGURE 14

SCALE HEIGHT = 75 km $(Z_0 = 10^4)$ $\eta = 2$

LINEAR ABSORPTION ALONE (17%)

LINEAR + NONLINEAR ABSORPTION (50%) AT $I_{inc} = 50 \mu W/m^2$

RADIATION PHASE, $\phi(z)$, IN RADIANS

DISTANCE Z IN UNITS OF $c/\omega$

FIGURE 15

C56

SCALE HEIGHT = 75 km. $(Z_0 = 10^4)$ $\eta = 2$

NEGATIVE POYNTING FLUX, $-J/J_{inc}$

LINEAR + NONLINEAR
ABSORPTION (50%)
AT $I_{inc} = 50\,\mu W/m^2$

LINEAR ABSORPTION
ALONE (17%)

DISTANCE Z IN UNITS OF $c/\omega$

FIGURE 16

C57
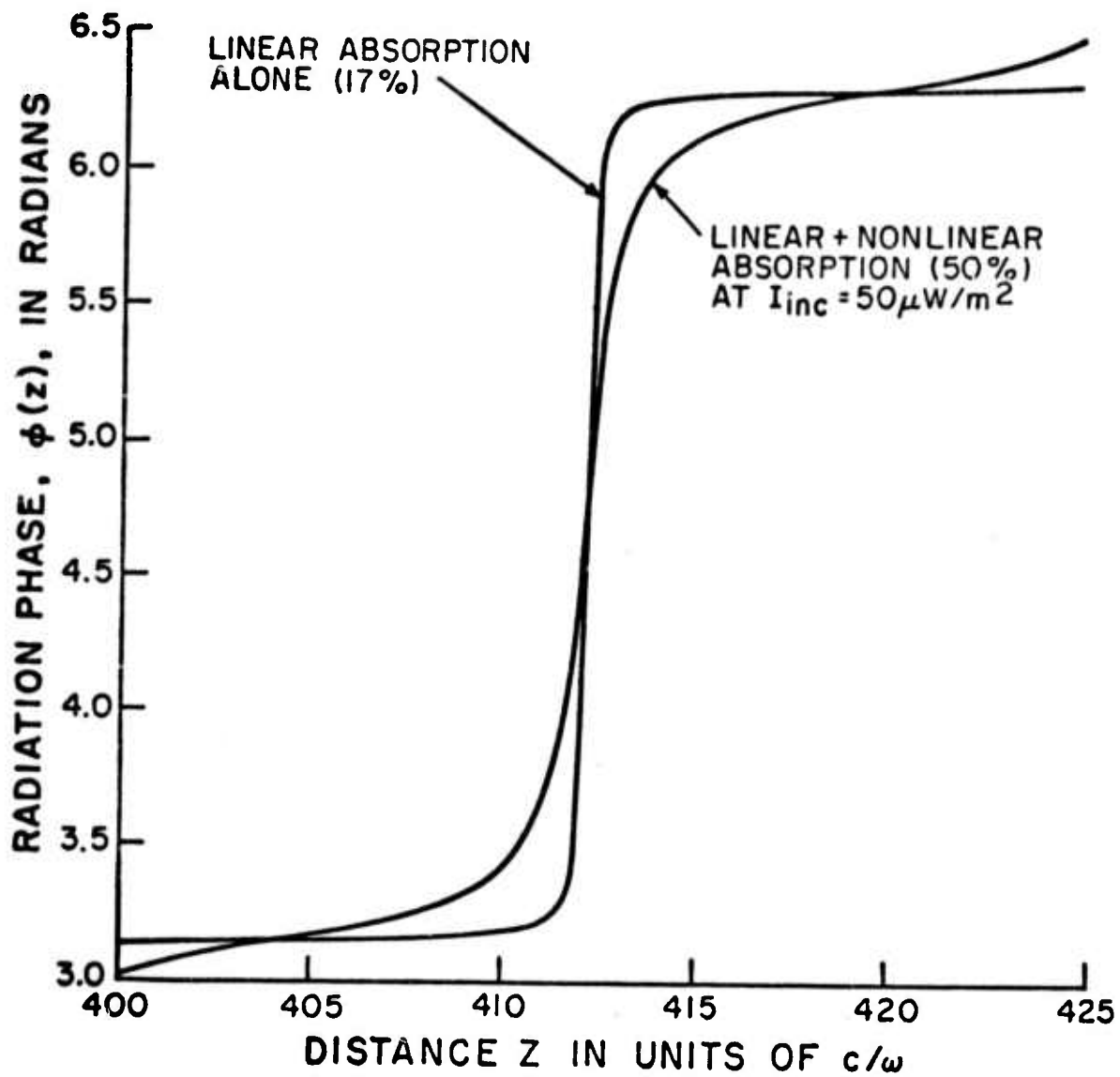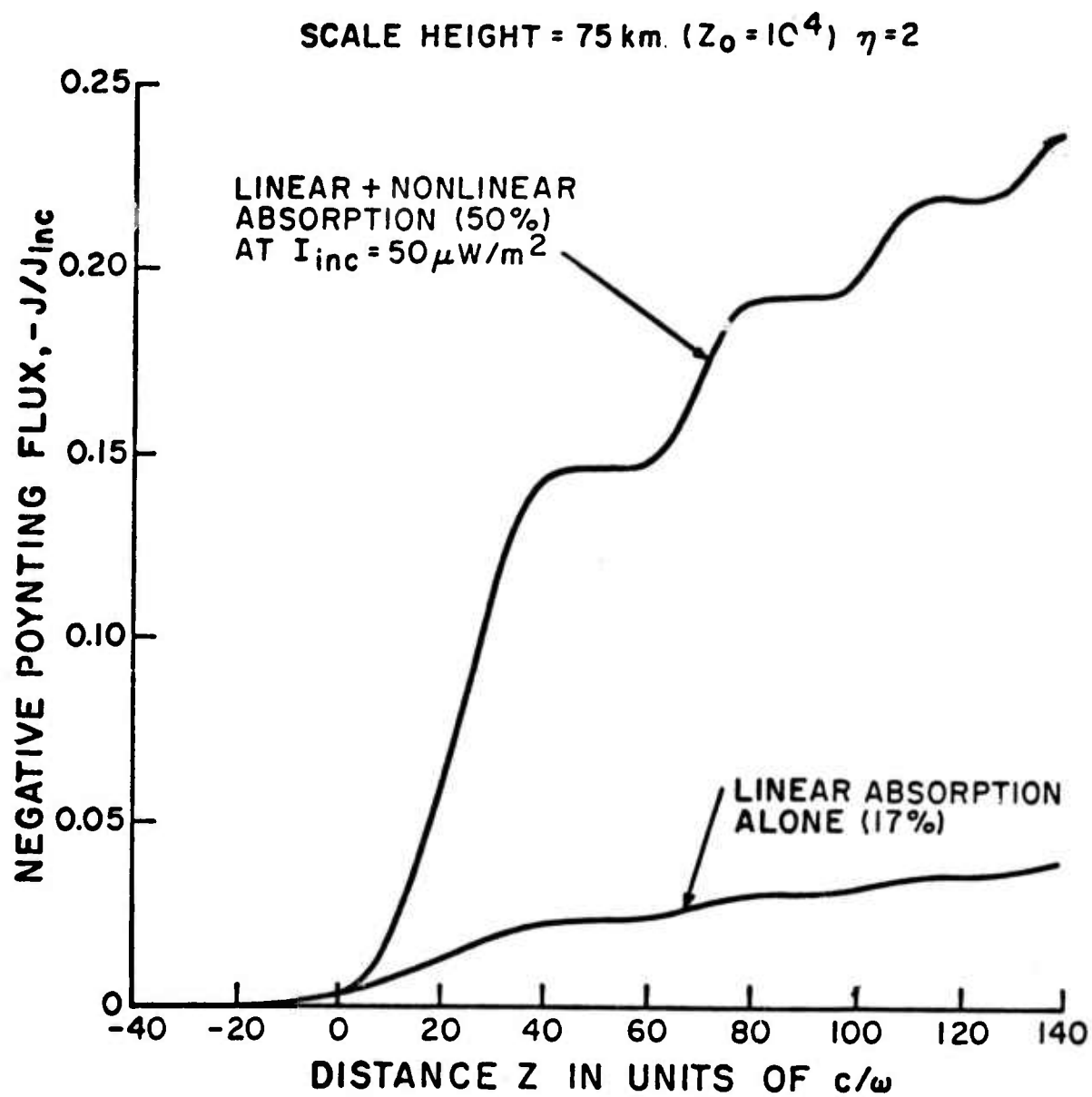
SCALE HEIGHT = 75 km ($Z_0 = 10^4$) $\eta = 2/3$

✘ AIRY SWELLING FACTOR

LINEAR ABSORPTION ALONE
(17% ABSORPTION)

LINEAR + NONLINEAR
ABSORPTION (31%)
AT $I_{inc} = 50 \mu W/m^2$

$|E_0/E_{inc}|^2$

DISTANCE Z IN UNITS OF $c/\omega$

FIGURE 17

C58

## References

1. D.F. DuBois and M.V. Goldman, _Physical Review Letters_ 14, 544 (1965); and _Physical Review_ 164, 207 (1967).

2. D.F. DuBois and M.V. Goldman, _Physical Review Letters_ 28, 218 (1972).

3. E. Valeo, C. Oberman, and F.W. Perkins, _Physical Review Letters_ 28, 340 (1972).

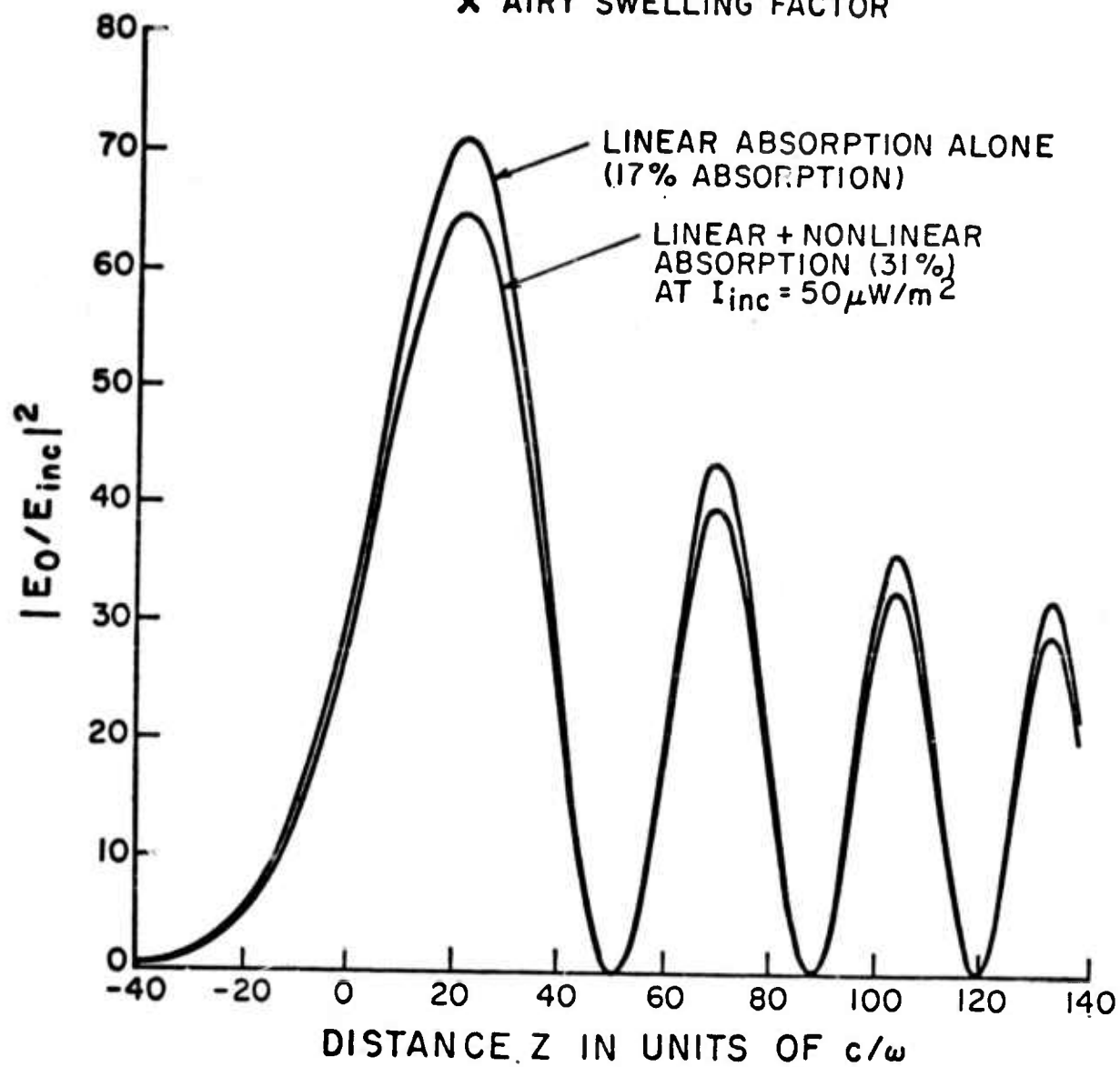4. M.V. Goldman and D.F. DuBois,"Nonlinear Laser Heating of a Plasma," Technical Report #AFWL-TR-72-101, Kirtland Air Force Base, Albuquerque, New Mexico, September, 1972. Also reported on at the Anomalous Absorptive Conference, Boulder, Colorado, March, 1972.

4a. D.F. DuBois and M.V. Goldman, _Physics of Fluids_ 15, 919 (1972).

5. W.L. Kruer and E.J. Valeo, "Nonlinear Evolution of the Decay Instability in a Plasma with Comparable Electron and Ion Temperatures," PPL MATT-919, August 1972 (to be published in _Phys. Fluids_).

5a. J.A. Fejer and Y.Y. Kuo, "Structure in the Nonlinear Saturation Spectrum of Parametric Instabilities," Preprint December, 1972.

6. W.L. Kruer and J.M. Dawson, _Physics of Fluids_ 15, 446 (1972).

7. F.W. Perkins and P.K. Kaw, _Journal of Geophysical Research_ 76, 282 (1971).

8. R. Cohen and J.D. Whitehead, _Journal of Geophysical Research_ 75, 6439 (1970).

9. E. Valeo, F. Perkins and C. Oberman, _Phys. Rev. Lett._ 28, 340 (1972).

10. K. Nishikawa, _Journal of Physical Society of Japan_ 24, 916, 1152 (1968).

10a. The neglect of the purely growing mode is justified at least for moderate pump ratios if $\gamma_L \ll \gamma_a$ where $\gamma_L$ and $\gamma_a$ are the total damping rates of Langmuir and ion acoustic waves respectively.

11. F.W. Perkins and J. Flick, Princeton University, Plasma Physics Laboratory Report No. MATT-833 (1971).

12. D.F. DuBois, V. Gilinsky and M.V. Kivelson, _Physical Review_ 129, 2376 (1963).

13. B. Bezzerides and J. Weinstock, _Physical Review Letters_ 28, 481 (1972); Also see Appendix A.

14. Summary of ARPA Theoretical Meeting of 17 November 1972.

15. T.H. Stix, The Theory of Plasma Waves, McGraw-Hill, New York, 1962.

16. H. E. Carlson, W.E. Gordon, R.L. Showen, "High Frequency Induced Enhancements of the Incoherent Scatter Spectrum at Arecibo." J. Geophys. Research 77, 1242-1250 (1972).

17. I. J. Kantor, "Plasma Waves Induced by HF Radio Waves," Ph.D. Thesis submitted 7/72 to Rice University.

18. N.M. Tomljanovich, "Self-Focusing of Electromagnetic Waves in Plasmas," Summary of ARPA Theoretical Meeting of 17 November 1972, p. 94.

ELECTRON ACCELERATION

Jerome Weinstock and Bandel Bezzerides

## ELECTRON ACCELERATION:

The electron velocity distribution function is substantially changed during modification. This change is evidenced by large enhancements of natural 6300Å (red) and 5500Å (green) airglow observed over Boulder and 6300Å observed over Arecibo. These alterations of the electron velocity distribution can have important consequences. For examples, the formation of energetic tails may (1) create new plasma wave instabilities such as the ion-acoustic instability, (2) change the saturated spectrum of short scale turbulence, and (3) change the radar scattering cross-section of the turbulence.

We have developed a theory for quantitatively predicting the change in the velocity distribution of electrons. Such changes are primarily due to acceleration of electrons by short wavelength plasma waves propagating in the Landau damped region, where typical wavelengths are about 15 cm (about 5 Debye lengths). Such short scale waves are excited in the bottom of the modified region as indicated in Figure 1.

The electron velocity distribution function $f = f(\underline{v}, z)$ satisfies the diffusion equation

$$\frac{\partial f}{\partial t} + \frac{\partial f}{\partial z} - \frac{e}{m} \; \underline{E}_o \cdot \frac{\partial f}{\partial \underline{v}} = \frac{\partial}{\partial \underline{v}} \cdot \left[ \underline{\underline{D}} \cdot \frac{\partial f}{\partial \underline{v}} \right] + \left( \frac{\delta f}{\delta \tau} \right)_c \tag{1}$$

where $\underline{v}$ is velocity, $\underline{E}_o$ is the pump field, $D(v,z)$ is the diffusion tensor. Horizontal stratification is assumed so that $f$ and $D$ depend upon height $z$. If we average (1) over a small enough vertical range $\Delta_z$ within the heated region such that

$$\frac{1}{\Delta_z} \int_{z}^{z+\Delta_z} dz \; \frac{\partial f}{\partial z} = 0 \tag{2}$$

D1

then (1) becomes

$$\frac{\partial \overline{f}}{\partial t} = \frac{\partial}{\partial \underline{v}} \cdot \overline{\left[ \underline{\underline{D}} \cdot \frac{\partial f}{\partial \underline{v}} \right]} \tag{3}$$

where the superbar denotes an average over the vertical range $\Delta_z$, and we have neglected the small effect of $E_o$ and of collisions upon $f$.

## RED AIR GLOW

The airglow measurements provide a direct measurement of the enhanced photon flux of atomic excitations. This photon flux is, in turn, a measure of the enhanced flux of electrons causing the excitations. The flux, and number density, of exciting electrons is determined by the quantity

$$\int d\underline{v} \ \sigma(v) \ f(\underline{v})$$

where $\sigma(v)$ is the excitation cross-section as a function of $v$. We can solve (1) for $\partial/\partial t \int d\underline{v} \ \sigma(v) \ f(\underline{v})$ and then determine the enhanced flux of exciting electrons. We multiply both sides of (1) by $\sigma(v)$ and integrate over $\underline{v}$ to obtain

$$\frac{\partial}{\partial t} \int d\underline{v} \ \sigma(v) \ f(\underline{v}) = \int d\underline{v} \ \sigma(v) \ \frac{\partial}{\partial \underline{v}} \cdot \left( \underline{\underline{D}} \cdot \frac{\partial f}{\partial \underline{v}} \right) \tag{4}$$

$$\frac{\partial}{\partial t} \int d\underline{v} \ \sigma(v) \ f(\underline{v}) = - \int d\underline{v} \ \frac{\partial \sigma(v)}{\partial v} \ \underline{v} \cdot \underline{\underline{D}} \cdot \frac{\partial f}{\partial v} \tag{5}$$

The diffusion tensor $\underline{\underline{D}}$ is given by

$$\underline{\underline{D}}(\underline{v},z) = \frac{e^2}{m^2} \ \text{Real} \int \frac{d\underline{k}}{(2\pi)^3} \ \langle E_{\underline{k}}^2 \rangle \int_0^\infty dt \ \exp \ [i(\omega - \underline{k} \cdot \underline{r}) t - \underline{k}^2 : \underline{\underline{D}} t^3] \tag{6}$$

and has been calculated in detail for modification conditions. The component of $\underline{\underline{D}}$ along the pump direction is described in Fig. 2.

D2

Note that D(v) is fairly narrowly peaked about the wave phase velocity. (This phase velocity is about 5 $v_e$ in the Landau damped regime.) Hence, the main contribution of the $\underline{v}$ integral in the right side of (5) comes from $v \approx \omega/k$

$$\frac{\partial}{\partial t} \int d\underline{v} \; \sigma(v) \; f(\underline{v}) = - \left[\frac{\partial \sigma(v)}{\partial v}\right]_{v=\omega/k} \int d\underline{v} \; \frac{\underline{v}}{v} \cdot \underline{\underline{D}} \cdot \frac{\partial f}{\partial \underline{v}} \tag{7}$$

Substituting (6), for $\underline{\underline{D}}$, into (7) we have

$$\frac{\partial}{\partial t} \int d\underline{v} \; \sigma(v) \; f(\underline{v}) = - \left[\frac{\partial \sigma}{\partial v}\right] \frac{e^2}{m_e} \; Re \int \frac{d\underline{k}}{(2\pi)^3} \; \langle E_k^2 \rangle \int d\underline{v} \int_0^\infty dt \; \frac{\hat{\underline{k}} \cdot \underline{v}}{v}$$

$$\times \quad \hat{\underline{k}} \cdot \frac{\partial f}{\partial \underline{v}} \; \exp[-i(\omega - \underline{k} \cdot \underline{v})t - \underline{k}^2 : \underline{\underline{D}} \; t] \tag{8}$$

We now note that velocity integral on the right side of (8) is proportional to the imaginary part of the nonlinear susceptibility $- \chi^{NL}(\underline{k}, \omega)$ so that, with $\underline{k} \cdot \underline{v} \approx \omega$, (8) can be written

$$\frac{\partial}{\partial t} \int d\underline{v} \; \sigma(v) \; f(\underline{v}) = \left[\frac{\partial \sigma}{\partial v}\right] \int \frac{d\underline{k}}{(2\pi)^3} \; \frac{\langle E_k^2 \rangle}{4\pi} \; k \; I_m \; \chi^{NL}(\underline{k}, \omega) \tag{9}$$

But

$$I_m \; \chi^{NL}(\underline{k}, \omega) \approx 2(\gamma_L^{NL} + \gamma_\chi)/\omega \tag{10}$$

where $\gamma_L^{NL}$ is the nonlinear damping rate of Langmuir waves and $\gamma_\chi$ is linear Landau damping. Furthermore, at saturation

$$\gamma_L^{NL} = \gamma_L \quad \text{(linear growth rate)}$$

$$= \gamma_L (P \; f(k) \; \cos^2\theta - 1) \tag{11}$$

where P is the pump ratio, $\gamma_L$ is the total linear damping ($\gamma_L = \nu + \gamma_\chi$)

D3

collisional + Landau damping, $f(k)$ is the width function, and $\theta$ is the angle between pump and $\underline{k}$. Substituting (10) and (11) into (9) we have

$$\frac{\partial}{\partial t} \int d\underline{v}\ \sigma(\underline{v}) = \left[\frac{\partial\sigma}{\partial v}\right] 2\int \frac{d\underline{k}}{(2\pi)^3}\ \frac{\langle F_{\underline{k}}^2\rangle}{4\pi}\ [\gamma_L\ Pf(k)\ \cos^2\theta - \nu] \tag{12}$$

Using the saturation spectrum for $\langle E_{\underline{k}}^2\rangle$ given in this report for the Landau damped region we finally have for (12)

$$\frac{\partial}{\partial t} \int d\underline{v}\ \sigma(v)\ f(\underline{v}) = \left[\frac{\partial\sigma}{\partial v}\right] \frac{4}{3}\ \gamma_L\ Pn_o\ \left(\frac{\langle(\delta E)^2\rangle}{4\pi m_o kT}\right)\ \frac{v_e^2 k}{\omega} \tag{13}$$

where $\langle(\delta E)^2\rangle$ is the total energy density of Langmuir waves, and $n_o$ is the ambient electron density.

The enhanced number density of exciting electrons is essentially determined by (13). Thus if we let $n^*(6300)$ denote the enhanced density of electrons exciting 6300Å airglow then we can write

$$\frac{\partial}{\partial t} \int d\underline{v}\ \sigma(v)f \equiv \langle\langle\sigma(v)\rangle\rangle\ \frac{\partial}{\partial t}\ n^*(6300) \tag{14}$$

where $\langle\langle\sigma(v)\rangle\rangle$ is defined as the average cross-section per exciting electron. But, from the right side of (7), together with (6), we see that the main contribution to $\partial f(\underline{v})/\partial t$ comes from $v \approx \omega/k$. Hence we approximately have from (14)

$$\frac{\partial}{\partial t} \int d\underline{v}\ \sigma(v)\ f(\underline{v}) \approx \sigma(\frac{\omega}{k})\ \frac{\partial n^*(6300)}{\partial t} \tag{15}$$

Substituting (15) in (13) yields

$$\frac{\partial n^*(6300)}{\partial t} = \left[\frac{\frac{\omega}{k}\left(\frac{\partial\sigma}{\partial v}\right)}{\sigma(\omega/k)}\right] \frac{4}{3}\ \gamma_L\ P\ n_o\ \left(\frac{kv_e}{\omega}\right)^2\ \frac{\langle(\delta E)^2\rangle}{4\pi mkT} \tag{16}$$

But, for energies less than 4 ev, $\sigma(v)$ is approximately given by

D4

$$\sigma(v) \; \alpha \; v^2$$

$$\left[ \frac{\partial\sigma/\partial v}{\sigma} \right]_{v=\omega/k} = \frac{2k}{\omega} \tag{17}$$

so that (16) becomes

$$\frac{\partial n^*(6300)}{\partial t} = \frac{8}{3} \; \gamma_L \; P \; n_o \left( \frac{kv_e}{\omega} \right)^2 \frac{\langle(\delta E)^2\rangle}{4\mathfrak{m}_o kT} \tag{18}$$

This describes the rate at which exciting electrons are produced. The saturation energy density $\langle(\delta E)^2\rangle/(4\mathfrak{m}_o kT)$ is given in this report as a function of P and $(kv_e/\omega)$, where k is the matching k. For a typical modification over Boulder $P \approx 3$ at the Landau damped height for which $k/k_D \approx 5$ so that $\langle(\delta E)^2\rangle/(4\mathfrak{m}_o kT) \approx 10^{-3}$, and $\gamma_\ell = \nu_c$ so that $\gamma_L \approx 1000$. Hence

$$\frac{\partial n^*(6300)}{\partial t} \approx 5 \times 10^4 \; \mathrm{cm}^{-3} \; \mathrm{sec}^{-1} \tag{19}$$

## FLUX OF EXCITING ELECTRONS

The flux of exciting electrons accelerated down the geomagnetic field, in the Landau damped region, is obtained by integrating $\partial n^*/\partial t$ over the height range of the Landau damped region for which $P \approx 3$. This height range is about 0.3 $k_m$. Hence

$$\mathrm{FLUX} = \int_{6\,k_m}^{6.3\,k_m} dz \quad \frac{\partial n^*(6300)}{\partial t}$$

$$= 0.3 \times 10^5 \; \mathrm{cm} \times \frac{\partial n^*(6300)}{\partial t} \tag{20}$$

Consequently, for typical modification conditions the flux of exciting electrons is with (20) and (19),

D5

$$\text{FLUX} \approx 10^9 \text{ electrons } \text{-cm}^{-2} \text{-sec}^{-1} \qquad (21)$$

To compare this flux with the experimental photon flux various loss mechanism of exciting electron must be taken into account such as collision with nitrogen. When this is done we find that the flux predicted in (21) can explain the observed 50 Rayleigh enhancements of the 6300Å airglow over Boulder.

In deriving (13) and (18) - (21) we have only had to calculate an average of the modified distribution function $f(\underline{v})$. The task that now remains is to solve (1) for $f(\underline{v})$ at all $\underline{v}$.
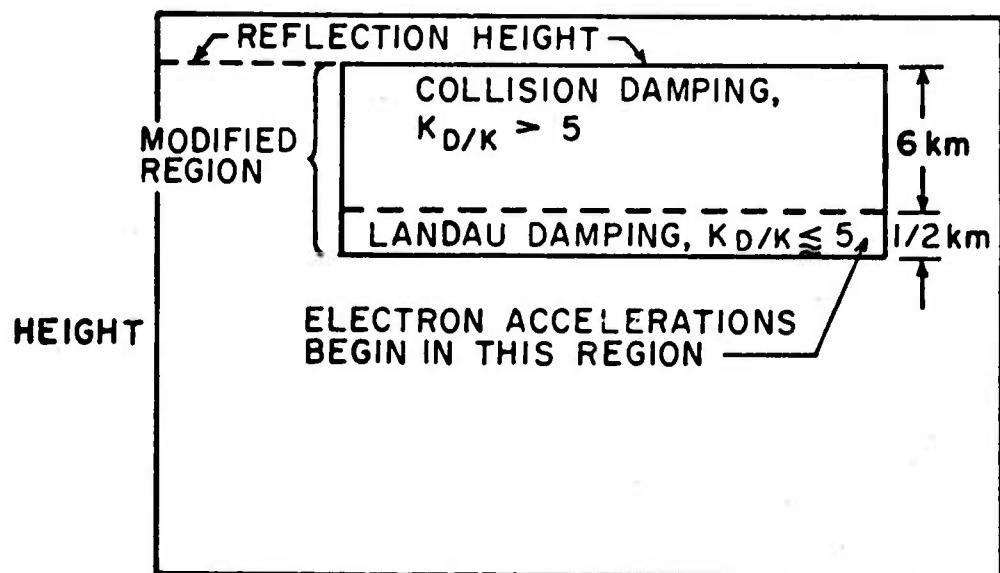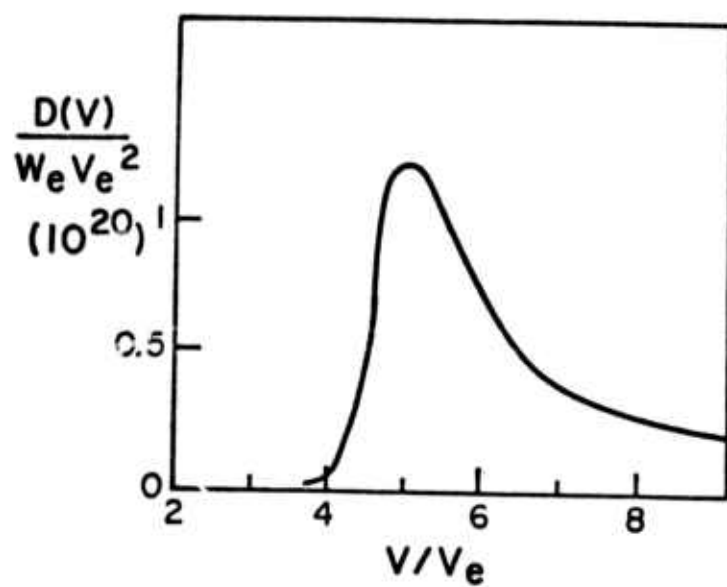
**FIGURE 1**

FIGURE 2

APPENDIX E:

# LINEAR THEORY OF DIFFUSION MODES

Martin V. Goldman, Donald F. DuBois,
Richard Berger, and Edward Williams

University of Colorado

# I. Linear Theory

We are concerned here with the linear properties of first order collisional-induced density diffusion across magnetic field lines in a homogeneous plasma. Section I gives the conditions for the simplest theory which ignores angular dependence and thermal fluctuations. Section II examines the diffusion mode for potential relevance to ionospheric modification experiments. Sections III and IV relax some of the approximations in I.

The elements and assumptions which go into the simplest linear fluid theory of the diffusion mode are listed below.

1. Electric fields produced by the diffusion are assumed electrostatic (only Poisson's equation is necessary):

2. The pressure is given by an isothermal equation of state, $p = N\theta$. The condition for this is $\frac{3}{2} n_e \omega \ll K_{e\perp} k^2$, where $K_{e\perp} = 5 n_e R_e^2 \nu_{ei}$ is the transverse electron thermal conductivity, $R_e$ is the electron gyroradius, and $\omega$ and $k$ are the frequency and wavenumber of the diffusion mode. This condition is only marginally satisfied in the simple theory presented here, although the theory is easily generalized in Section IV to include the thermal equations.

3. Viscosity terms are neglected. This neglect is justifiable provided the wavelength of the diffusion mode is sufficiently long, or $kR_i \ll (m_i/m_e)^{\frac{1}{2}}$, where $R_i$ is the ion gyroradius. A more general theory, in which viscosities are retained, has been presented by Dawson and Okuda[1] who are concerned with diffusion phenomena associated with ion-ion collisions rather than electron-ion collisions.

4. Electron-ion momentum transfer terms are retained in the electron momentum equations. These terms and electron cyclotron motion terms dominate the inertial terms ($|\omega| \ll \nu_{ei} \ll \omega_{ce}$).

5. The Ion charge density response, $\rho_1$, to the electrostatic field $\hat{k}E_1$ is the static Debye-screened response,

$$4\pi\rho_1 = - \frac{1}{k} \frac{k^2_{D1}}{k} E_1$$

where $k_{D1}$ is the ion Debye wavenumber.

6. In the linear theory we may assume quasineutrality: $n_e \simeq n_1$. Off resonance, the linear dielectric function for the diffusion mode is given by

$\epsilon = \chi_e + \dfrac{k^2_{D1}}{k^2}$ , where $\chi_e$ is the electrostatic susceptibility defined by

$$4\pi\rho_e = -ik\chi_e E_1$$

and to be evaluated below.

7. Diffusion along the magnetic field lines occurs on a much faster time scale than the diffusion across the field lines we are considering here (satisfied when $\omega_{ce} \gg \nu_{ei}$).

The most important property of the diffusion mode for our purposes is its extreme aspect sensitivity. This diffusion mode exists only for wave vectors k which are extremely close to perpendicular to the magnetic field lines. In Section III of this paper we show that the mode changes from diffusion-like to wavelike over an angle to the perpendicular to $\underset{\sim o}{B}$ given by

$$\alpha \simeq \frac{\nu_{ei}}{\omega_{pe}} \frac{k}{k_{D1}}$$

For the parameters over Boulder this is of the order of $10^{-6}$ radians.

8. For the present, assume $\underset{\sim o}{B}$ in the z-direction and first order spatial variation of all quantities is in the y-direction. With these approximations the first order electron fluid equations are given by

(9)      $\dfrac{\partial n}{\partial t} + n_o \dfrac{\partial}{\partial y} v_y = 0$

(10)      $0 = - \Theta y \dfrac{\partial n}{\partial y} - en_o (E_1\hat{y} + \dfrac{\overset{\twonotes}{v}}{c} \times \underset{\sim o}{B}) - \nu_{ei} \underset{\sim \perp}{v} n_o m_e$

E2

Combining these gives, to within the above approximations, for the first order electron density, n,

$$(11) \qquad \frac{\partial n}{\partial t} - \nu_{ei} R_e^2 \frac{\partial^2 n}{\partial y^2} - \frac{\nu_{ei} e n_o}{m_e \omega_{ce}^2} \frac{\partial}{\partial y} E_1 = 0.$$

Fourier transforming equation (11), we find for the electron susceptibility defined in (6),

$$(12) \qquad \chi_e(\underline{k}_1 \omega) = \frac{k_{De}^2}{k^2} \frac{i\nu_{ei} R_e^2 k^2}{\omega + i\nu_{ei} R_e^2 k^2},$$

where $R_e$ is the electron gyro-radius, defined by $R_e^2 = \theta_e / m_e \omega_{ce}^2$. We shall use $\chi_e$ in the next paper. Setting equal to zero the dielectric function $\epsilon$ (defined above in (6)) gives the dispersion relation

$$(13) \qquad \omega = - iDk^2,$$

where

$$(14) \qquad D \equiv \nu_{ei} R_e^2 (1 + \theta_i/\theta_e).$$

Equation (13) is characteristic of a diffusion process in which D is the diffusion coefficient. To see the process more clearly we can bypass equation (12) through (14) and put directly into equation (11) the static ion response $n_i$ to E given in (5), and the quasineutrality condition $n_e \approx n_i$. This gives the diffusion equation,

$$(15) \qquad \frac{\partial n}{\partial t} - D\frac{\partial^2 n}{\partial y^2} = 0.$$

Figure 1 sketches out how an initial density disturbance uniform along the z-axis but confined to y = 0, diffuses out in y as a function of time. Figure 2 shows the related particle motions.

E3

## II.   Potential Relevance to Central-Line Phenomenology

The diffusion mode is of interest in connection with experimental results because it has an aspect sensitivity confining this mode to less than about $0.1^{\circ}$. At present we have no plasma theory to account for the observed results. However, it is interesting to note the following:

The 157 Mhz central-line data results probe a several-Hz-wide field aligned disturbance of wave number

(16) $k = .066 \text{ cm}^{-1}$      $(\lambda = 95 \text{ cm})$

Inserting this into equation (13) gives

(17) $|\omega| = 15 \text{ Hz}$

where we have used the following parameters:

(18) $\begin{cases} \nu_{ei} = 400 \text{ Hz} \\ \theta_e = \theta_i = 0.2 \text{ eV} \\ B = 0.5 \text{ gauss} \\ \omega_{ce} = 8.8 \times 10^6 \text{ rad/sec} \\ R_e = 2.1 \text{ cm} \end{cases}$

Thus, aspect sensitivity and observed frequencies suggest the possible participation of the diffusion mode in the central line scattering, although there is at present no theory which predicts the strong intensities at the probed wavelengths or the dependence at these wavelengths on the modifier intensity.  In the next paper we describe how the modifier can drive unstable diffusion modes at wavelengths between 50 and 500 meters with low thresholds (close to that of the decay instability).

E4

## III. Behavior of Diffusion Mode for $\underline{k} \cdot \underline{B}o \neq 0$.

In order to determine the behavior of the diffusion mode for wavevectors $\underline{k}$ at an angle to $\underline{B}o$, we include spatial variation of first order quantities in both the y- and z- direction. For the present, we do not assume that the ions are static or that $|\omega| \ll \nu_{e1}$. With these exceptions we retain the assumptions in Section I. The first order fluid equations are given by:

(19)
$$\frac{\partial n_1}{\partial t} + n_o \underline{\nabla} \cdot \underline{V}_j = 0,$$

(20)
$$\frac{\partial \underline{V}_j}{\partial t} = \frac{e_j}{m_j} \left( - \underline{\nabla}\phi + \frac{\underline{V}_j}{c} \times \underline{B}o \right) - \nu_{e1}\underline{V}_j - \frac{\theta_j}{m_j n_o} \underline{\nabla}n_j,$$

where

$$\underline{\nabla} = \hat{y} \frac{\partial}{\partial y} + \hat{z} \frac{\partial}{\partial z}$$

and $j$ is a species index, i.e., $j = i$ for ions and $j = e$ for electrons. These equations, when coupled with the linearized Poisson's equation,

(21)
$$\nabla^2\phi = - 4\pi \sum_j e_j n_j,$$

are sufficient to obtain the dielectric function for non-perpendicular wavenumbers. Equations (19) - (21) are Fourier analyzed in space and time. The three components of the Fourier analyzed equation (20) are solved for $\underline{V}_j$ in terms of the scalar potential $\phi$ and the perturbed density $n_j$. Then equation (19) can be used to express the density in terms of the potential. When this result is folded into Poisson's equation, we find the linear dielectric function $\epsilon(k,\omega)$, given by

(22)     $\epsilon(\underline{k}, \omega) =$

$$1 - \sum_j \frac{\omega_{pj}^2 \left[ (\omega + i\nu_{e1})^2 - \omega_{cj}^2 \sin^2\alpha \right]}{\omega(\omega + i\nu_{e1}) \left[ (\omega + i\nu_{e1})^2 - \omega_{cj}^2 \right] - k^2 V_j^2 \left[ (\omega + i\nu_{e1})^2 - \omega_{cj}^2 \sin^2\alpha \right]}$$

E5

The normal modes, found by setting $\epsilon(\underline{k}, \omega) = 0$, are given by

$$(25) \qquad \omega_{\pm} = \frac{-i\nu_{ei}k^2}{2k_{Di}^2\omega_{ce}^2} \left\{ 2\omega_{pe}^2 \left(1 + \frac{\theta e}{\theta i}\right) + \omega_{ce}^2 \frac{k_{Di}^2}{k^2} (1 \pm R) \right\}$$

where

$$R^2 = 1 - \frac{4\alpha^2 \omega_{pe}^2 k_{Di}^2}{\nu_{ei}^2 k^2} \left(1 + \frac{\theta e}{\theta i}\right).$$

In obtaining equation (25), we have made use of the inequalities $k^2 Ti/m_e \omega_{ce}^2 \ll 1$ and $k_{Di}^2 \gg k^2$. For perpendicular propagation, $\alpha = 0$, $R \to 1$, and the normal modes are $\omega_+ = -i \nu_{ei}$ and $\omega_- = -i k^2 D$ so that we recover the results of equations (13) and (14). However, for finite $\alpha$, $R^2$ rapidly becomes negative and the roots $\omega_{\pm}$ become complex which corresponds to heavily damped oscillations. The angle $\alpha_c$ at which this crossover occurs is found by setting $R^2 = 0$ or

$$(26) \qquad \alpha_c = \frac{k\nu_{ei}}{2k_{Di}\omega_{pe}} \left(1 + \frac{Te}{Ti}\right)^{-\frac{1}{2}}.$$

Therefore, as mentioned in Section I, the cross-field diffusion mode is limited to angles less than $10^{-5}$ radians.

## IV. EFFECT OF THERMAL FLUCTUATIONS ON DIFFUSION MODE

As we have seen in Section II the diffusion mode exists only for wave-vectors nearly perpendicular to the external field $\underline{B}_o$. Therefore, in examining the thermal effects we shall assume as in Section I that $\underline{k} \cdot \underline{B}_o = 0$. Moreover, we retain Eqs. (1) and (4)-(7) but not Eqs. (2) and (3). We consider only the first order electron fluid equations. These are the equation of continuity,

$$(27) \quad \frac{\partial n}{\partial t} + n_o \frac{\partial}{\partial y} V_y = 0,$$

the equation of motion in the y-direction,

$$(28) \quad 0 = \frac{-1}{m_e} \frac{\partial \theta_1}{\partial y} - \frac{\theta_o}{n_o m_e} \frac{\partial n}{\partial y} + \nu_{ei} V_y$$

$$+ \frac{.73}{3} \frac{\theta_o}{m_e \nu_{ei}} \frac{\partial^2 V_y}{\partial y^2}$$

$$+ \frac{e}{m_e} \frac{\partial \phi}{\partial y} + \omega_{ce} V_x,$$

the equation of motion in the x-direction,

$$(29) \quad 0 = -\nu_{ei} V_x + \frac{3}{2} \frac{\nu_{ei}}{m_e \omega_{ce}} \frac{\partial \theta_1}{\partial y} - \omega_{ce} V_y,$$

and the heat balance equation for electrons,

$$(30) \quad (4) \frac{\partial \theta_1}{\partial t} + \frac{2}{3} \theta_o \frac{\partial V_y}{\partial y} = - \frac{\theta_o \nu_{ei}}{\omega_{ce}} \frac{\partial V_x}{\partial y}$$

$$+ \frac{\eta \theta_o}{m_e \omega_{ce}^2} \nu_{ei} \frac{\partial^2 \theta_1}{\partial y^2} - \frac{2m_e}{m_i} \nu_{ei} \theta_1,$$

where $\eta = 2/3(4.66)$.

In obtaining Eq.(30), we assumed equal ion and electron background

temperatures and neglected the ion temperature fluctuation. The viscous terms in Eq. (29) were neglected because they are of order $k^2 R_e^2 \ll 1$. For the same reason all viscous terms except one are neglected in Eq. (28). The viscous heating terms in Eq. (30) are neglected because they are quadratic in first order quantities. The first two terms on the right hand side of Eq. (30) are the divergence of the electron heat flux and the last term is the collisional heating of electrons by ions (for equal ion and electron temperatures and no ion thermal fluctuations). This last assumption is justified provided $k^2 R_i^2 \gg 1$. In this regard, we note that Eq. (3) is no longer necessary as viscous terms have been included where they are important. Equations (21) and (27)-(30) are Fourier transformed, and the resulting system of equations solved for the dielectric function $\epsilon(\underline{k},\omega)$ where

(31) $\qquad \epsilon(\underline{k},\omega) = 1 + k_{Di}^2/k^2 + \chi_e(\underline{k},\omega)$

and

(32) $\qquad (\chi_e)^{-1} = \dfrac{k^2}{k_{De}^2} \left\{ \dfrac{\omega}{ik^2 R_e^2 \nu_{ei}} + 1 + \dfrac{\omega/6}{6\omega + \dfrac{2m_e}{m_i} i\nu_{ei} + (n-3/2)\, ik^2 R_e^2 \nu_{ei}} \right\}$

If we include only the first two terms in curly brackets in Ew. (32), we recover the results of Section I. The additional term in Eq. (32) is due to thermal fluctuations; and, for frequencies $\omega \sim ik^2 R_e \nu_{ei}$, it is clearly not negligible. The viscous terms however can be consistently neglected provided $k^2 R_e^2 \ll 1$. The dispersion equation, $\epsilon(\underline{k},\omega) = 0$, has two roots $\omega_\pm$ defined by

(33) $\qquad \omega_\pm = \eta^\pm\, ik^2 R_e^2 \nu_{ei}$

$\qquad\qquad \eta^\pm = -1.9 - \gamma \pm \left[\gamma^2 - 3\gamma + .4\right]^{1/2}$

$\qquad\qquad \gamma = .62 \, (\dfrac{m_e}{m_i})/k^2 R_e^2$

E8

For the ionosphere $\omega_{pe} \sim 4\omega_{ce}$ and $k \sim 0.1\, k_{De}$ so that $\gamma \ll 1$. Thus, with the inclusion of thermal effects, the dispersion relation has two diffusion modes where there was one (Eq.13) without thermal effects. However, for $\theta_e = \theta_i$, both these modes (Eq. 33) differ in value from the mode uncorrected by thermal effects (Eq. 13) only by 10%. Since each mode still has zero real frequency, we don't expect the inclusion of thermal effects to alter the conclusions of Appendices E or F.

$$\frac{\partial n_{1e}}{\partial t} - D \frac{\partial^2 n_{1e}}{\partial y^2} = 0, \quad n_e \approx n_i$$

$$D = \nu_{ei} R_e^2 \left(1 + \frac{\Theta_e}{\Theta_i}\right)$$



$n_{1e}(t_0)$     $n_{1e}(t_1)$     $n_{1e}(t_2)$

FIGURE 1

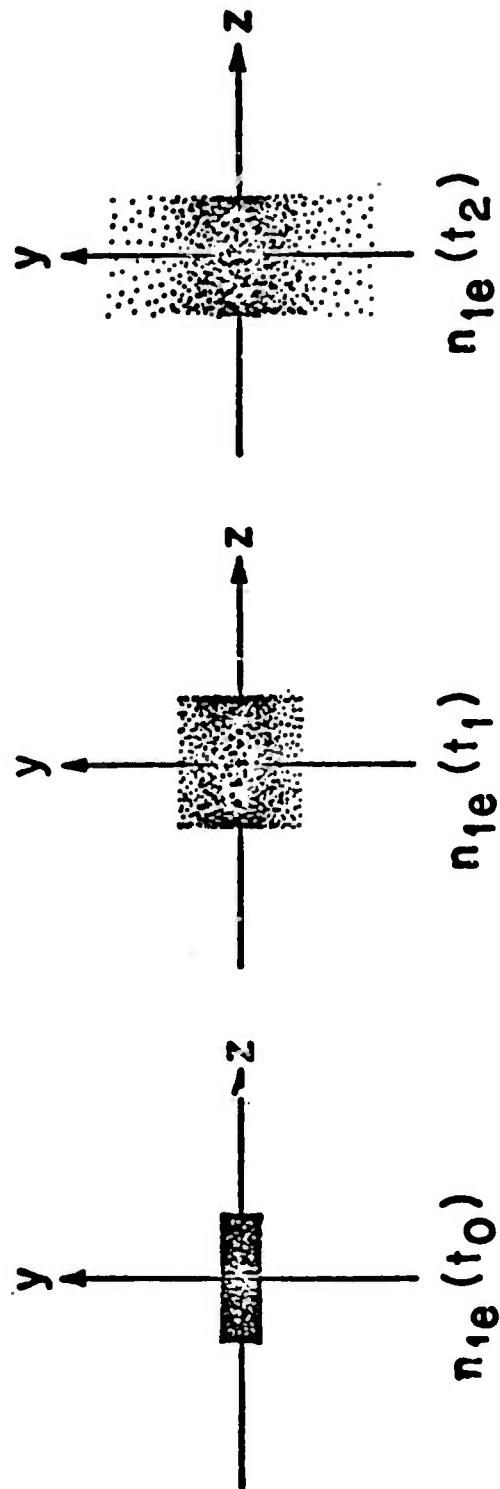FIRST ORDER DIFFUSION IN A HOMOGENEOUS PLASMA

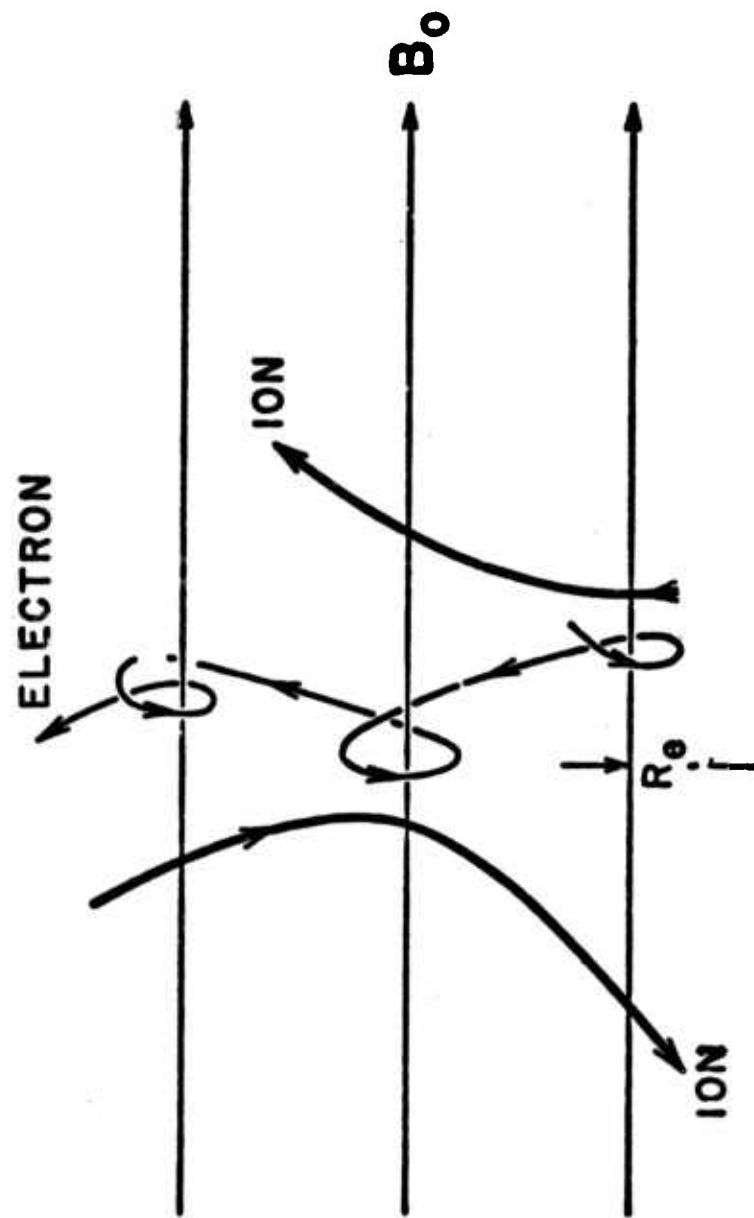FIGURE 2

## FOOTNOTES

1. H. Okuda and J. Dawson, "Theory and Numerical Simulation on Plasma Diffusion Across a Magnetic Field," Princeton University, MATT Report, 1972.

2. S.I. Braginskii, "Transport Processes in a Plasma," Reviews of Plasma Physics, Vol 1, pg. 205.

APPENDIX F:

STIMULATED DIFFUSION SCATTERING

M.V. Goldman and D.F. DuBois
University of Colorado

In this note we discuss a new electromagnetic parametric instability in which an O-wave heater acts as a pump to drive unstable the diffusion mode described in the previous note together with a scattered O-wave. The threshold and growth rates for this instability (to be called stimulated diffusion scattering, or SDS) are computed under the simplifying assumption that the pump linewidth is zero. We also consider possible relevance to spread-f.

Figure (1a) shows the simple geometry for which the calculation has first been performed. The incident and scattered wave vectors are orthogonal to $\underline{B}_o$ and the wave vector of the diffusion mode therefore also orthogonal (the lowest threshold occurs for $k_{diffusion} \approx 2k_{inc}$ as shown). Figure (1b) shows a more realistic stimulated scattering geometry for the ionosphere in which $\underline{k}_{inc}$ is at an angle to the geomagnetic field, and $\underline{k}_{scatt}$ is such that $\underline{k}_{diff}$ is still perpendicular to $\underline{B}_o$. We do not expect too much quantitative difference between (1a) and (1b), although we here only look at (1a).

We assume the validity of the fluid equations with pump, $\underline{A}_o \cos(\omega_o t - ky)$ and scattered radiation $\underline{A}_1$. These are combined with the Poisson and wave equations. The vector potentials $\underline{A}_o$ and $\underline{A}_1$ belong to the incident and reflected O-waves, respectively. The use of a monochromatic pump is possibly a serious oversimplification here. In the fluid equation, the velocity variable is related to canonical momentum by

$$\underline{u} = \underline{v} + \frac{e}{mc} (\underline{A}_o \cos(\omega_o t - k_o y) + \underline{A}_1).$$

This velocity variable $\underline{u}$, given by the canonical momentum divided by the mass has been used by many and perhaps most recently by Bodner and Eddleman[1] in their treatment of stimulated Brillouin scattering (SBS), which is similar to our treatment of SDS. We assume that the zero order fluid velocity is zero $(\underline{u} = 0)$.

The dominant terms in the fluid equations for the first order electron density and canonical momentum are given below.

$$\frac{\partial n_1}{\partial t} + n_o \underline{\nabla} \cdot \underline{u}_1 = 0 \tag{1}$$

$$\frac{\partial \underline{u}_1}{\partial t} - \frac{e}{mc} (\underline{u}_1 \times \underline{B}_o) + \frac{\theta}{mn_o} \underline{\nabla} n_1 + \nu_{ei} \left[ \underline{u}_1 - \frac{e}{mc} \underline{A}_1 \right] = \tag{2}$$

$$- \frac{e}{m} \left[ \underline{E}_1 + \frac{e}{mc} \underline{\nabla} \underline{A}_o \cdot \underline{A}_o \cos (\omega_o t - k_o y) \right]$$

$$\underline{\nabla} \cdot \underline{E}_1 = 4\pi (\rho_e + \rho_1) \tag{3}$$

$$(\nabla^2 - \frac{1}{c^2} \frac{\partial^2}{\partial t^2}) \underline{A}_1 = \frac{4\pi e^2}{c^2 m} \left[ n_1 \underline{A}_o \cos (\omega_o t - ky) + n_o \underline{A}_1 \right] \tag{4}$$

The momentum equation (2) includes momentum transfer to the ions through electron-ion collisions $\nu_{ei}$ and the force associated with the $\underline{\nabla A}_1 \cdot A_o$ non-linearity. (From a Hamiltonian point of view this force arises from the $\rho A^2$ coupling which adds to the $\rho\phi$ coupling.) Equations (1) and (2) tell us that the electron charge density responds to the indicated nonlinearity in exactly the way that it linearly responds to an electrostatic field $E_1$; that is, through a linear electrostatic susceptibility $\chi_e$ (cf our first note). When this information is put into Poisson's eq. (3), we obtain

$$\varepsilon(\underline{k},\omega) \ E_1(\underline{k},\omega) = \frac{i v_D}{2c} k \ \chi_e \ (\underline{k},\omega) \ A_1 \ (\omega - \omega_o) \tag{5}$$

in which the pump beats against the scattered wave to act as a source for driving the diffusion mode. Maxwell's equation for the scattered wave, driven

F2

by the diamagnetic current is

$$\left[ (\omega - \omega_0)^2 - \omega_p^2 - c^2 |\underline{k} - \underline{k}_0|^2 + \frac{i\nu_{ei}\omega_p^2}{\omega - \omega_0} \right] A_1(\omega - \omega_0) = \tag{6}$$

$$\frac{i v_D c}{2} k \, \chi_e(k,\omega) \, E_1(\omega)$$

$$v_D = \frac{eE_0}{m\omega_0}, \quad \chi_e = \frac{k_{De}^2}{k^2} \frac{i\nu_{ei}R_e^2 k^2}{\omega + i\nu_{ei}R_e^2 k^2}$$

In this current the pump beats against the first order charge density which is again expressed via the linear susceptibility $\chi_e$ and leads to equation (6).

Equations (5) and (6) comprise the coupled equations for the electrostatic field $\underline{E}_1$ associated with the diffusion mode and the vector potential $\underline{A}_1$ associated with the scattered O-wave. The regenerative interaction of these two modes through the pump $\underline{E}_0$ leads to the instability. The effects of $\underline{E}_0$ are contained in the conventional driven velocity $v_D$. The linear susceptibility $\chi_e$ which is essentially the coupling coefficient is derived in Appendix E. The results of the linear theory are briefly summarized, and the diffusion mode dispersion relation is written as

$$\varepsilon = 1 + \frac{k_{Di}^2}{k^2} + \chi_e. \qquad \underline{\text{Uncoupled}} \text{ diff. mode:}$$

$$\varepsilon = 0 \quad \text{at} \quad \omega = -\frac{1}{\tau_D} = -i\nu_{ei}k^2 R_e^2 \left(1 + \frac{\theta_i}{\theta_e}\right) \tag{7}$$

where $\tau_D$ is the diffusion time.

The scattered radiation consists generally of a downshifted Stokes frequency

$$\omega_s = \omega_0 - \omega \approx \left[\omega_p^2 + c^2(\underline{k}_0 - \underline{k})^2\right]^{\frac{1}{2}}$$

F3

and an upshifted anit-Stokes frequency

$$\omega_A = \omega_0 + \omega \approx \left[ \omega_p^2 + c^2 (\underline{k}_0 + \underline{k})^2 \right]^{\frac{1}{2}} .$$

The wave vector $\underline{k}_0 - \underline{k}$ is associated with the Stokes frequency, and $\underline{k}_0 + \underline{k}$ with the anti-Stokes frequency. Since the frequency $\omega$ is assumed $\ll \omega_0$, the pump, and Stokes frequencies are approximately equal and, hence, we must have

$$\left| \underline{k}_0 - \underline{k} \right| \approx k_0 .$$

This is possible only for $\underline{k} \approx 2k_0$ or $k \ll k_0$. The former is backward scattering and the latter is forward scattering. If the anti-Stokes mode is to participate, $\omega_A$ cannot be far from $\omega_0$, and then we must also have

$$\left| \underline{k}_0 + \underline{k} \right| \approx k_0 \quad \text{for anti Stokes.}$$

This is obviously only possible for forward scattering which we do not treat here. For backward scattering the anti-Stokes mode would be too far off its linear frequency to participate, and we have the strictly 3-mode interaction described by eq. (3), (5) and (6).

The threshold obtained from solving the dispersion relation implied in equations (5) and (6) is given by

$$\frac{v_D^2}{v_e^2} = \frac{\nu_{ei}}{2\omega_T} \left[ 8 \left( \frac{2\Theta_e}{\Theta_i} + 1 \right) \left( 1 + \frac{\Theta_i}{\Theta_e} \right)^{\frac{1}{2}} \right] \tag{8}$$

$$= 12 \sqrt{2} \; \frac{\nu_{ei}}{\omega_T} \quad \text{for } \Theta_e = \Theta_i \quad \text{(ionospheric O-wave)}$$

$$= 18 \frac{\theta_e \nu_{ei}}{\theta_i \omega_T} \quad \text{for } \theta_e \ll \theta_i$$

(compare with SBS threshold, $\dfrac{v_D^2}{v_e^2} = 8 \dfrac{\nu_{ei}}{\omega_T} \dfrac{\gamma_a}{\omega_a}$ ).

For the ionosphere, with $\theta_e \approx \theta_i$, the threshold value of $v_D^2/v_e^2$ (directed velocity squared to thermal velocity squared) is $12 \sqrt{2} \ \nu_{ei}/\omega_o$. This is about a factor of two higher than the threshold for stimulated Brillouin scattering or the parametric decay instability. Both SDS and SBS have an advantage over the decay instability in the sense that neither SDS nor SBS involves Languir waves and Landau damping. This leads to a much wider range of altitudes for which these instabilities can in principle occur. We compute the threshold below for a typical set of parameters:

$$( v_D^2/v_e^2)_{threshold} = 1.3 \times 10^{-4} \text{ for}$$

$$\nu_{ei} = 300 \text{ Hz}, \ \omega_o = 2\pi f_o = 4 \cdot 10^7 \text{ radians.}$$

On the other hand, a heater with local vacuum intensity of 50 $\mu w/m^2$ incident upon a plane-layered plasma with scale length 100 km gives rise to a maximum local value of

$$v_D^2/v_e^2 \Big|_{1st \ max} = 2 \times 10^{-3},$$

which is 15 times the threshold for this instability.

The frequency-matching condition for SDS is given by

$$\omega_o(\underline{k}_o) - \omega_T(\underline{k} - \underline{k}_o) = \frac{1}{\tau_D} \frac{1}{\sqrt{1 + \Theta_i/\Theta_e}} \qquad (9)$$

$$|\underline{k} - \underline{k}_o| \simeq k_o \implies \underline{k} \simeq 2\underline{k}_o$$

and leads to the conclusion that the instability is strongest when the wave number of the low frequency mode is twice that of the incident 0-wave. There is some latitude in the frequency-matching condition insofar as it affects the threshold, but since the difference between $\omega_o$ and $\omega_T$ is always smaller than either frequency, the momentum-matching condition $\underline{k} \simeq 2\underline{k}_o$ remains approximately satisfied.

The dispersion relation for the scattered wave which corresponds to-minimum threshold (or maximum growth rate) turns out to be exactly the uncoupled dispersion relation:

$$\omega = \omega_T(\underline{k} - \underline{k}_o) \equiv \omega_p^2 + c^2|\underline{k} - \underline{k}_o|^2$$

Thus, $\omega_o - \omega$ is a _real_ frequency given by $1/\sqrt{2}\ \tau_D$. The coupling has therefore converted the diffusion mode into a wave-like mode of (low) frequency of order of the former diffusion rate. This situation is exhibited in Figure 2 which shows the uncoupled normal modes (dots) and the coupled (new) normal modes (crosses).

Two expressions are given for the growth rates above threshold associated with SDS:

$$\text{Im } \omega = \begin{cases} \dfrac{1}{\tau_D} \dfrac{1}{4.25} \dfrac{1}{1 + \Theta_e/\Theta_i} \left[ \dfrac{v_D^2/v_e^2}{(4\nu_{ei}/\omega_T)\sqrt{1 + \Theta_i/\Theta_e}} - (2\dfrac{\Theta_e}{\Theta_i} - 1) \right] & \quad (10) \\[1em] \qquad \text{(for Im } \omega \gg \tau_D^{-1} \text{ only)} \\[1em] \dfrac{\sqrt{3}}{2} \omega_T \left[ \dfrac{\tau_D^{-2}}{4\omega_o^2} \dfrac{\omega_p^2}{\omega_o^2} \dfrac{v_D^2}{v_e^2} \dfrac{1}{8} \right]^{1/3} , \quad \text{(for Im } \omega \gg \nu_{ei} \text{ only)} & \quad (11) \end{cases}$$

The first is valid only for growth rates less than $\tau_D^{-1}$, and the second only for growth rates larger than $\nu_{ei}$. We have not yet completed the numerical work necessary to give the growth rates in the intermediate range. To compute the growth rate we first need the diffusion rate

$$\frac{1}{\tau_D} = 2\nu_{ei} k^2 R_e^2. \qquad (12)$$

The wave number k is twice the _local_ pump wave number. We look first near the first Airy maximum, where the electric field vector of the pump is largest. There the local pump wave number is related to the free space wave number by

$$k_{o_{local}} = \frac{\omega_o}{c} \frac{\pi}{2} \left( \frac{c}{\omega_o L} \right)^{1/3} , \qquad (13)$$

where, L is the density scale length. For L = 100 km and $\omega_o = 4 \times 10^7$ radians, eq. (13) gives

$$k_{o_{local}} = .066 \frac{\omega_o}{c} . \qquad (14)$$

The diffusion rate is then given by

$$\frac{1}{\tau_D} = 8.3 \times 10^{-4} \text{ Hz, or } \tau_D \approx 20 \text{ minutes} \tag{15}$$

This extraordinarily slow rate implies that a more accurate theory is required taking into account the finite pump linewidth when it exceeds $10^{-3}$ Hz. Inserting (15) into equation (10) we find for the growth rate,

$$\text{Im } \omega = 5.2 \frac{1}{\tau_D}$$

which violates the conditions of validity for equation (10), but is probably roughly accurate (eqn. (11) gives a far worse violation of validity conditions). This leads to a growth time of about 4 minutes, which is rather long in comparison with common spread-f onset times.

Since the growth rate goes as $\tau_D^{-1}$ and hence as $k^2_{local}$, we have examined the growth rate at somewhat lower altitudes, where the ratio of the local pump wave number to the free-space wave number is larger than .066. However, the Airy function swelling factor for the pump is smaller at these altitudes and the gain in wave number appears to be generally offset in intensity, so that the magnitude of the growth rate is not appreciably changed from that at higher altitudes. (As an example, at the $100^{th}$ Airy node, $k^2_{local}$ is 22 times larger than at the first node, but the swelling factor is down by a factor of 10 and the growth rate is numerically unchanged.)

Work is in progress on several other features of this instability. In addition to folding in a finite pump bandwidth, the competition of this instability with other parametric instabilities, such as SBS and the decay instability, must be studied. Stimulated Brillouin scattering may be especially interesting, because the growth rates are larger, although the unstable ion-acoustic waves are not field aligned.
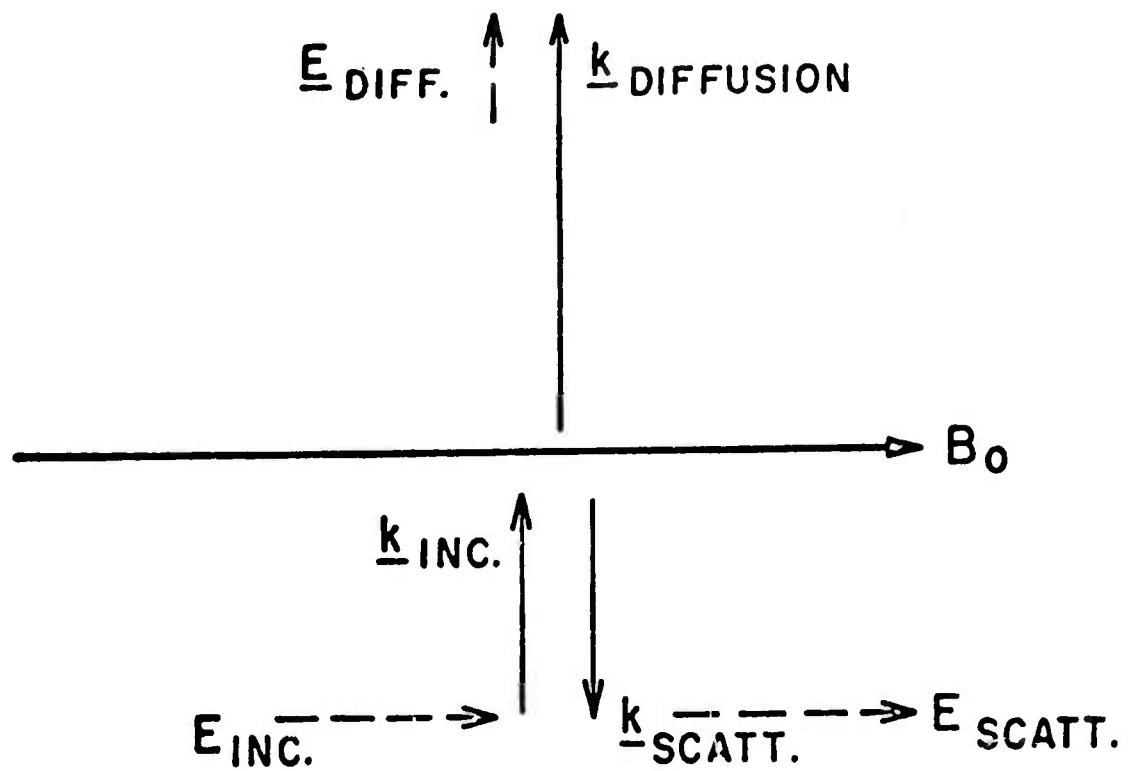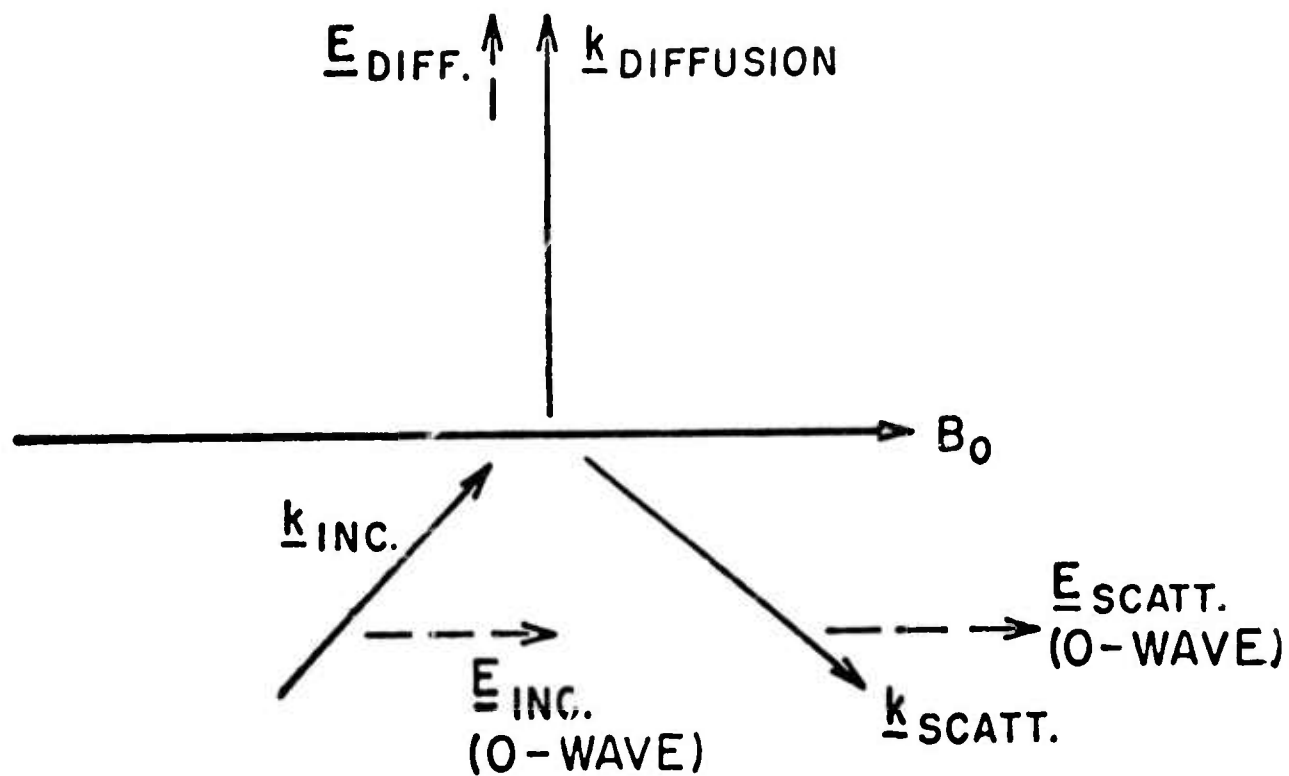
F8

$\underline{E}_{DIFF.}$ $\qquad$ $\underline{k}_{DIFFUSION}$

$B_O$

$\underline{k}_{INC.}$

$E_{INC.}$ $\qquad$ $\underline{k}_{SCATT.}$ $\qquad$ $E_{SCATT.}$
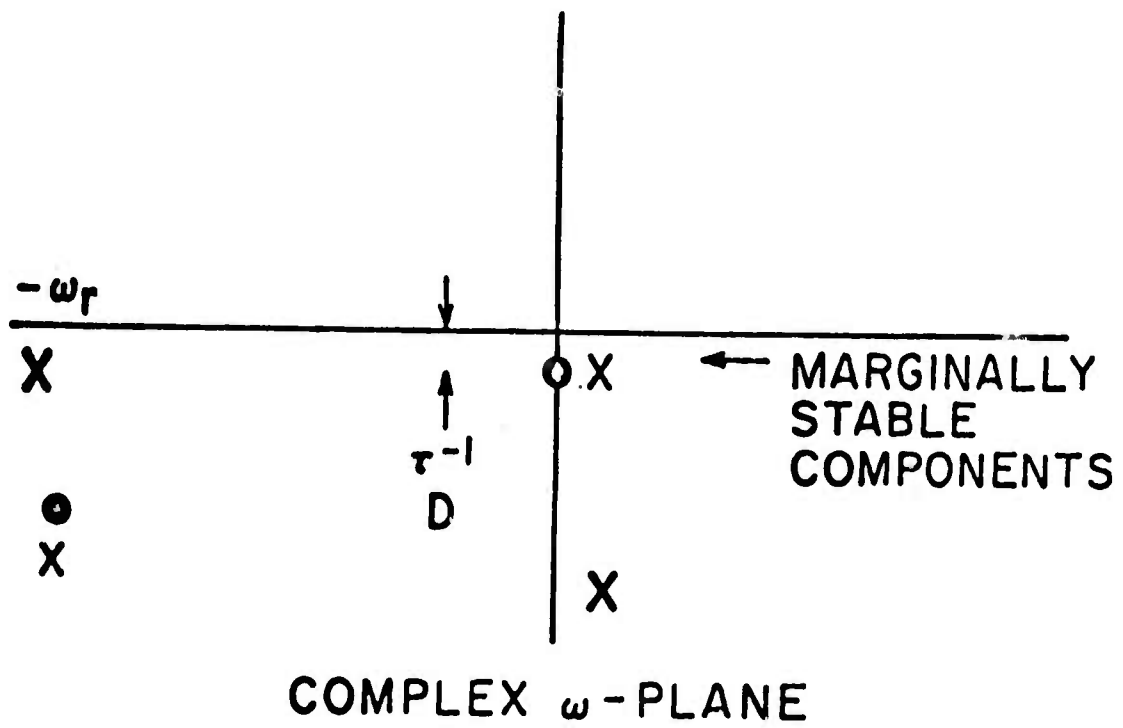
FIGURE 1a

FIGURE 1b

F10

COMPLEX ω-PLANE

FIGURE 2

F11

# References

1.  S.E. Bodner and J.L. Eddleman, "Stimulated Brillouin Scattering in
    Plasmas". University of California Radiation Laboratory, preprint
    #73378, August 31, 1971.

NONLINEAR SATURATION OF PARAMETRICALLY EXCITED

FIELD ALIGNED IRREGULARITIES

Jerome Weinstock and Bandel Bezzerides

Goldman and Dubois have shown that a low frequency unstable wave propagating across the magnetic field is excited during modifications (see these proceedings). Here we calculate the nonlinear saturated amplitude of this wave. The parametric excitation of this wave can be illustrated as follows:
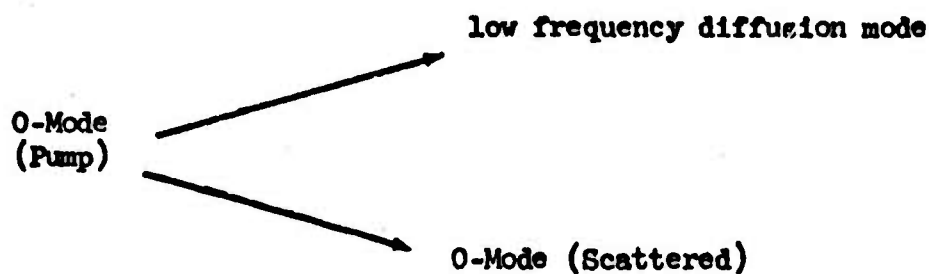


Low Frequency Mode at Threshold

$$\omega = k_\perp^2 D_{\perp a} - i\, k_\perp^2 D_{\perp a} , \qquad (1)$$

where $k_\perp$ is the wavenumber and is typically of the order of tens of meters, $D_{\perp a}$ is the ambipolar diffusion coefficient normal to the magnetic field.

$$D_{\perp a} = \frac{\nu_e v_e^2}{\Omega_e^2}\left(1 + \frac{T_e}{T_i}\right)$$

with $\nu_e$, $\Omega_e$, $v_e$ the electron collision frequency, gyrofrequency and thermal speed.

G1

The linear growth rate $\gamma^L$ of the mode is roughly given by

$$\gamma^L(k) \approx \left[ P \frac{2\cos^2\theta - 1}{\cos^2\theta} f(k) - 1 \right] k_\perp^2 D_{\perp a}, \quad 2\cos^2\theta \geq 1 \qquad (2)$$

where P is the ratio of pump intensity to threshold intensity, $\theta$ is an angle in the plane perpendicular to the magnetic field between the wave vector and the vertical plane, $f(k)$ is unity for the matching k and is very narrowly peaked

The nonlinear wave equation for this mode is given by

$$\frac{\partial I_{\underline{k}}}{\partial t} = \left( \gamma^L(\underline{k}) - \gamma^{NL}(\underline{k}) \right) I_{\underline{k}} + S \qquad (3)$$

where $I_{\underline{k}}$ is the spectral intensity at wave vector $\underline{k}$, $\gamma^{NL}$ is the nonlinear damping decrement due to waves, and S is the noise source.

$\gamma^{NL}(\underline{k})$ is determined by calculating the perturbation of electron and ion orbits due by the unstable waves. This result is found to be [see Eq's. (39) and (52) of Weinstock and Williams, Phys. Fluids 14, 1472 (1971)].

$$\gamma^{NL}(\underline{k}) = \frac{2c^2}{B^2} \int \frac{d\underline{k}'}{(2\pi)^3} \left( \frac{\hat{\underline{z}} \times \underline{k}_\perp}{k_\perp} \right)^2 I_{\underline{k}'} \frac{\gamma^{NL}(\underline{k}')}{\omega_R^2 + [\gamma^{NL}(\underline{k}')]^2} \qquad (4)$$

where c is the speed of light, B is the magnetic field strength, $\hat{\underline{z}}$ is a unit vector along the magnetic field, and $\omega_R$ is the real part of the frequency of the unstable mode. In the present case

$$\omega_R \approx \gamma^{NL}(\underline{k}') \qquad (5)$$

To approximately solve the wave Eq. (3) for the saturated value of $I_{\underline{k}}$ we set $\partial I_{\underline{k}}/\partial t = 0$, and neglect S as being relatively small to obtain

$$\gamma^{NL}(\underline{k}) \approx \gamma^L(\underline{k}) \qquad (6)$$

G2

Substituting (2) into (6) we have

$$\gamma^{NL}(\underline{k}) \approx \left[ P \frac{2\cos^2\theta - 1}{\cos^2\theta} f(k) - 1 \right] k_\perp^2 D_{\perp a} \tag{7}$$

Equations (4) and (7) can be solved for the total wave energy density

$\int \frac{d\underline{k}'}{(2\pi)^3} \frac{I_{\underline{k}'}}{4\pi n \theta_e}$ . The solution is

$$\int \frac{d\underline{k}'}{(2\pi)^3} \frac{I_{\underline{k}'}}{4\pi n \theta_e} = \frac{2 P^2 (k_\perp^2 D_{\perp a})^2 \Omega_e^2}{\langle\langle k_x^2 \rangle\rangle v_e^2 \omega_{pe}^2} \tag{8}$$

where $\langle\langle k_x^2 \rangle\rangle \equiv$ is the mean wave vector component in the normal plane defined by

$$\langle\langle k_x^2 \rangle\rangle \equiv k_\perp^2 \int \frac{d\underline{k}'}{(2\pi)^3} \frac{\sin^2\theta \cos^2\theta}{2\cos^2\theta - 1} I_{\underline{k}'} \quad , \tag{9}$$

$\omega_{pe}$ is the electron plasma frequency. The value of $\langle\langle k_x^2 \rangle\rangle \approx$ is found to be roughly given by

$$\langle\langle k_x^2 \rangle\rangle \approx 10^{-1} k_\perp^2 \tag{10}$$

The mean square density fluctuation $(\delta n)^2$ at saturation can be obtained from (8) by making use of the relation     .

$$i \underline{k} \cdot \underline{E}_{\underline{k}} = 4\pi n_{\underline{k}} \frac{k^2}{k_D^2} \tag{11}$$

so that

$$\langle |E_{\underline{k}}^2| \rangle = (4\pi e)^2 \frac{k^2}{k_D^4} \langle |n_{\underline{k}}^2| \rangle \tag{12}$$

Substituting (12) into (8), with $\langle E_{\underline{k}}^2 \rangle = I(\underline{k}) \times$ Volume, we have finally

$$\int \frac{d\underline{k}'}{(2\pi)^3} \frac{\langle |n_{\underline{k}}^2| \rangle}{n_o^2} = 2 P^2 \frac{k_\perp^2}{\langle\langle k_x^2 \rangle\rangle} \left(1 + \frac{T_e}{T_1}\right)^2 \left(\frac{\nu_e}{\Omega_e}\right)^2$$

$$\left(\frac{\delta n}{n_o}\right)^2 = 2 P^2 \frac{k_\perp^2}{\langle\langle k_x^2 \rangle\rangle} \left(1 + \frac{T_e}{T_1}\right)^2 \left(\frac{\nu_e}{\Omega_e}\right)^2 \tag{13}$$

Equation (13) is the mean square density fluctuation. For typical values of

$$\left(\frac{\nu_e}{\Omega_e}\right)^2 \approx 10^{-8}$$

$$P \approx 12$$

$$\frac{k_\perp^2}{\langle\langle k_x^2 \rangle\rangle} \approx \frac{1}{10}$$

we find, from (13), that

$$\left(\frac{\delta n}{n_o}\right)^2 \approx 1.1 \times 10^{-4}$$

We note, from (13), that the level of density fluctuations depends upon the angular spectrum, but does not depend upon the absolute value of the wavelength.

## DOCUMENT CONTROL DATA - R & D

*(Security classification of title, body of abstract and indexing annotation must be entered when the overall report is classified)*

| 1. ORIGINATING ACTIVITY *(Corporate author)* | 2a. REPORT SECURITY CLASSIFICATION |
|---|---|
| The University of Colorado<br>Department of Astro-Geophysics<br>Boulder, Colorado 80302 | Unclassified |
| | 2b. GROUP |

**3. REPORT TITLE**

THEORY OF IONOSPHERIC MODIFICATION

**4. DESCRIPTIVE NOTES** *(Type of report and inclusive dates)*

Final Report

**5. AUTHOR(S)** *(First name, middle initial, last name)*

Martin V. Goldman          Jerome Weinstock
Donald F. DuBois           Bandel Bezzerides

| 6. REPORT DATE | 7a. TOTAL NO. OF PAGES | 7b. NO. OF REFS |
|---|---|---|
| 1 February 1973 | 223 | 73 |

| 8a. CONTRACT OR GRANT NO. | 9a. ORIGINATOR'S REPORT NUMBER(S) |
|---|---|
| F30602-72-C-0343<br>b. PROJECT NO.<br>ARPA Order No. 1423<br>Program Code No. 2820 | |
| | 9b. OTHER REPORT NO(S) *(Any other numbers that may be assigned this report)*<br>RADC-TR-73-88 |
| d. | |

**10. DISTRIBUTION STATEMENT**

N/A

| 11. SUPPLEMENTARY NOTES | 12. SPONSORING MILITARY ACTIVITY |
|---|---|
| Monitored by:  RADC/OCSE<br>GAFB, NY  13441 | Advanced Research Projects Agency<br>1400 Wilson Blvd.<br>Arlington, VA  22209 |

**13. ABSTRACT**

Theoretical results are presented for nonlinear plasma wave effects of ionospheric modification by high power radio waves. UHF and L-band scattering models have been constructed and nonlinear deviative absorption computed. The effects of parametric instabilities on the electron distribution function and observed airglow are computed. Linear low frequency electromagnetic plasma instabilities associated with the geomagnetic field are derived.

DD FORM 1473

| 14 KEY WORDS | LINK A | | LINK B | | LINK C | |
|---|---|---|---|---|---|---|
| | ROLE | WT | ROLE | WT | ROLE | WT |
| Parametric instability | | | | | | |
| Nonlinear spectrum of plasma instabilities | | | | | | |
| Saturation of Plasma waves | | | | | | |
| Stimulated Diffusion Scattering | | | | | | |
| Airglow | | | | | | |
| Electron acceleration by Plasma waves | | | | | | |
| UHF scattering model | | | | | | |
| Induced scattering of Langmuir waves | | | | | | |
| Larmor Orbit Perturbation | | | | | | |
| Decay instability | | | | | | |